# Fouling and process design in reverse electrodialysis

## a study with natural waters

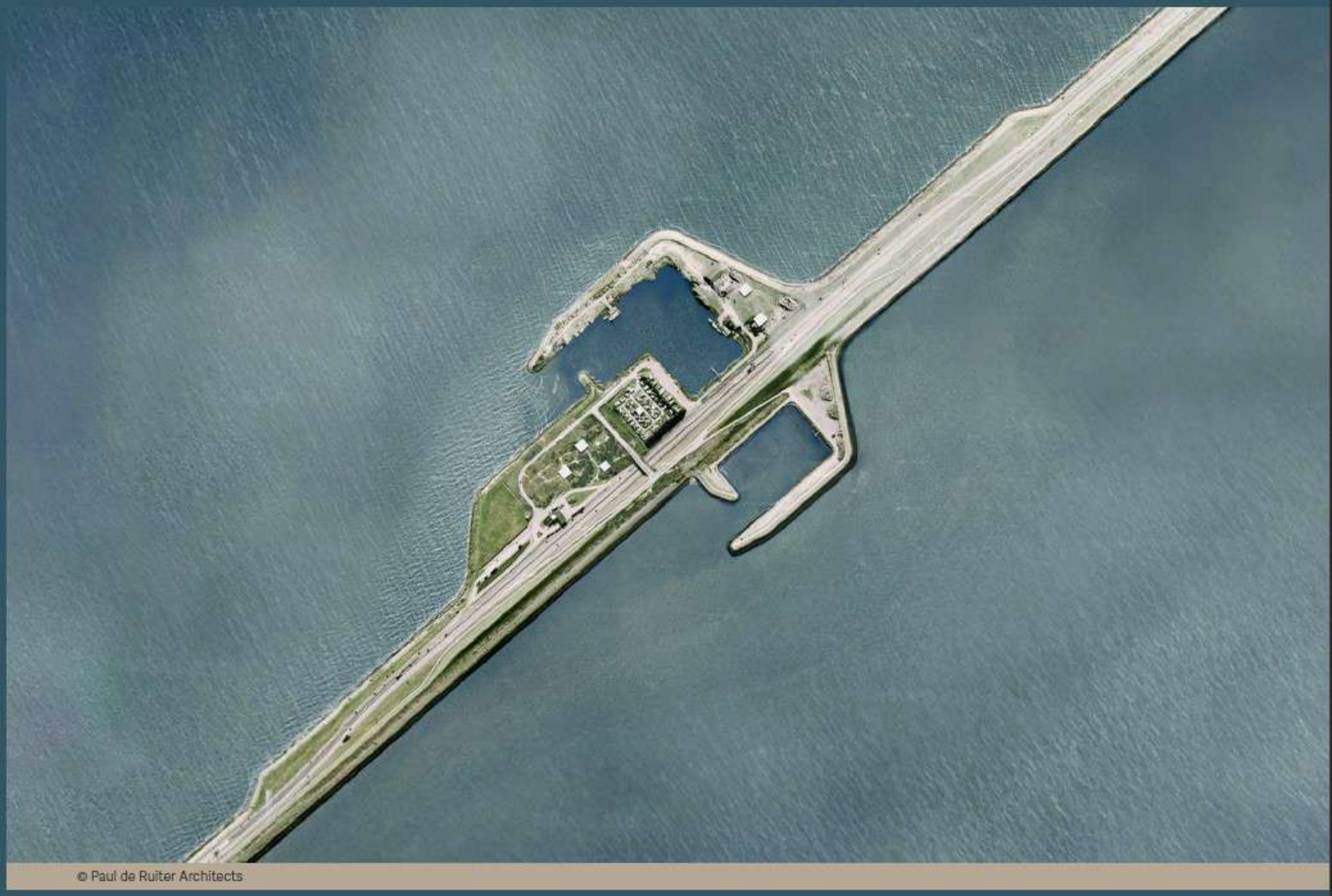

© Paul de Ruiter Architects

Bárbara Vital

**Propositions**

1. Working with natural water sources brings unpredictable results, but they are more meaningful than using artificial feeds.
   (this thesis)

2. There is no direct measurement for biofouling impact in reverse electrodialysis.
   (this thesis)

3. Reduction of energy demand is crucial for energy transition.

4. Increasing the life span of a product is key for its sustainability and must be the focus of industry.

5. Companies that caused environmental damage in the past must be held accountable for the harm they caused.

6. The behaviour of an individual serves as a model for the rest of the society.

7. Governmental subsidies and allowances must be less universal.

8. Developing job opportunities in small cities is needed to spread people more evenly over the world.

**Propositions belonging to the thesis, entitled**

**Fouling and process design in reverse electrodialysis: a study with natural waters.**

Bárbara Vital,

Wageningen, 11 September 2023

# Fouling and process design in reverse electrodialysis: a study with natural waters

Bárbara Vital

**Thesis committee**

**Promotor**

Prof. Dr H.V.M. Hamelers

Special Professor, Electrochemical Resource Recovery

Wageningen University & Research

**Co-promotors**

Dr T. Sleutels

Scientific project manager

Wetsus - European Centre of Excellence for Sustainable Water Technology, Leeuwarden

Dr M.C. Gagliano

Theme Coordinator Biofilms

Wetsus - European Centre of Excellence for Sustainable Water Technology, Leeuwarden

**Other members**

Prof. Dr L.C.P.M. de Smet, Wageningen University & Research

Prof. Dr W.G.J. van der Meer, University of Twente, Enschede

Prof. Dr D.C. Nijmeijer, Eindhoven University of Technology

Prof. Dr J.G. Crespo, Universidade Nova de Lisboa, Portugal

This research was conducted under the auspices of the Graduate School for Socio-Economic and Natural Sciences of the Environment (SENSE).

# Fouling and process design in reverse electrodialysis: a study with natural waters

Bárbara Vital

**Thesis**

submitted in fulfilment of the requirements for the degree of doctor

at Wageningen University

by the authority of the Rector Magnificus,

Prof. Dr A.P.J. Mol,

in the presence of the

Thesis Committee appointed by the Academic Board

to be defended in public

on Monday 11 September 2023

at 4 p.m. in the Omnia Auditorium.

Bárbara Vital

Fouling and process design in reverse electrodialysis: a study with natural waters, 194 pages

PhD thesis, Wageningen University, Wageningen, the Netherlands (2023)

With references, with summary in English

ISBN: 978-94-6447-779-5

DOI: https://doi.org/10.18174/633990

*“We don’t inherit the earth, we borrow it from our children.”*

*Native American proverb*

**Table of Contents**

## Summary

The use of fossil fuels and its impact on the environment, together with the increasing energy demand and the difficulty to find energy sources that can supply energy continuously in a sustainable way all around the world, drives the need for a mix of renewable and sustainable energy. A few renewable sources are already exploited at scale, such as wind and solar energy, but there is a need for the development of other sources that can supply energy more constantly.

Salinity Gradient Energy (SGE), also popularly known as "Blue Energy," uses the controlled mixing of the salinity gradient between fresh and sea water to produce electrical energy and is a promising energy source that can be considered for exploitation at large scale at river deltas and shoreline regions. Reverse Electrodialysis (RED) is the technological process that allows the harvest of this energy, by using a series of alternating anion (AEM) and cation (CEM) exchange membranes. The alternating membranes are stacked into an electrochemical cell, creating compartments for fresh and sea water, and due to the natural movement of ions from the more concentrated solution to the less concentrated solution and the presence of electrodes and electrolyte solution, energy from the mixing can be harvested in the form of electrical energy.

Fouling, the attachment of unwanted compounds to ion-exchange membranes and spacers, is a severe problem within RED applications under natural conditions. Fouling can significantly decrease the power output and decrease the lifetime of the ion exchange membranes. The compounds causing fouling can have different nature, such as organic matter, particulate, biofouling, and scaling. These diverse types of foulants have different impacts on the membrane process and the knowledge on fouling behaviour within RED applications is scarce. In this thesis, first steps were taken to identify the different foulants from these different water sources and relate them to the performance of the RED process (Chapters 2 and 3). For that, a fouling fractionation setup was used, where foulants from natural feed waters were treated at various levels. The presence of the different sizes in foulants was related to the performance of stacks and to the remaining foulants on membrane surface. After two months of operation, the presence of particulate matter after dual media filtration was related to an increase of pressure drop when treating both fresh (~100 mbar) and sea (~500 mbar) water but could help limit biofouling development on the membrane surface. The presence of biofouling did not seem to impact electrical performance of the stacks. Due to the high pumping power losses in seawater treatment at the end of the designated operation time, a simple and chemical free cleaning procedure was performed and showed that 90% of the fouling build-up was reversible, recovering the pumping losses accumulated over 2 months of operation in a few minutes.

This knowledge built the base for the development and optimization of a suitable and cost-effective pre-treatment for RED, a dual media filtration system (Chapter 4). The use of activated filter media (AFM), sand and anthracite were coupled with a high flow velocity of filtration that led to a decrease of the area needed for filtration and still allowed for an adequate pre-treatment. Also, the use of profiled membranes in combination with dual media filtration, showed that is possible to limit the pumping power losses related to fouling in RED, using realistic operation conditions with natural feed waters.

After the improvement of the pre-treatment, a more energy efficient way of connecting stacks, called multi-stage, was studied and analysed in the view of fouling (Chapter 5). Multistage enables the use of salinity gradient further than a single pass, which implies that the treated water is used more efficiently, reducing the treatment need. The behaviour of multivalent ions in this configuration showed that in the second stage uphill transport did not occur, limiting the performance loss associated with these ions. The stack autopsy revealed microorganisms with sizes ten times larger than the cartridge filter nominal pore size (5 µm) and biofilm covering part of the spacer open area, contributing to the increasing pressure drop in the stacks.

Lastly, in Chapter 6, due to pressure drop caused by particles after dual media pre-treatment still leading to pumping power losses, studying simple and chemical free cleaning regimes became of importance for RED application. Cleaning with air sparging and a technique called reverse flow and feed switch yield the best results, keeping pressure drop over the stacks below 100 mbar over more than 2 months continuous operation of the stacks.

Finally, a discussion of the relevance of the findings of this thesis to prospects of RED and SGE is presented. Considerations about the pre-treatment energy requirement are discussed, and the impact of the feedwater quality on the feasibility of the process is extrapolated to distinct locations. The energy requirement to run the pre-treatment with dual media filter accounts for around 20% of the energy production with stacks, even when using a low power density of 0.3 $W/m^2$. In addition, an overview of points of attention for future development of the technology and its sustainability and ecological impact are discussed.

# Chapter 1

## Introduction

### 1.1 Background information

The growth of world population, together with the development of new technologies and needs associated with a modern life has led to a constant increase in energy demand over the past decades. Currently, most energy production derives from fossil fuels. The generation of energy occurs through combustion of these carbon-based fuels, found in deposits from a deep layer of the Earth. Besides releasing energy, the combustion process also emits carbon to the atmosphere, mostly in the form of carbon dioxide ($CO_2$). These emissions are directly associated with worldwide issues, namely greenhouse effect, climate change and air pollution [1,2] and are being enhanced by the higher demand and use of energy from fossil fuels.

These negative impacts have been addressed in scientific and political discussion for several years and yet, no clear solution has been widely implemented. It is evident that addressing these challenges requires a societal response and can only be achieved with an integrated approach. The shift from fossil fuels to renewable energy sources has not been completely successful yet. The establishment of new policies is a promising approach to promote changes in the energy sector, for example with the so-called world goals or sustainable development goals by the United Nations (UN). Some of the goals are related to energy production and pollution by energy sources, for instance, goals 7 (Affordable and Clean energy) and 13 (Climate Action) [3].

The European Union (EU) faces a major challenge to achieve these UN goals related to energy. Even though energy is available for almost the entire population (one of the targets of goal 7), a large portion still comes from non-renewable sources, representing 78% in 2020 of the total energy consumption of the EU [4]. One of the goals in the EU is that $CO_2$ emissions must drop 45% by 2030 and reach a net zero by 2050 [2,5]. Only 37.5% of the gross electricity consumption is coming from renewable sources, namely hydropower, wind, solar, thermal and biofuels [4]. In the Netherlands, this share is only 12.3% and leaves the country in the third last position among European countries [4].

Wind and solar energy have developed immensely in the last decades, and are the ones leading the increase of the share of the renewable energy sources worldwide [2,3]. Wind and solar energy are known for their availability all around the world, large exploitable power output and being modular. They can be used in power plants to produce large amounts of energy or more locally producing energy for small scale business or even households [1]. The arising of these energy sources created a new market on the energy sector, called green energy, and it has been constantly growing in the last years [6]. Their development as energy sources in Europe has been expanding and there is still room for further improvement. However, their dependency on weather conditions and the lack of a stable energy production is a problem without a direct solution at the time. Concerns about the life cycle of the materials involved in their operation also need to be considered. They

include separation of the components, energy costs and lack of policies for recycling solar panels and wind turbines, which have an average life cycle of 25 years [7–9]. On top of that, citizens are often disturbed by the visual and sound pollution of wind turbines in certain environments and some communities are now organized against the installation of the turbines in their areas. Similarly, large areas with solar panels are increasingly getting opposition from social movements that claim that the land area could have a more beneficial use than energy production, such as food production or biodiversity goals. All in all, these issues, especially the high variability of energy production from solar and wind sources, drastically prevent the expansion of these well-established renewable energy sources. This reinforces the need for alternative renewable and sustainable energy sources, so that the goals set for the years to come can be accomplished.

A promising alternative energy source is **Salinity Gradient Energy (SGE)**, popularly known as **Blue Energy**, which exploits the salinity gradient energy from the controlled mixing of fresh water and seawater [10]. Blue energy relies on the **Reverse electrodialysis (RED) technology** to produce energy sustainably; the principle is that by using a stack of alternatingly anion exchange and cation exchange membranes, with alternating high and low concentration solutions compartments, it is possible to harvest the mixing energy emerging from this configuration (Fig. 1.1).

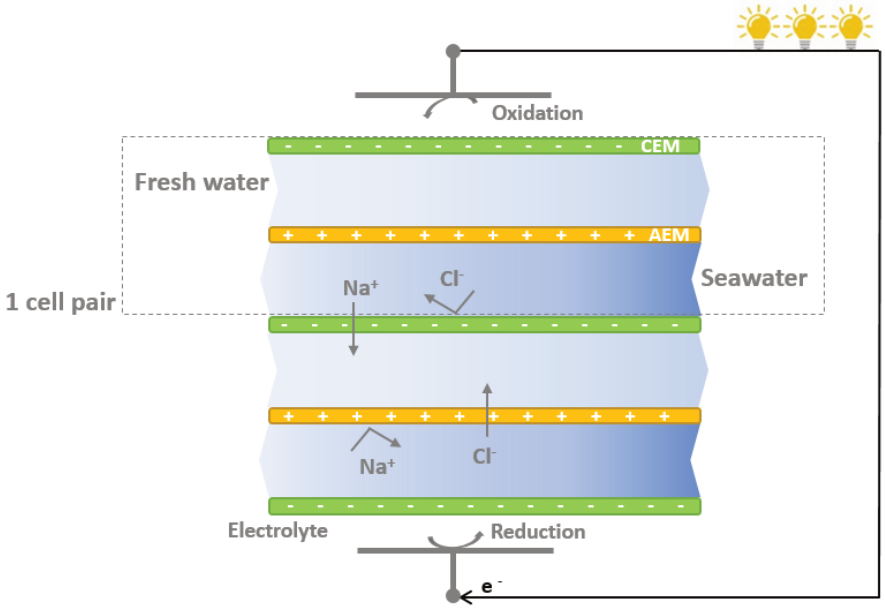


**Figure 1.1** Scheme representing the reverse electrodialysis principle.

Blue energy has the advantage of being an energy production technology with low dependence on weather conditions. It is to be noted that the process is affected by temperature and salinity gradient, which changes with the seasons and precipitation. However, the impact is to a lower extent than wind and solar energy sources [11]. Wind and solar are known to be able to significatively generate energy under limited weather conditions and for their variability in the available power due to the day-night cycle and seasons. Blue Energy offers the possibility of a continuous operation, since the salinity gradient is always present and the impact of rainfall and other weather and seasonal variations is of less relevance [12]. In addition, Blue Energy can be considered a sustainable energy source due to the use of only sea and fresh water, or other waste solutions from industrial processes. The main by-product of the process is brackish water, and in the case that the location of the power plant is in river deltas, the mixing of sea and fresh water would already occur naturally.

### 1.2 Characterization of Reverse electrodialysis

The theoretical energy that can be harvested from the mixing of two solutions with different concentrations is given by the Gibbs energy of mixing (J):

$$\Delta G_{mix} = G_b - (G_{sw} + G_{fw}) \quad \text{(Eq. 1.1.)}$$

where $G_b$ is the Gibbs free energy (J) of the brackish solution after the mixing of the previous two solutions, $G_{sw}$ is the Gibbs free energy of the concentrated solution, in this case seawater, and $G_{fw}$ is the Gibbs free energy of low concentration solution, which in this case is fresh water from a lake.

The alternating high and low salinity compartments result in a difference of potential over each membrane, and the sum of all the voltages differences of each pair of compartments that are stacked between an anode and cathode gives the voltage of the cell [10,13]. Due to the potential, ions move from the high salinity compartment to the low salinity compartment by selectively permeating through cation and anion exchange membranes [10]. By redox reactions on the electrode compartments an electrical current occurs and, by closing the circuit, electrical power can be harvested by an external load [10,14,15].

By measuring the stack voltage, V (V) and current, I (A), the gross power ($P_{gross}$, W) that can be generated by a stack is defined as:

$$P_{gross} = V \cdot I \quad \text{(Eq. 1.2)}$$

The pumping losses related to the stack operation are calculated as the energy needed to pump both sea and fresh water, $P_{pump}$ (W) to the stack, as:

$$P_{pump} = \phi_{fw} \Delta P_{fw} + \phi_{sw} \Delta P_{sw} \quad \text{(Eq. 1.3)}$$

With ΔP (Pa) being the difference of pressure drop between inlet and outlet of the stack for each feed water compartment and $\phi$ ($m^3/s$) is the flow rate of the feed water being pumped.

The net power density ($P_{net}$, W) is obtained by subtracting the power consumed for pumping the feed water from the gross power, as:

$$P_{net} = P_{gross} - P_{pump} \quad \text{(Eq. 1.4)}$$

### 1.3 Technological challenge

One of the challenges for RED to be a feasible energy source is the limitation in net energy output due to fouling. Fouling occurs due to interaction of the membrane and compounds found in the feed waters, known as foulants, that may cause deterioration of the membrane properties and reduce the efficacy of the process [16]. As all membrane processes, RED is susceptible to fouling when using natural water sources, which comprises a large range of possible foulants. RED makes use of two different water sources (low and high salinity) and in this thesis, the low salinity solution is fresh water from the IJsselmeer (the Netherlands), and the high salinity water source is seawater from the Wadden Sea (the Netherlands). RED uses two types of membranes, anion exchange membrane (AEM) and cation exchange membranes (CEM), with opposite charge on the membrane surface, which can have a great influence on how foulants will interact with the membrane. This means that there are four possible fouling interactions in RED, which makes fouling prevention more complex than many other processes previously studied [17]. Figure 1.2 shows the possible fouling interactions in RED and other process.

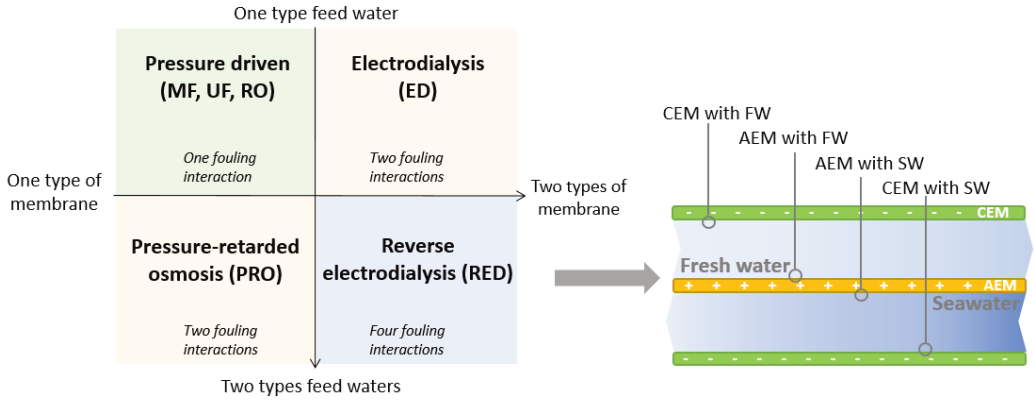


**Figure 1.2.** Possible interactions causing fouling on various membranes processes based on the characteristics of different types of membranes and feed waters, together with the specification of the four possible fouling interactions in RED. Adapted from [17].

### 1.4 Fouling definition

Fouling in RED is caused by the attraction/attachment/adsorption of substances present in the feed water source to an ion-exchange membrane or spacer, resulting in a lower performance of the process. Process deterioration occurs due to a decreased selectivity of the membrane towards the ions of interest, or to an increased resistance to exchange of ions, which impacts the gross power that can be obtained. In addition, fouling may cause an increase of pressure drop over the inlet and outlet of the feed compartments. This translates into an increase of pumping power required for the process, reducing the available net power output [11,18]. Foulants can also interact with the surface of spacers, when present, to form a fouling layer. The main categories of foulants that are relevant for this process are described below:

a. ***Particulate matter:*** Comprises inorganic and organic particles and aggregates with sizes usually in the range of micrometres (> 1 μm). The most common compounds forming this type of fouling are silt, clay, aluminium precipitates and high molecular weight organic substances and their aggregates, which can present similar behaviour to inorganic colloids [19].
b. ***Organic fouling*:** Usually refers to organic foulants that are dissolved or in the liquid phase of the feed stream, also known as natural organic matter (NOM). It is mostly originated from the decomposition of organic materials. In terms of composition, more than half of organic foulants are humic substances [20]. Proteins and carbohydrates are also present, and the main mechanism for fouling formation is by adsorption [21].
c. ***Inorganic fouling:*** accounts for deposition of inorganic salts due to precipitation on the membrane surface. Calcium, sulphate, and magnesium ions are known to lead to inorganic fouling. pH and concentration are some of the conditions that [22] affect the solubility of inorganic salts and, as a result, are directly associated with this type of fouling [16].
d. ***Microorganisms and related fouling****:* living microorganisms can adhere and grow on the membrane surface, forming a biofilm. The mechanisms responsible for this attachment are called bioadhesion and bioadsorption. Their occurrence depends on characteristics of the stream, surface and microorganisms [23]. The biofilm is an aggregate of living and dead cells, surrounded and entangled by extracellular polymeric substances (EPS) [24]. More than half of the organic matter in a biofilm comes from EPS, which are polymeric substances excreted by active microorganism. EPS is also present in aquatic systems in the form of mucus, slimes and lysis products [24,25]. Transparent exopolymer particles (TEPs) are another category of foulants produced by phytoplankton and bacteria [26]. They are acidic polysaccharides excreted by these microorganisms that are sticky and exist as

filtrable particles (0.2 μm). They are found in high concentrations in coastal areas and can be visualize by microscopy with the use of alcian blue [26].

The experiments carried in this thesis delt with natural water sources, so weather and seasonal variations are expected. Such variations can impact the RED process and fouling formation. For instance, wind and rain affect the availability of particulate matter in the feed water, due to resuspension of the particles in the waters. Similarly, warmer months and with more light result in a higher incidence of algae and living microorganisms in the feed, while the opposite is true for the colder and darker months, especially in northern Europe. In the specific case of this thesis, the water sources are located near areas with human activities as well, resulting in unexpected variations due to opening of sluices, passage of ships or dredging activities.

In this study, we focused on developing the RED technology using natural water with the least intervention as possible, so the results can be used for decision making in real conditions of operation. The operation time of the experiments are kept as long as possible for a good representation of the changing weather and seasonal conditions and to allow fouling build-up in a natural way (without high concentrations of most known foulants or supplying nutrients for bacterial growth, for example).

### 1.5 Feedwater pre-treatment for RED

Considering all types of foulants listed above, several pre-treatments of feed waters have been proposed to limit fouling. The costs and energy consumption of the pre-treatment are of crucial importance for design of RED process. Ideally, the pre-treatment process is robust, with simple operation and maintenance, sustainable and uses mainly natural resources [27,28]. It is also important that the treated water is used in the most efficient way, maximizing the energy yield per volume of treated water, making the best use of the costs associated with the pre-treatment [29].

The use of **cartridge filters** was adopted since the first pilot applications of RED, as it is an easy and efficient way to remove most of the particulate matter coming from the feed waters [30]. However, they are not feasible for use in large-scale applications, due to high costs and the necessity of disposal of the filters when they are saturated. Other membrane process, such as **ultrafiltration and nanofiltration** modules were studied to remove the particulates as well, but due to their high energy consumption, they are also not a viable alternative [11,28].

The use of a **drum filter** was also studied, both technically and economically for RED applications by Post and colleagues [31]. In their study, special attention was given to the water fluxes and head losses, and due to its capability of treating large volumes of water at a low cost per $m^3$, the drum filter was chosen for installation in the RED Pilot Plant at the Afsluitdijk, the Netherlands. However, long term experiments showed that the cut-off

screen of 40 µm was not able to avoid substantial pressure drop losses over the inlet and outlet of the stacks [32].

**Media filtration** might be a better alternative for RED pre-treatment due to its low energy consumption, easy regeneration (backwash), large-scale application and low environmental impact (i.e. no use of chemicals) [33] . The use of different media types is possible, with sand and anthracite as the most commons materials used in rapid filtration [34]. Other media recently investigated in RED were granulated activated carbon (GAC) and activated filter media (AFM), both showing good results in short term laboratory tests [28]. The combination of medias, known as dual media filter (DMF) is widely applied in other water treatment process, such as drinking water treatment, with the use of an anthracite layer with larger grains acting as a buffer for larger foulants and a second layer of fine sand to remove smaller suspended solids [35]. Due to the few studies available, more knowledge on the design and operation of the media filter for application for RED is needed. The most important factors to consider in the media filtration are the definition of the media (chemical-physical characteristics) and the flow velocity applied during the pre-treatment.

### 1.6 Cleaning techniques for RED stacks

To avoid a loss of performance when operating RED stacks for long periods, the combination of a robust pre-treatment and tailored cleaning strategies is required [27,36,37].

Most studied cleaning techniques for IEM processes had application in the food industry and rely on the use of chemical agents to restore the membrane performance, as the processes are heavily impacted by fouling [37–39]. For RED applications, it is to note that the cleaning technique needs to clean the membranes while maintaining a sustainable process by not forming toxic by-products. Therefore, chemical cleanings, using agents such as acids and bases, are not desired and different cleaning strategies are needed.

The most common techniques investigated previously that do not use chemicals are mechanical cleanings. These can comprise the use of gases in the form of bubbles to disturb/detach the fouling layer [40,41] or changing operational configuration of the stack (such as the flow, and compartment switch) that could have an effect on the fouling layer [40].

A combination of techniques can be considered to tackle different types of fouling without the use of chemical agents, maintaining the concept of sustainability and low energy requirements that are important for RED. For example, combining a mechanical strategy that can be carried out with almost no energy expenditure, with a regular frequency and a more intensive cleaning in longer periods of operation, would be the optimal approach to address the fouling issues in RED.

### 1.7 Role of RED in a renewable energy system

It is relevant to consider how RED is placed in a context of other renewable energy producing technologies, including well-established and emerging ones. The main benefit of RED, when compared to wind and solar energy, is having a more constant energy output and being relatively independent on weather conditions, since the driving force is more stable and reliable than sun and wind. Also, when comparing the available power output in the Netherlands, RED can reach between 7 to 21 PJ per year, which is similar to energy produced with wind offshore currently in the Netherlands (17 PJ), even though many uncertainties are still present for RED [42].

Dynamic Tidal Power (DTP) is another energy source that has been getting some attention in the Dutch context and has similar characteristics to RED [42]. This energy source is based on harvesting the energy from ocean currents, that occur naturally and in cycles, with the use of dams. Blue Energy and DTP share some features, as using the energy present in seawater and being more stable and predictive energy output than the current applied renewable energies. Blue Energy is still more advantageous because of its higher technical readiness level, lower impact on the ecology as well higher synergy with other technologies [42].

Among all renewable energies, hydropower is the source with the highest energy density considering the required land, with solar being the second [43]. Both are highly variable and dependant on location characteristics, for example topography for hydro and sun incidence for solar.

A simple comparison between RED and hydropower in terms of energy density can be done for the use of the potential of the Paraná River in Brazil. There, one of the biggest hydropower plants in the world is installed, named Itaipu. Due to the regularization of the flow of the river caused by the construction of the dam, flows of 8,000 $m^3/s$ is achieved more than 90% of the time [44]. This results in a production of more than 10,000 MW per year, achieving an energy efficiency of 1.25 $MW/m^3/s$. In the same river, the potential energy efficiency estimated for RED, already accounting for stratification and other losses, is of 1.5 $MW/m^3/s$ [45]. It is to be noted that the environmental impact caused by such a large plant for RED is impossible to be estimated at the moment. However, RED would potentially cause less environmental impact than Itaipu hydropower plant, as it would preserve the flooded area that was required for the construction of the dam (>1,350 $Km^2$).

On the prospects for 2050 from IEA, hydro and solar energies sources, together with wind are going to take over the lead of energy production worldwide and overcome oil and coal [46]. This scenario, with a strong share of renewables in the energy matrix, shows that RED has the potential to become an important key stone for a stable renewable energy supply

since it can stabilize electricity production in a system based on wind and solar and potentially cause less environmental impact than hydropower [47].

The estimates of the potential energy that can be harvested with RED varied in many previous studies, from 3 % to 74% of global electricity demand [45]. However, even considering the lower estimation, the prospections for RED are still highly promising. It represents a relatively clean energy source, which may be readily implemented due the potential transfer of knowledge and personnel from Oil and Gas industry. In addition, the increased demand in coastal areas aligned with the constructions of more dikes due to sea level rise also support the further development and use of Blue Energy [48,49].

The main disadvantage of Blue energy remains the price per Kwh produced, when compared with wind offshore for example [42]. That is mainly due to the high prices of the ion exchange membranes. These high costs can be mitigated in the future, by increasing the demand for these membranes. Additionally, other electrochemical process that use ion-exchange membranes can also contribute to lower membrane prices. Other crucial aspects were evaluated, such as ecological impact, synergy and potential available (in the Netherlands) and RED still competes well with offshore wind. For estimation of the cost of the technologies by 2050, RED reaches similar levels, even though this technology still faces many uncertainties.

### 1.8 Aim of the research

The aim of this research is to understand how the different classes of foulants, often present in the natural water sources used to feed RED stacks, can interact and affect the process of harvesting energy from mixing fresh and sea water. Gaining knowledge on the behaviour of foulants in RED stacks allowed us proposing enhanced strategies for fouling control (i.e., pre-treatment and cleaning procedures) and incorporating them in the process design. This research was performed with natural water under real live conditions over longer periods of time, making it a one of kind study.

### 1.9 Outline of this thesis

This thesis is divided into two main sections. The first one (chapters 2 and 3) evaluates the impact of different foulants in RED, found in both fresh and sea water sources, and how different types of pre-treatments influence the fouling layers formed on the IEMs surface. In the second section, (chapters 4, 5 and 6), the process design parameters for RED are studied in more detail. It covers the assessment on the effect of new configurations for pre-treatment, cleaning strategies, and staging of stacks.

**Chapter 2** investigates how foulants in the freshwater feed source are affected by two different types of pre-treatments, namely dual media filtration and microfiltration. This chapter focuses on how these foulants impact on the RED process performance.

In **Chapter 3**, a similar approach as in Chapter 2 was applied to investigate specifically the impact of the fouling from seawater feed on RED process. It also includes strategies on reversing the fouling after long-term operation with a series of simple cleaning procedures.

**Chapter 4** studies how different configurations of media and flow velocity affect the pre-treatment with dual media filtration for RED process. Profiled membranes are used for the first time in combination with a dual media filter.

**Chapter 5** describes an advantageous staging configuration for RED, tested with natural waters for the first time. The investigations zoomed-in on how staging of stacks affects the formation of fouling layer, and again simple cleaning procedures are tested for their efficiency.

In **Chapter 6**, simple cleaning procedures are tested and compared for their feasibility and efficiency on long-term operation in RED. Special attention is given to how the different cleaning strategies affect the main categories of foulants present in the fouling layer.

Finally, in **Chapter 7**, an outlook of how this thesis contributes to expanding the knowledge for process design of RED is given.

**References**

[1] International Energy Agency (IEA), Global Energy Review: CO2 Emissions in 2021, IEA, Paris, 2022.
[2] European Environment Agency (EEA), Energy and climate change, 2017.
[3] United Nations (UN), The Sustainable Development Goals Report, UN, New York, 2022.
[4] Eurostat, Renewable Energy statistics, 2023.
[5] European Comission, The European Green Deal. COM 640 final, Brussels, 2019.
[6] International Energy Agency (IEA), Renewable Energy Market Update: Outlook for 2022 and 2023, IEA, 2022.
[7] Jonas Pagh Jensen, Evaluating the environmental impacts of recycling wind turbines, Wind Energy 22 (2019) 316–326.
[8] Y. Xu, J. Li, Q. Tan, A.L. Peters, C. Yang, Global status of recycling waste solar panels: A review, Waste management (New York, N.Y.) 75 (2018) 450–458.
[9] M.S. Chowdhury, K.S. Rahman, T. Chowdhury, N. Nuthammachot, K. Techato, M. Akhtaruzzaman, S.K. Tiong, K. Sopian, N. Amin, An overview of solar photovoltaic panels' end-of-life material recycling, Energy Strategy Reviews 27 (2020) 100431.
[10] J.W. Post, Blue energy: Electricity production from salinity gradients by reverse electrodialysis. Wageningen, Univ., Diss., 2009, 2009.
[11] S. Chae, H. Kim, J. Gi Hong, J. Jang, M. Higa, M. Pishnamazi, J.-Y. Choi, R. Chandula Walgama, C. Bae, I.S. Kim, J.-S. Park, Clean power generation from salinity gradient using reverse electrodialysis technologies: Recent advances, bottlenecks, and future direction, Chemical Engineering Journal 452 (2023) 139482.
[12] E.H. Hossen, Z.E. Gobetz, R.S. Kingsbury, F. Liu, H.C. Palko, L.L. Dubbs, O. Coronell, D.F. Call, Temporal variation of power production via reverse electrodialysis using coastal North Carolina waters and its correlation to temperature and conductivity, Desalination 491 (2020) 114562.
[13] A. H. Galama, J. W. Post, H. V. M. Hamelers, V. V. Nikonenko, P. M. Biesheuvel, On the Origin of the Membrane Potential Arising Across Densely Charged Ion Exchange Membranes: How Well Does the Teorell-Meyer-Sievers Theory Work?, Journal of Membrane Science & Research 2 (2016) 128–140.
[14] J. Veerman, M. Saakes, S.J. Metz, G.J. Harmsen, Reverse electrodialysis: evaluation of suitable electrode systems, J Appl Electrochem 40 (2010) 1461–1474.
[15] D. Pintossi, Fouling in Reverse Electrodialysis - Monitoring, Modeling, and Control (2021).
[16] K. Solonchenko, A. Kirichenko, K. Kirichenko, Stability of Ion Exchange Membranes in Electrodialysis, Membranes 13 (2023) 52.
[17] B. Vital, E.V. Torres, T. Sleutels, M.C. Gagliano, M. Saakes, H.V. Hamelers, Fouling fractionation in reverse electrodialysis with natural feed waters demonstrates dual media rapid filtration as an effective pre-treatment for fresh water, Desalination 518 (2021) 115277.
[18] S. Pawlowski, R.M. Huertas, C.F. Galinha, J.G. Crespo, S. Velizarov, On operation of reverse electrodialysis (RED) and membrane capacitive deionisation (MCDI) with natural saline streams: A critical review, Desalination 476 (2020) 114183.
[19] S. G. Yiantsios, A. J. Karabelas, The effect of colloid stability on membrane fouling, Desalination 118 (1998) 143–152.

[20] Wei Yuan, Andrew L. Zydney, Humic acid fouling during microfiltration, Journal of Membrane Science 157 (1999) 1–12.
[21] W. Guo, H.-H. Ngo, J. Li, A mini-review on membrane fouling, Bioresource technology 122 (2012) 27–34.
[22] D. E. Potts, R. C. Ahlert, S. S. Wang, A critical review of fouling of reverse osmosis membranes, Desalination 36 (1981) 235–264.
[23] H. Ivnitsky, I. Katz, D. Minz, E. Shimoni, Y. Chen, J. Tarchitzky, R. Semiat, C.G. Dosoretz, Characterization of membrane biofouling in nanofiltration processes of wastewater treatment, Desalination 185 (2005) 255–268.
[24] G.-P. Sheng, H.-Q. Yu, X.-Y. Li, Extracellular polymeric substances (EPS) of microbial aggregates in biological wastewater treatment systems: a review, Biotechnology advances 28 (2010) 882–894.
[25] R.S. Wotton, EPS (Extracellular Polymeric Substances), silk, and chitin: vitally important exudates in aquatic ecosystems, Journal of the North American Benthological Society 30 (2011) 762–769.
[26] U. Passow, Transparent exopolymer particles (TEP) in aquatic environments, Progress in Oceanography 55 (2002) 287–333.
[27] A. Nazif, H. Karkhanechi, E. Saljoughi, S.M. Mousavi, H. Matsuyama, Recent progress in membrane development, affecting parameters, and applications of reverse electrodialysis: A review, Journal of Water Process Engineering 47 (2022) 102706.
[28] J. Ju, Y. Choi, S. Lee, C.-G. Park, T. Hwang, N. Jung, Comparison of Pretreatment Methods for Salinity Gradient Power Generation Using Reverse Electrodialysis (RED) Systems, Membranes 12 (2022).
[29] H. Kim, S. Yang, J. Choi, J.-O. Kim, N. Jeong, Optimization of the number of cell pairs to design efficient reverse electrodialysis stack, Desalination 497 (2021) 114676.
[30] M. Tedesco, C. Scalici, D. Vaccari, A. Cipollina, A. Tamburini, G. Micale, Performance of the first reverse electrodialysis pilot plant for power production from saline waters and concentrated brines, Journal of Membrane Science 500 (2016) 33–45.
[31] J.W. Post, C.H. Goeting, J. Valk, S. Goinga, J. Veerman, H.V.M. Hamelers, P.J.F.M. Hack, Towards implementation of reverse electrodialysis for power generation from salinity gradients, Desalination and Water Treatment 16 (2010) 182–193.
[32] D.A. Vermaas, D. Kunteng, M. Saakes, K. Nijmeijer, Fouling in reverse electrodialysis under natural conditions, Water research 47 (2013) 1289–1298.
[33] B. Vital, T. Sleutels, M.C. Gagliano, H.V. Hamelers, Reversible fouling by particulate matter from natural seawater reduces RED performance while limiting biofouling, Desalination 548 (2023) 116262.
[34] M. Vanoppen, T. van Vooren, L. Gutierrez, M. Roman, L.J.-P. Croué, K. Verbeken, J. Philips, A. Verliefde, Secondary treated domestic wastewater in reverse electrodialysis: What is the best pre-treatment?, Separation and Purification Technology 218 (2019) 25–42.
[35] Environmental Protection Agency Ireland, Water treatment manuals: Filtration, 1995.
[36] S. Mikhaylin, L. Bazinet, Fouling on ion-exchange membranes: Classification, characterization and strategies of prevention and control, Advances in colloid and interface science 229 (2016) 34–56.

[37] I. Merino-Garcia, S. Velizarov, New insights into the definition of membrane cleaning strategies to diminish the fouling impact in ion exchange membrane separation processes, Separation and Purification Technology 277 (2021) 119445.
[38] N. Pismenskaya, M. Bdiri, V. Sarapulova, A. Kozmai, J. Fouilloux, L. Baklouti, C. Larchet, E. Renard, L. Dammak, A Review on Ion-Exchange Membranes Fouling during Electrodialysis Process in Food Industry, Part 2: Influence on Transport Properties and Electrochemical Characteristics, Cleaning and Its Consequences, Membranes 11 (2021).
[39] K. Chon, N. Jeong, H. Rho, J.-Y. Nam, E. Jwa, J. Cho, Fouling characteristics of dissolved organic matter in fresh water and seawater compartments of reverse electrodialysis under natural water conditions, Desalination 496 (2020) 114478.
[40] D.A. Vermaas, D. Kunteng, J. Veerman, M. Saakes, K. Nijmeijer, Periodic feedwater reversal and air sparging as antifouling strategies in reverse electrodialysis, Environmental science & technology 48 (2014) 3065–3073.
[41] J. Moreno, N. de Hart, M. Saakes, K. Nijmeijer, CO2 saturated water as two-phase flow for fouling control in reverse electrodialysis, Water research 125 (2017) 23–31.
[42] TNO-Nederlandse Organisatie voor Toegepast Natuurwetenschappelijk Onderzoek, Stroom uit water: Onderzoek potentieel elektriciteitsopwekking uit water ten behoeve van de Verkenning Elektriciteit uit Water, TNO, 2021.
[43] J.K. Nøland, J. Auxepaules, A. Rousset, B. Perney, G. Falletti, Spatial energy density of large-scale electricity generation from power sources worldwide, Scientific reports 12 (2022) 21280.
[44] Itaipu Binacional, Principais características técnicas, 2022, https://www.itaipu.gov.br/sites/default/files, accessed 28 March 2023.
[45] O.A. Alvarez-Silva, A.F. Osorio, C. Winter, Practical global salinity gradient energy potential, Renewable and Sustainable Energy Reviews 60 (2016) 1387–1395.
[46] IEA, International Energy Agency, Net Zero by 2050 - A Roadmap for the Global Energy Sector.
[47] K.E. Mueller, J.T. Thomas, J.X. Johnson, J.F. DeCarolis, D.F. Call, Life cycle assessment of salinity gradient energy recovery using reverse electrodialysis, Journal of Industrial Ecology 25 (2021) 1194–1206.
[48] J.H. Nienhuis, J.R. Cox, J. O'Dell, D.A. Edmonds, P. Scussolini, A global open-source database of flood-protection levees on river deltas (openDELvE), Nat. Hazards Earth Syst. Sci. 22 (2022) 4087–4101.
[49] M.Z.A. Khan, H.A. Khan, M. Aziz, Harvesting Energy from Ocean: Technologies and Perspectives, Energies 15 (2022) 3456.

# Chapter 2

# Fouling fractionation in reverse electrodialysis with natural fresh water

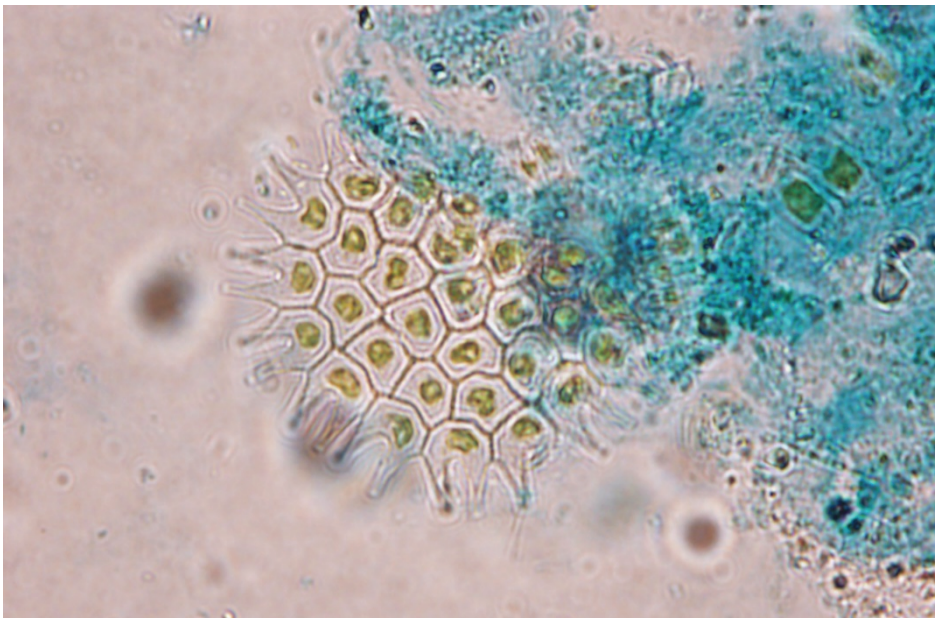

**Abstract:**

Reverse electrodialysis (RED) is a process to harvest renewable energy from the salinity gradient obtained by the controlled mixing of fresh and seawater. When using natural waters, (bio)fouling is an inevitable process which has a negative impact on the obtained power density. Specific characteristics of RED do not allow the direct transfer of knowledge from previous fouling studies in other membranes process. More insight on how fouling is impacting RED is needed to design effective pre-treatment solutions. In this study, fresh water was fractionated based on particle size for 54 days, revealing the impact that specific foulants have on the RED process. A combination of turbidity and particle size measurements coupled with stack performance throughout the experiment showed that particles with an average diameter of 10 µm are responsible for a reduction in obtained stack power density of around 25%. Visualization of extracellular microbial polymers by confocal laser scanning microscopy confirmed that the role of biofouling only was of lesser concern compared to the impact of these suspended particles. According to these results, the removal of suspended particles >10 µm using a dual media filter has shown to be a simple and effective pre-treatment for fresh water in RED applications.

This chapter has been published as:

B. Vital, E.V. Torres, T. Sleutels, M.C. Gagliano, M. Saakes, H.V. Hamelers. Fouling fractionation in reverse electrodialysis with natural feed waters demonstrates dual media rapid filtration as an effective pre-treatment for fresh water, *Desalination,* 518 (2021) 115277.

## 2.1 Introduction

In the last decades, Salinity Gradient Energy (SGE) – also called Blue Energy – has been receiving substantial attention as an alternative renewable energy source. Reverse electrodialysis (RED) is a technology that can harvest the potential of SGE in river estuaries and turn it into electrical energy [1]. In RED a fresh and a saltwater stream are separated by ion-exchange membranes, and the concentration difference between the two water streams results in an electrochemical potential difference over the membranes[1–4]. This potential difference can be harvested when the ions selectively move through ion-exchange membranes, i.e., anions through anion exchange membrane (AEM) and cations through cation exchange membranes (CEM). The ionic current can be converted into an electrical current via redox reactions, and harvested if an external load is connected [1,5].

Since 1954, RED has been studied with model synthetic solutions with promising results [6,7]. However, there is a lack of studies focussing on fouling issues when using natural waters in RED systems [3,4]. Membrane fouling is a phenomenon resulting from the joint action of foulants depositing on the membrane surface [8,9], lowering the power generation [4,5]. Natural waters contain a variety of compounds that can cause fouling, namely fine particles, colloids, microorganisms and (in)organic compounds [4,8]. One of the main effects of fouling is an increase of pressure drop over a stack's feed compartment, resulting in a higher energy consumption to pump the feed waters through the stacks. This increased energy consumption leads to a reduction of the overall net power density produced by the RED process [2,5,10,11]. Fouling can also include the clogging of the inlets' feed compartments, which affects flow distribution inside the stack and can reduce the obtained power density [10]. Finally, fouling of the ion-exchange membranes can hinder ion transport and thereby increases the internal resistance of the stack, reducing the power density that can be harvested [2].

Substantial knowledge about fouling is available for pressure driven membranes processes like e.g. ultrafiltration or reverse osmosis [12]. As RED is not a pressure driven process, the mass transport phenomena are different and different fouling processes and effects can be expected. Electrodialysis (ED) is a process that shares more similar characteristics with RED and its fouling has been studied in more detail; however there are still substantial differences in configuration between the two processes, such as larger intermembrane distance, opposite current direction and higher current densities for ED [13,14]. These differences do not allow for a direct transfer of fouling knowledge from ED to RED applications. Furthermore, in RED two types of ion exchange membranes are in contact with the two different water streams, resulting in four different combinations of natural water and ion exchange membranes and therefore four different types of fouling interactions need to be understood. Figure 2.1 outlines the possible fouling interactions of membranes process including RED and highlights the complexity for describing and

understanding the fouling in RED and the need to distinguish the different fouling interactions.

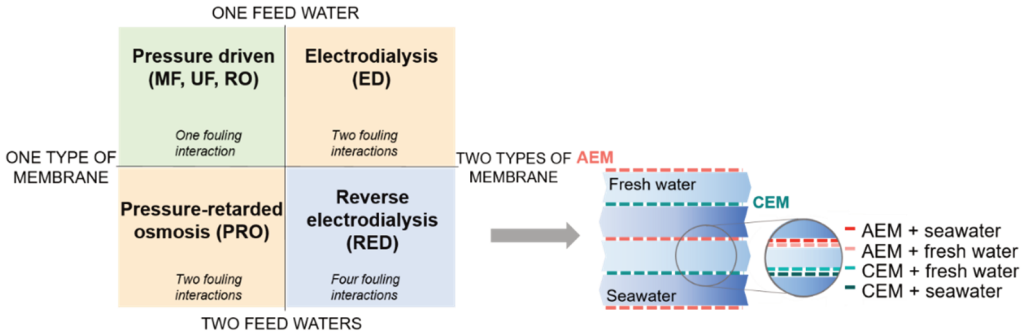


**Figure 2.1.** Possible fouling interactions on various membranes process based on the different types of membranes and feed waters, and specification of possible fouling interactions on RED.

Overall RED performance is usually characterized using two types of measurements: pressure drop over inlet and outlet of each water compartment and electrochemical measurements derived from stack voltage and current. The first measurement gives an indication of fouling from each specific water stream, as it is measured for every compartment separately. The second measurement only gives an overall indication of the electrical performance as it can only be measured for the full stack and therefore does not allow separating the source of the fouling. For a full evaluation of the four possible interactions of fouling, a membrane autopsy is needed.

Fouling in RED applications using natural waters depends on intricate physical and chemical interactions between diverse compounds in the waters and the chemical groups on membrane and spacer surfaces [8,9]. Previous studies have shown that the possible four interactions can result in distinctive types of fouling. For example, the combination of seawater and CEM can possibly lead to scaling, due to higher concentration of multivalent ions in the seawater compartments that can precipitate on the membrane surface [2]. The combination of fresh water and AEM is known for the incidence of organic and colloidal fouling, since these compounds are present in relevant concentrations in fresh water and are mostly negatively charged [2,9,15]. Clay particles are also negatively charged and thus more prone to cause fouling in AEMs than in CEMs [2,3]. The four possible interactions in RED should be studied separately to propose adequate measures for fouling control.

Feed water composition is a key factor determining fouling and therefore impacting the power output of the RED process [16]. Previous studies on water composition and fouling with synthetic solutions showed to which extend certain foulants would impact RED performance, mostly investigating the effect of multivalent ions and model organic compounds, such as humic acids (HA) and sodium dodecyl benzene sulfonate (SDBS) [17,18]. These compounds caused fouling and uphill transport of ions, increasing

membrane resistance and significantly impacting the obtained power density [4,17,18]. In the work of Post et al. [19], the effect of biofouling and mitigation measures to prevent biofouling were studied. They used sodium chloride and nutrient rich solutions inoculated with natural waters as feed and results showed a steep increase of pressure drop, resulting in a loss of performance, even after applying measures to mitigate biofouling. Unfortunately, these findings can hardly be translated into the real world, as natural waters entering the RED stacks are a mixture of potential foulants (ranging from soluble compounds to particulate matter) that can interact in unpredictable ways. The main foulants usually found in surface waters (both fresh and sea) are the following [8]:

- Particulate matter: inorganic or organic suspended particles and aggregates usually in the size range of micrometres that can block membrane surface. The most common found in surface water are silt, clay, precipitated iron and aluminium oxides and silicates, organics aggregates and cellular debris. Suspended particulate matter size in fresh water bodies usually varies between 1-100μm, with peak concentrations around 30 μm [20,21].
- Organic: dissolved components and colloids, such as humic and fulvic acids, or extracellular polymers produced by algae or microorganisms, that can attach to the membrane surface by sorption interactions. Colloids are usually classified in the size range below 1 μm until 0.001 μm, and dissolved organic matter with molecular weight (MW) of 300-100,000 Da. These compounds originate of residues from decomposition of animal and plants and form a complex heterogeneous mixture. Humic substances usually account for more than 50% of this fraction in surface water, while proteins, amino acids and carbohydrates vary from 20-40%.
- Inorganic: mostly insoluble compounds, such as calcium carbonate ($CaCO_3$), calcium phosphate ($Ca_3(PO)_4$) and silica ($SiO_2$) or as well cations $Mg^{2+}$, $Ca^{2+}$ that can precipitate on the membrane surface, usually due to pH change or by concentrations exceeding their solubility.

- Micro-organisms and EPS (extracellular polymeric substances): mainly algae and microorganisms that can adhere to membranes and grow on top of these in the form of a biofilm. Biofilm is an aggregate of living and dead cells, embedded in EPS, which are polymeric substances excreted by active microorganism or present in aquatic systems in the form of mucus, slimes and lysis products [22]. EPS is rich in polysaccharides and proteins, forming the larger fraction of biofilms (50-80% of organic matter). In membrane processes, EPS from water can accumulate causing fouling phenomena, because of their ability to bind water, molecules and ions and thus alter the membrane functions.

Based on the above-mentioned classes of foulants found in natural waters, the goal of this work was to fractionate these and associate each fraction with variations in the

performance of the RED process. For this purpose, a pilot-scale dual media rapid filter was used as pre-treatment for the influent natural water and then further fractionated with a micro cartridge filter. A dual media filter is considered environmental friendly and low energy-intensive, which are key characteristics for a pre-treatment on a RED system [23,24]. Analytical techniques were used to determine feed water quality and study the fractionated foulants. Foulants on the membrane surface were studied using microscopic techniques in membrane autopsies after the experiment was finished. The impact of the specific foulants was linked to the RED stack performance. This combination of performance measurements and water and membrane analysis aims to detect and understand and to possibly predict fouling in its distinctive and interrelated dimensions.

To the best of our knowledge, this is the first study addressing foulants phenomena in a RED process via natural foulants fractionation while a pilot scale dual media rapid filter is used as pre-treatment for RED. This approach gives insights in which components, among the whole spectrum found in feed waters, are the ones that affect the performance the most and in which way. This study is a fundamental approach and provides a knowledge base for designing future effective pre-treatments methods for RED processes.

## 2.2 Materials and methods

The experiment was performed in the Afsluitdijk Pilot Plant of REDstack BV (The Netherlands). Seawater (SW) was supplied from the Wadden Sea (Breezanddijk, The Netherlands) and fresh water (FW) from the IJsselmeer (The Netherlands) and the intake points are shown in Figure S2.1.

### 2.2.1 Foulant fractionation setup

***Feed waters pre-treatment:*** Figure 2.2 displays a schematic representation of the set-up used in this study. Both fresh and seawater first went through a drum filter with a 20 µm pore size mesh, and then to a 30m³ storage tank that was refilled continuously. After, the feed water passes through a dual media rapid filter pre-treatment, ending in the setup buffer tanks. Dual media rapid filters were composed of a 50 cm layer of anthracite (1.2 – 2.0 mm Ø) on top of a 50 cm layer of sand (0.5 – 1.0 mm Ø), placed into 11 cm Ø PVC pipe. Sand and anthracite were supplied by Filcom (SCR-Sibelco N.V., Belgium). The filters were individually backwashed twice a week by flushing with compressed air and processed water, for a minimum of 10 minutes or until no colour was seen in the effluent.

After the dual media filters, the two feed waters were further treated differently. The treatment of seawater aimed to remove as many foulants as possible, so the fouling incidences on the RED stack performances can only be associated to foulants coming from fresh water.

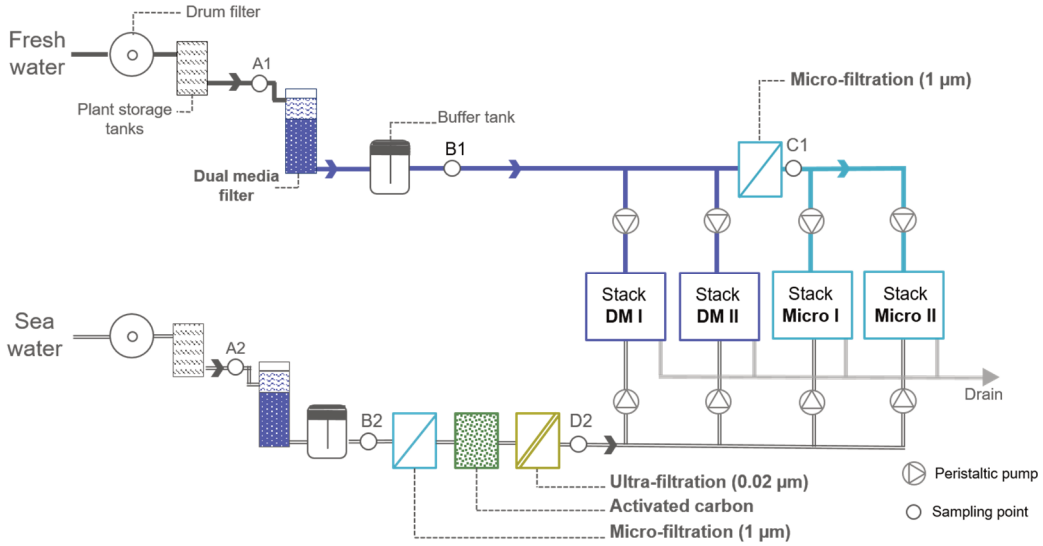


**Figure 2.2.** Schematic representation of the experimental set-up in the Afsluitdijk pilot REDStack facility at Breezanddijk in the Netherlands. Fresh water passes a dual media rapid filter (stacks DM I and II) and a micro-filtration unit (1 $\mu m$) (stack Micro I and II). Sampling points A represent the effluent of the drum filters of the pilot plant, sampling points B the effluent of the dual media filtration, point C the effluent of microfiltration and point D the effluent of ultrafiltration.

The freshwater pre-treatments aim to remove certain types of foulants in each fractionation step, so the performance of each stack can be attributed to the remaining foulants in their feed water. For this reason, stacks DM I and II (after dual media filtration - Fig. 2.2) received fresh water directly after the dual media rapid filter pre-treatment, while Stacks Micro I and II received fresh water after a step of micro-filtration with cut-off pore size of 1 µm (gradient cartridge filter DGD.2501.20, Pentair, The Netherlands). For seawater, the stream feeding all the stacks was pre-treated with the same micro-filtration cartridge, a granular activated carbon filter (GAC-10", Pentair, The Netherlands) and finally an ultra-filtration module of 0.02 µm pore size (R-21 module, Pentair, The Netherlands). All stacks received their feed waters after their pre-treatment by using adjustable peristaltic pumps (Cole-Parmer, Masterflex L/S Digital drive, USA).

Feed waters were characterized at six different sampling points every 3 days (detailed in section 2.2.2.). Three sampling points were established for each water stream (Fig. 2.2), where points A represent the feed waters in the beginning of the process, points B represent the waters treated after the dual media filter, point C represents the fresh water after microfiltration, and point D2 represents seawater after full treatment (last treatment is ultrafiltration). Point D2 was used as control for seawater that actually fed the stacks, but due to its extensive treatment, the detection limit of equipment and methods used to detect physicochemical characteristics was not reached, thus results are not shown. The

experiment lasted for 54 days, and membrane autopsy was performed afterwards (detailed in section 2.2.3).

***Stack configuration:*** Four 10 cm x 10 cm REDstack X-flow stacks were built in the lab with housing supplied by REDstack BV (Sneek, Netherlands). Stacks contained 10 cell pairs of flat CEM and AEM of the Fuji BE series (non-commercial membranes, Fujifilm Manufacturing Europe B.V., Netherlands), which membrane specifications are listed in Table 2.1.

**Table 2.1.** Membrane properties of cation and anion exchange membranes of Fujifilm BE series.

| Membrane | Dry thickness [μm] | Permselectivity (0.05 – 0.5M NaCl) | Electrical resistance (0.5 M NaCl) [Ω.cm2] |
|---|---|---|---|
| CEM BE | 45 | 96 % | 1.42 |
| AEM BE | 53 | 94 % | 0.70 |

Within each stack, membranes were separated by 480 μm woven netting spacers (PES 740/53, Saati S.p.A. Italy) and integrated silicon rubber (Deukum GmbH, Germany) acting as a sealer. Stacks were operated at 0.5 cm/s flow velocity and pressure drop over the outlet and inlet of the stacks was continuously measured by a pressure difference transmitter (EJA110E, Yokogawa, Japan). The electrolyte solution was composed of 0.05 M $K_3Fe(CN)_6$, 0.05 M $K_4Fe(CN)_6$ and 0.25 M NaCl (VWR, USA) dissolved in Milli-Q water. The electrolyte compartments were shielded with an additional CEM and kept at an over pressure of 0.3 bar. At both sides of this membrane pile, titanium electrodes (mesh 1.7 $m^2/m^2$) with a galvanic platinum coating of 2.5 μm and with an active area of 10 cm x 10 cm were used as the anode and cathode (Magneto Special Anodes B.V., Netherlands). Temperature and conductivity of the feed waters after the buffer tank were measured using a sensor and recorded every 60 seconds using a data logger (GX10, Yokogawa, Japan).

***Electrochemical measurements:*** Chronopotentiometric series were applied using a potentiostat (Iviumstat, Ivium Technologies, Netherlands) connected to a peripheral differential amplifier to measure voltage and calculate the open circuit voltage, stack resistance and gross power density, using the same well established method as described in [2,9]. The chronopotentiometry series consisted of constant current density steps of 4 $A/m^2$, 5 $A/m^2$, 6 $A/m^2$ and 7 $A/m^2$ applied for 60 s each – to reach a constant voltage value – which were separated by steps of 20 s with no current when the OCV was measured. The rest of the time, the stacks were operated at constant current density of 5 $A/m^2$ to simulate a RED process.

### 2.2.2 Feed waters characterization

Feed waters were sampled at the sampling points (Fig. 2.2) and were subjected to diverse physicochemical analysis:

***Ion concentration:*** relevant anion ($Cl^-$, $Br^-$, $SO_4^{2-}$ and $NO_3^-$) and cation ($Na^+$, $Ca^{2+}$, $K^+$ and $Mg^{2+}$) concentrations were measured by ion chromatography (Metrohm Compact IC Flex 930, Schiedam, Netherlands).

***Organic carbon concentration*** was calculated by measuring total carbon (TC) and its fractions of total organic carbon (TOC) and inorganic carbon (IC) via a total organic carbon analyser (TOC-L, Shimadzu, Japan).

***Concentration of particulate matter:*** total suspended solids (TSS) and volatile suspended solids (VSS) were determined using a standard protocol [25].

***Particle size distribution:*** analysis performed using a particle size analyser DIPA-2000 (Donner Technologies, Netherlands).

***Turbidity:*** analysis performed using the turbidimeter 2100N IS (Hach, USA).

***pH and conductivity***: These parameters were monitored by using a calibrated bench top multi-parameter quantifier (Mettler Toledo, USA).

### 2.2.3 Membrane autopsy

Autopsy of the membranes was performed at the end of the experiment by opening the stacks and observation of samples was made using different microscopic approaches to visualize existing fouling. The cell pairs located in the centre of the membrane pile were sectioned in its central area for microscopic analyses (Fig. S 2.5), described next.

#### *Optical microscopy and EPS staining*

To visualize if extracellular polymeric substances (EPS) were causing biofouling, the cut sections of each membrane were placed on a clean microscopy glass slide and stained with crystal violet 0.1% solution (Crystal Violet / ammonium oxalate solution, Boom B.V., Netherlands). Crystal violet was applied to visualize the organics (protein and carbohydrates) of EPS [26]. After 30 minutes of staining, samples were washed with Milli-Q and then observed with phase contrast microscopy (Leica DM750, Leica, Switzerland) at 10, 20 and 40X magnification. Images were taken using the software LAS 4.12 (Leica, Switzerland).

***Fluorescent staining and Confocal scanning laser microscopy (CSLM)***

A further characterization of the EPS fraction of fouling layers was carried out by applying fluorescent staining of proteins and carbohydrates. Sections of the membranes were placed on a 6-well plate and first treated with calcofluor white (CW) (Sigma-Aldrich Chemie B.V., Netherlands) for visualization of β-polysaccharides, and subsequently with Sypro™ Red (Molecular Probes, Thermo Fisher Scientific, USA) for visualization of proteins. Both staining's procedures were carried out for 60 minutes in the dark and after membrane sections were washed with PBS to remove excess dye. Finally, the membrane samples were observed with Confocal Laser Scanning microscopy (CSLM) via a Zeiss LSM 880 (Zeiss, Germany). Images were acquired through the software ZEN black (ZEISS, Germany).

Before the CLSM analysis, clean membrane supports were tested for fluorescence emission with the staining. Due to the slight negative charge of the dyes used in this study, they were interacting with the clean AEM membranes (Fig. S 2.6), making impossible to apply this analysis on them.

***Scanning electron microscopy (SEM) and energy-dispersive X-ray spectroscopy (EDX)***

Sections of the membranes were placed on a 6-well plate and fixed in 2.5% glutaraldehyde overnight at 4ºC. After, they were rinsed twice with Milli-Q and dehydrated in graded ethanol solutions (30, 50, 70 and 90%) for 20 minutes each, and finally 99.6% ethanol was applied twice for 30 minutes. The samples were dried for 30 minutes at 55ºC before SEM analysis with a JEOL JSM-6480LV (JEOL, Japan) at an acceleration voltage of 6 kV and magnifications up to 30,000X. Identification and quantification of relevant chemical elements was carried out with energy dispersive X-ray detector (x-act SSD-EDX, Oxford Instruments, UK) coupled with the SEM imaging. The images were processed using JEOL SEM Control User Interface software (version 7.07).

## 2.3 Results and discussion

Fouling in the RED process using natural feed waters was studied by analysing the fractionated feed waters, looking at stack performance and membrane autopsy after the 54-day experiment.

### 2.3.1 Fractionation of feed water and their characteristics

The fractionation of fresh feed water and the sampling points are shown in Fig. 2.2. Each sample was characterized by its turbidity, Total Suspended Solids (TSS), average particles size, ion composition, and total carbon, inorganic carbon, and total organic carbon (TOC) and the results are presented in Tables 2.2 and 2.3.

**Table 2.2.** Physicochemical characteristics of fresh (1) and sea (2) feed water samples from the Afsluitdijk Pilot Plant. Sampling point A is the effluent of the drum filter and influent of the dual media filter, sampling point B is the effluent of the dual media filter and influent of microfiltration, and sampling point C is the effluent of microfiltration. * Values below detection range

| Parameter | Fresh water | | | Seawater | |
|---|---|---|---|---|---|
| | Influent dual media A1 | Effluent dual media B1 | Effluent Micro filter C1 | Influent dual media A2 | Effluent dual media B2 |
| Turbidity (NTU) | 12.2 ± 5.5 | 6.8 ± 3.6 | 2.5 ± 0.6 | 22.1 ± 13.2 | 5.0 ± 3.1 |
| TSS (mg/L) | 34.9 ± 21.3 | 14.6 ± 4.4 | * | 78.4 ± 19.3 | 31.3 ± 8.6 |
| Average particle size ($\mu m$) | 18.2 ± 4.5 | 10.4 ± 2.4 | * | 21.9 ± 5.0 | 6.4 ± 2.5 |

**Table 2.3.** Chemical characteristics of fractionation of fresh (1) and sea (2) water from the Afsluitdijk Pilot Plant. Sampling point A is the effluent of the drum filter and influent of the dual media filter, sampling point B is the effluent of the dual media filters and influent of microfiltration, and sampling point C is the effluent of microfiltration.

| Parameter (mg/L) | Fresh water | | | Seawater | |
|---|---|---|---|---|---|
| | Influent dual media A1 | Effluent dual media B1 | Effluent Micro filter C1 | Influent dual media A2 | Effluent dual media B2 |
| Sodium | 86.0 ± 8.1 | 100.8 ± 9.3 | 119.3 ± 18.9 | 6,534 ± 332 | 6,485 ± 352 |
| Calcium | 44.8 ± 3.4 | 46.3 ± 3.0 | 43.4 ± 4.9 | 271.7 ± 11.1 | 273.6 ± 14.1 |
| Magnesium | 14.2 ± 0.7 | 16.0 ± 1.1 | 22.1 ± 13.3 | 779.3 ± 38.8 | 777.3 ± 42.4 |
| Potassium | 6.4 ± 0.4 | 7.0 ± 0.4 | 14.1 ± 10.8 | 241.2 ± 32.3 | 234.5 ± 28.0 |
| Chloride | 146.5 ± 13.7 | 172.8 ± 16.5 | 187.5 ± 40.0 | 11,826 ± 604 | 11,768 ± 622 |
| Sulphate | 63.2 ± 3.4 | 67.9 ± 3.6 | 57.8 ± 8.9 | 1,695 ± 78 | 1,685 ± 85 |
| Total Carbon (TC) | 31.1 ± 0.9 | 32.1 ± 0.9 | 30.2 ± 0.8 | 38.6 ± 4.0 | 39.2 ± 6.4 |
| Inorganic carbon (IC) | 21.5 ± 3.0 | 23.5 ± 1.0 | 22.5 ± 1.0 | 27.5 ± 4.2 | 27.1 ± 4.0 |
| Total Organic Carbon (TOC) | 7.7 ± 0.6 | 7.9 ± 0.7 | 7.7 ± 0.5 | 8.4 ± 3.2 | 7.8 ± 3.7 |

Turbidity, TSS and particle size, (Table 2.2) all show a reduction of suspended solids after each fractionation step for both fresh and seawater. From the turbidity values and average

particle size, it is clear that dual media rapid filtration removes bigger particles (up to approximately 10 µm in fresh water and up to 6 µm in seawater) and microfiltration removes smaller suspended particles between 10 µm and 1 µm in diameter, as expected and based on the potential of removal of the selected filters. The dual media filter allows for a more constant number of suspended particles in the effluent when compared to the drum filter, as seen in lower standard deviation in the measurement related to the dual media filter (Table 2.2).

Over the 54 days of experiment, among the 15 samples of fresh water taken after the dual media filter, just two of them had a turbidity exceeding 10 NTU. This shows that dual media rapid filter treatment is a reliable method even considering natural variations in water turbidity. For comparison, a pressurized full-scale sand/dual media rapid filter with coagulation pre-treatment can deliver an effluent with turbidity lower than 1 NTU [23]. This shows that it is possible to achieve even better results with an automated full-scale filter in the future. Reduction in turbidity after microfiltration is also relevant, as most values are below 3 NTU, with only two samples being around 5 NTU. These turbidity values support that the suspended particles are removed in the fractionation steps.

Also, for seawater, dual media filtration shows promising results as pre-treatment, reaching an average effluent quality of 5 NTU with turbidity removal of 71%).

The two consecutive fractionation steps applied on the freshwater stream did not remove ions and organic/inorganic carbon, as shown by similar values for ions (sodium, calcium, magnesium, potassium, chloride, and sulphate) and TC, IC, and TOC (Table 2.3). Notably, both dual media and microfiltration were not able to remove the organic carbon from the influent water, which can be related to the subsequent bio- and organic fouling of the membranes.

### 2.3.2 Stack performance is mostly impacted by suspended particles

Stack performance is evaluated by pressure drop over the inlet and outlet of feed waters in the stack, internal stack resistance and gross power density obtained from the process. These measurements allow the assessment of eventual fouling and enable comparison with previous studies.

***Pressure drop***

The pressure drop between inlet and outlet of fresh water during the 54 days of experiment is presented in Figure 2.3. An increase in pressure drop was observed approximately one month after the start of the experiment. By the end of the experiment (day 54), a clear difference in pressure drop can be seen for the stacks after the dual media filter (80 mbar) when compared to the stacks after microfiltration (20 mbar) (Fig.2.3). This

shows that the microfiltration pre-treatment can lead to a lower build-up of fouling in long term operation. This comes with the expense of additional treatment procedure.

As all chemical parameters do not significantly change in the fractionation steps (Table 2.3), the differences in stack performance can relate to the fouling due to particles with average diameter of 10 µm or lower, which are passing through the dual media rapid filter. Therefore, the highest impact on performance is caused by suspended particles. This is also the case for other parameters that determine the stack performance (internal resistance and gross power density) presented in the next section. Even though the rapid filter reduces fouling significantly when compared to the 20 µm mesh drum filters, the dual media filter effluent still contains a relevant amount of foulants, which still impacts the performance in the long term.

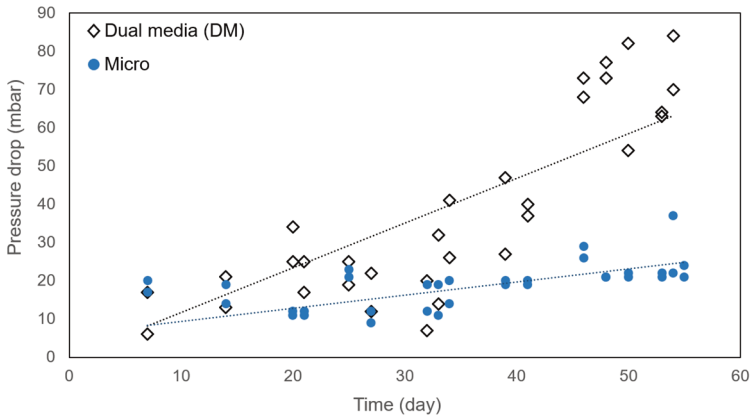


**Figure 2.3.** Pressure drop measurements for freshwater flow through stacks after dual media filtration (in black) and microfiltration (in blue). Duplicate measurements are shown as markers and the trend of the average of the two measurements are represented as lines.

The values of pressure drop in stacks DM I and II, without applying any cleaning strategy, are very low when compared to other pre-treatment methods used before. For example, Vermaas et al. 2013 reached around 1.5 bar with fresh water after 25 days of operation when using only a drum filter of 20 µm mesh as pre-treatment and stacks with intermembrane distance of 240 µm. Moreno et al. (2017), using the same pre-treatment, reported a total pressure drop increase, accounting for both fresh and sea water, of around 900 mbar and the stack had to be stopped after 45 days of operations, due to this high pressure drop. In the present study the contribution of seawater to the pressure drop is low (<10 mbar), since this stream is fully treated, resulting in a total pressure drop of 90 mbar (considering fresh and seawater streams).

***Internal stack resistance and gross power density***

The initial and final internal stack resistance and gross power density for the two fractionation steps of fresh water are presented in Figure 2.4 and the extended data over time is presented in Figure S 2.3. This stack resistance was corrected for the resistance associated with the conductivities of waters and therefore only represents the resistance of the membranes and associated fouling in the stack.

The internal resistance of all stacks in the beginning of the experiment was comparable, around 8 Ω (Fig. 2.4). By the end of the experiment, the stacks after the dual media filtration step reached an average of 10.8 Ω, an increase of about one third of the initial value. For the stacks after the microfiltration step, the average resistance was 9.3 Ω, representing an increase of around 15% of the initial value. This increase in resistance can be attributed to fouling of the spacers and membranes, as other conditions were unchanged. The increase in resistance of the stack after the microfiltration is around half of the increase of stacks receiving fresh water pre-treated with dual media filtration, and according to water samples and membrane autopsy the fouling in those stacks is mostly from organic soluble colloids and EPS. Thus, these compounds influence the performance of the stacks to a lower extent than particulate matter.

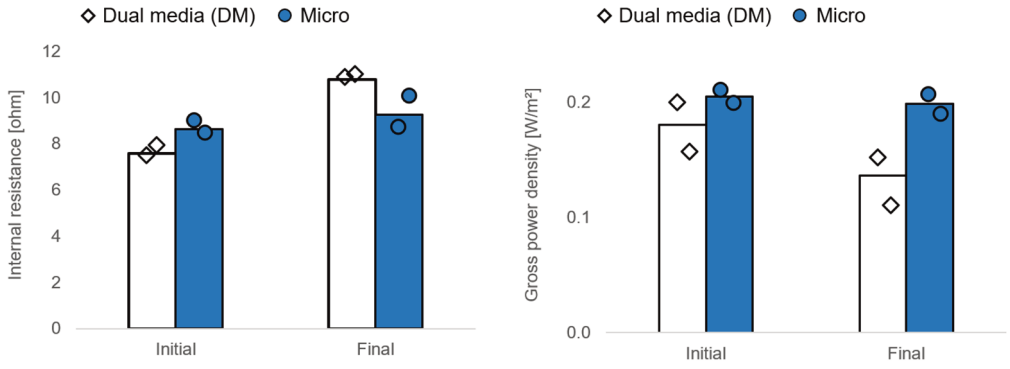


**Figure 2.4.** Internal resistance of the stacks and gross power density at the initial and final stage of the experiment after dual media and micro fractionation step. Duplicate measurements are shown as dots and the average of the two measurements is represented as bars.

The gross power density and the internal resistance are inversely related, thus an increase of internal resistance corresponds to a decrease in gross power density, [5]. In the initial stage of the experiment, the power density of the stacks fed with dual media filtered and micro filtered freshwater was comparable (0.20 – 0.21 W/m$^2$). The exception was one of the stacks after dual media filter fractionation (stack DM II), which after the first day of the experiment had a lower OCV (resulting in 0.16 W/m² after applying a load), probably due to an internal leakage. During the experiment, performance stabilized with a slightly lower value of OCV and gross power density than the other stacks (DM I, Micro I and II).

As observed in the previous sections, stacks DM I and II suffered a higher impact in performance due to fouling compared to the ones after microfiltration. This translated in a reduction of 25% of gross power density in these stacks, while only a small reduction of 3% was registered after the microfiltration step. Of course, this comes with the investment of an additional treatment.

Still, the performance of the stacks receiving the water treated with dual media filtration is promising. The increase in resistance (~35%) is lower compared to previous studies. For example, Vermaas et. al. 2013 reported an increase in resistance of 70% in 25 days when using a drum filter as pre-treatment and stacks with spacers (240 µm), while stacks with profiled membranes showed an increase of 40% in 25 days. The power density in the same study varied between 0.05 and 0.14 W/m², with the best results for stacks with profiled membranes. Moreno et. al. (2017) compared cleaning strategies for fouling removal and performance recovery and the best results were achieved with flushing $CO_2$, which reached a power density of 0.17 W/m² after 55 days of operations.

When dual media filtration is applied as pre-treatment, a similar performance (power density of 0.16 W/m²) could be achieved as with profiled membranes or cleaning with $CO_2$. This shows the robustness of this pre-treatment and the potential it has to put Blue Energy in a better competing position with other sustainable energy sources.

### 2.3.3 Membrane autopsy reveals particulate fouling after dual media filtration and biofouling after microfiltration

At the end of the experiment (day 54) membrane samples were taken from the stacks and were prepared for visual analyses, and representative pictures are shown in Figure 2.5. AEMs were covered by a brown coloured layer (Fig. 2.5 B and D), which was not observed for the CEMs (Fig. 2.5 C and E) and can be attributed to the presence of humic acids. The negative charge of humic acids favours its attachment to AEMs which are positively charged, as reported before [2,3].

Particulate fouling was observed on both membrane types on stacks DM I and II (Fig. 2.5 B and D) but not after the microfiltration step (Fig. 2.5 C and E). The same can be seen for the spacers, where more particulate fouling accumulated after dual media filtration than after microfiltration (Fig. S 2.7).

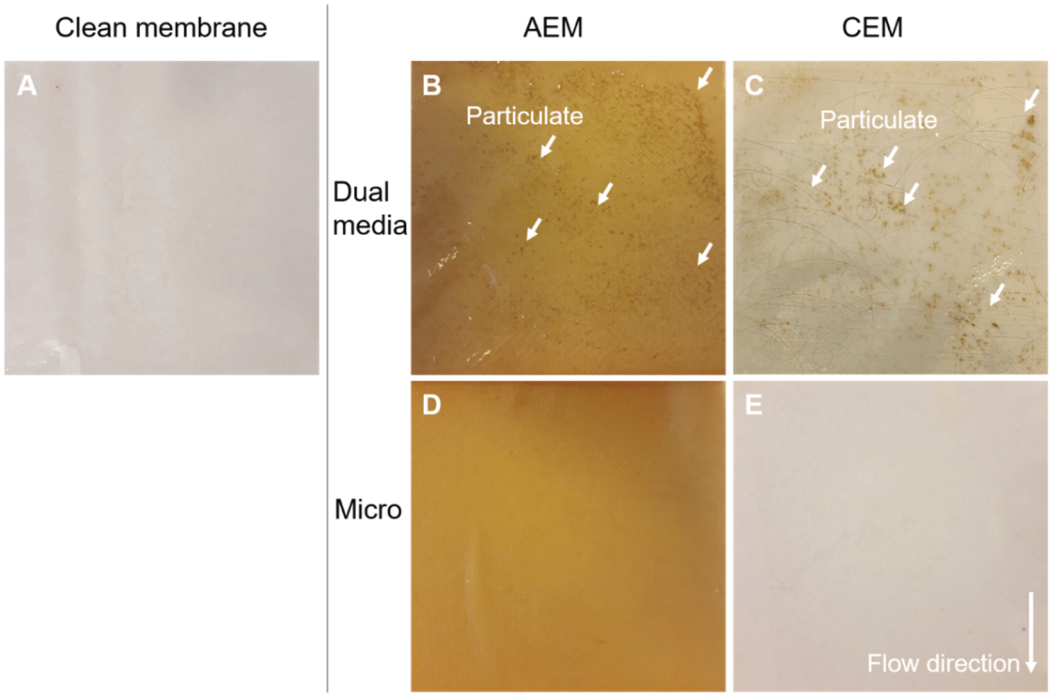


**Figure 2.5.** Visual analysis of membranes (B to E) in contact with fresh water after 54 days experiment. For comparison, a clean membrane is shown (A), with no visual distinction between a clean AEM and CEM.

To identify organic components in the fouling layers, first crystal violet was used as a fast method to stain the EPS present on the membrane (Fig. S 2.8). Floccular EPS accumulated in some spots on the AEM and CEM of stacks DM I and II (Fig. S 2.8 A and B) and Micro I and II (Fig. S 2.8 C and D). This EPS could have originated either from accumulation from the feed waters, where it can be present as excretion or mucus or from microbial secretion, after cells attachment and growth on the membranes [22]. The amount and morphology of EPS fouling looked similar for both the membranes after the two different treatments (Fig. S 2.8), as expected since organic polymers and cells were present in the feed water even after 1 µm filtration. EPS presence was further evaluated by the application of two fluorescent dyes targeting EPS main components, namely proteins (with SyproRed, in red) and polysaccharides (with CW, in blue). These dyes were applied on CEM membrane sections, and stained sections were analysed using confocal microscopy (Fig 2.6).

CLSM images of CEM membranes showed the presence of EPS after both fractionation steps although with a different structural pattern (Fig. 2.6 A to D). After the dual media filtration step, most of the EPS and cell structures detected were rich in proteins (red signal, Fig. 2.6 A and B). The most common pattern detected were coccoid cells clustered to form

aggregates near the membrane support fibres (Fig. 2.6 A and B). Majority of the detected cells were positive to SyproRed, while polysaccharides were rarely detected, and always in combination with proteins (purple signal, Fig. 2.6 B) mostly surrounding biological structures resembling nematodes and fungi (Fig. 2.6 B and S 2.9 A). On the other hand, EPS in stacks Micro I and II seems to be connected with the formation of a lattice rich in polysaccharides (Fig. 2.6 C and D, purple signal) with a linear pattern, which was not observed on the membranes of stacks DM. The presence of a polysaccharides lattice, forming a network of linear junctions, could be related to the attachment and growth of different sort of cells [27] in comparison to the ones observed in stacks DM I and II (Fig. 2.6 A and B). Since it was not possible to analyse AEM membranes via CLSM, these were analysed via SEM, and similarities could be observed with the respective CEM counterpart. Indeed, AEMs from DM stacks presented EPS/biofouling as little coccoid cells (Fig. 2.6 E), and EPS aggregates. (Fig. 2.6 F). This EPS aggregates often contained diatomic reminiscent and other particles (Fig. S 2.9 B). Interestingly, a likely polysaccharides lattice pattern was visualized also in AEM after microfiltration (Fig. 2.6 G) together with grouped cells (Fig. 2.6 H).

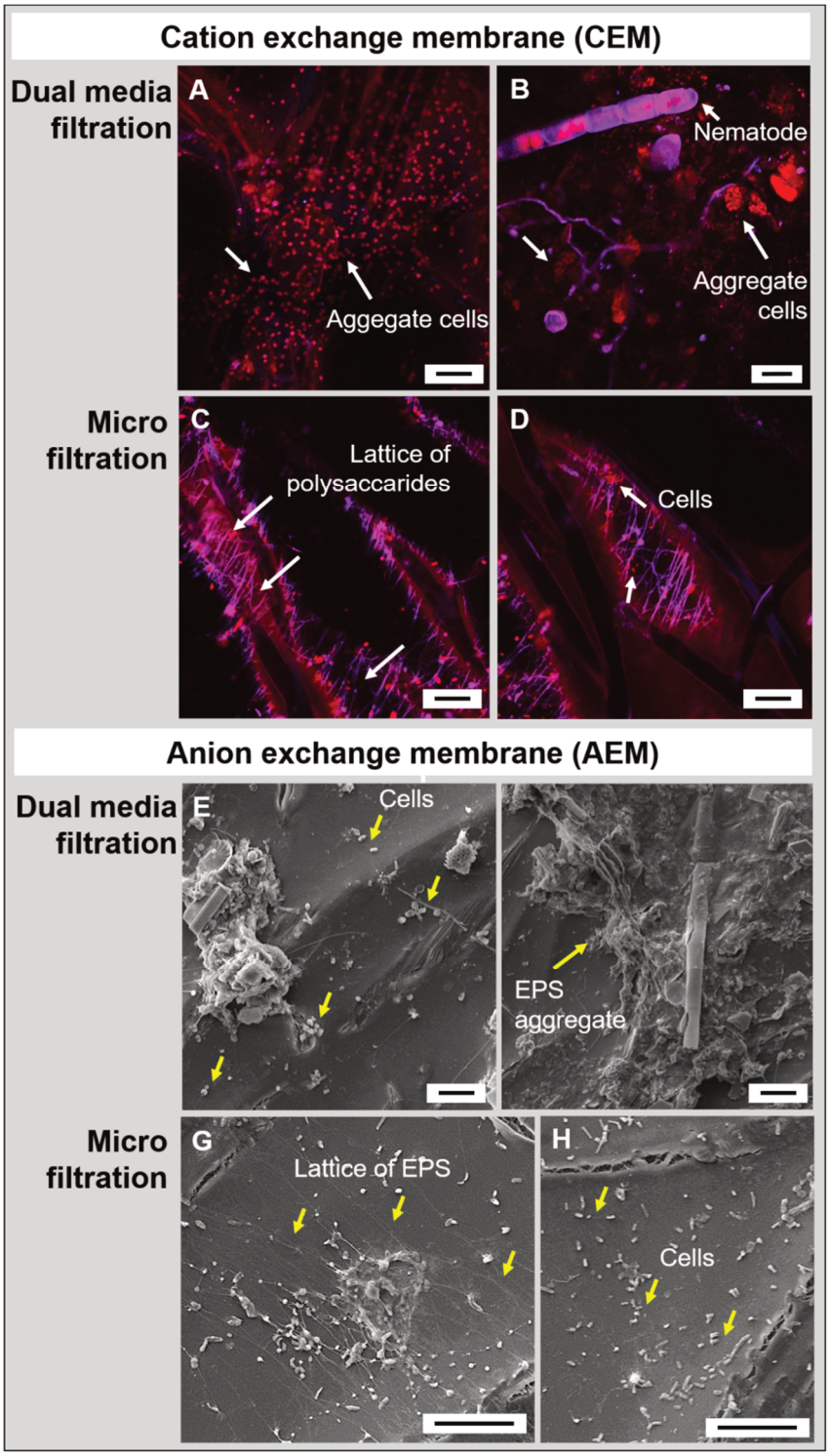
Cation exchange membrane (CEM)
Dual media filtration
A
Aggegate cells
B
Nematode
Aggregate cells
Micro filtration
C
Lattice of polysaccarides
D
Cells
Anion exchange membrane (AEM)
Dual media filtration
E
Cells
EPS aggregate
Micro filtration
G
Lattice of EPS
H
Cells

**Figure 2.6.** Microscopic images of the biofouling developed on CEM and AEM analysed via CLSM and SEM, respectively. From A to D, CLSM dataset showing the combination of SyproRed (proteins, in red), and Calcofluor White (polysaccharides, blue). Purple indicates co-localization of the two staining signals, while white arrows indicate details. Stacks DM showed aggregate cells with a proteic outer layer adhering on the CEM membranes (A, B). In stacks Micro, biofouling was visualized as a lattice rich in polysaccharides, surrounding (C) and in within the membrane fibres, together with cells (D). From E to H, SEM images of AEM after fixation and dehydration. Yellow arrows indicate details. In stacks DM, cells (E) and EPS aggregates (F) were visualized. In stacks Micro, a lattice of EPS (G) and many cells (H) were present. Scale bar is 10 µm.

Combined CLSM and SEM results thus, unlike crystal violet staining (Fig. S 2.8), highlighted a different shape of fouling after dual media and microfiltration treatments (Fig. 2.6). Different kind of cells were attaching and growing on top of CEM and AEM after the two pre-treatment steps, likely the result of a selection of certain types of microorganisms by the microfiltration step [28]. It is possible that the microorganisms that are able to pass the microfiltration step find less competition and more space to grow on the available membrane surface [29]. Another reason why we do not observe the same pattern observed in Micro stacks as in DM stacks could be related to the presence of particulate fouling (as clearly observed in Fig. 2.5) on the membrane surface. The adhesion of particles to the membrane surface form a sort of protective layer to bacterial adhesion, since it creates a less ideal surface for microbial growth [30]. Most probably the difference in EPS and biofouling is a combination of these two factors.

The water analysis presented in section 2.3.2 showed that there were no consistent differences in TOC levels in the feed waters entering the stacks and after the different fractionation steps. However, the results from the membrane autopsy and microscopic analysis showed that there were substantial differences in the structure of biofouling due to the fractionation process and therefore fractionation can have an impact on fouling characteristics, in turn affecting stack performance.

Although there is this indication of a microbial/EPS fouling on the membrane surface after the microfiltration step, process performance in terms of pressure drop, internal resistance and gross power density, indicates that the impact in the RED process is small in comparison to particulate fouling. Future studies with an even longer duration to allow more development of biofouling might unravel in detail the effective role of such foulants on RED performance.

## 2.4 Conclusions and implications

The fractionation of foulants from natural waters leads to a better understanding how each type of foulant can affect the RED process. Suspended particles with average diameter

of 10 µm are responsible for a reduction in stack performance of around 25% in gross power density after operation of 54 days without cleaning measures.

Membrane autopsy of the stacks shows the presence of a polysaccharidic lattice of EPS formed after microfiltration treatment with potential development of more complex biofouling on the membrane surface. However, their impact in performance as a foulant is of lesser concern than the suspended particles found after the dual media rapid filtration step.

More studies are needed to investigate the effect of specific foulants on RED performance, such as studying a fractionation step for removal of organics and testing fractionation of seawater, to understand if the similar dynamics apply to this type of water.

It was shown that the use of a dual media filter is a simple yet effective pre-treatment method for RED applications, considering freshwater feed, when compared to the use of a 20 µm drum filter. The possibility of backwashing this type of filter with only air and water is an ecological acceptable cleaning tool for blue energy since no aggressive chemical cleaning agents are needed. Also, the media material (sand and anthracite) are durable materials that do not need to be replaced often.

**Supporting Information**

### Feed waters

Figure S 2.1 shows the intake points of the feed waters, in the Wadden sea and IJsselmeer lake. The pilot plant is located at Breezanddijk area in the Afsluitdijk in the Netherlands.

Figure S 2.2 shows the daily average of water temperature of the two waters used in the experiment.

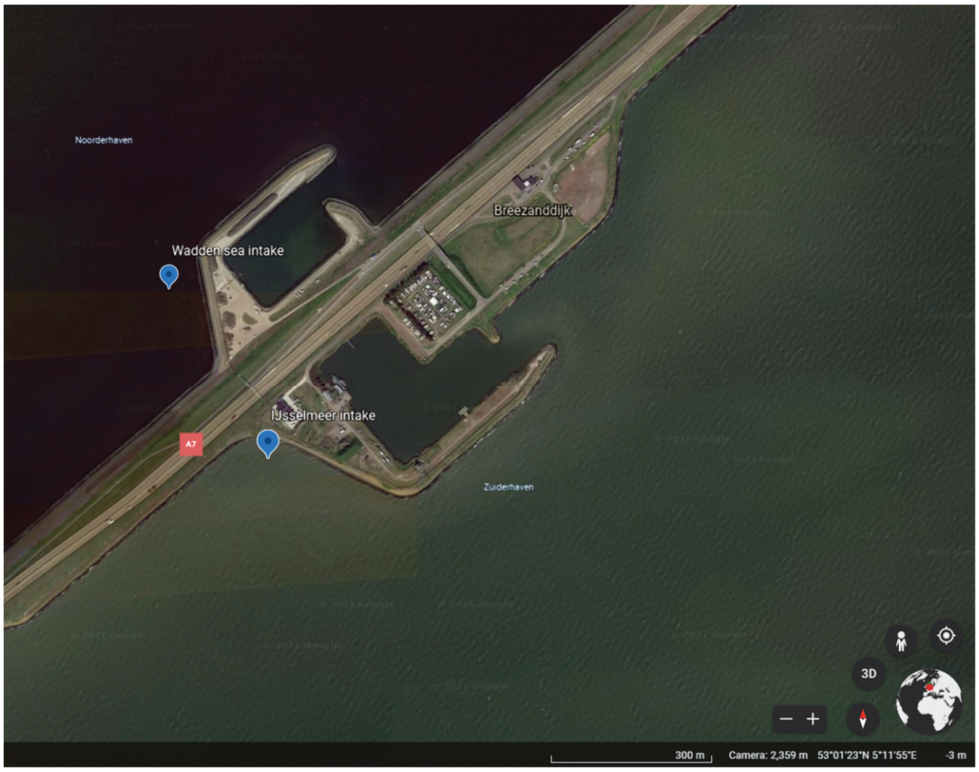


**Figure S 2.1**. Digital satellite photo of the pilot plant in the Afsluitdijk, the Netherlands. Intake points of seawater and fresh water are marked in the picture [31].

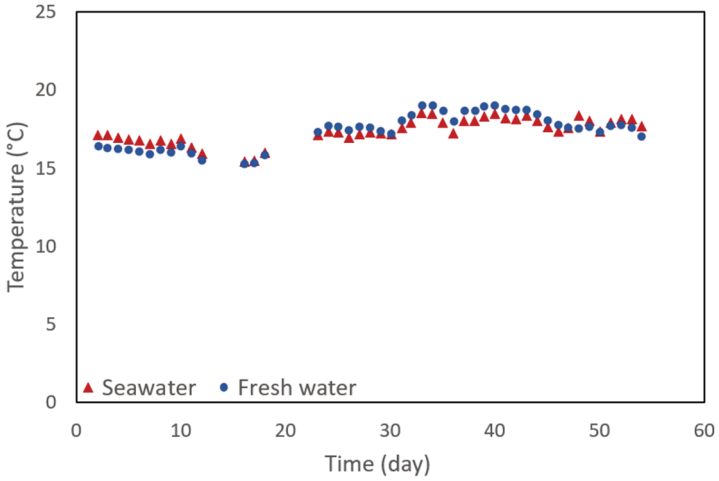


**Figure S 2.2.** Daily average water temperature measurements for fresh and seawater during the time of experiment

### Internal resistance and gross power density data of stacks

Figure S 2.3. shows the extended data of internal resistance and gross power density of the four stacks operated in the experiment. The fluctuation of the data can be partially attributed to the natural conditions, such as waters temperature and conductivity, and to stagnant bubbles and issues with flow distributions in the stacks. On day 35 an intervention was made to prevent the issues with bubbles in the setup and even though stacks were kept running no measurements were made. After the intervention the behaviour of stacks is more stable and a clear distinction on performance can be seen when comparing stacks receiving the water after treatment with dual media filtration and microfiltration.

Figure S 2.4 shows I-V curve of the four stacks on the initial and final stage of operation.

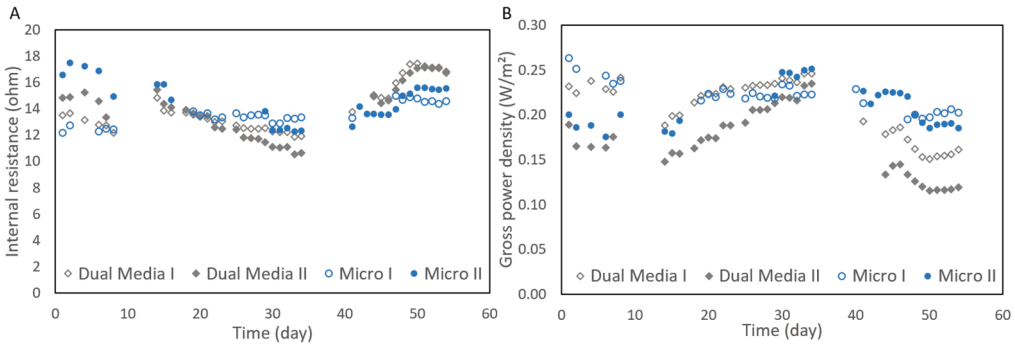


**Figure S 2.3.** (A) Internal resistance and (B) gross power density of the four stacks over the time of operation. Points are daily average of measurements.

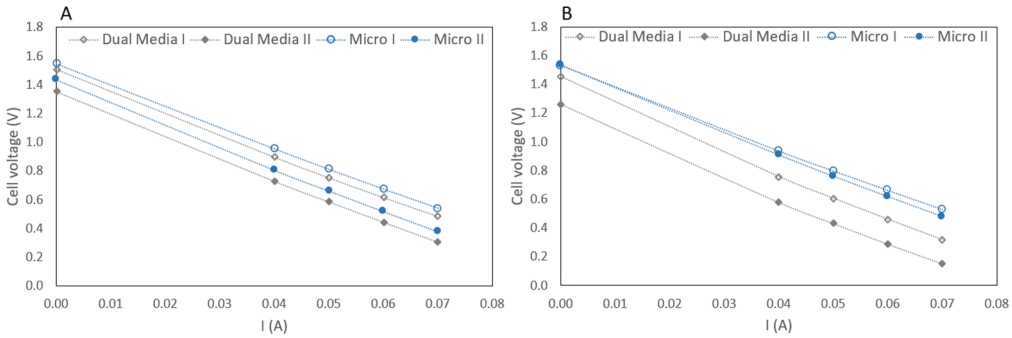


**Figure S 2.4**. I-V curves of start (A) and end (B) of the experiment of the four stacks. Lines were added to guide the eye. These are examples of I-V curves, representing one single measurement, while internal resistance and gross power density reported before were calculated with the daily average of at least 10 measurements.

### Membrane autopsy

Figure S 2.5 shows how the membranes were sectioned for the membrane autopsy. Figure S 2.6 shows how a clean AEM membrane reacted with the stains used in the autopsy, emitting signal, and not allowing its use for identification of foulants in the membrane surface. Figure S 2.7 presents a comparison of fouled spacers from the stacks fed with dual media filter or with microfiltration, both spacers were from freshwater compartments. Finally, figures S 2.8 and S 2.9 present additional images from the membrane autopsy, highlighting the identified structures and patterns.

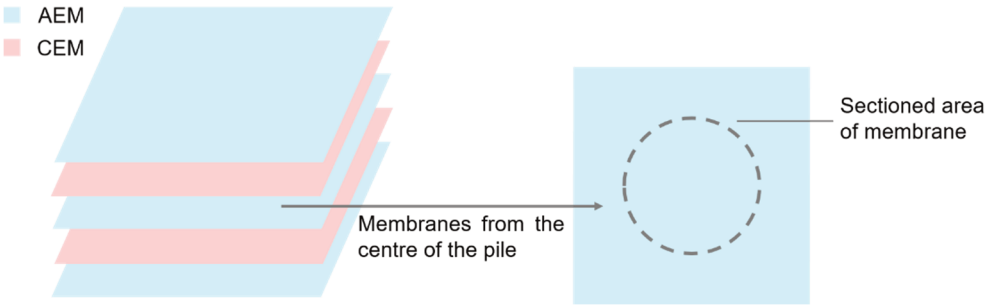


**Figure S 2.5** Scheme showing how membranes were sectioned for membrane autopsy. Membranes from the centre of the membrane pile, which consisted of 10 cell pairs, were chosen, and cut in a central area for representative pieces for microscopy analysis.

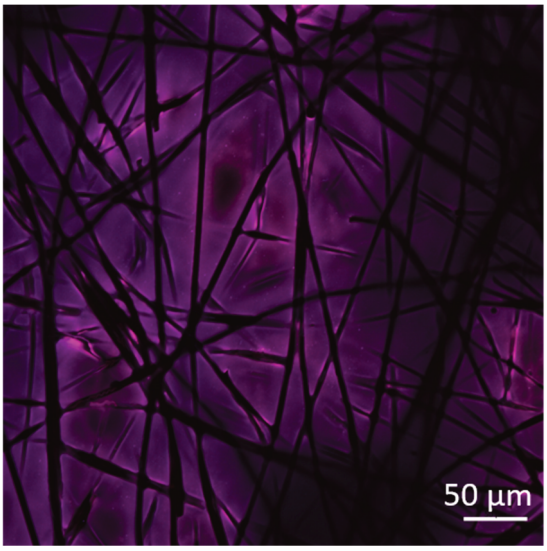


**Figure S 2.6** Clean AEM membrane stained with SyproRed and Calcofluor white (CW). Purple colour correspond to the signal from both dyes (red and blue).

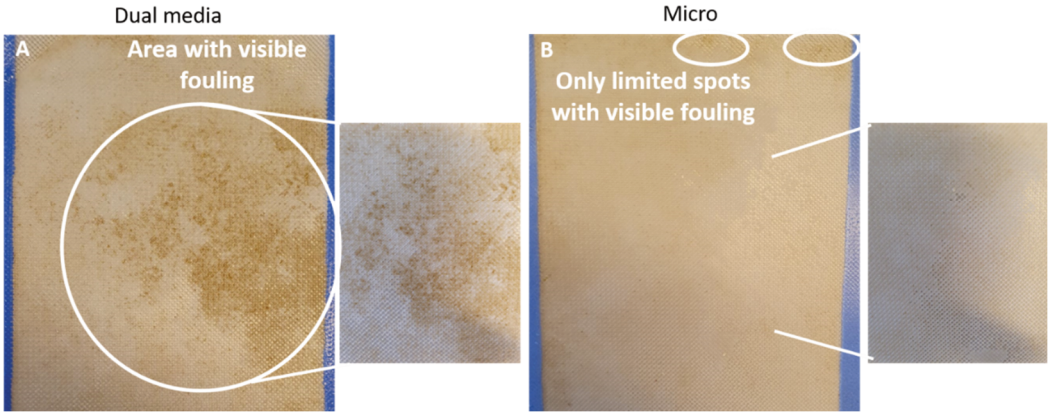


**Figure S 2.7** Visual analysis of spacers after dual media filtration (A) and microfiltration (B) treatments, in contact with fresh water after 54 days experiment.

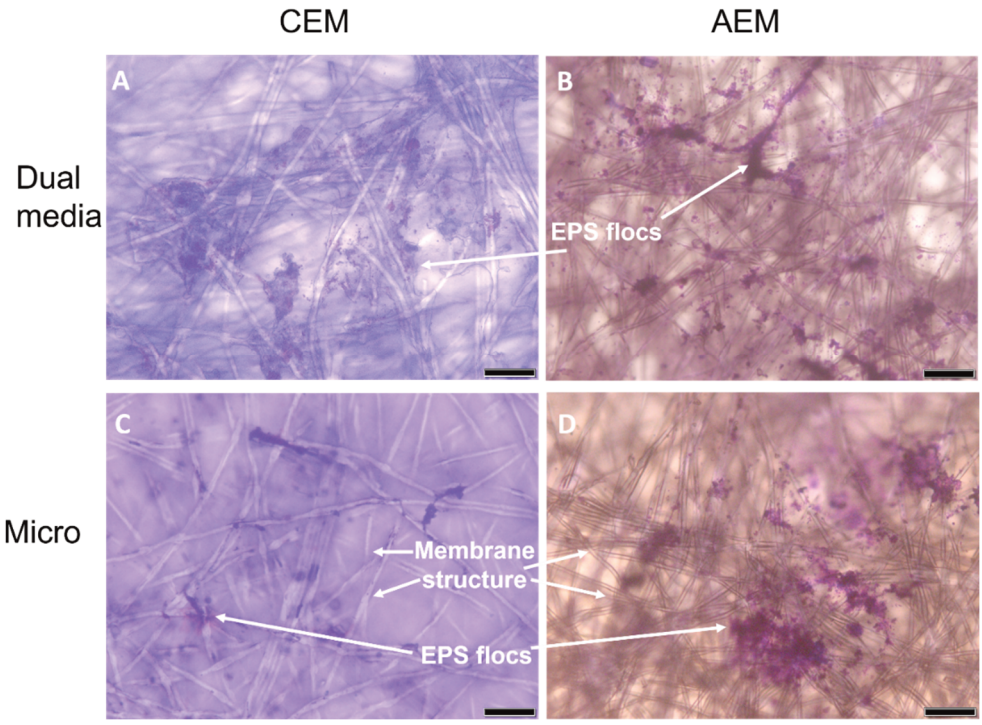


**Figure S 2.8** Optical microscopy pictures of CEM (A, C) and AEM (B, D) after dual media and microfiltration, stained with crystal violet, to detect extracellular polymeric substance (EPS). No clear difference in EPS fouling was observed on the membrane surface after the different fractionation steps. Scale bars represent 50 µm.

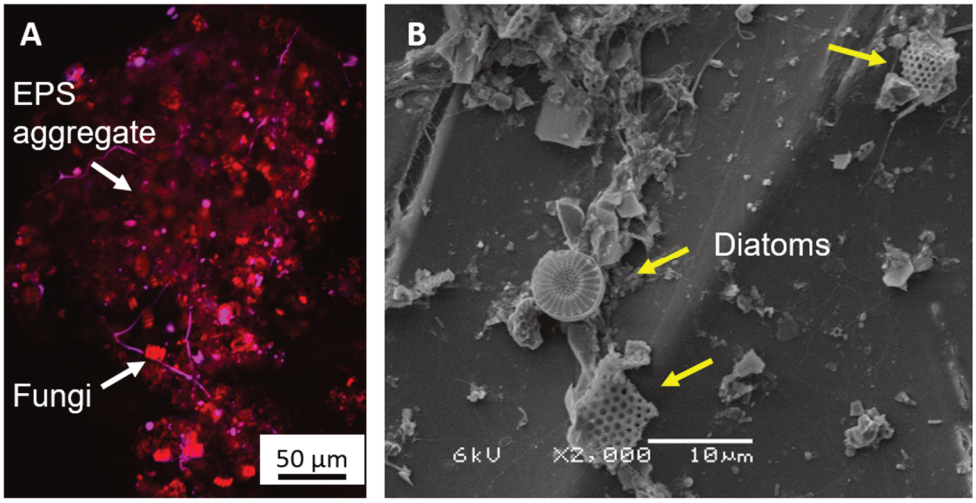


**Figure S 2.9 -** Microscopy images of the biofouling developed on CEM (A) and AEM (B) after dual media rapid filtration analysed via CLSM and SEM, respectively. The CLSM image is showing the combination of SyproRed (proteins, red), and Calcofluor White (polysaccharides, blue). Purple indicates co-localization of the two staining signals. On the CEM, different kind of protein-rich, EPS aggregate were visible (in red), and bigger structures, likely fungi (A). On the AEM, with SEM it was possible to visualize several diatoms reminiscent (B).

**References**


[1] J.W. Post, J. Veerman, H.V. Hamelers, G.J. Euverink, S.J. Metz, K. Nymeijer, C.J. Buisman, Salinity-gradient power: Evaluation of pressure-retarded osmosis and reverse electrodialysis, Journal of Membrane Science 288 (2007) 218–230.

[2] D.A. Vermaas, D. Kunteng, M. Saakes, K. Nijmeijer, Fouling in reverse electrodialysis under natural conditions, Water research 47 (2013) 1289–1298.

[3] T. Rijnaarts, J. Moreno, M. Saakes, W.M. de Vos, K. Nijmeijer, Role of anion exchange membrane fouling in reverse electrodialysis using natural feed waters, Colloids and Surfaces A: Physicochemical and Engineering Aspects 560 (2019) 198–204.

[4] S. Pawlowski, R.M. Huertas, C.F. Galinha, J.G. Crespo, S. Velizarov, On operation of reverse electrodialysis (RED) and membrane capacitive deionisation (MCDI) with natural saline streams: A critical review, Desalination 476 (2020) 114183.

[5] J. Moreno, N. de Hart, M. Saakes, K. Nijmeijer, CO2 saturated water as two-phase flow for fouling control in reverse electrodialysis, Water research 125 (2017) 23–31.

[6] Signe Kjelstrup, Torleif Holt, Liv Fiksdal, Effect of biofilm formation on salinity power plant output on laboratory scale, Industrial Membrane Processes 82 (1986) 39–44.

[7] R.E. Pattle, Production of Electric Power by mixing Fresh and Salt Water in the Hydroelectric Pile, Nature 174 (1954) 660.

[8] W. Guo, H.-H. Ngo, J. Li, A mini-review on membrane fouling, Bioresource technology 122 (2012) 27–34.

[9] S. Mikhaylin, L. Bazinet, Fouling on ion-exchange membranes: Classification, characterization and strategies of prevention and control, Advances in colloid and interface science 229 (2016) 34–56.

[10] D.A. Vermaas, M. Saakes, K. Nijmeijer, Power generation using profiled membranes in reverse electrodialysis, Journal of Membrane Science 385-386 (2011) 234–242.

[11] J. Di Luque Salvo, A. Cosenza, A. Tamburini, G. Micale, A. Cipollina, Long-run operation of a reverse electrodialysis system fed with wastewaters, Journal of environmental management 217 (2018) 871–887.

[12] M.B. Dixon, S. Lasslett, C. Pelekani, Destructive and non-destructive methods for biofouling analysis investigated at the Adelaide Desalination Pilot Plant, Desalination 296 (2012) 61–68.

[13] D.A. Vermaas, M. Saakes, K. Nijmeijer, Enhanced mixing in the diffusive boundary layer for energy generation in reverse electrodialysis, Journal of Membrane Science 453 (2014) 312–319.

[14] M. Vaselbehagh, H. Karkhanechi, R. Takagi, H. Matsuyama, Biofouling phenomena on anion exchange membranes under the reverse electrodialysis process, Journal of Membrane Science 530 (2017) 232–239.

[15] R.S. Kingsbury, F. Liu, S. Zhu, C. Boggs, M.D. Armstrong, D.F. Call, O. Coronell, Impact of natural organic matter and inorganic solutes on energy recovery from five real salinity gradients using reverse electrodialysis, Journal of Membrane Science 541 (2017) 621–632.

[16] E.H. Hossen, Z.E. Gobetz, R.S. Kingsbury, F. Liu, H.C. Palko, L.L. Dubbs, O. Coronell, D.F. Call, Temporal variation of power production via reverse electrodialysis using coastal North Carolina waters and its correlation to temperature and conductivity, Desalination 491 (2020) 114562.

[17] E.J. Bodner, M. Saakes, T. Sleutels, C. Buisman, H. Hamelers, The RED Fouling Monitor: A novel tool for fouling analysis, Journal of Membrane Science 570-571 (2019) 294–302.

[18] J. Moreno, V. Díez, M. Saakes, K. Nijmeijer, Mitigation of the effects of multivalent ion transport in reverse electrodialysis, Journal of Membrane Science 550 (2018) 155–162.

[19] J.W. Post, Blue energy: Electricity production from salinity gradients by reverse electrodialysis. Wageningen, Univ., Diss., 2009.

[20] M.A. de Lucas Pardo, D. Sarpe, J.C. Winterwerp, Effect of algae on flocculation of suspended bed sediments in a large shallow lake. Consequences for ecology and sediment transport processes, Ocean Dynamics 65 (2015) 889–903.
[21] J. Bouchez, J. Gaillardet, C. France-Lanord, L. Maurice, P. Dutra-Maia, Grain size control of river suspended sediment geochemistry: Clues from Amazon River depth profiles, Geochem. Geophys. Geosyst. 12 (2011) n/a-n/a.
[22] R.S. Wotton, EPS (Extracellular Polymeric Substances), silk, and chitin: vitally important exudates in aquatic ecosystems, Journal of the North American Benthological Society 30 (2011) 762–769.
[23] Environmental Protection Agency, EPA Water Treatment Manual - Filtration, 1995.
[24] A.H. Earn Tan, A.W. Ze Chew, A. Wing-Keung Law, Deployment of Recyclable Polycarbonate as Alternative Coarse Media in Dual-media Rapid Filters, Energy Procedia 143 (2017) 475–480.
[25] APHA, Standard Methods for the Examination of Water and Waste Water: Method 2540 D, 21st ed., Water Environment Federation, Washington, 2005.
[26] O'Toole, G. A., Pratt, L. A., Watnick, P. I., Newman, D. K., Weaver, V. B., and Kolter, R., Genetic approaches to study of biofilms., Methods Enzymol 310 (1999) 91–109.
[27] S.J. Kassinger, M.L. van Hoek, Biofilm architecture: An emerging synthetic biology target, Synthetic and systems biotechnology 5 (2020) 1–10.
[28] T. Suchecka, E. Biernacka, W. Piatkiewicz, Microorganism Retention on Microfiltration Membranes, Filtration & Separation 40 (2003) 50–55.
[29] N. Lebleu, C. Roques, P. Aimar, C. Causserand, Role of the cell-wall structure in the retention of bacteria by microfiltration membranes, Journal of Membrane Science 326 (2009) 178–185.
[30] Sara BinAhmed, Anissa Hasane, Zhaoxing Wang, Aslan Mansurov, and Santiago Romero-Vargas Castrillón, Bacterial Adhesion to Ultrafiltration Membranes: Role of Hydrophilicity, Natural Organic Matter, and Cell-Surface Macromolecules, Environmental science & technology 52 (2018) 162–172.
[31] Google Earth, Breezanddijk overview, Google Earth, 2021. Access date: 02/07/2021

Chapter 3

# Reversible fouling by particulate matter from natural seawater reduces RED performance while limiting biofouling

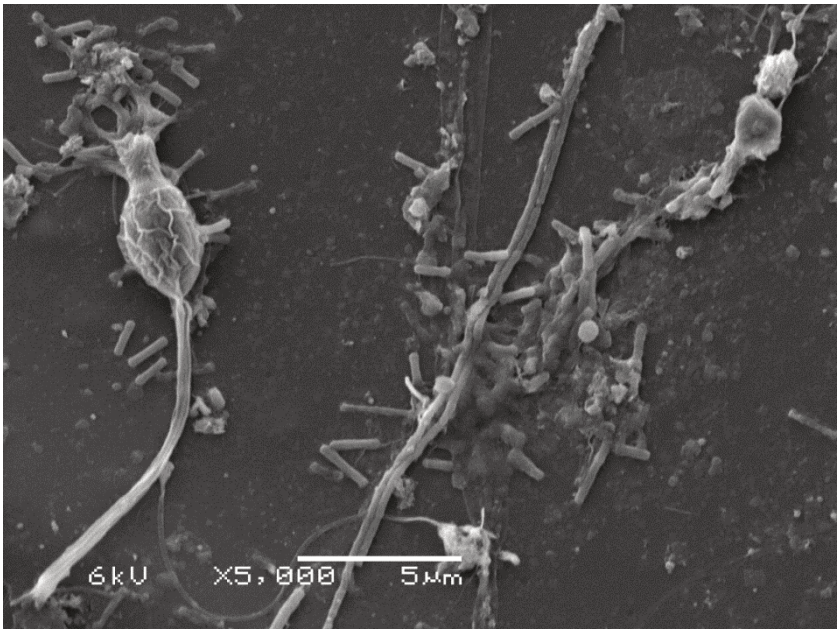

**Abstract:**

Reverse Electrodialysis (RED) has shown to be a promising technology for electricity production, but membrane fouling can influence the energy yield, thus, it is crucial to gain knowledge on the impact and prevention of fouling. We used a sequence of pre-treatments (dual media filter, microfilter and activated carbon filter) to fractionate foulants in seawater based on size and investigated its effect on RED. Fouling reversibility was studied by applying a cleaning procedure with reversal and increased flow and air sparging at the end of the experiment. After 63 days of operation, when using only the dual media filter as pre-treatment, the pressure drop increased by 520 mbar in the seawater compartments without affecting the electrochemical measurements. The application of the cleaning procedure allowed to recover 90% of the pumping power losses. A membrane autopsy showed the development of a biofilm layer on the membrane of the stacks receiving the most treated water while it was not detected when only the dual media filter was used, which showed that the presence of particulate matter could help limit biofouling development. Together with the performance recovery, we concluded that the application of the dual media filtration system is a suitable and cost-effective pre-treatment for RED.

This chapter has been published as:

B. Vital, T. Sleutels, M.C. Gagliano, H.V.M. Hamelers. Reversible fouling by particulate matter from natural seawater reduces RED performance while limiting biofouling. *Desalination,* 548 (2023) p.116262

### 3.1 Introduction

Blue Energy, also known as Salinity Gradient Energy (SGE), is a promising renewable source to complement the renewable energy matrix. Reverse electrodialysis (RED) is one of the technologies that can be used to harvest the salinity gradient that naturally occurs when fresh water reaches the sea [1,2]. RED makes use of a low and high salinity stream separated by ion-exchange membranes, namely anion exchange membrane (AEM) and cation exchange membranes (CEM), which are alternatingly stacked, creating an electrochemical potential difference [2,3]. This series of alternated membranes allows anions to be directed to the cathode and cations to the anode of a cell or stack, where electrodes are located and electrical energy can be harvested through redox reactions [2].

One of the main challenges to make this technology viable is the prevention of fouling of spacers and membranes, as fouling leads to reduction of the available power density and possibly a lower life-span of membranes [4,5]. Most common foulants found in seawater are particulates, colloids, organic and inorganic foulants, and microorganisms. Particulates and colloids can be distinguished based on their size, with the first considered solids with dimension > 1µm and the latter solids and dissolved compounds that are smaller than 1 µm, and both can have an organic and inorganic fraction [6,7]. Microorganisms can adhere and grow on the membrane and spacers surface and excrete an extracellular polymeric substances (EPS) matrix, forming a biofilm, which is known as biofouling [6].

When using natural waters, RED is subject to feed waters containing a variety of foulants that interact in unpredictable ways. Research in RED with natural waters is still new and the effect of foulants from each water stream is not fully understood [5]. Vital and colleagues [8] showed how RED has four possible different interactions of foulants from water streams and types of membrane, highlighting the importance to study them separately and understand the effect of each of these combinations in the overall performance. A foulant fractionation study in RED for fresh water was performed, where results showed that particulate fouling was the main cause for a decrease in performance over long-term operation.

Fouling is considered irreversible or permanent when even with the use of extensive cleaning techniques it cannot be removed from the membranes [5,9]. Irreversible fouling layers are mostly caused by natural organic matter (NOM) depositing or biofilms forming on the membrane surface, and this depends mostly by the physiochemical characteristics and interactions of the soluble organic compounds and membrane charged groups [9–11].

Cleaning procedures to remove fouling can vary greatly, from simple techniques such as backwashing as to more aggressive cleaning, such as chemical treatment with basic and acidic solutions [12]. The utilization of mechanical cleaning by changing the operational parameters (flow direction, velocity, etc.), can be seen as a sustainable and good

operational practice in contrast to the addition of chemicals as cleaning agent. Chemical cleaning has been used as the preferred method to restore performance of ion-exchange membrane processes in previous studies, even though the addition of a cleaning agent can lead to production of toxic by-products/waste and damage the membranes structure [12]. To keep RED sustainable and membrane lifespan as long as possible, an environmentally friendly procedure without the use of chemicals and with low energy consumption is required [12–14]. Some procedures that have been studied before include alternating seawater and fresh water compartments to create an osmotic shock [15,16], reversing inlet and outlet to push out accumulated foulants in the inlet [15], and more widely used membrane cleaning procedures, such as chemical cleaning with acid and base, air sparging and two-phase cleaning with $CO_2$ [12,14,16]. Combinations of these techniques have not been tested for use in RED so far.

The reversibility of fouling in RED has previously been studied using natural waters, with application of different cleaning techniques. Vermaas et al. (2014) [16] studied the performance of RED stacks fed with natural waters when applying two anti-fouling strategies: periodic switching of feed waters compartment to create an osmotic shock and periodic air sparging, to disturb flow channels with pressurized air. When compared to a control stack that was not subjected to any cleaning procedure, both techniques were beneficial to delay fouling impact and recover stack performance, by reversing fouling partially. Periodic air sparging presented superior performance, but at the cost of being a more energy intensive process. Moreno and colleagues [14] extended the work of Vermaas and compared the use of short pulses (2 s and 6 s) of air and $CO_2$, which consumed less energy than the air sparging previously studied. The use of short pulses of $CO_2$ demonstrated to be more beneficial to recover stack performance, since when using only air, stagnant bubbles were trapped in the spacer's mesh, while $CO_2$ could dissolve better in the feed water and not cause this issue [14].

The goal of the present study was to fractionate seawater foulants and associate each fraction with variations in the performance of the RED process. The fractionation was performed by using different types of filters (dual media filter, microfilter and activated carbon filter) that focused on removing the most relevant foulants found in seawater in a series of treatments. In addition, the reversibility of fouling after 2 months of operation was assessed by performing simple and environmentally friendly cleaning strategies. Finally, membrane autopsies gave insight on the type of fouling forming and persisting with and without cleaning from each feed water and membrane combination. All results combined allow for an evaluation of preferred pre-treatment and cleaning strategy and set the base knowledge for further developments in this field.

## 3.2 Materials and Methods

### 3.2.1 Foulant fractionation setup

Figure 3.1 displays a schematic representation of the set-up used in this study, which was built in the Pilot Plant installation of REDstack B.V. in the Afsluitdijk (the Netherlands). Untreated feed waters first went through a drum filter and then a rapid dual media filter, consisting of two distinct layers: first, an anthracite buffer for bigger particles followed by a sand layer (0.5 mm – 1.0 mm). After this treatment, the feed waters were stored in 30 $m^3$ tanks, which were continuously refilled to keep waters representative and avoid particles settlement.

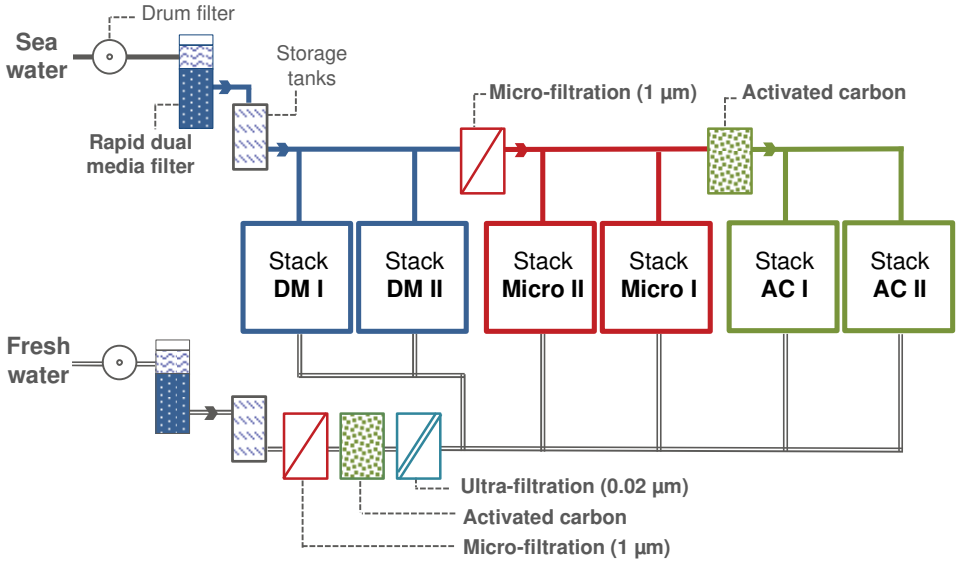


**Figure 3.1.** Schematic representation of the experimental set-up used in this study for the foulant-fractionation experiment of seawater. Stacks DM I and II received seawater after pre-treatment with a rapid dual media filter, for stacks Micro I and II this water is further treated with a micro filter and for stacks AC I and II seawater is further treated with an activated carbon filter. For fresh water all stacks received the water with same pre-treatment, with a final ultra-filtration to avoid fouling as much as possible.

The first two stacks (DM I and II) received the seawater treated only by the dual media filter, while the water fed to the two next stacks (Micro I and II) went through an additional microfiltration step (DGD - 2501.20, Pentair, The Netherlands) with 1 µm pore size (Fig. 3.1). Finally, the seawater fed to the last two stacks (AC I and II) went through a third step of treatment, which was done with an activated carbon cartridge filter (NCP-20BB, Pentair, the Netherlands). The three pre-treatment steps had the objective to make a fractionation of the foulants in the fed seawater, and each pair of stacks represented duplicates of feed

water conditions. The fresh water was treated equally for all the 6 stacks, receiving the strictest pre-treatment available for this experiment. This aimed at reducing fouling as much as possible on the river water compartments so that the findings could be attributed to seawater fouling effects only. Thus, fresh water passed through all the above-mentioned pre-treatments and additionally through an ultra-filtration module of 0.02 μm pore size (R-21 module, Pentair, The Netherlands). All feed waters were pumped through the stacks using adjustable peristaltic pumps (Cole-Parmer, Masterflex L/S Digital drive, USA).

The experiment lasted for 63 days, and performance of stacks was monitored in terms of pressure drop and electrical parameters, as described in the following paragraphs.

***Stack configuration***

Six 100 mm x 100 mm REDstack X-flow stacks were built with housing supplied by REDstack B.V. (Sneek, The Netherlands). Stacks contained 10 cell pairs (0.2 m² membrane area) of flat CEM and AEM of the Fuji Type 10 membranes (Fujifilm Manufacturing Europe B.V., The Netherlands) and membrane characteristics can be found in [17]. The membranes were separated by 480 μm woven netting spacers (Saati PES 740/53 S.p.A., Italy) to allow for long term operation of stacks and with integrated silicon rubber (DEUKUM GmbH, Germany) acting as a sealer, with stacks operating at 0.5 cm/s flow velocity. Pressure drop over the outlet and inlet of the stacks was continuously measured by a pressure difference transmitter (EJA110E, Yokogawa, Japan). The electrolyte solution was composed of 0.05 M $K_3Fe(CN)_6$, 0.05 M $K_4Fe(CN)_6$ and 0.25 M NaCl (VWR, USA). The electrolyte compartments were shielded with an additional CEM and kept at an overpressure of 0.3 bar. At both sides of this membrane pile, titanium electrodes (mesh 1.7 $m^2/m^2$) with a galvanic platinum coating of 2.5 μm and with an active area of 10 cm x 10 cm were used as the anode and cathode (Magneto Special Anodes B.V., The Netherlands). Temperature and conductivity of the feed waters after the buffer tank were measured using a sensor and recorded every 60 seconds using a data logger (GX10, Yokogawa, Japan).

***Electrochemical measurements***

Chronopotentiometric series were applied to the stacks using a potentiostat (Iviumstat, Ivium Technologies, The Netherlands) connected to a peripheral differential amplifier to measure voltage, including open circuit voltage (OCV) and calculate the stack internal resistance and gross power density [4,18]. The chronopotentiometry series consisted of constant current density steps of 4 $A/m^2$, 5.5 $A/m^2$, 7 $A/m^2$, 8.5 $A/m^2$ and 10 $A/m^2$ applied for 60 s each – to reach a constant voltage value – which were separated by steps of 60 s with no current [19,20]. The rest of the time, the stacks were operated at constant current density of 5 A/m² to simulate a RED process. The net power density was calculated using

the same method as in [14], accounting for the pumping power losses due to the increasing pressure drop caused by fouling.

### 3.2.2 Reversible fouling assessment with cleaning

A cleaning procedure was performed in stacks DM I and AC I one day before stopping the experiment, to assess if the fouling accumulated during 62 days of the experiment was reversible. By day 62, the stacks Micro I and II were not comparable in performance, so it was decided not to clean either of them, to avoid compromising the membrane autopsy and to compare the difference in fouling. Thus, the cleaning procedure was performed only in stack DM I and AC I, and stacks DM II and AC II were kept as reference for the fouling accumulated during the whole experiment.

The cleaning procedure consisted of three steps. The first step was flow reversal, done by switching the inlet with the outlet of the stack, based on the fact that fouling starts to accumulate in the entrance of the stack [14], and by switching the inlet with the outlet, part of the foulants can be pushed out of the stack. The next step was triplicating the original flow of the feed waters (maintaining the configuration from step 1), by enhancing the flow velocity part of the loosely deposited foulants were pushed out of the stack. The combination of flow reversal and increase can be seen as a backwashing procedure for RED. The final step was performing an air sparging, with a short, controlled introduction of pressurized air along with the feed water to disturb the fouling layer and flush foulants away. The air sparging was done twice for each stack with a regime of introducing air 3x for 2 sec at 2 bar, following the best results achieved with this approach in [14].

The outlet water after each cleaning step was collected and analysed with the procedure described in 3.2.3. Analysis of the effluent water from cleaning gave insight into which type of foulants could be removed in each step. All stacks were kept running for at least one more day before their removal for the membrane autopsy, to stabilize and allow for proper measurements before the autopsies were performed.

### 3.2.3 Feed waters analyses and membrane autopsy

Feed waters for each stack and inlet untreated waters were characterized at 7 different sampling points twice a week by various methods already described in [8]. In summary, the characterization was carried out for concentration of ions, in/organic carbon, suspended solids concentration, particle size distribution (PSD) and turbidity, pH, and conductivity.

After removing the stacks from the experimental setup, membrane autopsy was carried out in all stacks. Camera pictures were taken from cell pairs located in the centre of the membrane pile to visualize fouling appearance by naked eye. Membrane pieces were cut from an inlet central of the membrane in duplicate for observation under optical

microscope and scanning electron microscopy (SEM) together with energy-dispersive X-ray spectroscopy (SEM-EDX) as described in [8]. For optical microscopy, the membrane pieces were stained with crystal violet 0.1% solution (Crystal Violet/ammonium oxalate solution, Boom B.V., Netherlands) and Alcian Blue 8 GX 0.1% solution (Sigma Aldrich, the Netherlands) for visualization of organic fraction and the acidic polysaccharides within the EPS biofilm matrix, respectively [21,22]. For SEM-EDX, membrane samples were fixed with 2.5% glutaraldehyde solution and dried with ethanol in steps of increasing concentration [8].

To study particulate fouling in more detail, membrane pieces of 5x5 cm were cut and placed in 30 ml of 60 g/L NaCl brine to extract as much foulants as possible from the membrane surface to a draw solution. The samples were placed for 15 min on a shaker, followed by 30 min on the ultrasonic bath and lastly for 15 min on the shaker again. With the particulate matter in the brine solution, particle size analysis could be carried out with the same procedure used on the feed water analysis, described earlier in this section.

## 3.3 Results and discussion

Aiming at building a complete picture of fouling types and its effects, the fractions of foulants from seawater on RED stacks were studied in three different aspects: 1) evaluating stack performance, 2) the reversibility of foulants by subjecting the stacks to a cleaning procedure and 3) the detailed analysis of fouling by membrane autopsy.

### 3.3.1 Stack performance is mostly impacted by suspended particles

Stack performance and the effect of the foulants from the different fractions was evaluated through pressure drop over the inlet and outlet of feed waters in the stack, internal stack resistance and gross and net power density were monitored during the process and results are presented in Figure 3.2.

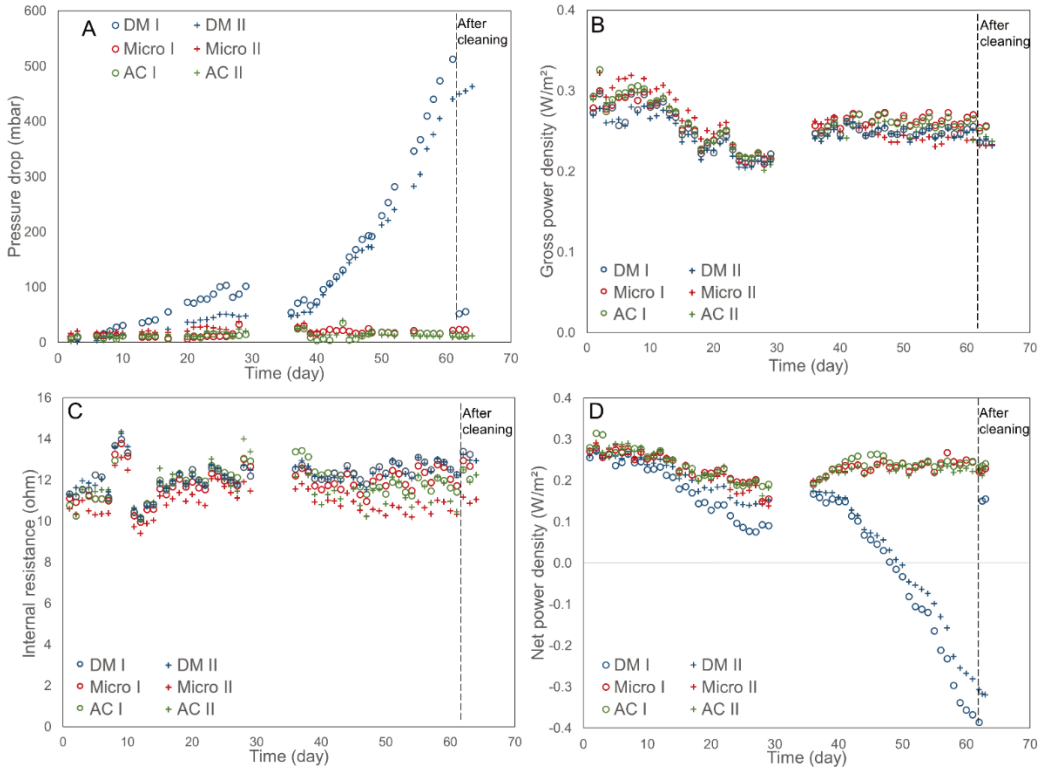


**Figure 3.2.** Pressure drop measurements (A) for seawater compartments fed with different pre-treated seawater. Gross power density (B), internal stack resistance (C) and net power density (D) for the six stacks operated during the experiment. The naming of the stacks is the same as shown on Figure 3.1. From day 29 until 36 no data is shown, as measurements were affected by adverse weather conditions in the pilot plant even though stacks were running normally. The cleaning procedure was performed in stacks DM I and AC I at day 62.

The pressure drop in the stacks receiving water from the dual media pre-treatment (DM I and DM II) started to increase after 10 days and reached values of over 500 mbar at the end of the experiment (Fig. 3.2A). Stacks Micro I, AC I and AC II did not show any relevant increase in pressure drop throughout the experiment. The pressure drop sensor on stack Micro II started to fail, thus no data are available after day 40.

The pressure drop measurements show that the pre-treatment with dual media filter only could not prevent a loss of performance, compared to additional microfiltration and activated carbon. This was likely caused by the presence of particulate fouling in seawater, as the average diameter of particles detected in samples taken after dual media filtration were 12 µm (Fig. S 3.1A), while after microfiltration and activated carbon no particle larger than 1 µm was expected. The impact caused by these particles in the DM stacks can be seen

in the net power density (Fig. 3.2D), as after day 49 the stacks produced a negative power density and thus consumed more energy than they could produce.

Even though the DM stacks suffered from fouling, no relevant changes in electrochemical performance were observed during the experiment in comparison to the other stacks (Fig. 3.2B and C). The cleaning procedure also did not influence the gross power density, showing that fouling was not affecting the electrical performance of the stacks. The only variations that could be observed were related to weather events that affected the process, such as seawater conductivity variation and lower temperature (Fig S 3.2) [23]. This stable performance can be attributed to two factors: first, a good efficiency of the membranes, with a low electrical resistance and high permselectivity [19] and second, the use of a dual media filter as the main pre-treatment, that removes a large size range of foulants and is able to keep a stable outlet water quality, even when due to natural events higher loads reached the filters [24,25]. When only a drum filter was used as pre-treatment, the decrease of gross power density over similar amount of time was of more than 40% of the initial value [14,16]. The removal of large solids (> 20 µm, Fig. S 3.1A) together with a reduction of more than 90% of the amount of solids (Fig. S 3.1B) by the dual media filter contributes for this better power performance of the stacks, even though the solids that are in the effluent of the filter can still cause decrease of performance due to increase of pressure drop. Overall, all the six stacks could be operated over two months without relevant losses of gross power density (Fig. 3.2B), thus all the pre-treatments applied have been demonstrated to enable a long and sustainable operation of RED stacks.

Since the reported pressure drop for the stacks DM I and II (Fig. 3.2A), caused by clogging of the feed channels, was not translated into an increase of stack resistance (Fig. 3.2C), such increase in pressure drop could be due mainly to the clogging of the spacers by particulate matter in seawater. Indeed, if the fouling had affected the membrane process this would be seen on the electrochemical parameters [4,26]. The use of spacers has been shown to be detrimental to stack performance in previous studies as well, mainly by supporting the attachment and accumulation of fouling when using natural waters [4]. The most developed alternative for the use of spacers is to use profiled membranes. Profiled membranes can promote a good flow distribution without offering as much area for fouling accumulation as spacers [27]. Next to that, when using profile membranes, most of the particulate fouling should be able to cross the flow channel and leave the stack. The channels' thickness is in the range of hundreds of micrometres, giving enough room for ~10 µm particles to pass [28]. The development of suitable profiled membranes that can replace spacers in RED stacks is needed for the further development of this technology [27].

### 3.3.2 Fouling caused by particulate matter is mostly reversible

A series of cleaning methods were performed after 62 days of operating the stacks to assess the reversibility of fouling. The developed procedure, described in 3.2.2, considers the

requirements of Blue Energy to be a sustainable technology. Therefore, the cleaning should be simple and effective, without the presence or production of any harmful or toxic substances [5,12]. Moreover, the procedure should be a cost-effective solution that can help stablish Blue Energy as a renewable energy source [29].

The cleaning procedure consisted of three steps: flow reversal, increasing the flow three times its original value (3x flow) and air sparging. The impact of each cleaning step on stack DM I is shown in Figure 3.3A and a comparison of the collected effluent waters for all stacks is presented in Figure 3.3B and C. The effect of the cleaning was evaluated by a reduction in pressure drop, which could only be detected in stack DM I.

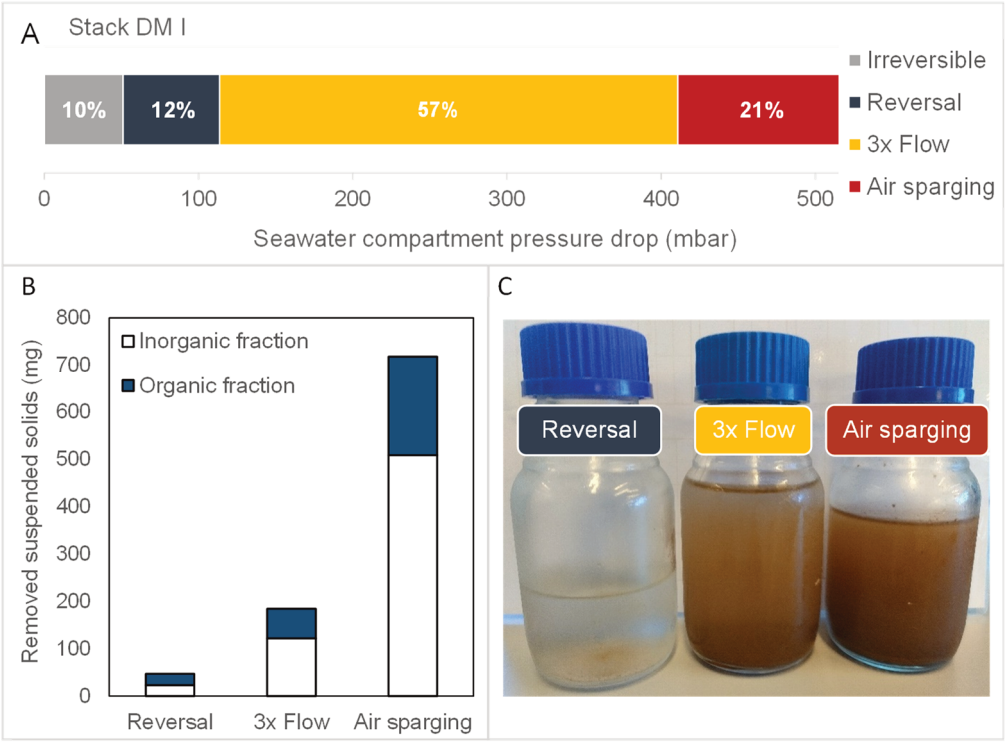


**Figure 3.3.** (A) Seawater compartment pressure drop measured on stack DM I after each of the three steps of the cleaning procedure. The fraction that was not removed by the cleaning procedure is considered irreversible fouling. In this picture, flow reversal is called reversal, the increase of flow rate is 3x flow and air sparging is represented with its full name. (B) Amount of suspended solids removed in each cleaning step, represented with their organic and inorganic fractions. (C) Picture from the outlet water collected after each cleaning step.

Flow reversal had the lowest impact on seawater pressure drop, accounting for a reduction of only 12% of the pressure registered before the cleaning step (520 mbar) (Fig. 3.3A). Flow reversal is a mechanical type of cleaning, that can be also seen as a good operational

practice and does not have the potential to remove large amounts of fouling, and thus a reduction of more than 10% of accumulated value is remarkable. As expected, flow reversal resulted in lowest amount of removed suspended solids (~50 mg - Fig. 3.3B).

The second step of the cleaning procedure, increasing the flow, was responsible for the largest reduction of the pressure drop in the seawater compartment, around 350 mbar (57% of total) (Fig. 3.3A). The effluent recovered in this step contained a mixture of large aggregates (> 50 µm) that would easily settle and medium and smaller solids (< 20 µm – Table S 3.2) that would be suspended for longer periods, causing turbidity in the water (Fig. 3.3C).

It is remarkable that 57% of the performance of a stack that was fouled for 62 days could be recovered simply by triplicating the original flow velocity for 2 minutes. This shows that most of the accumulated fouling during stacks operation is easily reversible with simple operational practices and cleaning procedures. Furthermore, this shows that a long-term and sustainable operation of RED can be enabled with a simple pre-treatment, such as a dual media filter, in combination with a frequent cleaning regime. Previous studies showed that tackling fouling formation in its early stages leads to higher percentages of performance recovery [30,31]. Thus, we believe that with only these two aforementioned steps of the cleaning procedure happening in an early stage of fouling formation, even a larger fraction of pressure drop could be recovered than the here reported 70%.

The last cleaning step - air sparging, yielded a reduction of an additional 21% of the original pressure drop value (Fig. 3.3A). Air sparging was responsible for removing the largest amount of solids in weight (700 mg) compared to the other two techniques (Fig. 3.3B). However, this large number of solids accumulated in the stack did not have a big impact on stack performance, reducing a smaller fraction of pressure drop than the increased flow (Fig. 3.3A). Of course, this outcome is heavily influenced by the order that the cleaning procedures took place. Thus, the first two procedures (reversal and 3x flow) removed mostly larger particles or aggregates (> 20 µm) compared to air sparging (> 10 µm – Table S 3.2) and these particles were the ones affecting pressure drop measurements the most. Therefore, during operation of RED stacks special attention should be given to preventing the settlement of these larger particles on the membrane surface, which can be achieved with a tailored and improved pre-treatment design and implementation of a frequent cleaning regime. Future studies should focus on these aspects of operation.

The remaining value of seawater pressure drop after the cleaning procedure was ~50 mbar, which is called an irreversible fraction of fouling, representing only 10% of the value that was build up during the experiment (> 500 mbar) [12]. This value (50 mbar) is in a similar scale to the one achieved by stack Micro I in the end of the experiment (~25 mbar), showing that the use of a dual media filter with an effective cleaning procedure can have comparable results to a microfiltration pre-treatment alone. Other more aggressive cleaning, such as

with the use of an environmental friendly cleaning agent, could possibly remove this remaining 10% of the maximum pressure drop value achieved in the experiment and restore it to the initial value [32].

### 3.3.3 Membrane autopsy shows biofouling development after activated carbon pre-treatment

Membrane autopsy after 63 days of process allowed to evaluate differences in membrane fouling in the stacks that received seawater after different pre-treatment, and for comparison of stacks that received same water treatment but with and without the cleaning procedure (DM I and II and AC I and II), as shown in Fig. 3.4 and Fig. S 3.3.

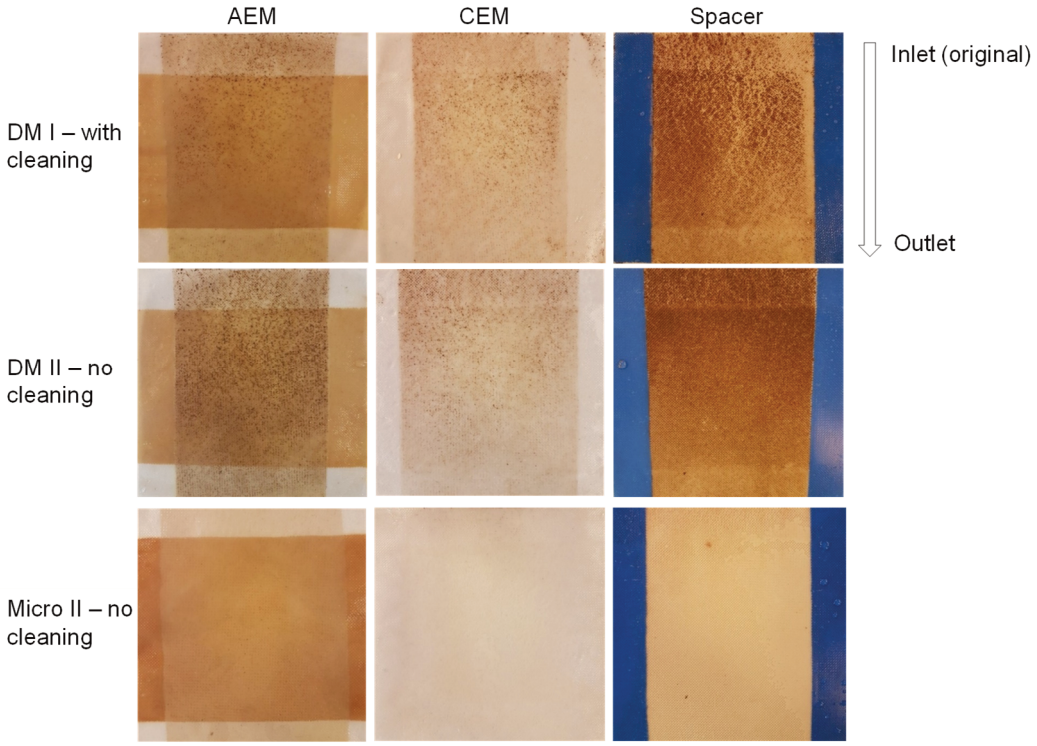


**Figure 3.4.** Representative images of AEM, CEM and spacer from stacks DM I, DM II and Micro II. Images of the remaining stacks can be seen in the supplementary information (Fig. S 3.3). The arrow indicates the flow of seawater through the stacks, from inlet to outlet. All pictures are showing the side of the membrane that was in contact with seawater during the experiment.

All AEMs presented a brown coloured layer on their surface (Fig. 3.4), that is attributed to the presence of humic acids, as previous studies also reported [4,33]. Humic acids are negatively charged which favours the interaction with the positively charged AEMs [33], but

their concentration in seawater is lower than in fresh water, leading to less fouling and reduction of performance when present in seawater fouling [34].

Particulate fouling could be seen on membranes and spacers of both stacks DM I and II and, as expected, DM I had a lower coverage of the membrane surface or spacers due to the cleaning procedures (Fig. 3.4). In all other stacks (Micro I and II, AC I and II) it was not possible to visually detect particulates on the membrane surface and/or spacers since the pre-treatment removed particles above 1 µm from the feed water. To further investigate the particulate fouling, the particle size distribution (PSD) of the particles extracted from membrane pieces from stack DM I and DM II was carried out (Fig. 3.5).

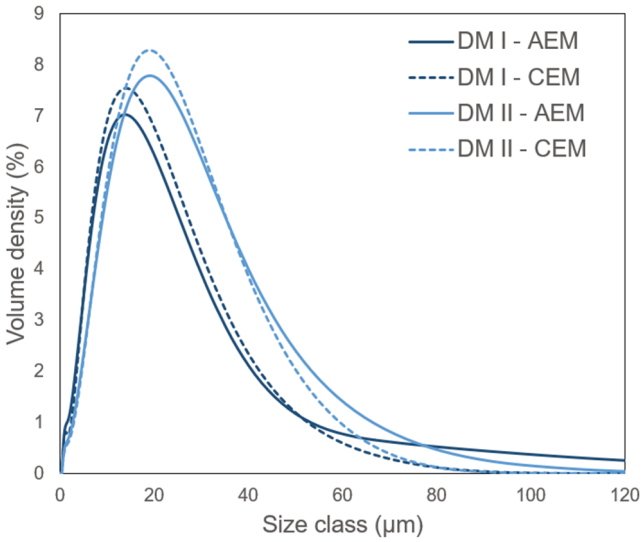


**Figure 3.5**. Particle size distribution (PSD) of particles extracted from membrane surface of stacks DM I and II.

The peak of the of the PSD curves from stack DM I corresponds to a smaller size class (~12 µm) than the ones of stack DM II (~20 µm), while the volume occupied by the particles (represented by the area below the curves) from stack DM I is smaller than DM II, showing that the cleaning procedure removed a considerable number of bigger particles (Fig 3.5). Larger particles contribute most to the pressure drop and once they were removed, the value of pressure drop decreased considerably (Fig. 3.3A).

The microscopy observation of the fouling accumulated on the membrane's samples (Fig. 3.6 and Fig. S 3.4) showed that the type of fouling detected in the membranes after different pre-treatments was remarkably different. In stack DM I (Fig. 3.6) and II (Fig.S 3.4) a quite general type of fouling was detected, with large entangled complex structures covering most of the membrane surface, and large deposits of silica and aluminium compounds, as

shown by EDX data (Table S 3.3). A few microorganisms' cells could be observed in these entangled structures, but not in such a significant amount to identify it as biofouling. For stacks Micro I and II, the coverage of the membrane by the fouling layer was lower than in stacks DM, with many more clean spaces on the membranes surface (Fig 3.6B and E). In this case, a few more cells and EPS structures were detected in comparison to stacks DM, but still not a significant amount that could hinder stack performance, confirming the results showed in Fig. 3.2. EDX measurements localized in the rare spots where fouling was visualized, showed lower amounts of silica and aluminium but more elements related to membrane composition and salts, such as carbon, sulphur, chloride, and sodium, showing that many membrane portions were not covered by particulate fouling.

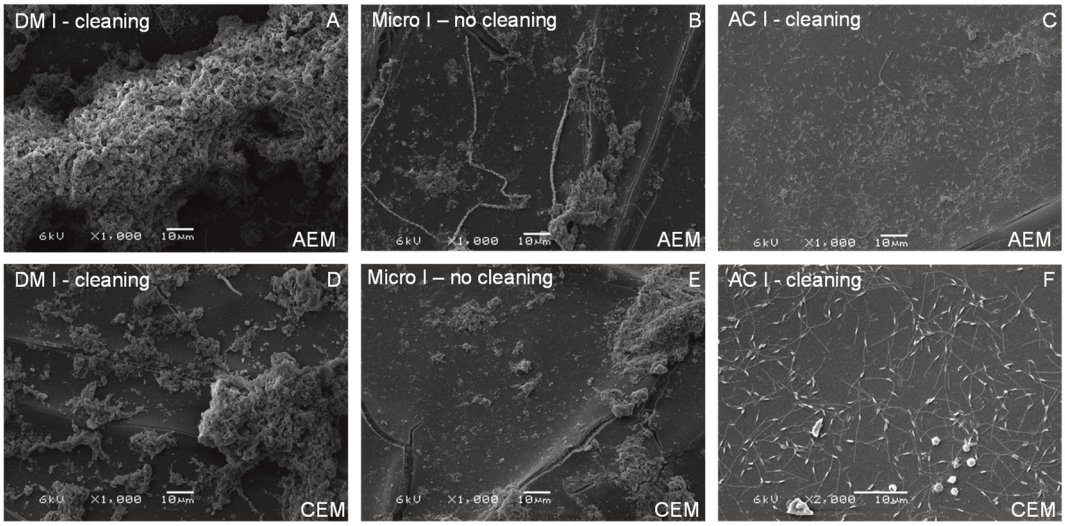


**Figure 3.6.** SEM representative images of stacks DM I, Micro I and AC I. Pictures A, B and C are from AEM and D, E, F are from CEM. The related EDX data are reported in Table S 3.3. More images of membranes from stacks DM II, Micro II and AC II can be found in the support information (Fig S 3.4).

Stacks AC I and II showed a different fouling profile, with both CEM and AEM membrane surfaces covered by groups of cells with same morphology, likely belonging to the same species, connected via a solid network of pili (Fig. 3.6C and F). The synthesis of bacterial appendages such as pili and flagella is thought to be an important stage starting bacterial adhesion on surfaces and driving the formation of a biofilm layer by several kind of bacteria [35]. The coverage of this kind of biofouling on the membrane surface was large, and other types of fouling structures were barely detected. A similar kind of biofouling was observed in an experiment with the same approach of fouling fractionation, applying microfiltration treatment on fresh water [8]. The latter would support the hypothesis that the microfiltration step and activated carbon filter was not removing all the bacteria in the inlet flow, but actually acting as selection parameter for a certain bacterial species, as highlighted

by observing the cell morphology (Fig. 3.6C and F). Indeed, cells of small size, so called "filterable bacteria" can pass through the filtration steps, and the lack of other bacterial competition can favour their growth even in such nutrients limited environments [36]. Moreover, the lack of silica-rich particulate fouling on these membranes could have likely favoured the adhesion of such cells via the synthesis of appendages, forming an interconnected network. Indeed, bacterial adhesion is strongly depending by the surface characteristics [37], and the polar characteristics of AEM and CEM could have likely favoured polar interactions between cell surface and membranes [11].

The addition of treatments in each fractionation step led to different type of fouling in the RED process. With stricter pre-treatment, less overall fouling was expected. However, with the strictest pre-treatment, presence of biofouling, covering extensive portions of membrane surface was surprisingly detected. This is especially interesting due to the interaction with other foulants, such as the small silica particulates. The presence of big silica particles after less strict pre-treatment, did not lead to presence of biofouling.

Despite the growth of the biofouling layer, the performance of the stacks was not hampered, and no pressure drop was observed during the process (Fig. 3.2 and 3.3). This finding confirms that biofouling is not a significant negative factor for RED stack operation, as previously observed in our work [8]. However, since the formation of biofouling can be detrimental for the membrane performance on the long run [5], the presence of particulate fouling, preferably with smaller particles (< 10 µm) that cause less impact on stack performance, which likely limited microbial attachment/growth, could be seen as an added value in light of the application of the sole dual media filter as a pre-treatment to operate Blue Energy technology.

### 3.4 Conclusions

The current work brings new and exciting insights for the prospects of the Blue Energy technology. The use of a dual media filter for the pre-treatment of seawater is adequate to reduce operational problems related to fouling. Indeed, even though the stacks fed with dual media filtered seawater had a loss of performance in the long term, the type of fouling formed (mainly due to particulate matter) was not irreversible neither damaging the membranes, and could be mostly reversed by a series of simple cleaning techniques. The cleaning by triplicating the original flow of stacks was responsible for reversing almost 60 % of the pressure drop increase in the stacks fed with water treated via dual media filtration after more than 2 months of operation, showing that this simple technique is very effective. In addition, the cleaning techniques applied were of low technical complexity and could be easily adopted in a more frequent regime since the beginning of fouling build-up to prevent fouling accumulation that hinders performance.

Membrane autopsy showed that the presence of particulate matter on the membrane surface, accumulated after the use of dual media filtration as pre-treatment, could prevent the formation of a connected network of cells, opposed to what happened when using a pre-treatment that does not allow for the presence of particulates (< 1µm), such as microfiltration and activated carbon.

This last finding is of relevance not only for future developments in Blue Energy and ion-exchange membranes technologies, but also for conventional membrane process, such as nanofiltration and reverse osmosis, as this input could give new ideas on how to prevent or at least delay and reduce biofouling formation, a known issue related to all membrane technologies.

Finally, the results show that 90% of the performance loss could be recovered with a simple cleaning procedure, reinforce that a dual media filter is sufficient for seawater pre-treatment for Blue Energy applications. The combination of a dual media filter and a simple cleaning procedure, without the use of chemicals, show that Blue Energy is a sustainable technology for the energy matrix, and that the by-products of this technology can be of natural origin and of low environmental impact.

## Support information

### Feed waters and cleaning

Table S 3.1 shows the water composition of each stream entering the stacks. The ions concentration is mostly not affected by the pre-treatments, keeping similar values through the whole setup. In this case the differences in performance detected during the experiments cannot be attributed to multivalent ions fouling, since all stacks are subject to the same ion concentrations.

**Table S 3.1.** Feed water composition for all the different treatment steps of the experimental setup.

| Parameter (mg/L) | Seawater | | | | Fresh water | | |
|---|---|---|---|---|---|---|---|
| | Untreated | Eff. dual media filter | Eff. Micro filter | Eff. Activated carbon | Untreated | Eff. dual media filter | Eff. Ultra filtration |
| **Chloride** | 12,209 ± 1,188 | 13,414 ± 854 | 13,536 ± 662 | 13,476 ± 943 | 133 ± 14 | 135 ± 15 | 137 ± 14 |
| **Sodium** | 7,225 ± 550 | 7,639 ± 483 | 7,733 ± 318 | 7,680 ± 509 | 83.0 ± 8 | 84.4 ± 9 | 83.9 ± 8 |
| **Sulphate** | 1,726 ± 161 | 1,899 ± 117 | 1,915 ± 94 | 1,845 ± 168 | 59.7 ± 6 | 60.5 ± 7 | 62.5 ± 5 |
| **Calcium** | 266 ± 21 | 278 ± 23 | 279 ± 12 | 281 ± 19 | 41.8 ± 4 | 41.8 ± 4 | 41.5 ± 4 |
| **Magnesium** | 844 ± 66 | 881 ± 62 | 911 ± 41 | 902 ± 63 | 14.2 ± 1 | 14.4 ± 1 | 13.9 ± 2 |
| **Potassium** | 265 ± 25 | 276 ± 30 | 275 ± 14 | 273 ± 23 | 6.9 ± 1 | 7.1 ± 0.5 | 7.0 ± 0.5 |

Further feed water characterization of particle size distribution and suspended solids are presented in Figure S 3.1 and conductivity and water temperature measured on the treated water with dual media filtration for both water streams are presented in Figure S 3.2. The graph of particle size shows the distribution of particle size by means of reference values, Dx 10, 50 and 90. Dx (90) means that 90% of particles present in the sample are smaller than the Dx (90) value. Proportionally, the same applies for Dx 10 and 50. Suspended solids are presented as the total of suspended solids (TSS) and its fractions, fixed suspended solids (FSS) and volatile suspended solids (VSS). The reduction of total suspended solids from untreated seawater compared to dual media filtered water is remarkable, with an average of 96% removal. A similar trend is seen for reduction on the particle size, showing that the pre-treatment retains the larger particles and only allows smaller particles to pass through.

The graph of seawater conductivity shows large variations from day 18 till 33, which happens due to weather events and operation of the Afsluitdijk locks, causing variations on the performance of stacks as shown on Figure 3.2.

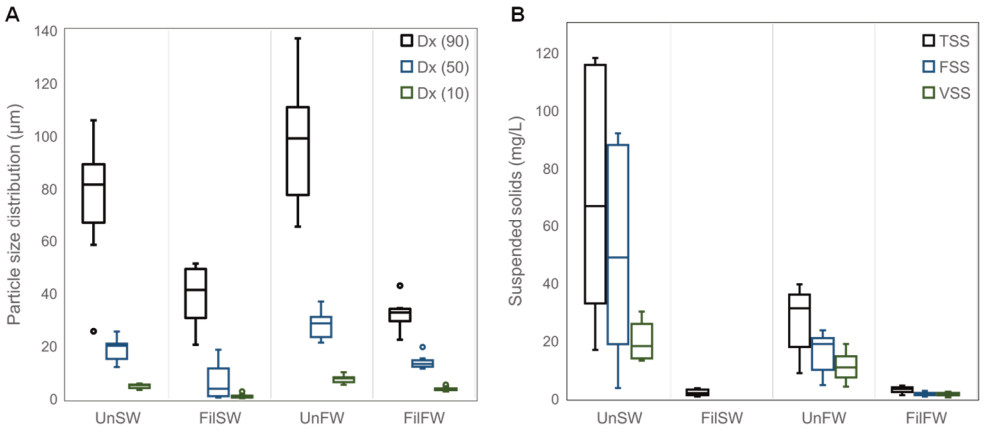


**Figure S 3.1.** Particle size distribution (A) and suspended solids (B) of 4 types of water samples: UnSW is Untreated seawater, FilSW is seawater after treatment with the dual media filter, UnFW is the untreated fresh water and FilFW is fresh water after treatment with the dual media filter. Samples of water that were further treated with microfiltration and activated carbon are not showed, as the parameters here analyzed were below detection limit on these samples.

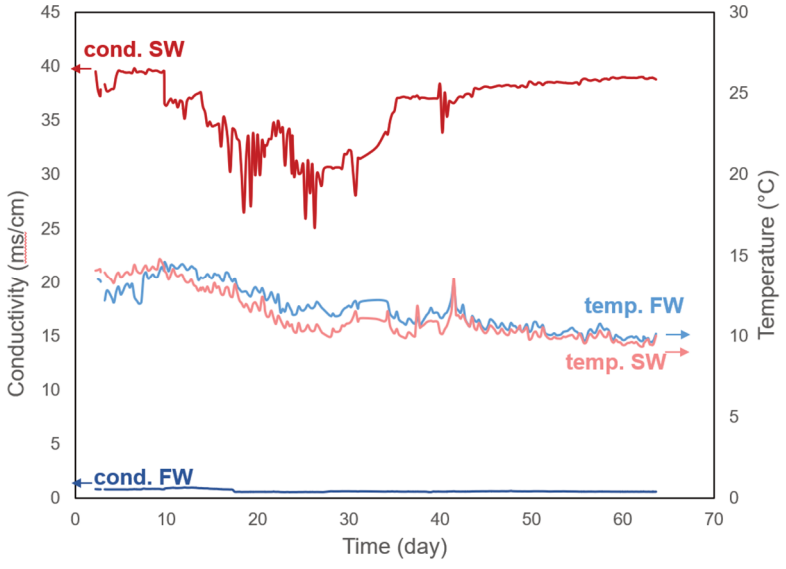


**Figure S 3.2.** Conductivity and temperature of sea and fresh water treated with dual media filtration system during the time of experiment.

The effluent during the cleaning moment from stack DM I was recovered and analysed for particle size distribution. A summary of the findings is presented on Table S 3.2. The reference values for particle size show that the size of the recovered particles in the cleaning with 3x flow was larger than air sparging, even though the latter was able to remove a greater amount of solids, as shown on Figure S 3.3.

**Table S 3.2.** Particle size distribution from effluent from cleaning procedure stack DM I.

| Sample | Dx (90) | Dx (50) | Dx (10) |
|---|---|---|---|
| 3x flow | 129.2 | 56.9 | 18.2 |
| Air sparging | 104.2 | 37.9 | 12.2 |

**Membrane autopsy**

Additional information of membrane autopsy is shown on Table S 3.3 and Figures S 3.3 and S 3.4. Table presents the atomic percentage of each element in representative samples of membrane pieces from all stacks. In the two stacks receiving feed water directly from the pre-treatment from dual media filter the presence of elements such as Silicon and Aluminium occurs with higher percentages than other stacks, showing that compounds such as Silica and Aluminium oxides are most likely present.

**Table S 3.3.** EDX elements identification on the 12 membrane samples. Labelling of samples is done with the abbreviation from the stack given in Figure 3.1 and following with the type of membrane (AEM or CEM). Measurements done on representative spots of the sample with an acceleration voltage of 15 kV. Results are presented in atomic percentage (%) of each element of the spot composition.

| Element | DM I AEM | DM I CEM | DM II AEM | DM II CEM | Micro I AEM | Micro I CEM | Micro II AEM | Micro II CEM | AC I AEM | AC I CEM | AC II AEM | AC II CEM |
|---|---|---|---|---|---|---|---|---|---|---|---|---|
| **C** | 37.7 | 52.4 | 41.4 | 61.9 | 75.3 | 68.0 | 96.3 | 71.3 | 96.0 | 78.8 | 96.0 | 68.1 |
| **O** | 52.2 | 39.5 | 39.2 | 26.9 | 21.3 | 26.6 | - | 22.8 | - | 17.8 | - | 24.2 |
| **Na** | - | - | - | 0.8 | - | 0.6 | - | 0.8 | - | - | - | 1.2 |
| **Mg** | - | 0.4 | - | 0.6 | 0.1 | 0.3 | - | 0.4 | - | 0.3 | - | 0.6 |
| **Al** | 2.0 | 1.2 | 2.3 | 0.4 | 0.5 | 0.5 | 0.1 | 0.1 | 0.1 | - | 0.1 | - |
| **Si** | 4.9 | 3.2 | 6.1 | 1.3 | 1.2 | 1.3 | 0.1 | 0.3 | - | - | - | 0.1 |
| **S** | - | 1.3 | - | 5.0 | 0.1 | 2.0 | - | 3.1 | 0.2 | 2.0 | 0.2 | 4.9 |
| **Cl** | 0.1 | 0.3 | 1.2 | - | 1.2 | 0.1 | 3.5 | - | 3.8 | - | 3.6 | - |
| **K** | 0.3 | 0.6 | 0.6 | 0.2 | 0.1 | 0.3 | - | 0.1 | - | - | - | 0.1 |
| **Ca** | 1.3 | 0.3 | 1.5 | 1.4 | - | 0.1 | - | 0.6 | - | 0.3 | - | 0.9 |
| **Mn** | - | 0.5 | 1.3 | 0.4 | 0.1 | 0.1 | - | 0.4 | - | 0.8 | - | - |
| **Fe** | 1.0 | - | 4.4 | 1.1 | 0.2 | - | - | 0.1 | - | - | - | - |

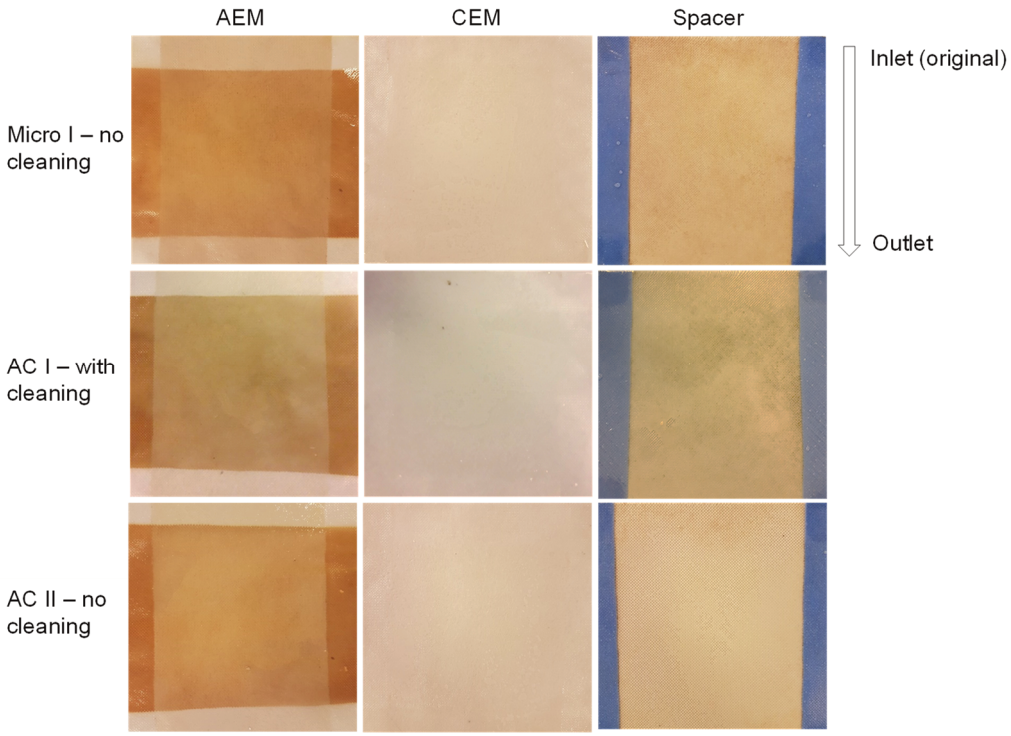


**Figure S 3.3**. Representative images of AEM, CEM and spacer from stacks Micro I, AC I and AC II. The arrow indicates the flow of seawater through the stacks, indicating the inlet and outlet. All pictures are shown with the side of the membrane that was in contact with seawater during the experiment.

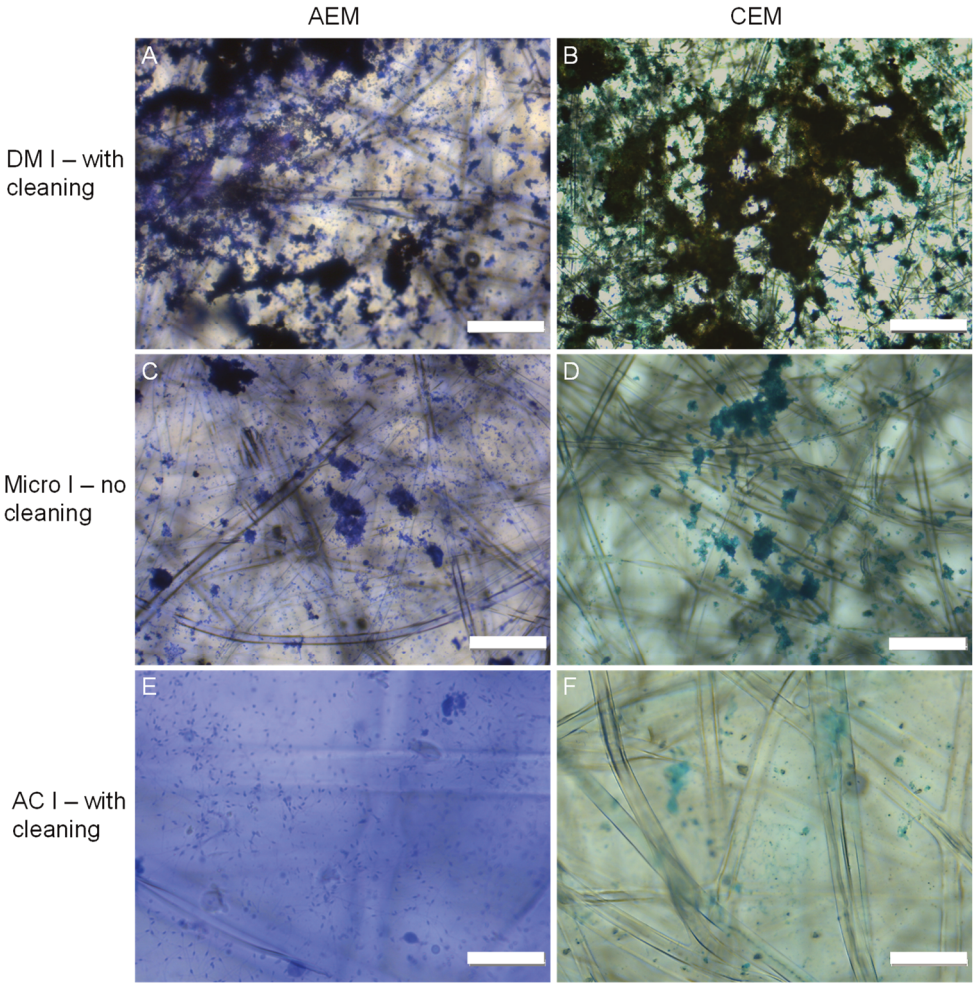


**Figure S 3.4**. Microscopic images of AEM stained with crystal violet and CEM with Alcian blue. The figure shows that in the stacks DM coverage of the membrane surface by large fouling aggregates, later identified as mostly silica compounds is dominant. In stacks Micro this is reduced and biofouling structures started to appear, while in stacks AC the network of connected cells is clearly visible covering most areas of the membrane surface. Scale bar of pictures A, C and D represent 100 µm, of picture B is 200 µm, for E is 20 µm and for F is 50 µm.

**References**


[1] R. E. Pattle, Production of Electric Power by mixing Fresh and Salt Water in the Hydroelectric Pile, Nature 174 (1954) 660.

[2] J.W. Post, J. Veerman, H.V. Hamelers, G.J. Euverink, S.J. Metz, K. Nymeijer, C.J. Buisman, Salinity-gradient power: Evaluation of pressure-retarded osmosis and reverse electrodialysis, Journal of Membrane Science 288 (2007) 218–230.

[3] R.E. Lacey, Energy by reverse electrodialysis, Ocean Engineering 7 (1980) 1–47.

[4] D.A. Vermaas, D. Kunteng, M. Saakes, K. Nijmeijer, Fouling in reverse electrodialysis under natural conditions, Water research 47 (2013) 1289–1298.

[5] S. Pawlowski, R.M. Huertas, C.F. Galinha, J.G. Crespo, S. Velizarov, On operation of reverse electrodialysis (RED) and membrane capacitive deionisation (MCDI) with natural saline streams: A critical review, Desalination 476 (2020) 114183.

[6] W. Guo, H.-H. Ngo, J. Li, A mini-review on membrane fouling, Bioresource technology 122 (2012) 27–34.

[7] R. Oliveira, Understanding adhesion: A means for preventing fouling, Experimental Thermal and Fluid Science 14 (1997) 316–322.

[8] B. Vital, E.V. Torres, T. Sleutels, M.C. Gagliano, M. Saakes, H.V. Hamelers, Fouling fractionation in reverse electrodialysis with natural feed waters demonstrates dual media rapid filtration as an effective pre-treatment for fresh water, Desalination 518 (2021) 115277.

[9] U. Metzger, P. Le-Clech, R.M. Stuetz, F.H. Frimmel, V. Chen, Characterisation of polymeric fouling in membrane bioreactors and the effect of different filtration modes, Journal of Membrane Science 301 (2007) 180–189.

[10] K. Kimura, Y. Hane, Y. Watanabe, G. Amy, N. Ohkuma, Irreversible membrane fouling during ultrafiltration of surface water, Water research 38 (2004) 3431–3441.

[11] M. Herzberg, S. Pandit, M.S. Mauter, Y. Oren, Bacterial biofilm formation on ion exchange membranes, Journal of Membrane Science 596 (2020) 117564.

[12] I. Merino-Garcia, S. Velizarov, New insights into the definition of membrane cleaning strategies to diminish the fouling impact in ion exchange membrane separation processes, Separation and Purification Technology 277 (2021) 119445.

[13] N. Pismenskaya, M. Bdiri, V. Sarapulova, A. Kozmai, J. Fouilloux, L. Baklouti, C. Larchet, E. Renard, L. Dammak, A Review on Ion-Exchange Membranes Fouling during Electrodialysis Process in Food Industry, Part 2: Influence on Transport Properties and Electrochemical Characteristics, Cleaning and Its Consequences, Membranes 11 (2021).

[14] J. Moreno, N. de Hart, M. Saakes, K. Nijmeijer, CO2 saturated water as two-phase flow for fouling control in reverse electrodialysis, Water research 125 (2017) 23–31.

[15] J.W. Post, Blue energy: Electricity production from salinity gradients by reverse electrodialysis, Wageningen University, Wageningen (NL), 2009.

[16] D.A. Vermaas, D. Kunteng, J. Veerman, M. Saakes, K. Nijmeijer, Periodic feedwater reversal and air sparging as antifouling strategies in reverse electrodialysis, Environmental science & technology 48 (2014) 3065–3073.

[17] J. Moreno, S. Grasman, R. van Engelen, K. Nijmeijer, Upscaling Reverse Electrodialysis, Environmental science & technology 52 (2018) 10856–10863.

[18] C. Simões, D. Pintossi, M. Saakes, Z. Borneman, W. Brilman, K. Nijmeijer, Electrode segmentation in reverse electrodialysis: Improved power and energy efficiency, Desalination 492 (2020) 114604.

[19] J. Moreno, V. Díez, M. Saakes, K. Nijmeijer, Mitigation of the effects of multivalent ion transport in reverse electrodialysis, Journal of Membrane Science 550 (2018) 155–162.

[20] J. Moreno, E. Slouwerhof, D.A. Vermaas, M. Saakes, K. Nijmeijer, The Breathing Cell: Cyclic Intermembrane Distance Variation in Reverse Electrodialysis, Environmental science & technology 50 (2016) 11386–11393.

[21] J. Ramus, Alcian blue: A quantitative aqueous assay for algal acid and sulfated polysaccharides, Journal of Phycology 13(4) (1977) 345–348.
[22] O'Toole, G. A., Pratt, L. A., Watnick, P. I., Newman, D. K., Weaver, V. B., and Kolter, R., Genetic approaches to study of biofilms., Methods Enzymol 310 (1999) 91–109.
[23] E.H. Hossen, Z.E. Gobetz, R.S. Kingsbury, F. Liu, H.C. Palko, L.L. Dubbs, O. Coronell, D.F. Call, Temporal variation of power production via reverse electrodialysis using coastal North Carolina waters and its correlation to temperature and conductivity, Desalination 491 (2020) 114562.
[24] A. Zouboulis, G. Traskas, P. Samaras, Comparison of single and dual media filtration in a full-scale drinking water treatment plant, Desalination 213 (2007) 334–342.
[25] Environmental Protection Agency, EPA Water Treatment Manual - Filtration, 1995.
[26] R.S. Kingsbury, F. Liu, S. Zhu, C. Boggs, M.D. Armstrong, D.F. Call, O. Coronell, Impact of natural organic matter and inorganic solutes on energy recovery from five real salinity gradients using reverse electrodialysis, Journal of Membrane Science 541 (2017) 621–632.
[27] D.A. Vermaas, M. Saakes, K. Nijmeijer, Power generation using profiled membranes in reverse electrodialysis, Journal of Membrane Science 385-386 (2011) 234–242.
[28] W. Choi, E.P. Chan, J.-H. Park, W.-G. Ahn, H.W. Jung, S. Hong, J.S. Lee, J.-Y. Han, S. Park, D.-H. Ko, J.-H. Lee, Nanoscale Pillar-Enhanced Tribological Surfaces as Antifouling Membranes, ACS applied materials & interfaces 8 (2016) 31433–31441.
[29] S. Pawlowski, J.G. Crespo, S. Velizarov, Profiled Ion Exchange Membranes: A Comprehensible Review, International journal of molecular sciences 20 (2019).
[30] D. Pintossi, M. Saakes, Z. Borneman, K. Nijmeijer, Electrochemical impedance spectroscopy of a reverse electrodialysis stack: A new approach to monitoring fouling and cleaning, Journal of Power Sources 444 (2019) 227302.
[31] D. Pintossi, M. Saakes, Z. Borneman, K. Nijmeijer, Tailoring the Surface Chemistry of Anion Exchange Membranes with Zwitterions: Toward Antifouling RED Membranes, ACS applied materials & interfaces 13 (2021) 18348–18357.
[32] K. Chon, N. Jeong, H. Rho, J.-Y. Nam, E. Jwa, J. Cho, Fouling characteristics of dissolved organic matter in fresh water and seawater compartments of reverse electrodialysis under natural water conditions, Desalination 496 (2020) 114478.
[33] T. Rijnaarts, J. Moreno, M. Saakes, W.M. de Vos, K. Nijmeijer, Role of anion exchange membrane fouling in reverse electrodialysis using natural feed waters, Colloids and Surfaces A: Physicochemical and Engineering Aspects 560 (2019) 198–204.
[34] M. Grzegorzek, K. Majewska-Nowak, The influence of humic acids on desalination process with the use of electrodialysis, E3S Web Conf. 17 (2017) 27.
[35] S.A. Etha, V.S. Sivasankar, H.S. Sachar, S. Das, Coating for preventing nonspecific adhesion mediated biofouling in salty systems: Effect of the electrostatic and van der waals interactions, Electrophoresis 41 (2020) 657–665.
[36] J. Liu, B. Li, Y. Wang, G. Zhang, X. Jiang, X. Li, Passage and community changes of filterable bacteria during microfiltration of a surface water supply, Environment international 131 (2019) 104998.
[37] Y. Yuan, M.P. Hays, P.R. Hardwidge, J. Kim, Surface characteristics influencing bacterial adhesion to polymeric substrates, RSC Adv. 7 (2017) 14254–14261.

# Chapter 4

# Dual media filtration allows for high-rate pre-treatment for RED application

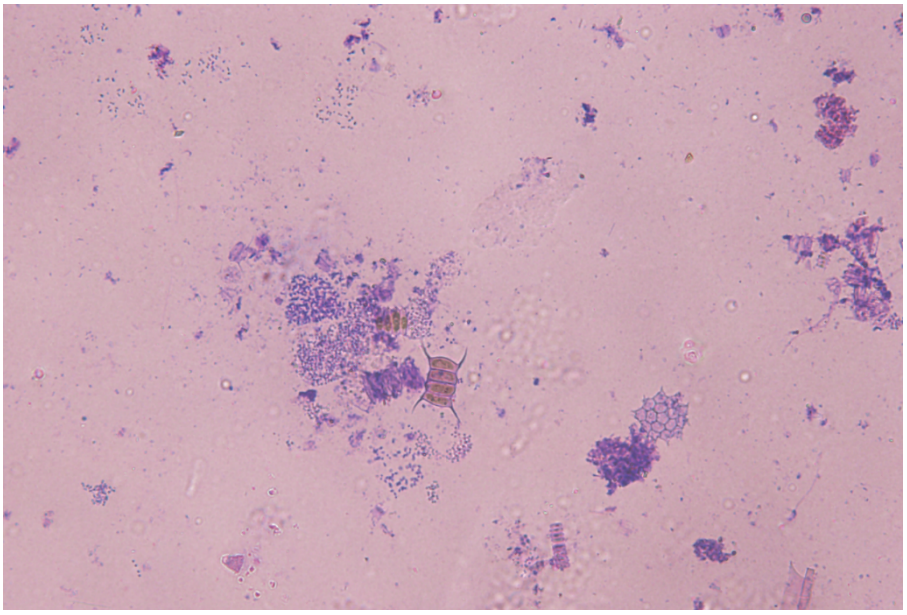

**Abstract:** Reverse electrodialysis (RED) is a technology to harvest the Salinity Gradient Energy (SGE) from the controlled mixing of fresh and sea water, by using ion-exchange membranes. Membrane fouling is one of the biggest challenges that needs to be overcome for suitability of the process for large scale application. Thus, the use of a pre-treatment to prevent the performance losses associated to fouling is needed. In this study, we combined the use of profiled ion-exchange membranes (200 µm thick compartments) with a pre-treatment with different configurations of dual media filter for both natural feedwaters (Ijsselmeer and Wadden Sea). We compared the performance of sand and activated filter media (AFM) as the second layer of the dual media filter and the application of low (~4 $m^3/m^2.h$) and high flow velocities (~20 $m^3/m^2.h$). The use of a high flow velocity showed to be suitable for pre-treatment applications for RED, even though the effluent presents higher turbidity than when treated at low velocity, since the increase of pressure drop in the stacks was limited to around 100 mbar. The use of AFM as filtration media at this high flow velocity showed to be better than sand, delivering better effluent quality. We concluded that the use of AFM and a high flow velocity in dual media filters for RED application is advantageous, allowing for more efficient treatment and reduction of the area occupied by the pre-treatment.

### 4.1 Introduction

Salinity Gradient Energy (SGE) is a renewable energy source that is found in nature where fresh and sea water mix. An advantage of SGE over the more exploited solar and wind power is that it is less dependent on weather conditions. SGE can be harvested using Reverse electrodialysis (RED) [1,2]. RED exploits the potential difference from the controlled mixing of a low and high salinity stream that are separated by ion-exchange membranes, which only allows the passage of either anions or cations. [1–3]. Anion exchange membranes (AEM) and cation exchange membranes (CEM) are alternated in a stack, creating high and low salinity compartments, with the ions moving according to the potential and membrane properties either towards the cathode or anode of a cell [4,5]. In the electrode compartments in the end of the stack pile, redox reactions take place and electrical energy can be harvested [2,4]. In recent years, a lot of attention has been paid to improving RED to be able to add this energy source to the renewable and sustainable energy matrix.

To make RED technology available for the energy market, the challenge with fouling of the ion exchange membranes needs to be addressed, since when using natural waters fouling leads to a reduction of the harvested net power [6,7]. Fouling in RED is influenced by the construction of the stack, and the feed channel's configuration is strongly influencing how fouling attachment occurs. The use of profiled membranes to create feed channels has shown to have benefits over using spacers, due to avoiding the spacer shadow effect [8], creating conditions for better flow distribution [9,10], promoting less fouling attachment [11,12] and avoiding gas bubbles entrapment during two-phase cleaning [12,13]. Thus, for this work the use of profiled membranes was preferred.

Prevention of fouling can be achieved with a suitable pre-treatment that removes a large fraction of the most critical foulants [14]. It is also important that the pre-treatment can withstand variable levels of incoming foulants, a variability that is caused by weather and seasonal variations common for the natural water bodies [15]. Also crucial for the sustainability and economic viability of the process, is that the pre-treatment consumes low amounts of energy since more energy will be available for the grid if less energy is spent in the process.

The use of intensive pre-treatment, such as membrane filtration (micro, ultra and nano filtration [16]), has been tested in lab scale, and although being effective in removing most of the potential foulants and yielding high gross power density, the energy expenditure of these processes is too high compared to the energy production of RED. Other low-energy pre-treatment methods were tested before, such as cartridge filter [13], coagulation with polyaluminum chloride (PAC) [17] or riverbank filtration [18], but either they are not desirable due to their impact on the environment or they are not able to maintain good performance of the stacks.

Previous studies [19,20] showed that a dual media filter can provide a stable effluent quality that does not allow impactful fouling build-up in RED stacks. This filtration system uses a layer of anthracite, a type of coal with high carbon content, which has a large grain size (1.0 - 2.0 mm) and acts as a filter for the larger particles, allowing middle and small particles to pass this filtration layer. The second layer with sand (0.5 - 1.0 mm grain size) filters out the middle range particles. Besides the granule material and the bed height, the operating conditions of such a filter can influence the effluent quality. The flow velocity, which is the velocity that a certain volume crosses the area of the filter (in $m^3/m^2.h$ or m/h), influences the filtration efficiency. At lower velocity, the residence time is longer and allows for better filtration, increasing the chances of particles being retained by the filter, resulting in better effluent quality. In addition, the flow velocity influences the economics of the overall process, since at a higher flow velocity, more treated water is produced using a smaller area of filtration. This will also have an effect on the capex costs of construction (lower capex), but in the operation as well, as the frequency of backwashing is higher (higher opex) [21]. Thus, the flow velocity represents a trade-off with the effluent quality and construction and operational costs.

Other media beyond sand and anthracite have been studied in the past for use for filtration of fresh and sea water [16]. The use of granular activated carbon (GAC) and activated filter media (AFM) showed to be effective in removal of organic matter from treated wastewater effluent in lab scale, but this has not been tested for fresh and sea water at pilot scale yet.

In this study, we combined the use of three different operational conditions of dual media filter pre-treatment of natural fresh and seawater with six RED stacks that were constructed using profiled ion-exchange membranes, which created water compartments of 200 µm thickness. The different operational conditions are based on different flow velocities (5 $m^3/m^2.h$ and 20 $m^3/m^2.h$), with the use of the higher velocity with the goal to reduce capex cost with water pre-treatment, and to compare the different type of media for the best performance (AFM and sand). These three different configurations were compared for their effluent quality and filtration performance, and in addition, the performance of the RED stacks receiving the three different pre-treatment configurations were analysed.

To allow the experimental conditions to be kept constant throughout the experiment, a fully automated dual media filter unit was specifically designed and applied for the water pre-treatment. Finally, only natural feed waters were used to represent the real concentration of foulants, and a membrane autopsy was performed to give insights on the residual fouling after the experiment.

## 4.2 Materials and Methods

### 4.2.1 Experimental Setup

The experiment was performed in the pilot plant installation at the REDstack BV facility located in De Afsluitdijk, a dike in Breezanddijk, the Netherlands. Three different configurations of pre-treatment were used to feed six stacks that were operated in parallel, in a way that every two stacks received the same treated feed water and were duplicates (Fig. 4.1). The three pre-treatment configurations were:

1. **Sand – Low:** dual media filter with a 77 cm layer of sand (0.5 mm – 1.0 mm) and 77 cm of anthracite (1.2 mm – 2.0 mm) operated at a low flow velocity (~ 4 $m^3/m^2.h$). This flow velocity is comparable to the traditional use of dual media filters for drinking water production [22].
2. **Sand – High:** dual media filter with a 40 cm layer of sand (0.5 mm – 1.0 mm) and 40 cm of anthracite (1.2 mm – 2.0 mm) operated at a high flow velocity (~ 20 $m^3/m^2.h$). The higher flow velocity allows for a smaller footprint of the filtration system.
3. **AFM – High:** dual media filter with a 40 cm layer of AFM (type 1) and 40 cm of anthracite (1.2 mm – 2.0 mm) operated at a high flow velocity (~20 $m^3/m^2.h$).

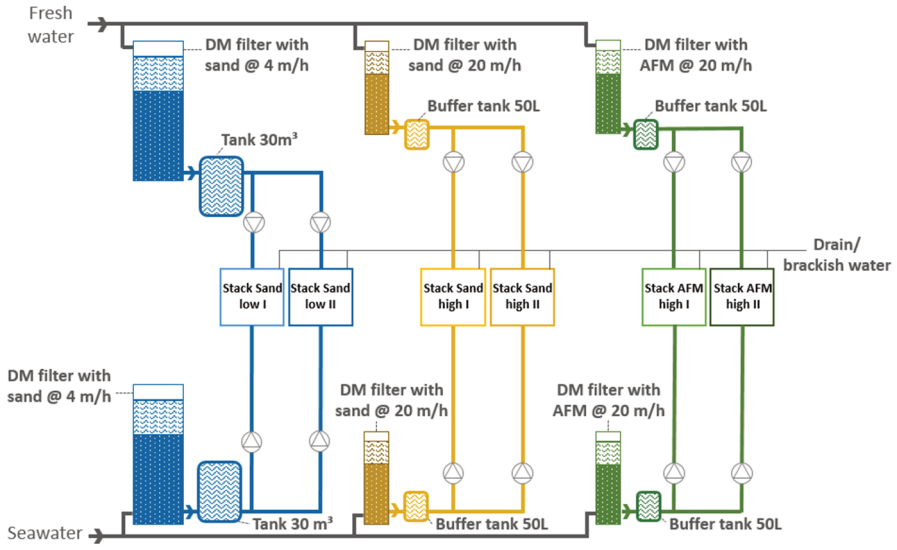


**Figure 4.1.** Schematic representation of the experimental set-up used for the experiments presented in this work. Six stacks were operated, with each couple of stacks as duplicates. The different conditions were in the pre-treatment of the feed waters.

Other conditions and operational configurations of the filters are given in Table 4.1. The experiment lasted for 16 days of continuous operation of the filters and the six connected stacks (Fig. 4.1).

**Table 4.1.** Configuration of the three different pre-treatments parameters

| Filter description | Flow velocity ($m^3/m^2.h$) | Media composition | Area filter ($m^2$) | Backwash frequency | Backwash procedure | Buffer tank ($m^3$) |
|---|---|---|---|---|---|---|
| Sand - Low | 4 | 77 cm anthracite + 77 cm sand | 4.9 | 12 hours | Air + backflow treated effluent | 30 |
| Sand - High | 20 | 40 cm anthracite + 40 cm sand | 0.052 | 6 hours or 600 mbar | Backflow treated effluent | 0.05 |
| AFM - High | 20 | 40 cm anthracite + 40 cm AFM | 0.052 | 6 hours or 600 mbar | Backflow treated effluent | 0.05 |

### 4.2.2 Profiled membranes and stack operation

10 x 10 cm crossflow stacks were supplied by REDstack BV (The Netherlands), and were built equally, with eight cell pairs each. They were operated in the same way, with a flow velocity of 1 cm/s. CMH-PES and AMH-PES membranes supplied by Ralex (Mega, Czech Republic) were used in the experiment and their properties can be found in a previous study [23]. The choice for heterogeneous membranes is due to the possibility of making profiles with the thermo-press method, as described in literature [23–25].

The profiles were made on both sides of the CEM membranes, to create the feed water compartments. A cross flow pattern was used; the profiles were positioned perpendicularly. The AEMs were positioned between the CEMs as delivered by the supplier. The profiling procedure consisted of pre-heating moulds for 2 minutes at 140 and then applying 200 bar of pressure for 10 minutes. The moulds were sprayed with releasing agent and the membranes were cooled to 50°C maintaining the applied pressure. The height of the profiles was around 200 µm, which is thus the intermembrane distance in the stack.

Titanium meshes with a galvanic platinum coating were used as electrodes of the stacks and were supplied by Magneto Special Anodes B.V. (The Netherlands). As the electrolyte rinse a solution of 0.05 M $K_3Fe(CN)_6$, 0.05 M $K_4Fe(CN)_6$ and 0.25 NaCl (VWR, USA) was recirculated in the electrode compartments and kept at 0.3 bar over pressure. Pressure difference was

continuously measured by a transmitter (Yokogawa, Japan) connected to the outlet and inlet of the stacks and logged with a data logger (Yokogawa, Japan) every 5 seconds.

A potentiostat (Iviumstat, Ivium Technologies, the Netherlands) was used to apply current and measure the voltage, by connecting it to a peripheral differential amplifier for independent measurement of each stack. Chronopotentiometric series were applied throughout the experiment allowing for measuring the open circuit voltage (OCV) and calculating gross power density based on I-V curves. When no chronopotentiometry was applied, the stacks were operated at constant current density to simulate the RED process.

#### 4.2.3 Fouling removal water analysis and membrane autopsy

Samples of the influent and effluent of sea and fresh water from all the filters were taken and analysed throughout the experiment to analyse the performance of the different configurations of filters. These samples were analysed for turbidity, total suspended solids and particle size distribution (PSD) using the same procedures described in [20].

To compare the different stress conditions that the filters were subjected to, the cumulative turbidity load removed by the filter in each cycle was defined as the cumulative difference of turbidity of the influent and effluent normalized by the volume of treated water per area of the filter, in $NTU.m^3/m^2$. A similar approach is used to define the total turbidity load received by the stacks, but in this case only the turbidity of the effluent of the correspondent filters and the volume of water that crosses the stack are used, resulting in the unit $NTU.m^3$.

All stacks were subjected to a membrane autopsy at the end of the experiment to analyse remaining fouling on the membrane and to determine how the different pre-treatment configurations affected the fouling layer. Fouling was evaluated by both naked eye, presented as camera photos, and by SEM-EDX microscopy images. Before SEM-EDX procedure, membrane pieces were fixed with 2.5% glutaraldehyde solution overnight and dehydrated with graded series (30, 50, 70, 90 and two times 100%) of ethanol for 20 minutes each step and finally dried for 30 minutes at 55ºC oven. The SEM analysis was performed with a JEOL JSM-6480LV (JEOL, Japan) at an acceleration voltage of 6 kV and magnifications up to 15,000X [20].

Finally, to quantify remaining fouling on the membrane surface, duplicate membrane pieces of 5x5 cm were cut and placed in 30 ml of 90 g/L NaCl solution, aiming to extract as much foulant as possible from the membrane surface. To create as much disturbance as possible on the membrane surface and allow the foulants to be solubilized, the membrane pieces were placed in a shaker for 30 min, followed by 30 min on the ultrasonic bath and left overnight at 4° C. The next day, the samples were again shaken for 30 min, and suspended solids and humic acids analysis were performed in the same way as the effluent water for the filter, as described earlier in this section.

## 4.3 Results and discussion

The effect of the different pre-treatment configurations was evaluated by monitoring the variations of influent and effluent quality of the filters in time along with the performance of the RED stacks fed with the filters' effluent. Finally, membrane autopsy was applied to identify residual fouling on the membrane surface.

### 4.3.1 Filters operation comparison

The performance of the dual media filtration pre-treatment was evaluated by the flow velocity (Fig. S 4.1), differential pressure across the filter (Fig. 4.2) and duration of filtration cycles (Fig. S 4.2), the time in between two backwashing events. The two main characteristics of the pre-treatment are the application of low versus high flow velocity and the use of sand or AFM as second bed media.

For both low and high velocity (~4 $m^3/m^2.h$ and 20$m^3/m^2.h$), the flow (Fig. S 4.1) is mostly maintained at the desired level. However, the flow fluctuated within each filtration cycle, due to the clogging of the filter, which increased the pressure over the filter. Most variations in flow therefore occurred due to high loads in the influent. In the case of Sand – High and AFM – High the flow through each of these filters was affected by the other one, as both filters were supplied by the same feed pump (one pump for both freshwater filters and another pump for both seawater filters).

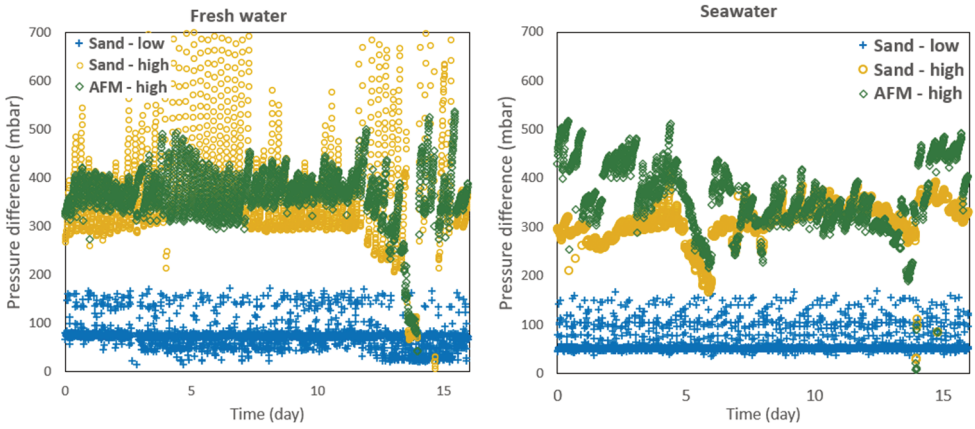


**Figure 4.2.** Pressure difference across the six filters. The legend refers to type of media used and flow velocity that was aimed to be maintained during operation.

The pressure difference across the filters is expected to increase during a filtration cycle, as foulants are being filtered and retained in the filtration media (Fig. 4.2). Thus, depending on the water quality of the influent, variations in pressure difference over the filters are expected. For the filter AFM-High in freshwater the increase of pressure during a cycle is

around 100 mbar, with some cycles between days 8 and 12 even having lower increase of pressure, around 50 mbar. However, the pressure difference on the filter Sand - High for freshwater varied more than expected during the experiment, exceeding 500 mbar in some days, due to a malfunction of the pressure meter is some days. For Sand – low filters the variation of pressure within a cycle are minimal, which can be due to the low filtration velocity and smaller foulants loads reaching the filters. For the seawater filters, the variability among cycles was greater than for freshwater, due to the large variations in the amount of received foulant loads. Still, mostly for Sand – High and AFM – High, the increase in pressure drop during a cycle is around 100 mbar. Other variations in the pressure difference are related to the flow and not the fouling, as in day 5 in seawater and day 14 in freshwater.

The fouling removed from the feed waters with the filters in terms of turbidity load is shown in Figure 4.3, from day 4 until day 10 of the experiment, which is the most stable period of operation.

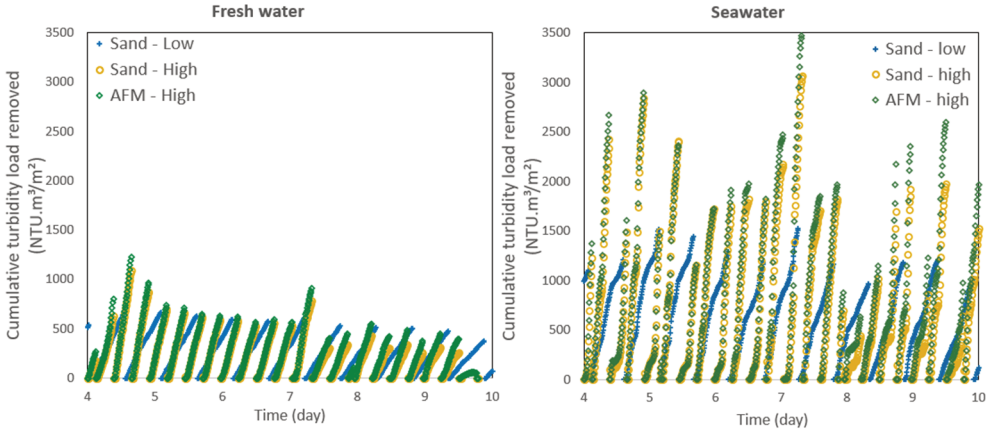


**Figure 4.3.** Cumulative turbidity load removed per cycle with each filter in NTU.m³/m², from day 4 until day 10 of the experiment.

For freshwater the benefit of the high velocity is limited when considering just the turbidity load removed, since the turbidity removed per cycle was similar to the one in the low velocity (Fig. 4.3). With the higher flow velocity, the turbidity load is removed from the filter faster, but the amount that is removed, which is intrinsically related to the flow and the duration of the filtration cycle, is similar to the removed at low velocity in one cycle. For example, during one cycle at low velocity (that lasts 12 hours) up to 1000 NTU.m³/m² is removed from freshwater feed. At high velocity, the cycle lasts 6 hours and removes a similar amount of turbidity, meaning that although it is possible to remove the load faster with the use of high velocity, the effluent quality is reduced and frequency of backwashing

increases. The ratio of increase in the flow velocity between the high and low velocity is around 5 times. Moreover, for seawater, the use of high velocity is more advantageous than for freshwater since the removed turbidity load during the high velocity filtration is about 4 times more than at low velocity when considered the same period (Fig. 4.3). The removal of turbidity load is lower than the ratio of the applied velocities due to a decrease of the effluent quality in the high velocity cycle, but the benefit lies in the faster removal of turbidity load with the high flow velocity. Thus, at high velocity, the removal of turbidity is more efficient, and the filter can reach a better balance of load received and backwashing need, using its capacity of treatment more efficiently.

The application of higher flow velocity during the filtration is an important parameter for the further development of RED, since it allows for the treatment of feed water with a lower area footprint filter than with the more usual flow velocity of 4 $m^3/m^2.h$, for example. With a smaller footprint of the filters, also the investment cost will be lower. On the other hand, the use of high flow velocities results in more frequent backwashing, which can be seen as an increase of the operation costs. A balance must be found between a higher production rate of water and the downtime of the pre-treatment due to backwashing.

To put this balance in perspective: the total amount of treated water produced in one cycle of 6 hours of the filter running at high velocity (20 $m^3/m^2.h$) is 120 $m^3$ per $m^2$ of filter area, while for the filter at low velocity (4 $m^3/m^2.h$), one cycle of 12 hours can produce 48 $m^3$ per $m^2$ of filter area. In both filters' configuration, backwashing is set in the same way with a total duration of 20 min and backwash velocity of 20 $m^3/m^2.h$ to allow proper bed expansion and a rinsing step for the settling of the bed. Thus, backwashing consumes around 7 $m^3$ per $m^2$ of filter. Thus, per cycle, the high flow velocity produces a net amount of 113 $m^3/m^2$ and operates 6.3 hours, while the low velocity cycle produces 41 $m^3/m^2$ and operates 12.3 hours. An effective flow velocity can be defined as the volume of treated water produced by area of the filter divided by the duration of the cycle, which represents the real flow velocity accounting for the downtime and use of treated water for backwashing. For the high velocity this real flow velocity is 17.9 $m^3/m^2.h$ while for the low velocity is 3.3 $m^3/m^2/h$.

This means that the ratio of produced treated water with the high velocity by the low velocity is 17.9 $m^3/m^2.h \div 3.3\ m^3/m^2.h = 5.35$, which is more than the factor of the high and low velocities applied (20 $m^3/m^2.h \div 4\ m^3/m^2.h$) = 5.0. This shows that the negative aspect brought in by the increase of backwashing with the higher flow velocity is offset by the benefit of producing more water in the same period.

### 4.3.2 Filtration efficiency based on influent and effluent water quality

The influent water quality was monitored inline by means of turbidity, as shown on Figure 4.4. In addition, offline measurements were made by taking samples for further analysis, such as particle size distribution and suspended solids, as shown on Figure 4.5.

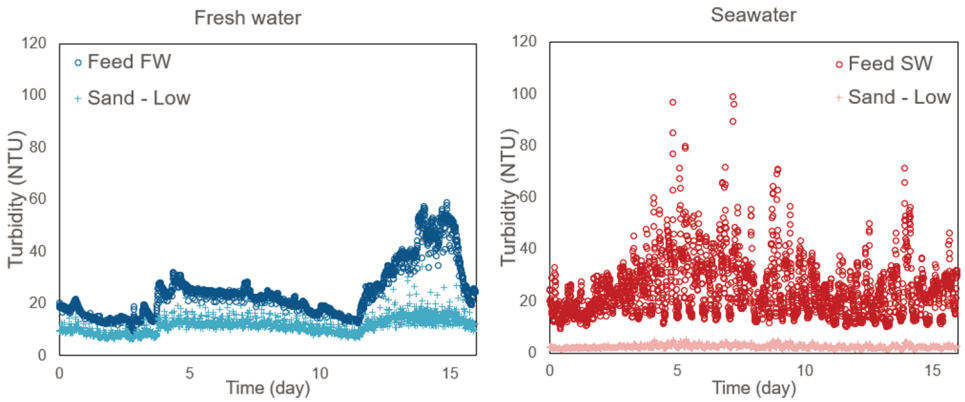


**Figure 4.4.** Turbidity measured continuously during the experiment. Influent fresh and sea water and the effluent of the filters sand low as reference.

Influent quality of seawater presents large daily variations, as seawater quality is heavily influenced by weather events, such as wind and rain. During the experiment, influent turbidity surpassed 50 NTU about 19 times (Fig. 4.4), showing that the high inflow of turbidity is frequent, but the duration is short. This demands that the filters can handle these momentously high loads without significative losses of effluent quality. This is achieved by the filtration with Sand - Low filters (Fig. 4.4), where the quality of the treated water remains rather constant (below 5 NTU) even with the variations of influent. As for the freshwater influent quality, the variations are less frequent and less intense in terms of loads, with steadier build-up or decrease of turbidity load. The amount in terms of turbidity is also lower, as 50 NTU is only surpassed 3 times during the experiment (Fig. 4.4). However, the effluent quality of the treated freshwater, represented by Sand-Low filter, is worse and it is more impacted by the influent quality variation than seawater treatment (Fig.4.4).

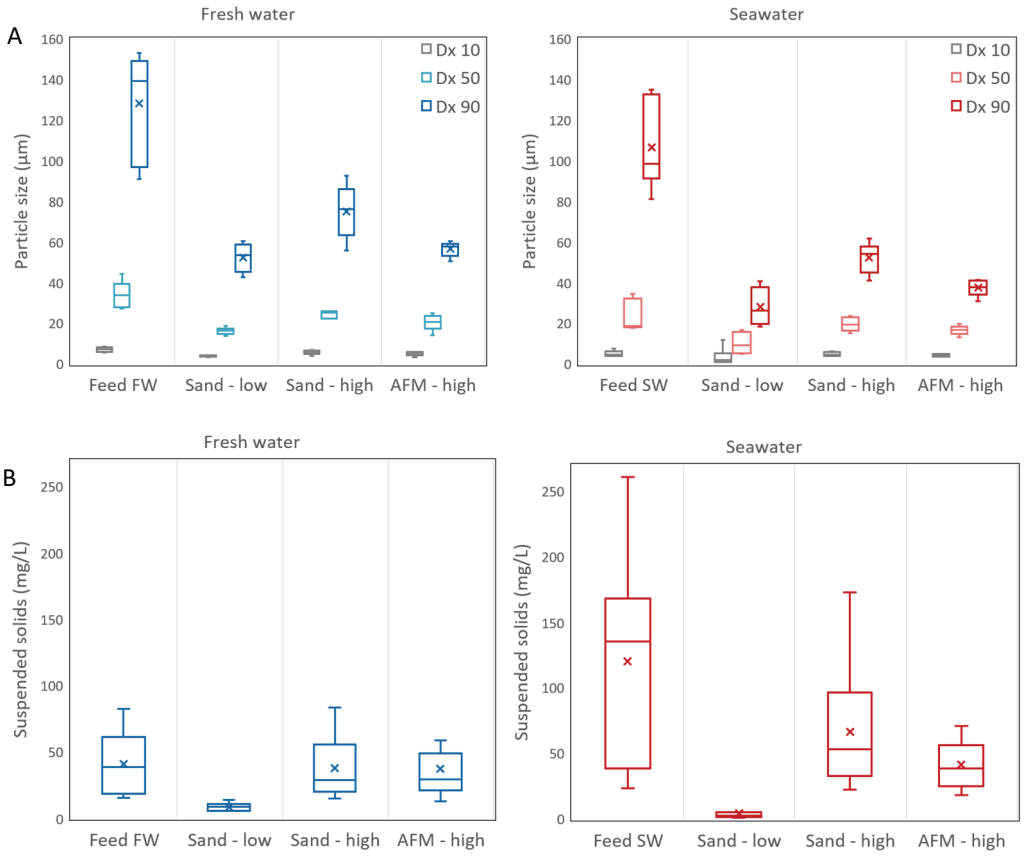


**Figure 4.5.** (A) Box plot distribution of particle size in the influent for the filters and in their respective effluent. Dx 10 value represent that 10% of the particles in the sample are smaller than this value, while Dx 50 is the same for 50% of the particles and Dx 90 for 90% of particles. (B) Box plot distribution of the values for total suspended solids of the samples collected during the experiment.

The particle size distribution (Fig. 4.5A) analysis gives insights in the reasons that can lead to the better filtration of seawater, since turbidity is a measurement that does not directly correlate with particle size. The particle size distribution for freshwater shows that 90% of the particles are smaller than 140 µm, while 50% is smaller than 40 µm. For seawater, the particle size distribution shows that 90% of the particles is smaller than 110 µm while 50% is smaller than 20 µm. This means that seawater has a larger fraction of medium range particles (< 100 µm) than freshwater. Thus, in the filtration of seawater mostly the removal of the particles above the medium value (20 µm) is required for good effluent quality, while for freshwater is needed to remove the large (140 µm) and medium particles (40 µm) for good effluent quality. Thus, the removal of these medium size together with the large particles seems to be more difficult to achieve with the dual media filtration, resulting in a worse effluent quality.

Besides the particle size distribution, also the concentration of particles is of importance, which is presented by the measurement of the suspended solids (Fig. 4.5 B). This shows that the seawater influent contains higher levels of particles, and their concentration had a larger variation among samples than in fresh water. This variation in concentration correlates with the high variation of turbidity measurements (Fig. 4.4) and the influence of weather events, such as rainfall and storms. For freshwater the concentrations of solids were lower (Fig. 4.5 B), as expected from the turbidity measurements, however due to the particle size, the filter efficiency is lower than in seawater.

In both of this measurements (particle size and suspended solids) AFM shows to filtrate better than sand, given that the effluent of AFM filtration presents smaller particles (Fig. 4.5A) and smaller concentration of solids (Fig. 4.5B) than sand, when comparing only the filters running at high flow velocity. This is probably due to the large active surface area of the material available for interaction with the foulants [26]

For the filters running at higher velocity, the treatment efficiency was reduced when the influent load in terms of suspended solids was lower (< 30 mg/L). This can, for example, be seen in the comparison of two days, day 9 and 15, with different influent qualities due to different amounts of solids (Fig. 4.6).

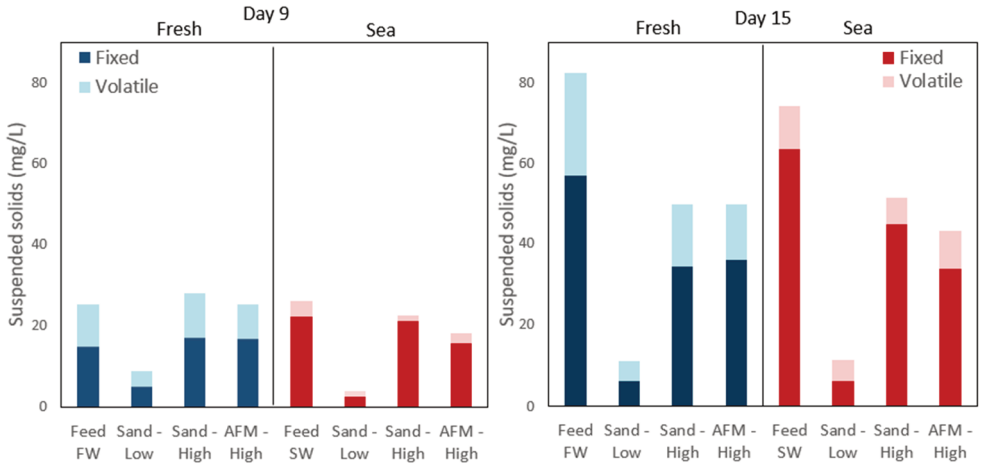


**Figure 4.6.** Comparison of suspended solids received by each filter in day 9 and 15 of the experiment.

On day 9, the influent load was low (< 30 mg/L) for both sea and fresh water and the filters at high velocity could not remove solids from the influent (Fig. 4.6). On day 15, the scenario was different, with high level of influent solids in both sea and fresh water (> 70 mg/L). In this case, the filters at high velocity managed to remove about 40 % of the solids from both the influent feed waters. The treatment in low velocity removed large amounts of solids in

both cases (65% to 95%) (Fig. 4.6), due to a longer residence time providing more time for interaction between foulants and bed media.

### 4.3.3 Stacks performance

To assess the effectiveness of the filtration pre-treatments, RED stacks receiving the effluent of the three filters configurations were also evaluated in terms of performance. The pressure drop between inlet and outlet of the stacks is the main parameter for indication of fouling and its increase during the experiment is shown in Fig. 4.7. The electrical performance of the stacks was not affected by fouling during the experiment, as shown on Fig. S 4.3.

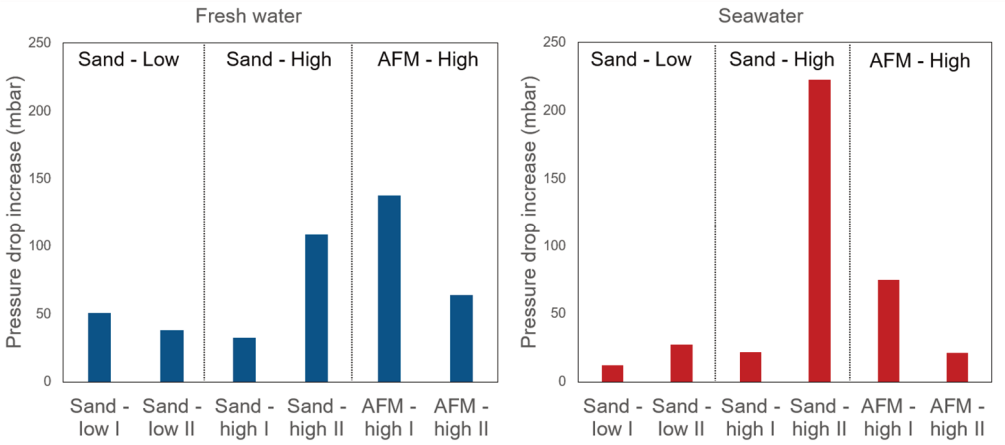


**Figure 4.7.** Pressure drop increase in the stacks' compartments, from the beginning until the end of the experiment.

The stacks receiving the treated water from Sand-Low filters had the lowest average increase of pressure, while Sand-High has the highest average value (Fig. 4.7). This is in agreement with the effluent quality of the water after the pre-treatment (Fig. 4.6 and 4.7), with the low velocity filtration yielding the best results. However, at a higher velocity, AFM was filtrating better than sand, and this can be seen by the lower increase of pressure drop in the AFM stacks (Fig. 4.7). Overall, the duplicate stacks had low similarity in results, especially for the stacks receiving the filtered water at high velocity (Fig. 4.7). The duplicate stacks received the same treated water, but it seems the accumulation of fouling in the compartments can be triggered by factors different than only the water quality. In the case of freshwater compartments, the stacks receiving treated water from the filter Sand-Low had the smallest pressure increase, followed by Sand-High and as last AFM-High (Fig. 4.7). In the case of seawater, most compartments presented an increase of pressure drop during the experiment below 50 mbar, while the stack Sand-High II showed a significant discrepancy in comparison to the other compartments, with a value above 200 mbar.

Overall, for the majority of feed water compartments of the stacks the increase of pressure drop during the experiment is below 100 mbar, which is reasonable and with the application of an adequate cleaning procedure, the related pumping losses can be mitigated [12].

The fouling build-up in the stacks can be estimated by the total load in terms of turbidity that each stack received during the experiment, as shown in Figure 4.8.

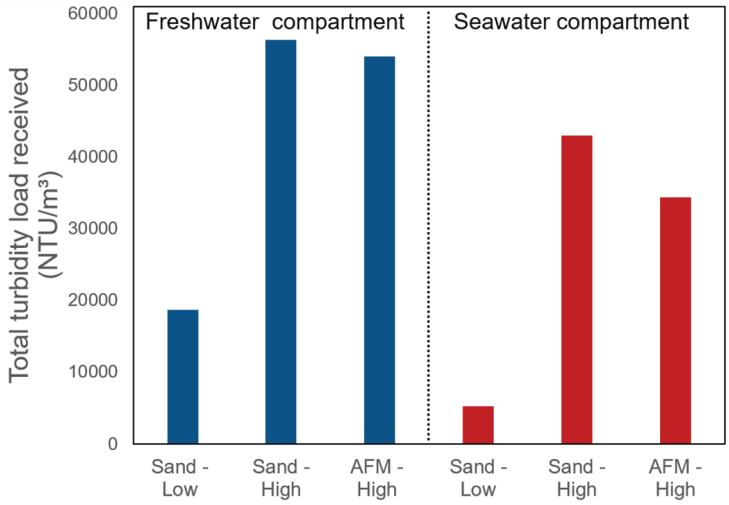


**Figure 4.8.** Total turbidity load received by the stacks during the experiment in NTU/m³.

Due to a lower turbidity of the effluent of the filters running at low flow velocity (Fig. 4.8), both in freshwater and seawater compartments, the received load of the stacks was lower than from the high velocity filters. In the fresh water compartment the load received in the stack after filtration at low velocity corresponds to about 35% of the load received by the filters at high velocity (Fig. 4.8). For seawater compartment this value was about 15%. This explains the increase of pressure drop in the stacks receiving the water treated at high velocity, even though the difference among the increase of pressure drop of the stacks (Fig. 4.7) is not necessarily the same as the values of total load received (Fig. 4.8). This could be due to the particulate foulants, represented by turbidity (Fig. 4.8), just crossing the stacks and not attaching to the membrane and not causing an increase in pressure drop. In RED, the direction of the water flow is parallel to the membrane surface, which lower the chances for interaction between foulants and membrane, allowing a fraction of the particles to just cross the stack and not be attracted to the membrane.

### 4.3.4 Membrane autopsy

At the end of the experiment (day 16) all stacks were subjected to a membrane autopsy, where membrane samples were visually analysed. Both visual observation (Fig. S 4.4) and SEM (Fig. S 4.5) showed that the stacks fed by the low velocity filtration pre-treatment

overall presented less fouling. This was also confirmed by the analysis of residual fouling on the membrane surface (Fig. 4.9) showing that suspended solids were found in higher concentrations on the membranes from stacks Sand – High (1.5 – 7 g/m²), followed by lower values in stacks receiving the treated water from AFM – High (1 – 2.7 g/m²) and even lower for the stacks Sand – Low (0.3 – 0.7 g/m²) (Fig. 4.9 A). The solids were not especially more attracted to the CEMs or AEMs, as the membrane with higher concentration of solids varies in each stack (Fig. 4.9 A).

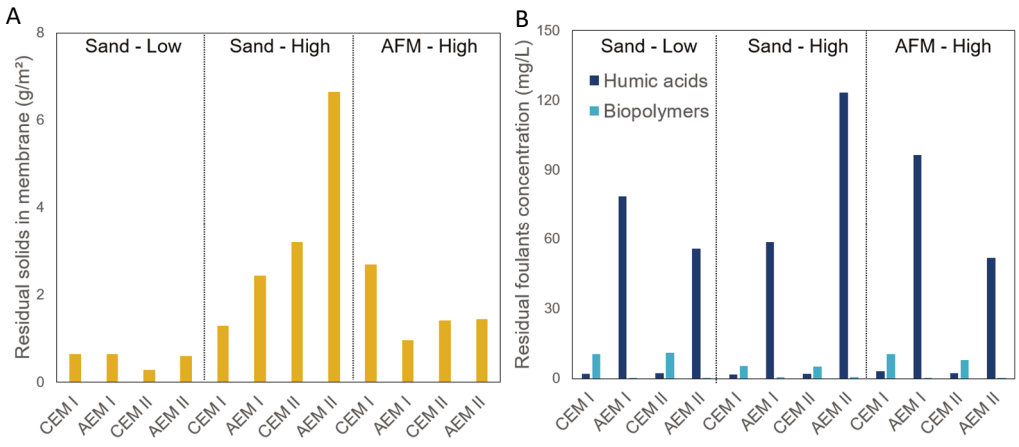


**Figure 4.9.** Estimation of residual membrane fouling (solids in A, humic acids and biopolymers in B) on membrane surface of CEM and AEM of each stack.

The residual fouling was mostly from humic acids for the AEMs (Fig. 4.9 B). The negatively charged humic acids have a strong interaction with the positive charges of the AEMs [27,28]. The CEMs however, accumulated instead, mostly biopolymers, even though observed values were at lower scale than for humic acids (Fig. 4.9 B). Humic acids values varied in each stack from 50 until 120 mg/L, and again stacks Sand – High had the highest concentrations, showing that especially stack Sand – high II was affected by humic acids fouling. Interestingly, this stack had the lowest value of fouling by biopolymers in the CEM (5 mg/L) (Fig. 4.9 B).

These results of the residual solids in the membrane surface (Fig. 4.9) are in in agreement with the effluent quality data (Fig. 4.6) and the increase of pressure drop data (Fig. 4.7), indicating that the stacks receiving the effluent treated with low velocity filtration were subjected to lower load of foulants (Fig. 4.8), which results in lower pumping losses in these stacks.

## 4.4 Conclusions

Different configurations for dual media filtration were tested, showing that a high flow velocity/loading rate (~20 m³/m².h) is suitable for pre-treatment applications for RED. As

expected, the effluent quality decreased with the higher loading rate, however the minimal level of treatment needed for RED was achieved, since the impact of fouling on the RED stacks is low (< 100 mbar). Also, due to fouling reaching the stacks being mostly composed of particles in the effluent of filtration, other studies [12] have shown that it is possible to control the pumping losses with in-situ cleaning techniques.

The variation of inflow turbidity was shown to affect the effluent quality of the filters, thus, when the feedwaters would have higher turbidity due to weather events, the effluents of all the filters configuration studied would also present higher turbidity, which would reach the stacks. The filters running at higher velocities were more affected by these events, due to receiving more load at shorter time interval. When the inflow of suspended solids loads was low (< 30 mg/L), the filters running at high velocity would barely remove the foulants, while with higher feed loads (> 70 mg/L) the removal could reach around 50%.

The frequency of backwashing of filters had to be increased with the use of a high velocity. However, comparison of the load removed during one filtration cycle showed that at high velocity the bed of the filter is used more efficiently and resulted in more turbidity removed than filtration at lower velocity for seawater. The main benefit of using the filters at high flow velocity lies in the reduction of the area needed for filtration, which leads to a reduction of construction costs of the filters. The use of AFM as media when applying high flow velocities is preferred, since this type of media can yield better effluent quality than sand in terms of suspended solids and size of particles.

**Supporting Information**

**Filters and stack performance**

The flow velocity achieved by the six different filters was logged during the experiment and it is presented in Figure S 4.1. Variations in the flow occurred during each cycle, due to accumulation of fouling causing a higher resistance for the filtration of the water and reducing the flow. Larger variations occurred due to high turbidity in the feed waters, causing the filters to clog and the flow to be reduced.

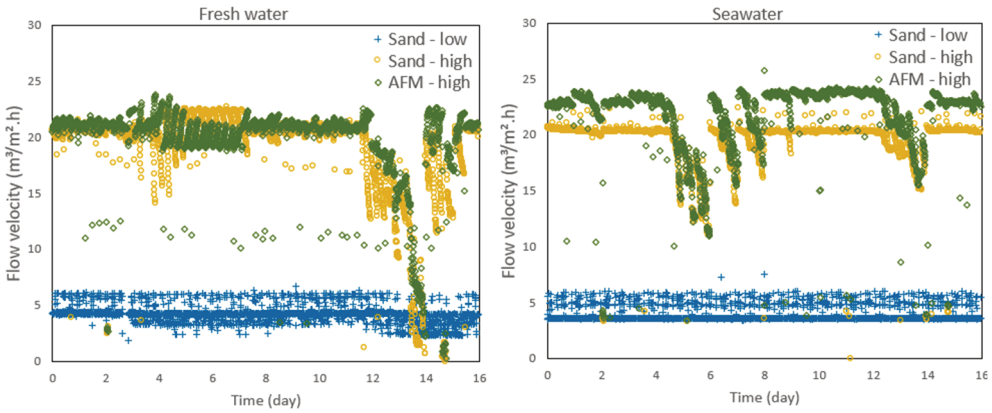


**Figure S 4.1**. Flow velocity for each of the six filters, separated by influent source (fresh water and seawater). The legend refers to type of media used and flow velocity that was aimed to be maintained during operation.

The duration of each filtration cycle is shown minutes in Figure S 4.2. The normal duration of the cycle at low velocity corresponds to 12 hours and for the cycle at high velocity to 6 hours. A few times the filters at high velocity had to be backwashed more frequently than 6 hours due to high turbidity in the feed waters.

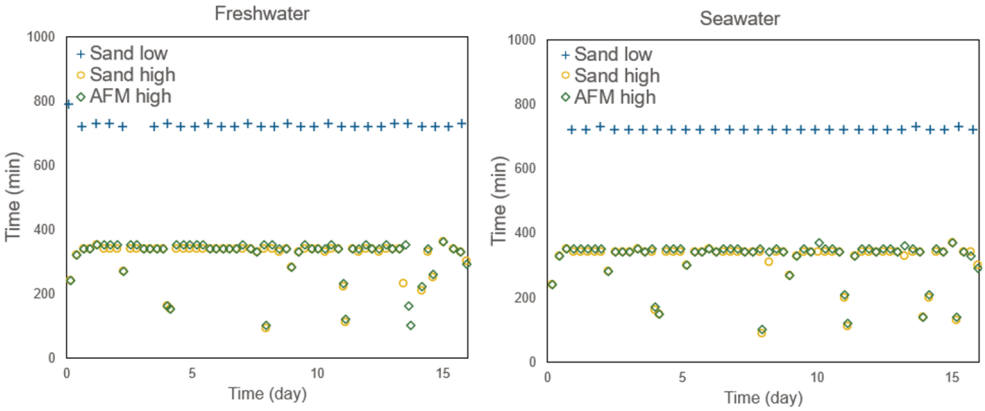


**Figure S 4.2.** Duration of filtration cycles for the six filters. The duration of the cycles is mainly due to time set to backwash.

The electrochemical performance of the stacks is shown in terms of open circuit voltage (OCV) in Figure S 4.3. The values remain constant during the experiment, except for variations due to the salinity of the waters, which impact all the stacks similarly.

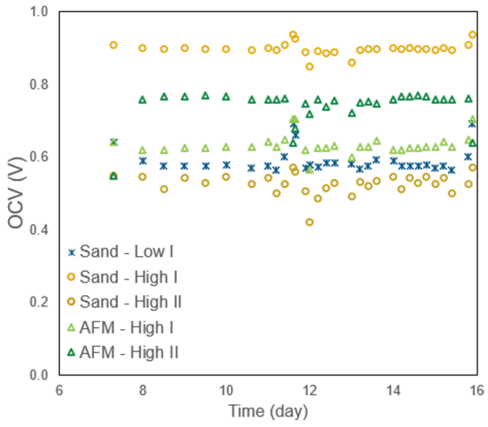


**Figure S 4.3.** Open circuit voltage (OCV), of the stacks during the experiment.

**Membrane autopsy**

Pictures of the membrane surface of both CEM and AEM of each stack is shown in Figure S 4.4. The stacks Sand – High and AFM – High had more incidence of solids on the CEMs.

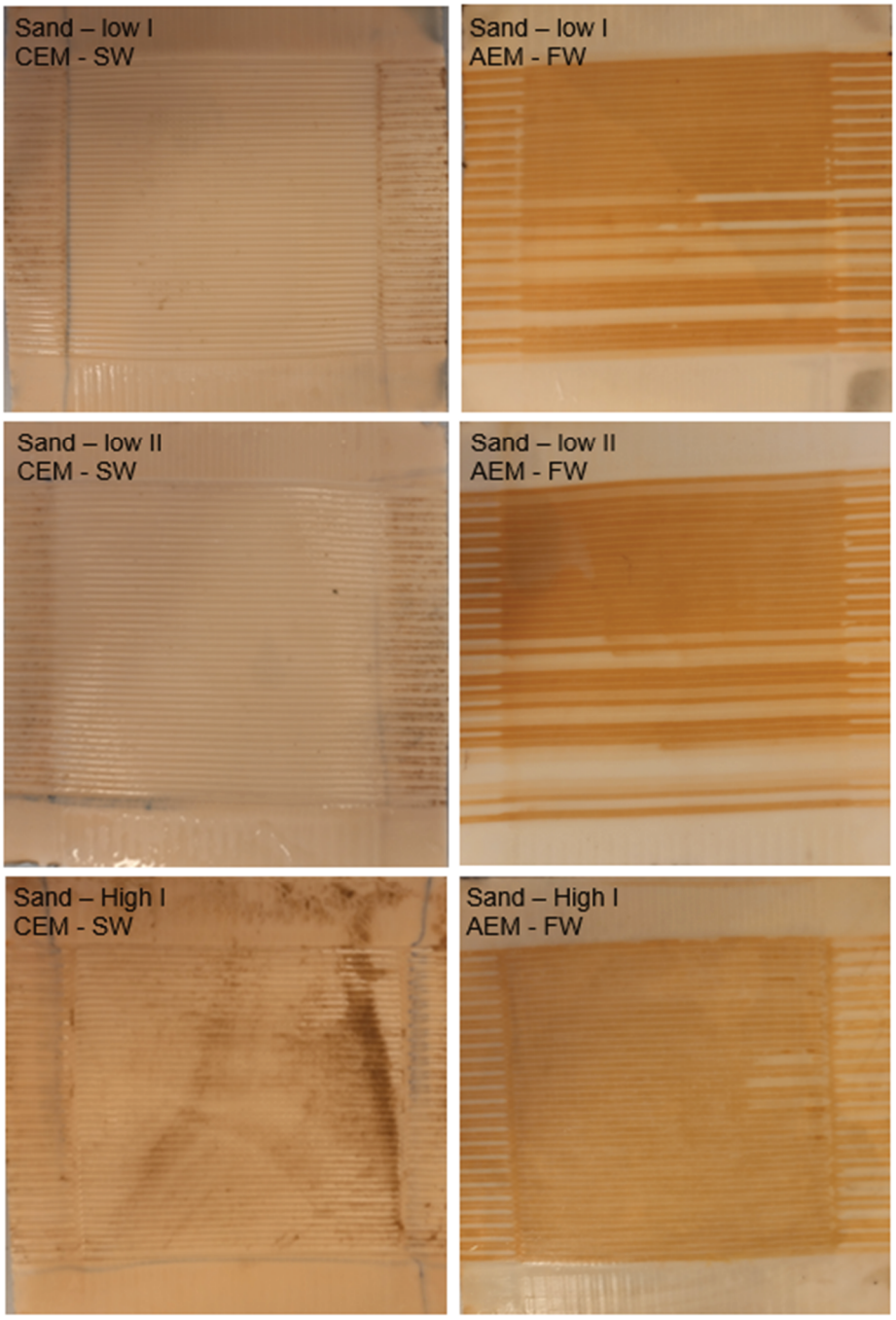

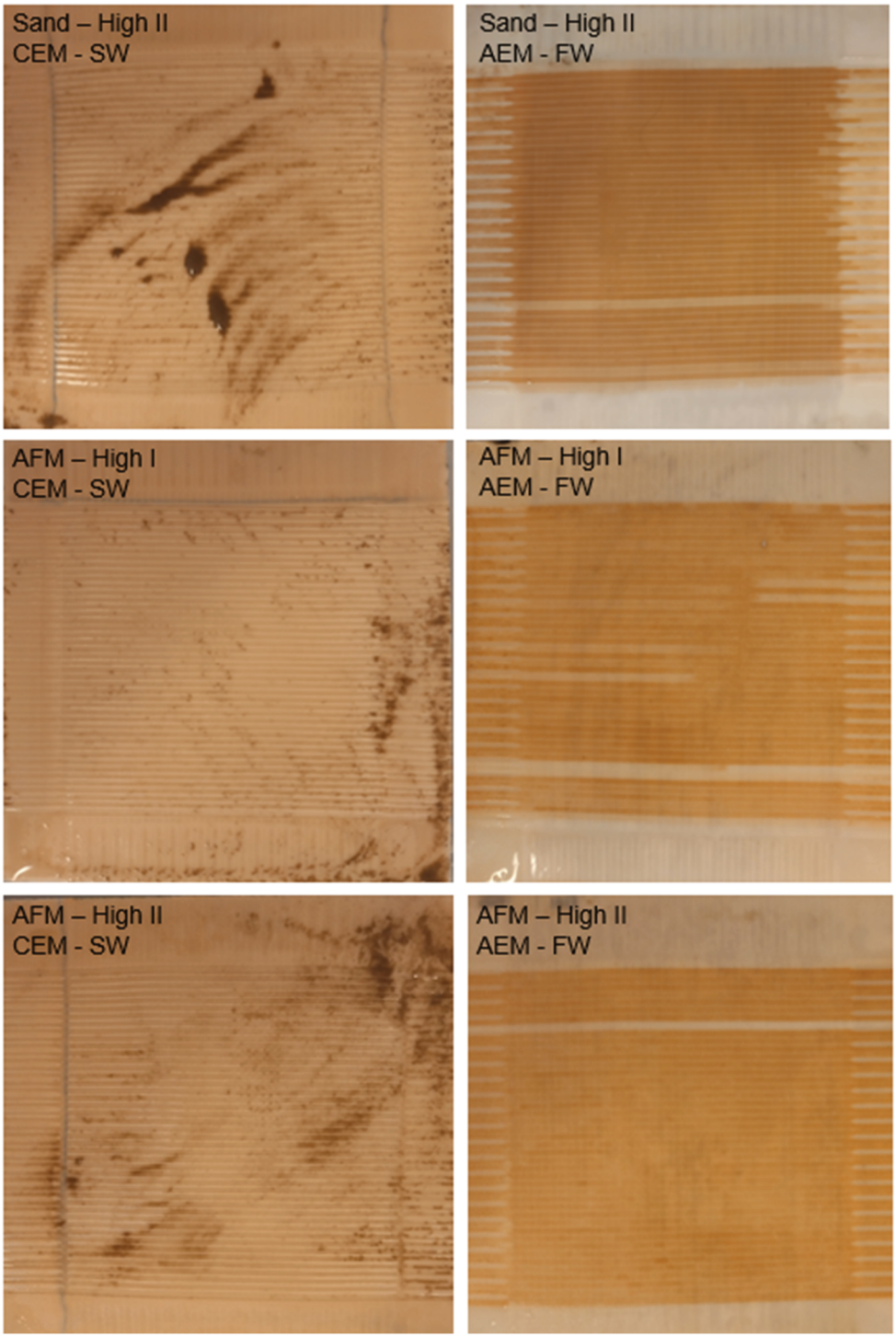


**Figure S 4.4.** Images of membrane surface of both CEM and AEM of each stack after the experiment

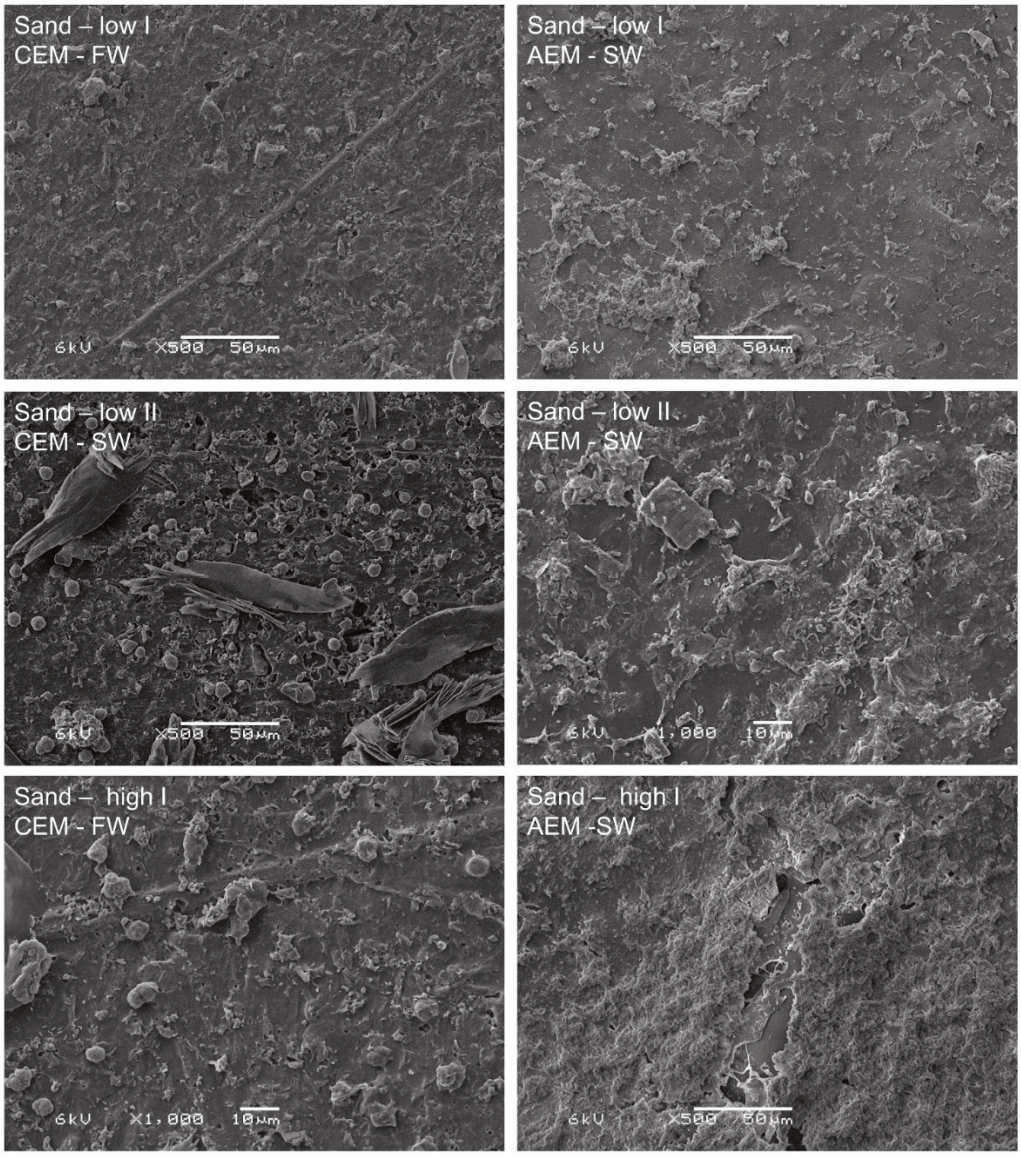


**Figure S 4.5.** SEM images of membrane surface of both CEM and AEM of each stack after the experiment

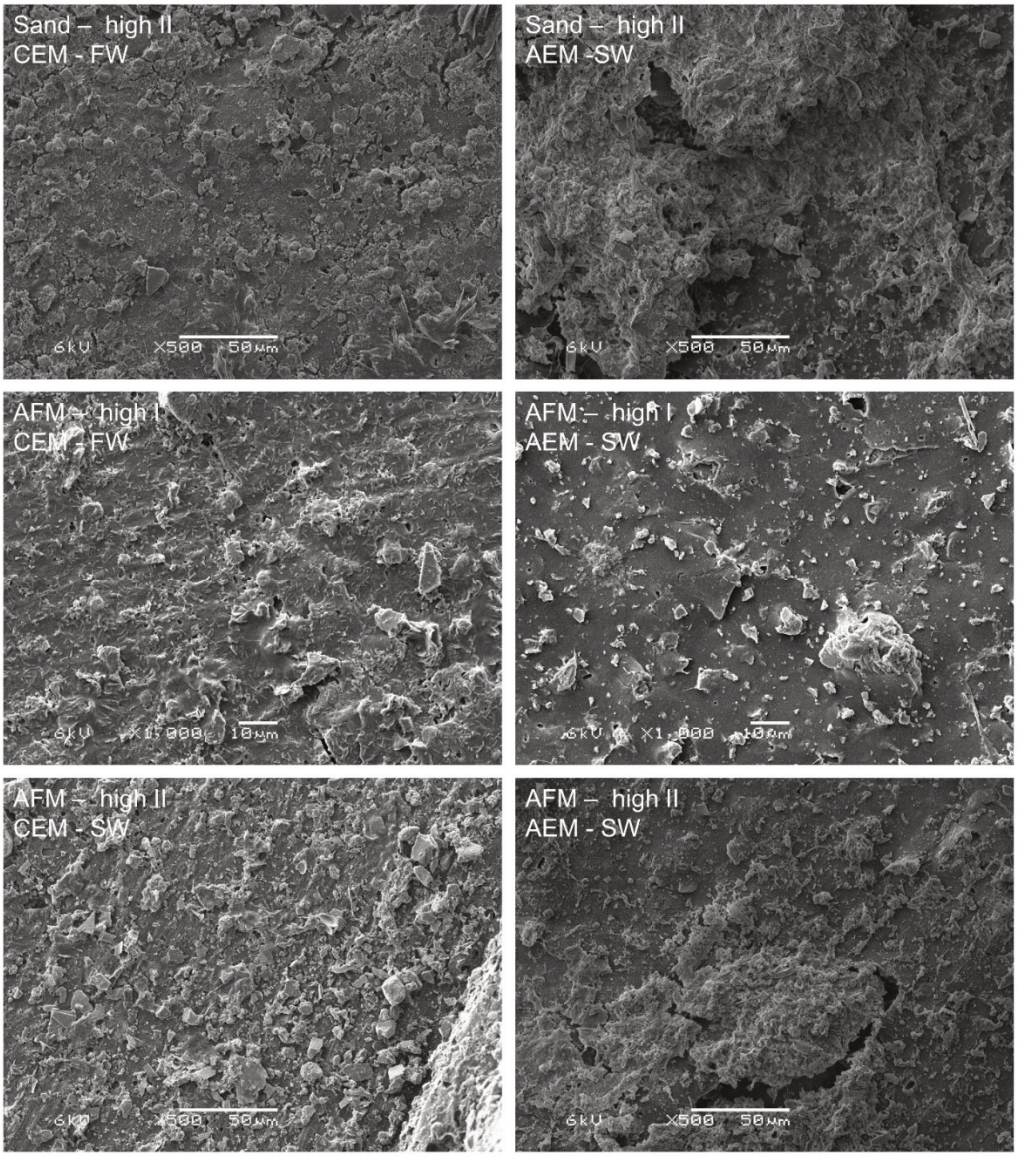


**Figure S 4.5.** SEM images of membrane surface of both CEM and AEM of each stack after the experiment

**References**


[1] R. E. Pattle, Production of Electric Power by mixing Fresh and Salt Water in the Hydroelectric Pile, Nature 174 (1954) 660.

[2] J.W. Post, J. Veerman, H.V. Hamelers, G.J. Euverink, S.J. Metz, K. Nymeijer, C.J. Buisman, Salinity-gradient power: Evaluation of pressure-retarded osmosis and reverse electrodialysis, Journal of Membrane Science 288 (2007) 218–230.

[3] R.E. Lacey, Energy by reverse electrodialysis, Ocean Engineering 7 (1980) 1–47.

[4] J.W. Post, Blue energy: Electricity production from salinity gradients by reverse electrodialysis. Wageningen, Univ., Diss., 2009, 2009.

[5] A. Nazif, H. Karkhanechi, E. Saljoughi, S.M. Mousavi, H. Matsuyama, Recent progress in membrane development, affecting parameters, and applications of reverse electrodialysis: A review, Journal of Water Process Engineering 47 (2022) 102706.

[6] D.A. Vermaas, D. Kunteng, M. Saakes, K. Nijmeijer, Fouling in reverse electrodialysis under natural conditions, Water research 47 (2013) 1289–1298.

[7] S. Pawlowski, R.M. Huertas, C.F. Galinha, J.G. Crespo, S. Velizarov, On operation of reverse electrodialysis (RED) and membrane capacitive deionisation (MCDI) with natural saline streams: A critical review, Desalination 476 (2020) 114183.

[8] D.A. Vermaas, M. Saakes, K. Nijmeijer, Early detection of preferential channeling in reverse electrodialysis, Electrochimica Acta 117 (2014) 9–17.

[9] E. Güler, R. Elizen, M. Saakes, K. Nijmeijer, Micro-structured membranes for electricity generation by reverse electrodialysis, Journal of Membrane Science 458 (2014) 136–148.

[10] S. Pawlowski, V. Geraldes, J.G. Crespo, S. Velizarov, Computational fluid dynamics (CFD) assisted analysis of profiled membranes performance in reverse electrodialysis, Journal of Membrane Science 502 (2016) 179–190.

[11] J. Choi, W.-S. Kim, H.K. Kim, S.C. Yang, J.-H. Han, Y.C. Jeung, N.J. Jeong, Fouling behavior of wavy-patterned pore-filling membranes in reverse electrodialysis under natural seawater and sewage effluents, npj Clean Water 5 (2022).

[12] D.A. Vermaas, D. Kunteng, J. Veerman, M. Saakes, K. Nijmeijer, Periodic feedwater reversal and air sparging as antifouling strategies in reverse electrodialysis, Environmental science & technology 48 (2014) 3065–3073.

[13] J. Moreno, N. de Hart, M. Saakes, K. Nijmeijer, CO2 saturated water as two-phase flow for fouling control in reverse electrodialysis, Water research 125 (2017) 23–31.

[14] E.J. Bodner, M. Saakes, T. Sleutels, C. Buisman, H. Hamelers, The RED Fouling Monitor: A novel tool for fouling analysis, Journal of Membrane Science 570-571 (2019) 294–302.

[15] A. Zouboulis, G. Traskas, P. Samaras, Comparison of single and dual media filtration in a full-scale drinking water treatment plant, Desalination 213 (2007) 334–342.

[16] J. Ju, Y. Choi, S. Lee, C.-G. Park, T. Hwang, N. Jung, Comparison of Pretreatment Methods for Salinity Gradient Power Generation Using Reverse Electrodialysis (RED) Systems, Membranes 12 (2022).

[17] S. Mehdizadeh, M. Yasukawa, T. Suzuki, M. Higa, Reverse electrodialysis for power generation using seawater/municipal wastewater: Effect of coagulation pretreatment, Desalination 481 (2020) 114356.

[18] M. Vanoppen, T. van Vooren, L. Gutierrez, M. Roman, L.J.-P. Croué, K. Verbeken, J. Philips, A. Verliefde, Secondary treated domestic wastewater in reverse electrodialysis: What is the best pre-treatment?, Separation and Purification Technology 218 (2019) 25–42.

[19] B. Vital, E.V. Torres, T. Sleutels, M.C. Gagliano, M. Saakes, H.V. Hamelers, Fouling fractionation in reverse electrodialysis with natural feed waters demonstrates dual media rapid filtration as an effective pre-treatment for fresh water, Desalination 518 (2021) 115277.

[20] B. Vital, T. Sleutels, M.C. Gagliano, H.V. Hamelers, Reversible fouling by particulate matter from natural seawater reduces RED performance while limiting biofouling, Desalination 548 (2023) 116262.

[21] S. Chae, H. Kim, J. Gi Hong, J. Jang, M. Higa, M. Pishnamazi, J.-Y. Choi, R. Chandula Walgama, C. Bae, I.S. Kim, J.-S. Park, Clean power generation from salinity gradient using reverse electrodialysis technologies: Recent advances, bottlenecks, and future direction, Chemical Engineering Journal 452 (2023) 139482.
[22] Environmental Protection Agency, EPA Water Treatment Manual - Filtration, 1995.
[23] D.A. Vermaas, M. Saakes, K. Nijmeijer, Power generation using profiled membranes in reverse electrodialysis, Journal of Membrane Science 385-386 (2011) 234–242.
[24] S. Pawlowski, J.G. Crespo, S. Velizarov, Profiled Ion Exchange Membranes: A Comprehensible Review, International journal of molecular sciences 20 (2019).
[25] S. Pawlowski, C.F. Galinha, J.G. Crespo, S. Velizarov, 2D fluorescence spectroscopy for monitoring ion-exchange membrane based technologies - Reverse electrodialysis (RED), Water research 88 (2016) 184–198.
[26] J. Ju, Y. Choi, S. Lee, Y.-G. Park, Comparison of different pretreatment methods for pressure retarded osmosis (PRO) membrane in bench-scale and pilot-scale systems, Desalination 496 (2020) 114528.
[27] K. Chon, N. Jeong, H. Rho, J.-Y. Nam, E. Jwa, J. Cho, Fouling characteristics of dissolved organic matter in fresh water and seawater compartments of reverse electrodialysis under natural water conditions, Desalination 496 (2020) 114478.
[28] J. Di Luque Salvo, A. Cosenza, A. Tamburini, G. Micale, A. Cipollina, Long-run operation of a reverse electrodialysis system fed with wastewaters, Journal of environmental management 217 (2018) 871–887.

# Chapter 5

# Scaled-up multistage reverse electrodialysis pilot study with natural waters

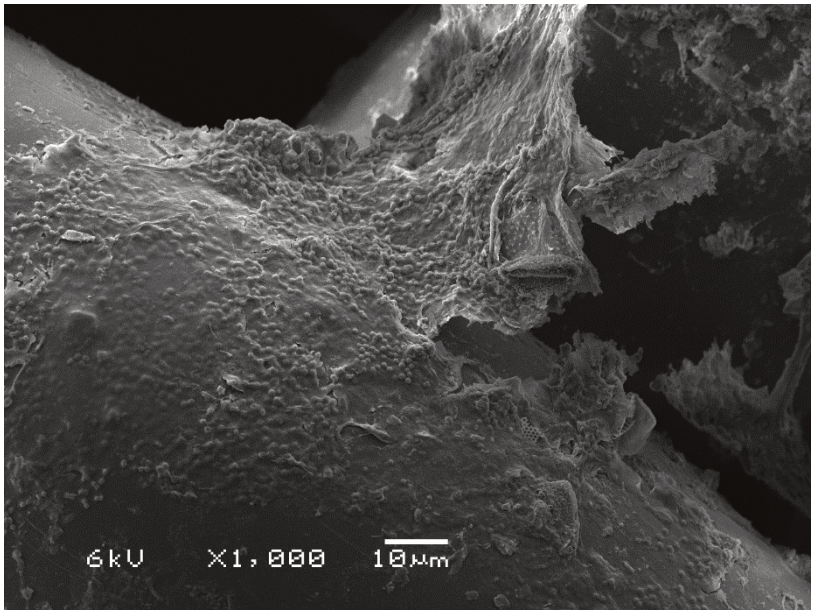

**Abstract:**

A multistage reverse electrodialysis system was studied at the REDstack research facility (the Afsluitdijk, the Netherlands) for over 30 days to describe the performance of such configuration under natural water conditions. The experiments were done with two 0.22 x 0.22 $m^2$ stacks in series comprising 32 cell pairs (3.1 $m^2$ of membrane area) for stage 1 and 64 cell pairs (6.2 $m^2$ membrane area) for stage 2. The total gross power density at the available salinity gradient was stable at around 0.35 $W \cdot m^{-2}$. The total net power density, corrected for the initial pressure drop of the stacks, was 0.25 $W \cdot m^{-2}$ at an energy efficiency of 37%. Throughout the operation, due to increased stack pressure drop, the actual total net power density lowered to 0.1 $W \cdot m^{-2}$. A distinct behaviour was found for multivalent ions in each stage. For stage 1, $Ca^{2+}$ and $SO_4^{2-}$ were transported from the fresh water to the seawater side, so-called uphill transport. For stage 2, uphill transport was not found, in line with Donnan potential calculations. Stack autopsy revealed microorganisms with sizes ten times larger than the cartridge filter nominal pore size (5 µm) and biofilm covering part of the spacer open area, both contributing to the increasing pressure drop in the stacks. This study showed that stable gross power densities and high energy efficiencies were obtained from feeding natural waters to a multistage reverse electrodialysis system, independent of fouling. In addition, it emphasized the importance of maintaining pumping power losses low for a viable deployment of the technology.

This chapter has been published as:

C. Simões, B. Vital, T. Sleutels, M. Saakes and W. Brilman. Scaled-up multistage reverse electrodialysis pilot study with natural waters. *Chemical Engineering Journal,* 450 (2022) p. 138412

### 5.1. Introduction

Renewable energy sources are a key element in fighting climate change, and $CO_2$ emissions and, simultaneously help fulfilling world energy requirements. One renewable energy source is salinity gradient energy (SGE), also known as “Blue Energy”. SGE results from the chemical potential difference between two solutions of different salinity, for instance, while mixing seawater and fresh water [1].

Reverse electrodialysis (RED) is an electro-membrane process that harvests the SGE in the form of electrical energy, using cation and anion exchange membranes (CEMs and AEMs) alternately piled in a stack [2]. Spacers keep the membranes apart and make the compartments to flow the feed solutions. Seawater and fresh water are fed alternately through these compartments. During operation, the concentration gradient across the membranes leads to ion transport from the seawater to the freshwater compartment and according to their selectivity, CEMs transport cations and AEMs transport anions. The resulting ionic current, generated through the stack, is converted into electric current, usually through redox reactions at the electrode end compartments [3].

The RED process was already introduced in 1954 [4]. However, it only gained more attention in the last two decades due to the call for new renewable energy sources and advances in ion-exchange membranes' performance and fabrication [5]. Despite technological advances during the last decade [6,7], the process has not yet met the targeted power density output of 2 $W/m^2$ and energy efficiency of 40% at long-term operation [8]. This is particularly true when natural waters are used, demonstrating the need to study natural water systems for the end application. Experiments towards natural seawater and freshwater applications have investigated the presence of divalent ions (e.g., $Ca^{2+}$, $Mg^{2+}$, $SO_4^{2-}$) which resulted in a decrease in the gross power density compared to NaCl solutions [9–12]. This is due to uphill transport, where divalent ions are exchanged with monovalent ions and are transported against the direction of the concentration gradient, and due to the larger hydration radius of divalent ions which increases the membrane electrical resistance. The use of monovalent selective ion exchange membranes has shown improvements in the gross power density [13–15]. Changes in temperatures have also been assessed, showing that lower temperatures affect negatively the performance of RED [16,17]. Other studies, focused on the fouling in natural waters, indicate that, when no anti-fouling strategies are in place, organic matter can decrease the gross power density up to 40 %, whereas inorganic fouling can decrease up to 8 % [18,19]. Anti-fouling strategies, such as water pre-treatment [20], cleaning strategies [21,22] or RED monitors [23,24] show a prospect of solving fouling issues and maintaining low stack pressure drops with the challenge of using less energy. The use of profiled membranes [25,26] was also suggested to decrease stack pressure drops. Another challenge brought by natural waters is the possible scaling at the electrodes of, for example, $Mg(OH)_2$ and $CaCO_3$, which increased the

energetic losses [27]. However, studies combining natural seawater and fresh water with control strategies, such as electrode segmentation [28] and multistage [29], are missing in the literature.

Multistage RED (MSRED) concept is gaining more attention as it increases the power output, consequently, the energy efficiency, while keeping the gross power density higher when compared to a single stage in the same conditions. MSRED enables different currents per electrode pair, as in electrode segmentation [28]. Moreover, it allows different configurations and materials per stage which can further improve the performance [30]. Veerman, who was the first to propose the MSRED concept in 2009 [31], recently published a model-based study with co- and counter-current flow in different multistage arrangements for maximum efficiency with different electrical controls [32]. Tedesco et al. simulated crossflow stacks for brine and brackish water mixtures up to three stages and 500 cell pairs per stage, showing more than 1000 W could be obtained [33]. Hu et al. showed through modelling that a multistage series control was more suitable in practice with a counter-flow arrangement for brine and freshwater concentrations in a RED heat engine system [29]. Their work continued with an experimental investigation where the process efficiency was five times higher than with single stage, preferably using low feed flow velocities [34]. Referring to natural waters, Wang et al. studied MSRED with natural seawater and brine to improve the process energy efficiency. However, the water composition was left out (only overall concentration was given), the test duration was rather short and only one stack was used to simulate the staging effect [35]. Besides the energy production aspect, MSRED is also used for improving the decolourization efficiency of azo dye wastewater [36], creating a system combined with multi-effect distillation [37] or producing hydrogen [38].

Our previous work investigated the application of MSRED for seawater and fresh water through modelling and experiments, using 0.5 M and 0.017 M NaCl solutions [30]. We concluded that the total power density and energy efficiency increased with a two-stage configuration using the “saving the gradient” strategy (stage 1 operated at a current density below the stage maximum power density) to achieve an overall higher maximum power. In addition, the pressure drop inherent to the feed compartments played an important role in the staging implementation [30]. Later, the same multistage model was extended to include magnesium and sulphate ions in solution, but it was validated only with single-stage experiments in controlled conditions [39]. The advantages of MSRED were moderated with the presence of divalent ions. The behaviour of multivalent ions in MSRED is limited to the model study and not experimentally verified. Thus, long-term testing of MSRED with natural seawater and fresh water, connecting two crossflow stacks in series, where the multivalent ions impact and fouling are evaluated daily, to our knowledge, has never been reported before.

In this study, we show for the first time the performance of two 0.22 x 0.22 $m^2$ crossflow stacks connected in series, fed with natural seawater and fresh water, at a geographical relevant location for RED implementation, over more than 30 days. The goal was to understand the impact of natural waters in an MSRED system concerning performance, ion transport and fouling and dealing with fluctuations associated with nature. Initially, the stacks were individually characterized at the laboratory using pure NaCl solutions (0.5 and 0.017 M NaCl) and, later were transported to the REDstack research facility (Afsluitdijk, the Netherlands), which allowed continuous water supply, and connected in series. For 30 days, the MSRED fed with natural waters was monitored continuously, revealing the fate of the ions (in particular divalent ions) and process performance. After a month of operation, cleaning techniques were tested in an attempt to lower the pressure drop across the stacks. At the end of the operation, a stack autopsy was conducted to evaluate the fouling extension.

## 5.2. Materials and methods

### 5.2.1. Experimental setup

Two crossflow RED stacks were provided and built by REDstack BV (Sneek, the Netherlands). The details of the stack design can be found elsewhere in the literature [40]. The stacks were connected in series with the fresh and seawater both fed to stack 1 and stack 2 received the outlet streams of stack 1 (Fig. 5.1). Stack 1 (or stage 1), which was the first stack receiving the feed waters in the multistage configuration, contained 32 cell pairs (3.098 $m^2$ of total active membrane area) and stack 2 (or stage 2) contained 64 cell pairs (6.196 $m^2$ of total active membrane area). The difference in the number of cell pairs resulted from model simulations, a shorter residence time increases the power density on stage 1 and a longer residence time, on stage 2, will exhaust further the salinity gradient increasing the energy efficiency while having lower pumping losses [30]. The active area of a single membrane was 0.22 m x 0.22 m. Each cell pair comprised one CEM (Fumasep FKS-30, Fumatech GmbH, Germany) and one AEM (Fumasep FAS-30, Fumatech GmbH, Germany). The shielding membranes were two fluorinated CEMs (Fumatech F-10150-PTFE, Fumatech GmbH, Germany), one being part of a cell pair and the other as the extra membrane. The ion exchange membranes properties can be seen in Table 5.1. Woven net spacers of 155 µm thickness (Deukum, GmbH, Germany) were used to make the compartments, with 55 % porosity. At the endplates, a pair of 0.22 m x 0.22 m platinized Ti-mesh electrodes were used as anode and cathode (MAGNETO special anodes BV, the Netherlands).

**Table 5.1** Ion exchange membranes properties.

| Properties | FKS-30 | FAS-30 | F-10150-PTFE |
|---|---|---|---|
| Thickness (dry) [α] [µm] | 25-35 | 25-35 | 140 – 150 |
| Permselectivity [α] [%] | > 98 | > 90 | > 95 |
| Electrical resistance [β] [Ω·cm$^2$] | 1.32 | 0.78 | 1.8 – 2.9 [γ] |
| Ion exchange capacity [γ] [meq·g$^{-1}$] | 1.43 | 1.6 – 2.0 | 0.7 – 0.9 |
| Dimensional swelling in H2O [α] [%] | < 3 | < 2 | < 5 |

[α] Fumatech Technical Data Sheet, provided upon the membrane purchase

[β] Measured in a six-compartment cell at 0.5 M NaCl, according to a literature procedure [41]

[γ] FUELCELL Store Technical Data Sheet, available online (www.fuelcellstore.com/fumatech)

The experiments were conducted first at the laboratory at Wetsus, for stacks validation with NaCl solutions, and later at the REDstack BV research facility (the Afsluitdijk, the Netherlands), where it took place the transition to natural feed waters and set up for two section 5.3.1), the 30-day run experiment (section 5.3.2 and 5.3.3) and only after the cleaning strategies and fouling investigation (section 5.3.4).

The electrode rinse solution (ERS), during the laboratory tests and first days of the pilot tests, was a mixture of 0.2 M $K_4Fe(CN)_6$, 0.2 M $K_3Fe(CN)_6$ and 0.15 M NaCl (VWR Chemicals, Belgium) recirculated at 300 mL/min. Although it worked in the laboratory and also with natural feed waters at a smaller scale [42,43], the hexacyanoferrate solution was found not to be suitable for scaled-up stacks using natural feed waters. $Mg^{2+}$ and $Ca^{2+}$ ions crossed the CEMs and reacted with $OH^-$ resulting from the reduction of water at the cathode and precipitated as salts. Figure S 5.1 shows the visual difference between the initial pristine solution and the used ERS in each stage and, Figure S 5.2 shows the scaling found at the autopsy. Therefore, to avoid scaling at the cathode, the ERS was replaced with single-pass seawater. Each electrode compartment for each stage was fed with seawater independently at a rate of 600 mL/min. Ag/AgCl reference electrodes were used to measure the potential difference across the membrane pile, excluding the overpotential at the electrodes. In a commercial application, voltages losses due to oxygen, chlorine and hydrogen evolution reactions need to be taken into account (around 1.5 to 2 V) or ERS that avoid such loss should be developed.

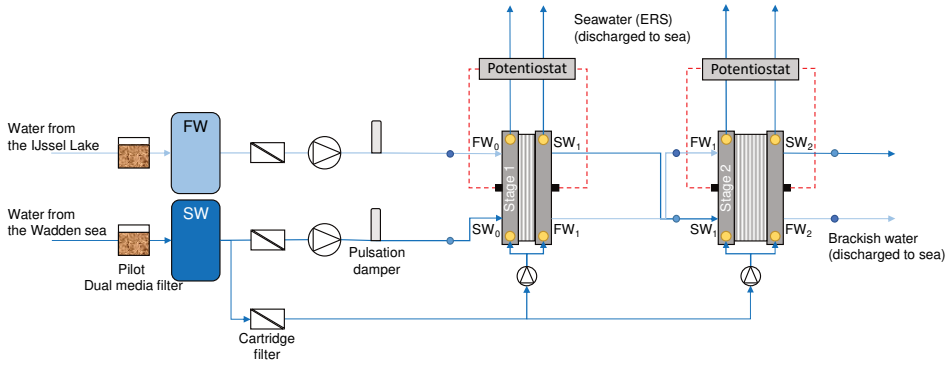


**Figure 5.1** Schematic diagram of the experimental setup at the research facility fed with fresh water (FW) and seawater (SW) and with single-pass seawater as the electrode rinse solution. Dots represent the sampling points in positions 0, 1 and 2. The three-way valves for water switching are not represented for simplicity but were installed before the stage 1 inlet.

The laboratory setup has been described in our previous work [30]. For the pilot setup (Fig. 5.1), the fresh water (FW) and seawater (SW) were pumped at a flow rate of 39.3 L/h, corresponding to 1.0 cm/s in stage 1 and 0.5 cm/s in stage 2, unless stated another flow rate. The spacer porosity was not included in the flow velocity calculation. The natural feed waters were automatically switched (changing compartment) every six hours to further mitigate scaling at the electrode compartments. By switching the feed waters, thus the polarity of the stack, cathode and anode were switched periodically, which helped lowering inorganic scaling at the cathode. Both valves installed for water switching were controlled by a Raspberry Pi (Raspberry Pi Foundation, United Kingdom), using an open-source Python code. Temperature and conductivity (Type 8228, Burkert, Germany) were measured inline, before stage 1 (position 0), between stages 1 and 2 (position 1) and after stage 2 (position 2). The pressure drop between inflow and outflow over the stack was measured with absolute pressure sensors (MIDAS SW, JUMO GmbH, Germany). Data were collected with a data logger (Yokogawa, Japan).

At the laboratory, both stacks were fed with pure NaCl solutions (Regenit, Esco, the Netherlands), which consisted of 1 g/L for the FW and 30 g/L for the SW at 24.5±0.5 °C. These values were chosen for consistency with previous studies with pure NaCl solutions. Afterwards, at the REDstack BV research facility at the Afsluitdijk, the Netherlands, the stacks were fed with natural waters from Lake IJssel (FW) and the Wadden Sea (SW), after being pre-treated with the research facility drum and sand filters, which was the pre-treatment adopted for this study, and a 50 - 5 µm nominal cartridge filter (Pentek DGD-5005-20, Pentair, USA) placed before the pumps. These waters were sampled at positions 0, 1 and 2 from both FW and SW (Fig. 5.1) and were characterized with an Ion Chromatograph (Metrohm Compact IC Flex 930, the Netherlands) for $Cl^-$, $SO_4^{2-}$, $Na^+$, $K^+$, $Mg^{2+}$

and $Ca^{2+}$. Before analysis, the samples were filtered using a 0.45 µm filter (Merck Millipore Millex-LCR, Germany). The typical composition of the natural feed waters, during the experiment, is given in Table 5.2.

**Table 5.2** Average natural seawater (SW) and fresh water (FW) characteristics during the experiment at the Afsluitdijk research facility.

| Source | Conductivity [mS·cm$^{-1}$] | Temperature [°C] | Typical ion concentration [mM] | | | | | |
|---|---|---|---|---|---|---|---|---|
| | | | $Cl^-$ | $SO_4^{2-}$ | $Na^+$ | $K^+$ | $Mg^{2+}$ | $Ca^{2+}$ |
| Wadden Sea (SW) | 31.4 | 18.6 | 342.5 | 17.9 | 283.8 | 6.2 | 33.2 | 6.8 |
| | ±4.1 | ±0.6 | ±37.6 | ±1.8 | ±32.6 | ±0.8 | ±3.8 | ±0.7 |
| Lake IJssel (FW) | 0.52 | 19.0 | 2.7 | 0.6 | 2.3 | 0.1 | 0.5 | 1.1 |
| | ±0.02 | ±0.7 | ±0.2 | ±0.1 | ±0.2 | ±0.1 | ±0.1 | ±0.1 |

### 5.2.2. Electrochemical measurements and calculations

The electrochemical measurements were done with a two-channel potentiostat (IVIUM n-stat, IVIUM Technologies BV, the Netherlands) and recorded with the IVIUMsoft software. The potential across the membrane, in volts, was calculated through the Nernst equation:

$$E = \frac{RT}{zF} ln\left(\frac{m_{SW}.\gamma_{\pm,SW}}{m_{FW}.\gamma_{\pm,FW}}\right) \quad \text{(Eq. 5.1)}$$

Where R is the gas constant (J/mol.K), T is the absolute temperature (K), z is the ion valency (-), F is the Faraday constant (C/mol), m is the molality (mol/kg $H_2O$) and $\gamma_\pm$ is the mean salt activity coefficient (-) estimated with the model of Ge et al. [44]. For the case of calculating the theoretical open circuit voltage (OCV), Eq. 5.1 was adapted to $OCV = E \cdot 2N \cdot \alpha_{IEM}$ , where $N$ is the number of cell pairs (-) and $\alpha_{IEM}$ is the average of the AEM and CEM permselectivity (-). The experimental OCV was measured when there was no current applied.

To define the power curve and maximum power density an I-V (current-voltage) measurement was done. It consisted of current steps of -0.5 A (at the Wetsus laboratory), and -0.4 A for stage 1 and -0.2 A for stage 2 (with natural waters at the Afsluitdijk) until the cell voltage reached zero. Displaying the results both current and voltage are made positive. The gross power density ($P_{d,gross}$ in W/m$^2$) of each stage was:

$$P_{d,gross} = \frac{I \cdot U}{A_{mem}} \quad \text{(Eq. 5.2)}$$

Where $I$ is the current applied (A), $U$ is the measured potential (volts) and $A_{mem}$ is the total active membrane area (m$^2$). The net power density (Eq. S 5.1) only considered pressure

drop losses from the stack (Eq. S 5.2). For the total power density ($P_{d,total}$ in W/m$^2$) of two stages, the contribution of each stage needs to be considered:

$$P_{d,total} = \frac{N_{S1}}{N_T} P_{dS1} + \frac{N_{S2}}{N_T} P_{dS2} \quad \text{(Eq. 5.3)}$$

Where $N_T$ is the total amount of cell pairs (-) and $N_{S1}$ is the amount of cell pairs in stage 1 and $N_{S2}$ is the amount of cell pairs in stage 2. To evaluate the power density and energy efficiency in the long term, the current was fixed during the experiments, after manually employing the "saving the gradient" strategy for the first days [30]. The strategy consisted of stage 1 working at 80% of its maximum power density and stage 2 at 95%. Providing a lower current to stage 1 to allow an "extra" salinity gradient for the following stage has proven that more power can be harvested than by setting each stage sequentially at its maximum power [30]. Applied current values and measured response voltage during the 30-day run are shown in Table S 5.1.

To verify how much of the available salinity gradient energy was harvested, the energy efficiency was calculated:

$$\eta = \frac{P_{gross}}{\Delta G_{in}} \quad \text{(Eq. 5.4)}$$

Where the $P_{gross}$ is the total gross power (W) and the $\Delta G_{in}$ is the Gibbs free energy per second at the inlet (W) [45]. To calculate $\Delta G$, the entropy ($\Delta S$ in W/K) and the absolute temperature ($T$ in K) are needed.

$$\Delta G = \Delta S \cdot T \quad \text{(Eq. 5.5)}$$

$$\Delta S = S_{mix} - S_{RW} - S_{SW} \quad \text{(Eq. 5.6)}$$

$$S = -R \cdot n_T \cdot \sum_i x_i \ln (x_i \cdot \gamma_i) \quad \text{(Eq. 5.7)}$$

$$i = H_2O, Cl^-, Na^+, K^+, SO_4^{2-}, Mg^{2+}, Ca^{2+}$$

Where $n_T$ is the total number of moles (mol/s), $x_i$ is the mole fraction (-) and $\gamma_i$ corresponds to the single ion activity coefficient of species i (-) as specified above. The single ion activity coefficient of species i, $\gamma_i$, was approximated by the mean salt activity coefficient, $\gamma_\pm$, for the following ions: $\gamma_{Cl^-} = \gamma_{NaCl}$, $\gamma_{Na^+} = \gamma_{NaCl}$, $\gamma_{K^+} = \gamma_{KCl}$, $\gamma_{SO_4^{2-}} = \gamma_{Na_2SO_4}$, $\gamma_{Mg^{2+}} = \gamma_{MgCl_2}$ and $\gamma_{Ca^{2+}} = \gamma_{CaCl_2}$. $\gamma_{H_2O}$ was assumed 1. With equations 4.5,4.6 and 4.7, the available power for mixing is calculated.

### 5.2.3. Cleaning and autopsy techniques

Cleaning strategies were implemented after more than 30 days of experiment, in an attempt to mitigate the reduction in net power density output. Both stages had visible signs of fouling and presented an increasing pressure drop with time. In the cleaning procedure, the inlet and outlet of the stacks were reversed, since most particulate fouling accumulated in the entrance of the stack and, by reversing the flow direction, this accumulation was pushed out of the stack. Following, the flow was doubled for 5 minutes, forcing the particles out. After that, air sparging was performed, with a configuration of 3 pulses of 2 seconds duration each at 3 bar air pressure. Air sparging is a sudden disturbance on the membrane and spacers surface by introducing compressed air for a short time along with the feedwater flow, to remove a large accumulation of foulants, mostly particulate fouling. During the cleaning procedure, water samples were taken at the outlet of each stack compartment (both fresh and seawater) and were analysed for suspended solids, according to the Standard Methods for the Examination of Water and Wastewater [46].

The multistage configuration was let to run for two more weeks after the cleaning, and at the end of the experiment, stack 1 was carefully opened and investigated concerning fouling. Since a membrane autopsy was destructive to the stack, stack 2 was kept intact for future research. Pictures of the AEM, CEM, spacers and electrodes were taken, and membrane and spacer pieces were cut for optical and electron microscopic investigation, always on an inlet, central area of the membrane. The procedure was the same as described in Vital et al. [20]. In short, membrane and spacer pieces were fixed and dried for microscopy analyses under scanning electron microscopy (SEM) and energy-dispersive X-ray spectroscopy (EDX), while other pieces were stained with Alcian Blue 8 GX 0.1% solution (Sigma Aldrich, the Netherlands) and observed with phase-contrast microscopy (Olympus BX40, Japan) at 10x and 20x magnification, for visualization of organic fraction of extracellular polymeric substances (EPS) and biofilm [47].

## 5.3. Results and Discussion

### 5.3.1. Transitioning between artificial and natural conditions

Both RED stacks were first tested at the laboratory, using pure NaCl solutions and at the same flow velocity (1.0 cm/s) to ensure reproducibility. Inlet conditions are shown in Table 5.3. OCV values were, 0.131 V and 0.133 V per cell pair for stacks 1 and 2, respectively (Fig. 5.2A). These values are close to the calculated theoretical OCV of 0.150 V per cell pair (Eq. 5.1, assuming permselectivity, $\alpha = 0.95$). The power density versus current density curves were similar (Fig. 5.2B). Stack 1 had a 1.5% higher gross power density; this minor difference can be attributed to different factors together, such as manual building or ionic shortcut currents from the increased cell pair number in stack 2 [48,49].

**Table 5.3** Test description and conditions for each stack/stage. At the laboratory reproducibility tests took place, thus the stacks are studied individually under equal conditions. At the research facility, the stacks, now named stages are already investigated in the two-stage series configuration.

| Test | Inlet conditions | SW | | FW | | Composition | Velocity |
|---|---|---|---|---|---|---|---|
| | | σ [mS/cm] | T [°C] | σ [mS/cm] | T [°C] | | [cm/s] |
| Validation | Stack 1 Lab | 47.83 | 24.9 | 2.03 | 24.8 | NaCl | 1.0 |
| Reproduci-bility | Stack 2 Lab | 47.78 | 25.3 | 2.03 | 25.1 | NaCl | 1.0 |
| Natural conditions | Stage 1 NW | 35.33 | 19.4 | 0.66 | 19.5 | Natural | 1.0 |
| | Stage 2 NW | 29.85 | 19.7 | 4.60 | 19.5 | Natural | 0.5 |

When the testing under natural conditions (Fig. 5.2C and 5.2D), the stacks were connected in series (Fig. 5.1) and are now referred to as stages 1 and 2. The initial test conditions can be seen in Table 5.3. Because of staging, the salinity gradient available for stage 2 is lower than stage 1, due to the mixing in stage 1. Furthermore, since stage 2 has twice the amount of cell pairs of stage 1, the flow velocity is halved to 0.5 cm/s. These two factors account for the 2.3 times lower maximum power density in stage 2, shown in Figure 5.2D. The effect of staging combined with the change in flow velocity seen here is comparable to the literature for NaCl solutions [30]. The maximum gross power density achieved in stack 1 lab was reduced by 41% with stage 1 NW (Fig. 5.2B and 5.2D). This was due to a combination of effects including the lower salinity gradient available which can be seen in Table 5.3 and calculated through Eq. 5.5, and the presence of multivalent ions like $Mg^{2+}$ and $Ca^{2+}$ (details in section 5.3.3). Vermaas et al. (2014) also reported a decrease of around 50% in gross power density with $MgSO_4$ (10%)/ NaCl (90%) solutions with a total salt concentration of 0.508 M and 0.017 M in artificial seawater and fresh water [10]. The lower temperature (Table 5.3), known to negatively influence the power density [11,17], further reduced the gross power density. The maximum gross power density of stage 2 NW (Fig. 5.2B and 5.2D) was even lower (0.3 $W/m^2$) because of the reasons mentioned above concerning initial concentration and flow velocity. Transitioning to natural waters shows multiple challenges that cannot be studied simultaneously in the laboratory.

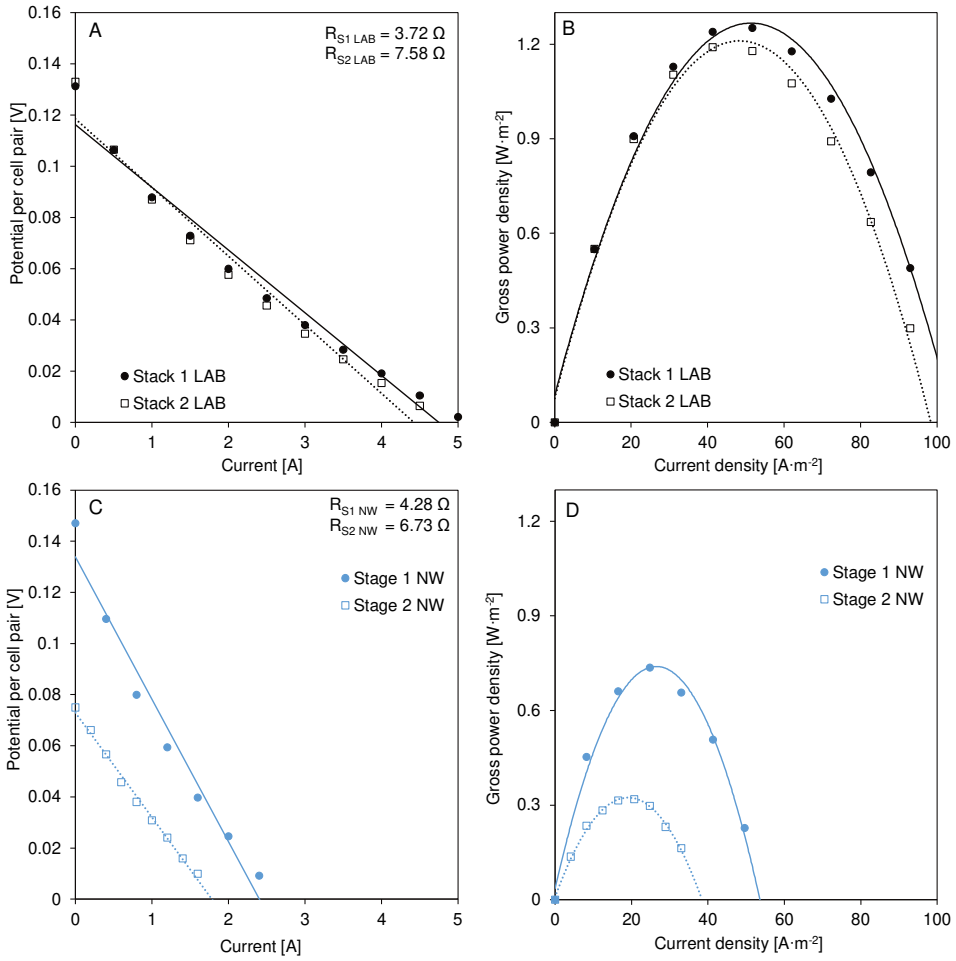


**Figure 5.2** (A) I-V curve, stack resistance and (B) gross power density vs current density for stacks 1 (circles and solid lines) and 2 (squares and dotted lines) as tested in the laboratory (LAB, black); (C) I-V curve, stack resistance and (D) gross power density vs current density for stages 1 (circles and solid lines) and 2 (squares and dotted lines) as tested at the research facility with natural waters (NW, blue). Conditions for these results are shown in Table 5.3. In these measurements ERS was still 0.2 M $K_4Fe(CN)_6$, 0.2 M $K_3Fe(CN)6$ and 0.15 M NaCl. Trend lines are added to guide the eye.

### 5.3.2. Continuous staging performance over a month

Figure 5.3 shows the gross power density and energy efficiency on the sampling moments for each stage and in total. Throughout the 30-day run, the total gross power density was quite stable at around 0.35 W/m$^2$ (Eq. 5.3). The contribution of each stage can be seen in Figure 5.3A, averaging 0.55 W/m$^2$ for stage 1 and 0.25 W/m$^2$ for stage 2 (Eq. 5.2). By reusing the waters in stage 2, thus extending their use at a reduced salinity gradient, and because of the longer residence time in this stage, there was an expected decrease in total power

density. The energy efficiency achieved values above 30% with a maximum of 37% (Fig. 5.3B, Eq. 5.4). Such energy efficiencies have not been reported for natural water studies and are found here to be comparable to theoretical [39,50] and laboratory studies [30,42]. The gross power density and the gross energy efficiency represent a good electrical performance of the multistage configuration. The gross power density would be increased if the salinity gradient of the natural waters was higher.

Some variations in performance as detected were explained by one of the following reasons: First, due to the natural change in salinity gradient between sea and fresh water (Figure S 5.3A) and second, due to changing the stack operation. For example, on days 27 and 28, an asymmetrical flow rate was tested (shaded green areas in Figures 5.3, 5.4, 5.5 and 5.6), with the seawater flow rate being half of the freshwater flow rate, or change in current applied (Table S 5.1). The temperature varied between 18 and 21 °C. These fluctuations can be seen in Figure S 5.3.

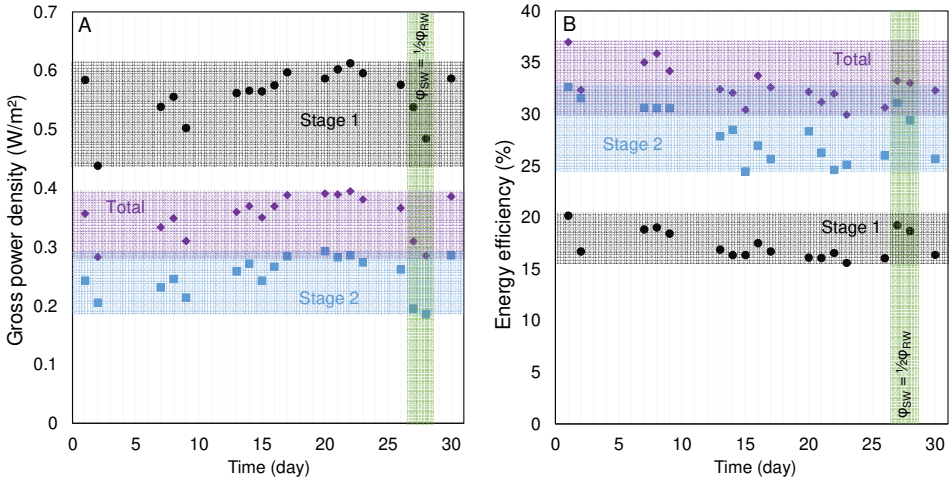


**Figure 5.3** Total and stage-related gross power density (A) and gross energy efficiency (B) for the sampling moments: Stage 1 (●), Stage 2 (■) and total (◆). The green shaded area corresponds to two days with an asymmetric flow rate, while FW was kept the same (39.3 L/h), and SW was reduced to half (19.6 L/h).

Figure 5.4 shows the multistage net power density (Eq. S 5.2) and the pumping power density per stage in two scenarios (Eq. S 5.1). If we would correct the gross power density only with the pressure drop of that stage to its starting value (0.3 bar for stage 1 and 0.15 bar for stage 2) and kept it constant, the total net power density amounts to 0.25 W/m$^2$. However, due to an increasing pressure drop in stage 1, at the start of the operation (Fig. S 5.3), the total net power density was mostly below 0.1 W/m$^2$ (Figure 5.4A). That is also why the constant and actual scenarios' net power density values do not match on day 1 of the 30-day run. Stage 1 was most affected, due to the higher flow velocity, and it was the first

in line to experience a pressure drop increase due to fouling (Fig. S 5.3), reaching, for most days, pumping power densities higher than the gross power density (Fig. 5.4B). Later on, stage 2 also showed an increase in pressure drop, indicating the fouling was not exclusive to stage 1 but remained with positive net power density values. The net power density per stage can be obtained from the difference between Figure 5.3A and Figure 5.4B. In our previous work [30], it was shown that variation of the stack residence time (and hence flow velocity and pressure drop) could be used for the optimization of the net power density production while increasing the energy efficiency. This strategy was not followed in this duration test.

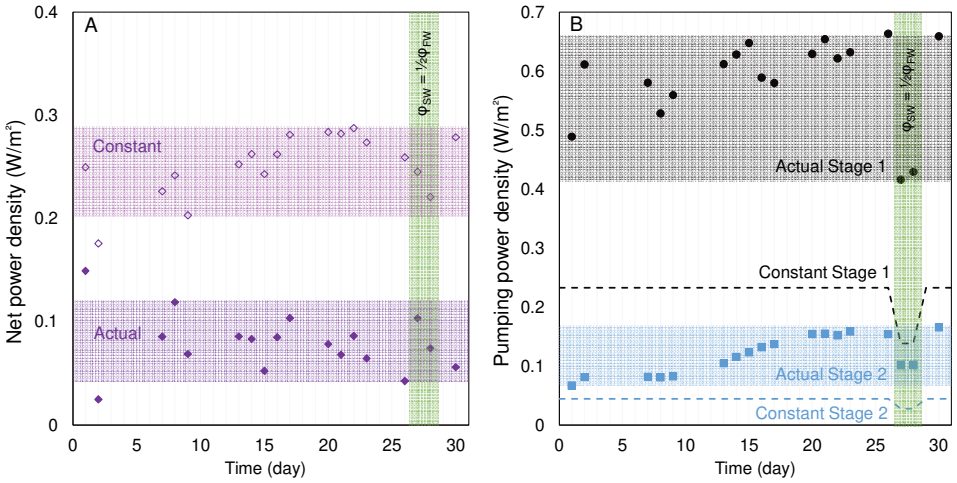


**Figure 5.4** (A) Total net power density of the multistage configuration for both the actual pressure drop and in case the pressure drop is taken as a constant and equal to the initial pressure drop. (B) Pumping power density calculated for stage 1 (black) and stage 2 (blue), actual values with symbols and constant values with dashed lines. The scenario actual uses the stage pressure drop at that moment and the scenario constant uses only the initial pressure drop value (Figure S 5.5). The green shaded area corresponds to two days with an asymmetric flow rate, while FW was kept the same (39.3 L/h), and SW was reduced to half (19.6 L/h).

The pressure drop can be partly attributed to visible fouling as algae growth was noticeable in the transparent tubing and the feedwater compartments. More details can be seen during the cleaning and stack autopsy in section 5.3.4. Interestingly, the gross electrical performance was not affected by the pressure increase and fouling [20]. We conclude that the electrical performance was dependent on the water's composition and concentration and mostly independent of the fouling for the period of testing. The fouling however affected the hydraulic performance, leading to a high loss in net power density output. Efforts towards maintaining the pumping power losses at a lower level in time are therefore needed.

The asymmetrical flow rate, with seawater being half of the freshwater flow rate, on days 27 and 28 did not show increasing performance values compared to the overall experiment. However, compared to the data points just before and after (days 26 and 30), which share more similar conditions, the energy efficiency increased (Fig. 5.3B). Although the gross power density decreased (Fig. 5.3A), the pumping power density lowered (Fig. 5.4B) subsequently increasing the net power density for the actual scenario. Thus, for controlled water conditions, the asymmetrical condition could work as an optimization. On the other hand, in a highly dynamic environment, as present in this study, there is no discernible benefit.

### 5.3.3. Ion's behaviour through staging: multivalent ions are transported differently per stage

During the 30-day run, natural waters were sampled at all positions to analyse the transport of ions through staging. The presence of multivalent ions, such as $Mg^{2+}$, $Ca^{2+}$ and $SO_4^{2-}$, leads to uphill transport of these ions, as described by Vermaas et al. [10]. Uphill transport occurs when a divalent ion is transported against its concentration gradient (usually from the fresh water to the seawater side) to obtain equilibrium in chemical potential at both sides of the membrane. This phenomenon results in losses for the RED process, since one divalent ion like $Mg^{2+}$ is exchanged with two monovalent ions like $Na^{+}$ at zero net charge.

Figure 5.5 shows the concentration of monovalent ions through the multistage process and the measured conductivity at the inlet (position 0), between the stages (position 1) and at the outlet (position 2). Both for the fresh and seawater sides, the conductivity coincides with chloride ($Cl^{-}$) and sodium ($Na^{+}$) concentration, which means that conductivity sensors can correctly indicate the salinity gradient when the natural water is mainly composed of $Cl^{-}$ and $Na^{+}$. This implies that an automated optimization of the RED performance could rely on the conductivity sensors that predict the available salinity gradient. All the monovalent ions show the same trend through staging.

While monovalent ions show a predictable behaviour through staging, multivalent ions have a different pattern. The uphill transport of sulphate ($SO_4^{2-}$) and calcium ($Ca^{2+}$) in stage 1 was expected and given in the literature [14,51]. Figures 5.6A and 5.6E show that both $SO_4^{2-}$ and $Ca^{2+}$ concentrations at the freshwater side decreased from position 0 to 1 (being 0 the inlet and 1 the outlet of stage 1). And the opposite occurred on the seawater side (Fig. 5.6B and 5.6F). In the case of magnesium ($Mg^{2+}$), uphill transport is not present (Fig. 5.6C and 5.6D) which is opposite to the literature [14]. In the work by Rijnaarts et al., the uphill transport of divalent ions was studied individually and not as a mixture, while also discarding the presence of $Ca^{2+}$. The uphill transport of $Ca^{2+}$ can be explained by the smaller hydrated ionic radius of $Ca^{2+}$ (0.412 nm) compared to $Mg^{2+}$ (0.428 nm) which makes $Ca^{2+}$

being transported more easily than $Mg^{2+}$. Guo et al. [11] compared the uphill transport of $Mg^{2+}$ and $Ca^{2+}$ for two different membranes.

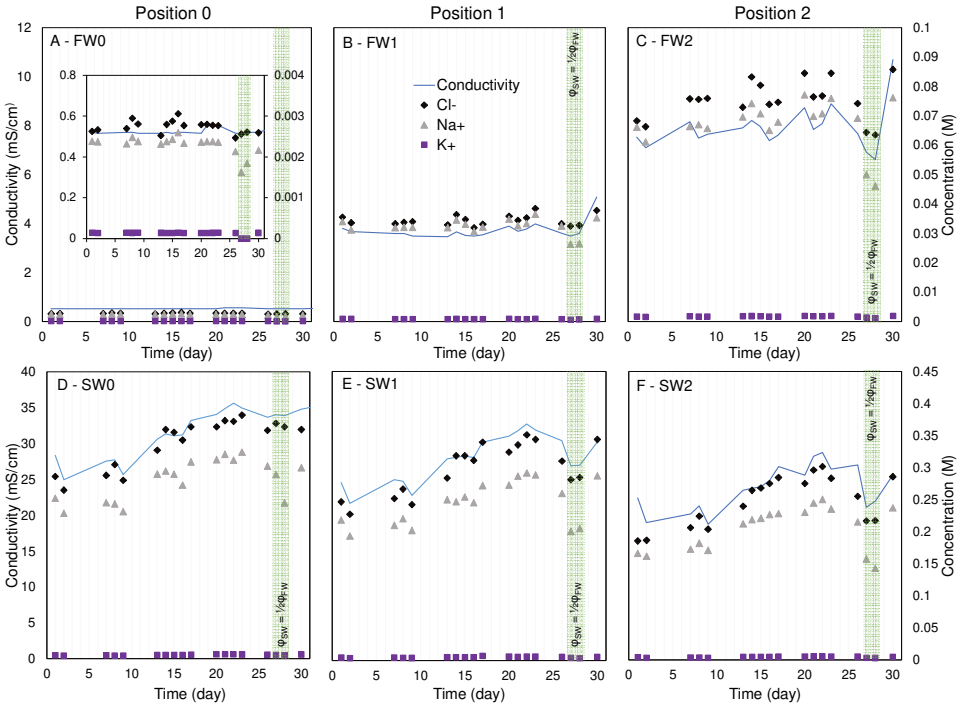


**Figure 5.5** Conductivity and concentration of monovalent ions at the inlet (0), between stages (1) and outlet (2) in fresh water (FW) (A, B and C) and in seawater (SW) (D, E and F) while operating at constant current density. The conductivity is represented with a line. The shaded area corresponds to two days with an asymmetric flow rate, FW was kept the same (39.3 L/h), and SW was reduced to half (19.6 L/h).

At lower temperatures, most of the uphill transport was attributed to $Ca^{2+}$ (which was ten times lower in concentration than $Mg^{2+}$ at the fresh waterside). In our case, $Ca^{2+}$ concentration (1.1 mM) in fresh water was higher than $Mg^{2+}$ concentration (0.5 mM). The higher concentration and the smaller hydrated radii triggered $Ca^{2+}$ to be preferably exchanged with $Na^{+}$ rather than $Mg^{2+}$.

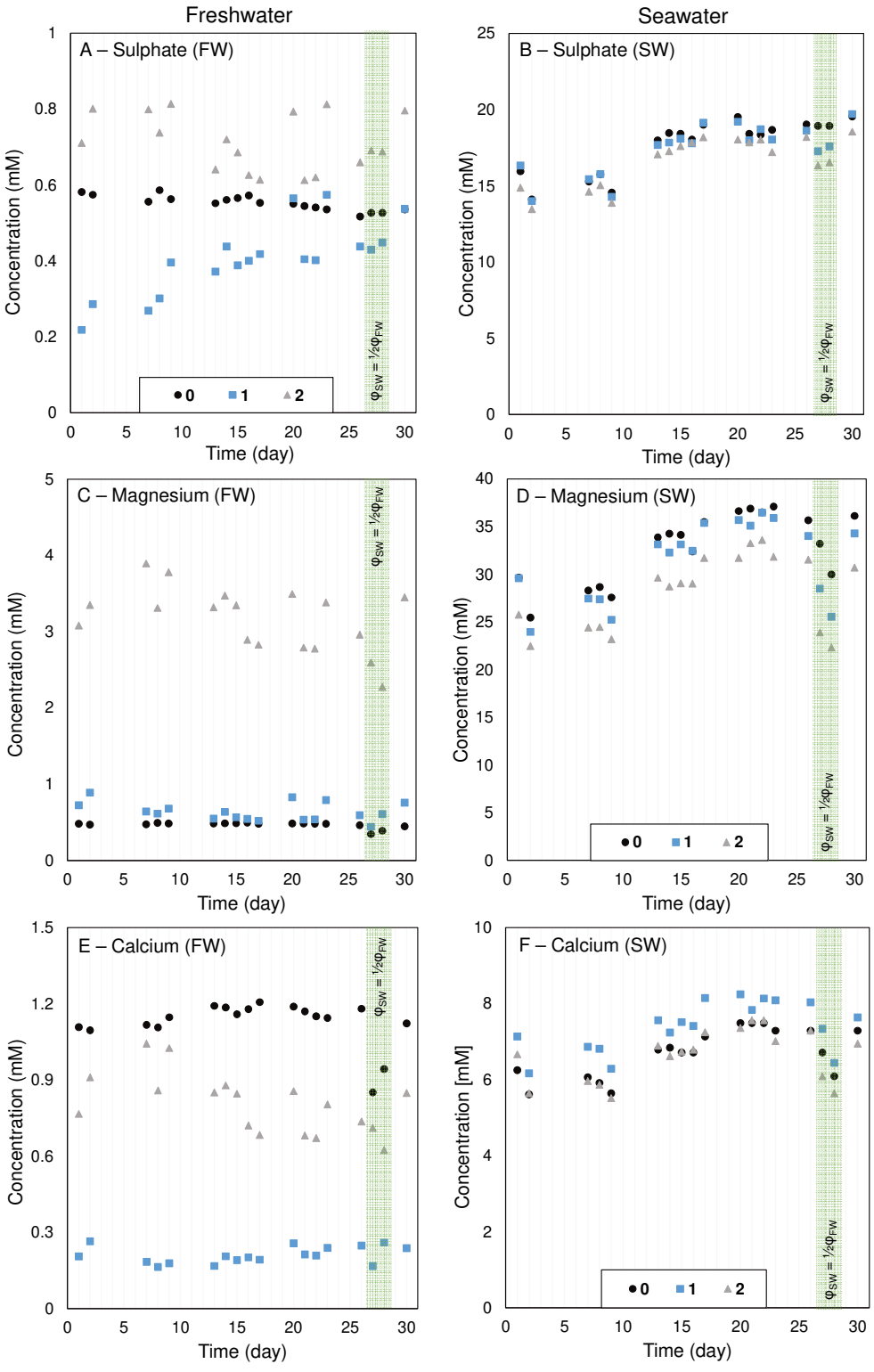
Freshwater
Seawater
A – Sulphate (FW)
B – Sulphate (SW)
C – Magnesium (FW)
D – Magnesium (SW)
E – Calcium (FW)
F – Calcium (SW)
Concentration (mM)
Concentration [mM]
Time (day)
0
1
2
φSW = ½φFW

**Figure 5.6** Sulphate (A and B), magnesium (C and D) and calcium (E and F) concentrations, in mM, in fresh water (FW, left side graphs) and seawater (SW, right side graphs) at the inlet (0), between stages (1) and outlet (2). Note that the y-axis values differ between graphs. The green shaded area corresponds to two days with asymmetric flow rate, FW was kept the same (39.3 L/h), and SW was reduced to half (19.6 L/h).

In stage 2, the transport pattern of multivalent ions was distinct from the previous stage. From positions 1 to 2, representing the inlet and outlet of stage 2, all ions follow downhill transport, following their concentration gradient, typically from the seawater to fresh water. Such behaviour has not been reported in the literature so far, given that experiments with multistage and multivalent ions are missing. The absence of uphill transport in stage 2 can be explained by the Donnan equilibrium. In stage 1, the multivalent ions exchange with the monovalent ions to obtain equilibrium in chemical potential between the membrane sides [52]. However, in stage 2, the Donnan potential for each ion is equilibrated at the inlet. Figure 5.7 shows the calculated Donnan potential (Eq. 5.1) for each ion on day 17 of the experiment. This day was randomly selected from the data. Stage 1 works as a removal step for multivalent ions, comparable to the principle of Donnan Dialysis [53]. The application of Donnan Dialysis as a pre-treatment step for RED was proposed earlier to improve the power density [54]. Since uphill transport was an intrinsic loss only for stage 1, stage 2 could benefit from this, resulting in a relatively better performance on that stage despite the lower salinity gradient.

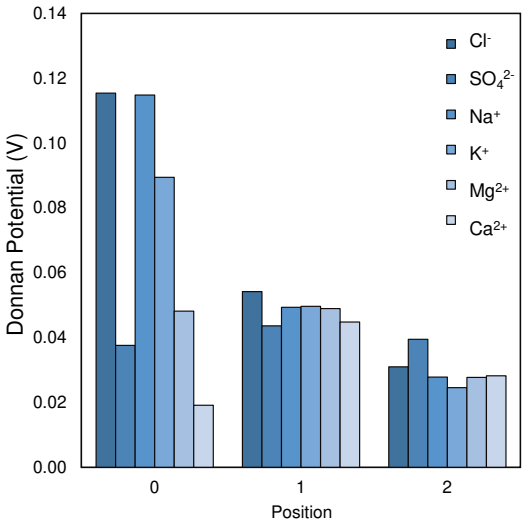


**Figure 5.7** Calculated Donnan Potentials (Eq. 5.1) for the ions at the positions 0, 1 and 2 on day 17 (randomly selected to represent the data). Each bar represents an ion, from left to right: chloride, sulphate, sodium, potassium, magnesium and calcium.

### 5.3.4. Cleaning and stack autopsy

The anti-fouling strategies adopted in the pre-treatment were not able to maintain the stacks' pressure drop close to the initial values. Increasing pressure drops lead to higher pumping power losses which decrease the available net power density. Thus, towards the end of the experiment, in an attempt to lower the pressure drop and possibly recover the initial value, three physical cleaning techniques were selected regarding low cost, sustainability and short system interruption, and applied to both stacks. The cleaning started with reversing the inlet and outlet, followed by increased flow rate and finally air sparging. Results achieved with the application of these cleaning techniques are presented in Figure 5.8.

The fouling removal on both stages was similar, achieving a recovery in pumping power losses of 0.03 W/m$^2$ for stage 1 and 0.01 W/m$^2$ for stage 2, which in both cases represented around 15% of the pumping power that could be recovered from stage 1 (~ 0.21 W/m$^2$) and stage 2 (~ 0.07 W/m$^2$). A higher removal of fouling on stage 1 was expected since the flow velocity in this stage was higher and it was also more likely to accumulate foulants, as it was the first stack to receive the feed waters. Most likely that could not be detected due to the cleaning being performed only after a long time of operation when fouling build-up was already established and reached similar levels in both stages. When looking at the amount of particulate removed that could be collected in the outlet of the stacks, we observed that on the seawater outlet of stage 1 a higher removal was achieved (Fig. 5.8). This indicates that more fouling was present and could be removed, even though the numbers presented are normalized for the membrane area, which in stage 2 is double of stage 1. For fresh water this did not happen, with similar removal in both stages, indicating that the fouling was not affected by the different hydraulic conditions of stages 1 and 2.

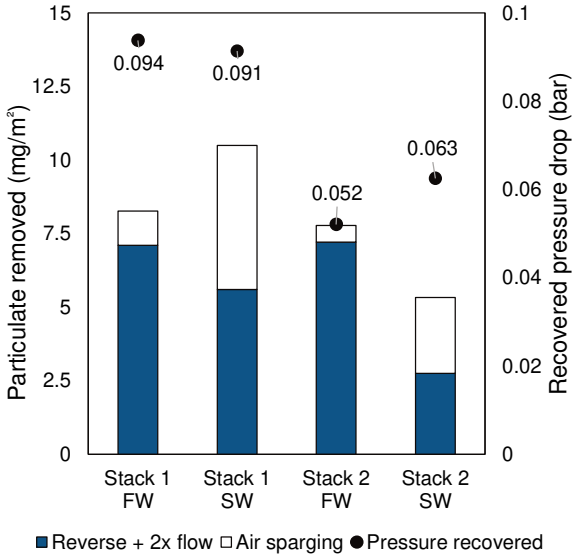


**Figure 5.8.** Bars represent the amount of particulate fouling removed per stack membrane area for each step of the cleaning procedure: cleaning with reverse and increased flow together and air sparging. The pressure drop that could be recovered from each water compartment at the end of the cleaning is presented with a round symbol on top of the bars (difference between right before and after cleaning). The pressure drop decrease after the cleaning procedure appeared only to be a small fraction of the pressure drop across the stages after long term operation.

After the cleaning, two fractions of particulate fouling were analysed, the first one collected after the reverse and increased flow, and the second after air sparging. For the fresh water compartments of both stages, the particulate removal was greater with the reverse and increase flow than with the air sparging. This probably happened due to the order in which the procedures took place, nonetheless, it showed that this simple technique could already remove a large part of the reversible fouling at a low energy cost and no additional agents had to be added (Fig. 5.8). For the seawater compartments of both stages, the removal of foulants with air sparging was similar to the amount achieved with the reverse and increased flow (around 50% of total particulate removed), showing that the addition of compressed air as a cleaning agent could result in better cleaning. This indicates that the remaining fouling from seawater could still be removed with increased shear stress near the membrane surface as caused by the use of compressed air, tackling a more resistant fouling layer. This shows that a dedicated cleaning procedure must be applied for a specific type of fouling.

The results show that the pumping power recovered achieved with the cleaning procedure was quite modest (15 %) compared to the power losses accumulated on the previous days of operation. Implementing the cleaning method earlier in the operation and

more frequent, may have prevented the cumulative increase of pressure drop [24]. In addition, other more intensive physical cleanings or chemical cleanings could be considered to reduce the fouling related pumping power losses [55].

Following the cleaning procedures, the configuration was kept running for two additional weeks to allow fouling regrowth and then stage 1 was opened for fouling investigation. Representative pictures of the membranes and spacers autopsy are shown in Figure S 5.6. In the autopsy no particulate fouling was visible, nor types of fouling could be seen by the naked eye, except the presence of organic fouling by humic acids on the AEMs, due to the characteristically brown colour of this type of fouling [43]. The positive charge of the AEMs attracts the negatively charged organic matter commonly found in freshwater bodies, widely known as humic acids, while CEMs do not suffer from this specific type of fouling, due to their negative charge being able to repel such foulants. However, under the microscope, many types of foulant could be identified, as shown in Figures 5.9 and 5.10.

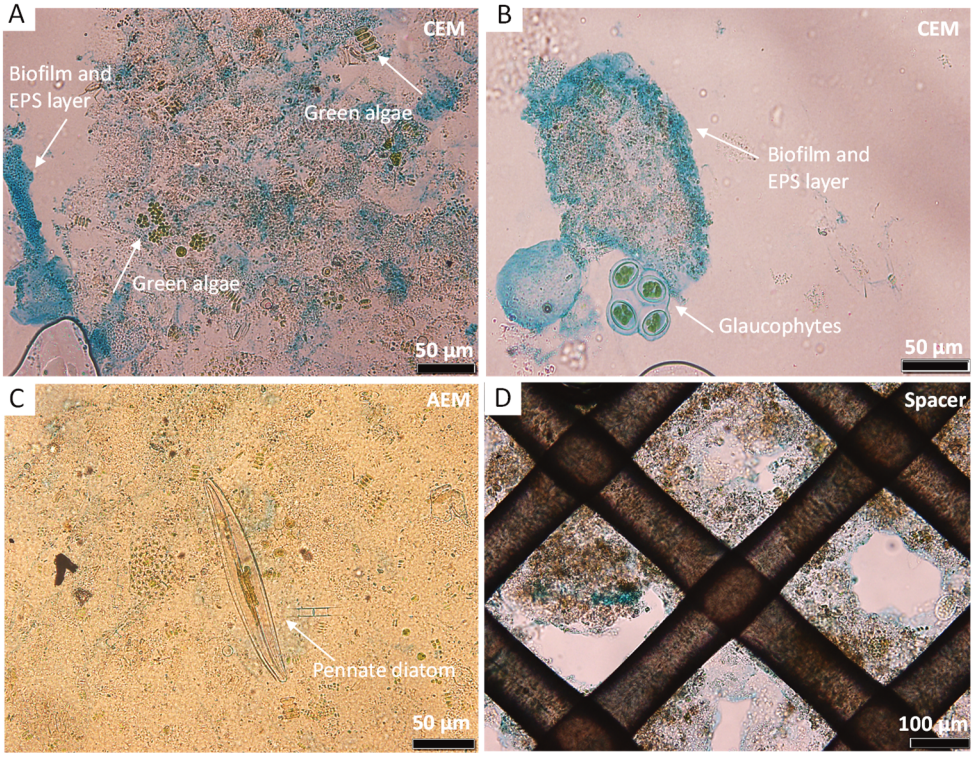


**Figure 5.9** Representative microscopic images of algae and other structures found on CEM (A and B), AEM (C) and spacer (D). The scale bar is 50 µm for A, B and C and 100 µm for D.

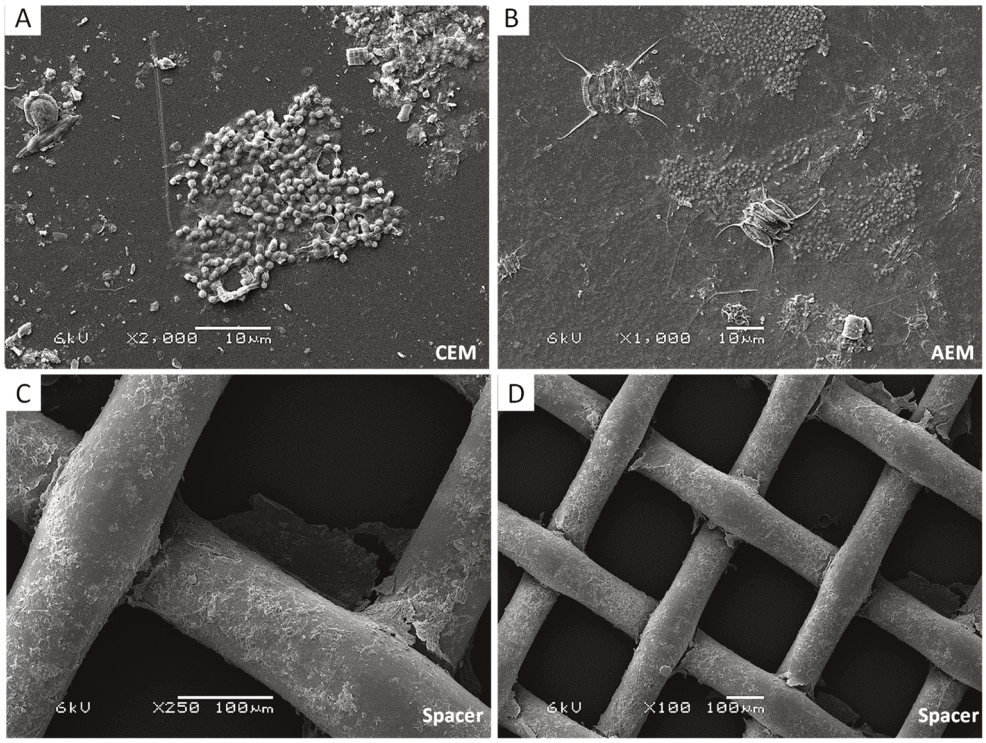


**Figure 5.10.** Scanning electron microscope representative images of CEM (A), AEM (B) and spacers (C and D). The scale bar is 10 µm for A and B, and 100 µm for C and D.

Figures 5.9A, 5.9B and 5.9C show agglomerations of organisms forming large structures, from 1 µm to approximately 50 µm. Most of the structures were identified as green algae, glaucophytes, and diatoms, all of them being commonly present in freshwater bodies [56,57]. The alcian blue dye reacted with biofilm and EPS layer, enabling their visualization and their presence was quite extensive on the surface of the membrane. SEM images, in Figures 5.10A and 5.10B, show similar structures, and biofilm formation can be seen more clearly, with an agglomerate of bacterial cells surrounded by the EPS layer. These types of foulants are consistent with the pre-treatment that was employed during the experiment since with a 5 µm filter as the last step of pre-treatment, a large part of particulate fouling was retained and only smaller foulants could pass through. The formation of structures larger than 5 µm resulted from the growth of living organisms and aggregation in communities.

Figures 5.9D, 5.10C and 5.10D also show an accumulation of fouling at the spacers at all four corners of the open mesh area. The presence of fouling reduced the available open area for the feedwaters to pass and consequently led to an increase in pressure drop. The spacers' thickness of 155 µm was remarkably thin and increased the sensitivity to fouling,

which may also have contributed to an increase of the pressure on the inlet compartment [58].

Unfortunately, the cleaning procedures were not effective in removing the remaining pressure drop to a large extent, as the type of fouling in this experiment was more intrinsically connected to the membrane surface than loosely particulate deposits. For future studies, an anti-fouling strategy to be applied against biofouling growth could be avoiding sunlight to reach the stacks and tubing. In a darker setting, most microorganisms' metabolism will be slower, preventing growth and accumulation [59]. Although there was a large effect of fouling on the hydraulic performance, the impact of fouling and scaling did not affect the gross electrical performance of the membrane pile, as the gross power density kept stable during the experiment. This positive outcome shows that the electrical optimization of the RED process (e.g., by multistage or electrode segmentation) and the minimization of the hydraulic resistance showed to be independent activities. The main influence of fouling was via the hydraulic resistance, affecting the required pumping power. This issue should be addressed using profiled membranes [25] or (in combination) with a more frequent cleaning procedure directly from the start of the experiment. The anti-fouling strategies (in pre-treatment and cleaning) should also be separately investigated and evaluated in view of their effectiveness, power consumption, system interruption and impact on environmental sustainability [20].

### 5.4. Conclusions

A multistage reverse electrodialysis system was operated with natural waters, at the Afsluitdijk, the Netherlands, for over 30 days with a stable gross electrical performance. The gross power density was between 0.3 and 0.4 $W/m^2$ and energy efficiency values were between 30 and 37%. A strong increase in pressure drop in stage 1 was observed in the first weeks, after which the net power density was stable at around 0.1 $W/m^2$. Considering the initial measured pressure drop the net power density would increase to around 0.25 $W \cdot m^{-2}$. Fouling did not affect the gross electrical performance of both stages but led to a higher pressure drop reducing the net power density output. The transport of multivalent ions was different in stage 1 and stage 2. For stage 1, $SO_4^{2-}$ and $Ca^{2+}$ showed uphill transport from fresh water to seawater, whereas $Mg^{2+}$, which is often linked to uphill transport in literature, did not. This was explained by the higher concentration of $Ca^{2+}$ than $Mg^{2+}$ in the fresh water. In stage 2, no uphill transport was observed. The cleaning procedures applied had limited effect on recovering the original pressure drop of the stacks. Stack autopsy revealed, at the membrane surface, microorganism structures larger than the cartridge filter (mean pore size of 5 µm) used as pre-treatment for the natural waters. The agglomeration and growth of these structures in-situ contributed to the increase in pressure drop through time in the compartments, as well as part of the spacers' open area that was covered with (bio)fouling.

Multistage reverse electrodialysis, with two stages in series, showed as a viable configuration to increase the energy efficiency with a stable gross power density, even at the low salinity gradient, available in this duration test. For optimal performance, the electrical control of the stages could be automated, taking into consideration the conductivity at the inlets and actual pressure drop. An improved stack design in combination with pre-treatment of the natural waters and periodical cleaning procedure of the stages is highly recommended, to avoid the power losses associated with the pressure drop increase across the stacks.

**Supporting information**

**Hexacyanoferrate solution**

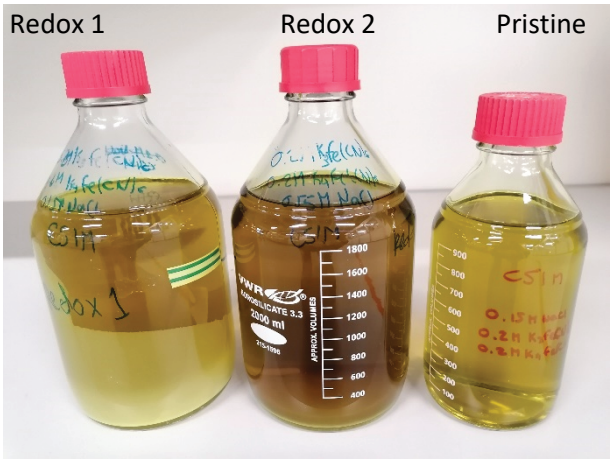


**Figure S 5.1** Pristine hexacyanoferrate solution (left) compared with the hexacyanoferrate solutions used as ERS at the electrode compartments of stages 1 (right) and 2 (middle) for four days.

The autopsy of the electrodes and spacers adjacent to the electrode compartments showed scaling in different forms, as seen in the pictures in Figure S 5.2.

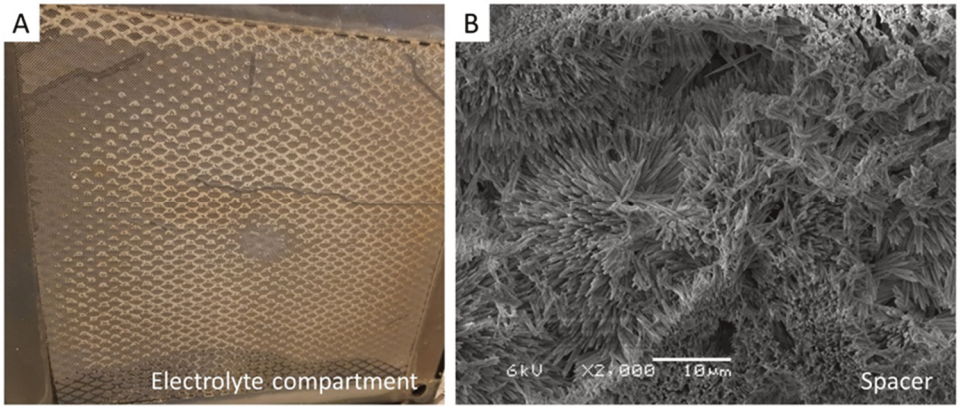


**Figure S 5.2** (A) Picture of the electrolyte compartment (spacer and electrode behind) and the white scaling on the spacer mesh (scaling). (B) SEM image of the spacer compartment, showing the crystals formed by scaling. With EDX the scaling was identified as $CaCO_3$ deposition.

The scaling was attached to the electrode, to the spacer net and the shielding membrane on the side facing the electrode. Using EDX, it is more likely that the scaling of the spacers was caused by $CaCO_3$ and on the electrodes scaling was a combination of $Ca(OH)_2$ and $Mg(OH)_2$. Since no cleaning was performed on the electrodes, the scaling as found may still

relate to scaling issues using the hexacyanoferrate electrode rinse solution on the transition to natural waters and, while the single-pass seawater, as ERS, was running without periodically switching the feedwaters (until day 5 of the 30-day run). The electrode scaling was more evident on one side than the other, which reinforces the assumption that this scaling developed at the start of the experiment. Scaling is more prone to occur at the cathode due to an increase in alkalinity. While switching the waters, both electrode compartments act as cathode or anode at some point, making a pH change in the compartment. During the period that the electrode acts as the anode, the precipitates can dissolve due to the formation of acid. To avoid scaling, reversal of polarity every six hours was found effective.

**Conditions during the installation phase and the 30-day run**

The seawater concentration, and thus conductivity, now and then drastically fluctuated due to the Afsluitdijk locks located at each end of the dyke (Fig. S 5.3A). These locks open for boats to cross and to discharge extra fresh water from Lake IJssel. For example, between day 0 to day 10 on the 30-day run the locks were frequently opened, due to intense rainfall in the region (Fig. S 5.4), the seawater conductivity even dropped to 15 mS/cm. In those moments, given the non-stable behaviour, both stages operated in OCV conditions (Fig. S 5.3B). These location-specific fluctuations reveal a vulnerability to operating with natural intakes. Note that also at other locations, the conductivity and temperature can change drastically during the seasons or specific weather events [16]. An automated control to adapt the current, given the inlet conductivities, could be a solution for better operation. In the present case, the temperature fluctuated between 18 and 21 °C and between day and night the change was 1 °C (Fig. S 5.3D).

The stages' pressure drops are shown in Figure S 5.3C. The higher initial pressure drop in stage 1 is due to increased flow velocity (1 cm/s) compared to stage 2 (0.5 cm/s). Stage 1 was the first to suffer from increased pressure drop since it is also the one receiving the feed waters first. This was probably caused by an accumulation of fouling at the membranes and in the very thin spacer used (155 µm). After the accentuated increase until day 6, for stage 1, water switching was used to mitigate scaling issues at the cathode in both stages. At the same time, this technique also helped with the increasing pressure drop where the rapid increase was replaced by a moderate increase over time and rejuvenated the performance of stage 1 (Fig. S 5.3B, days 4 to 6). It is hypothesized that the periodical osmotic shock caused by switching the seawater with the fresh water acted as an anti-fouling technique. It is also after day 6, with the switching, that the pressure drop of stage 2 starts to slowly increase. It seems that until then stage 1 was acting like a filter to stage 2, and later the filtering capacity of stage 1 was lost with the switching, thus the fouling was carried to the next stage.

**Figure S 5.3** (next page). (A) Inlet seawater (SW) and fresh water (FW) conductivity, (B) stage 1 and stage 2 gross power density, (C) SW and FW compartments pressure drop for stages 1 and 2, and (D) inlet SW and FW temperature, for the installation period and later 30-day run. When the water switching was active, the waters changed periodically, and with this, the line and colour do not indicate SW or FW but are fixed to the compartment (pressure drop plot). The zig-zag pattern on the pressure drop plot, after water switching, was thought to be caused by an asymmetry between pumps and compartments, but it was not further explored. The orange shaded areas correspond to OCV moments. The green shaded area corresponds to two days with asymmetric flow rate, FW was kept the same (39.3 L/h), and SW was reduced to half (19.6 L/h).

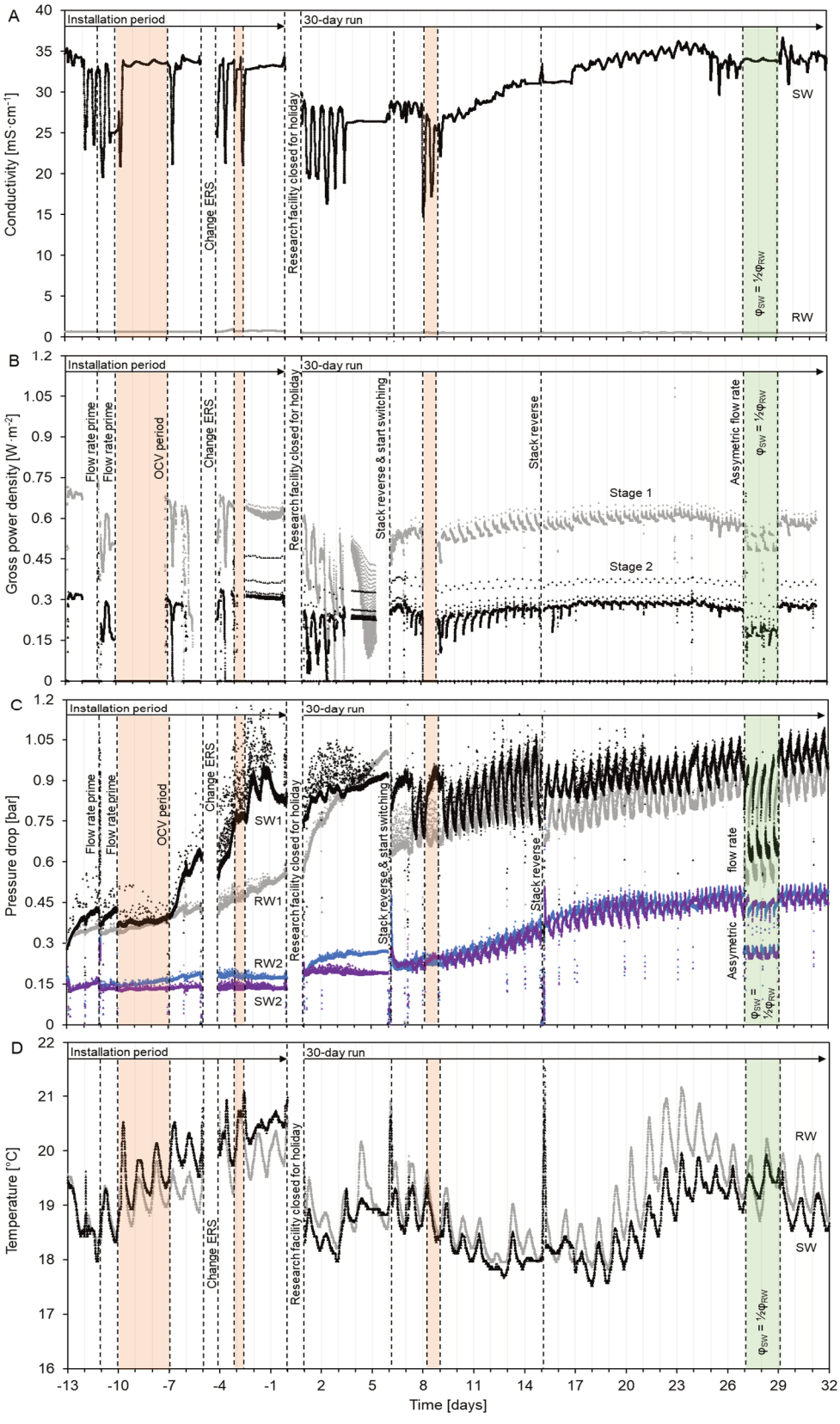
A
Installation period
30-day run
Conductivity [mS·cm⁻¹]
Change ERS
Research facility closed for holiday
SW
RW
φSW = ½φRW
B
Gross power density [W·m⁻²]
Flow rate prime
Flow rate prime
OCV period
Change ERS
Research facility closed for holiday
Stack reverse & start switching
Stack reverse
Stage 1
Stage 2
Assymetric flow rate
C
Pressure drop [bar]
SW1
RW1
RW2
SW2
Assymetric flow rate
D
Temperature [°C]
Time [days]

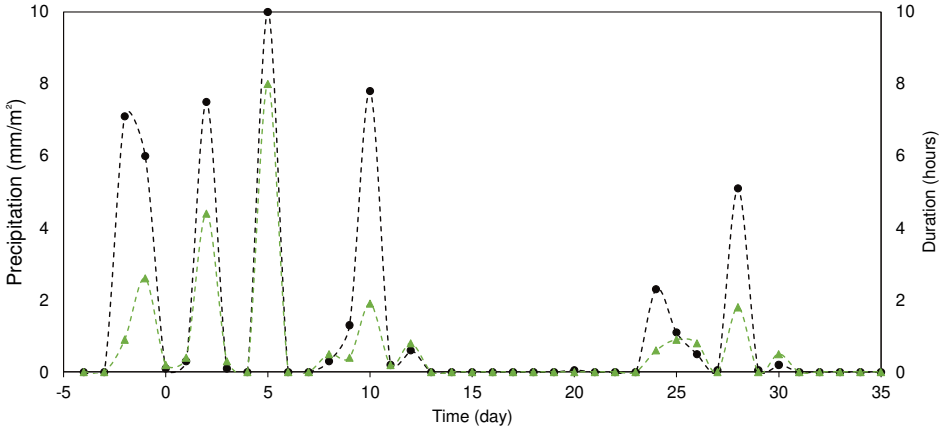


**Figure S 5.4** Rainfall as registered in Leeuwarden, the Netherlands, 5 days before and during the 30-day experiment [60], this figure does not comprise rainfall data from the installation period.

**Pressure drop calculations**

The pumping losses, or pumping power density ($P_{d,pump}$ in W/m$^2$), corresponding to the power lost for pumping SW and FW through a stack was calculated as:

$$P_{d,pump} = \frac{\varphi_{FW} \cdot \Delta P_{FW} + \varphi_{SW} \cdot \Delta P_{SW}}{A_{mem}} \quad \text{(Eq. S 5.1)}$$

Where $\varphi$ is the flow rate (m$^3$/s) and $\Delta P$ is the pressure drop across the compartment (Pa). By measuring the pumping losses, the net power density can be calculated as the difference between gross power and pumping power:

$$P_{d,net} = P_{d,gross} - P_{d,pump} \quad \text{(Eq. S 5.2)}$$

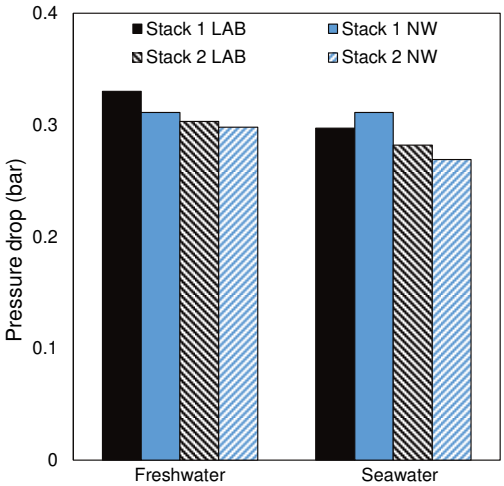

**Figure S 5.5** Pressure drop of fresh water and seawater in each stack at 1.0 cm/s (39.3 L/h for stack 1 and 78.6 L/h for stack 2) at the laboratory tests (LAB) and at the pilot plant with natural waters (NW) at initial conditions. Stack 1 = stage 1 and stack 2 = stage 2.

### 4.5.4. Switch position and current and stack potential measured during the 30-day run

**Table S 5.1** Switch position and applied current with the respective voltage response at the sampling moments. Since water switching occurred, two positions are defined: position A indicates the original/starting position, and position B indicates seawater is in the original fresh water compartment and vice-versa.

| Sample day | Position | $I_{S1}$ [A] | $E_{S1}$ [V] | $I_{S2}$ [A] | $E_{S2}$ [V] |
|---|---|---|---|---|---|
| 1 | A | 0.866 | 2.090 | 0.519 | 2.902 |
| 2 | A | 0.866 | 1.568 | 0.518 | 2.456 |
| 7 | B | 0.807 | 2.067 | 0.640 | 2.239 |
| 8 | A | 0.793 | 2.171 | 0.583 | 2.611 |
| 9 | B | 0.759 | 2.051 | 0.594 | 2.234 |
| 13 | B | 0.759 | 2.294 | 0.594 | 2.696 |
| 14 | B | 0.759 | 2.310 | 0.594 | 2.833 |
| 15 | B | 0.759 | 2.306 | 0.594 | 2.533 |
| 16 | A | 0.746 | 2.389 | 0.537 | 3.073 |
| 17 | A | 0.746 | 2.480 | 0.537 | 3.277 |
| 20 | B | 0.759 | 2.395 | 0.594 | 3.055 |
| 21 | A | 0.746 | 2.502 | 0.537 | 3.263 |
| 22 | A | 0.747 | 2.542 | 0.537 | 3.295 |
| 23 | B | 0.759 | 2.431 | 0.593 | 2.860 |
| 26 | A | 0.746 | 2.392 | 0.537 | 3.020 |
| 27 | B | 0.713 | 2.338 | 0.407 | 2.978 |
| 28 | A | 0.747 | 2.010 | 0.390 | 2.951 |
| 30 | B | 0.759 | 2.395 | 0.594 | 2.979 |

**Membrane autopsy**

Representative pictures of the membranes and spacer are shown in Figure S 5.6. Clean Fumasep FAS-30 and FKS-30 (Fumatech, Germany) membranes are translucent and transparent, as well as a clean spacer net. The membranes and spacers were found to be intact when opening the stacks at the autopsy, with no visible damage. Due to interactions with humic acids, AEMs turned brown after the experiment, while CEMs preserved the same characteristics of a clean membrane looking by the naked eye. On the spacers, some fouling accumulation can be seen on the connections of the mesh, mostly characterized by green light colour due to the presence of algae-like structures.

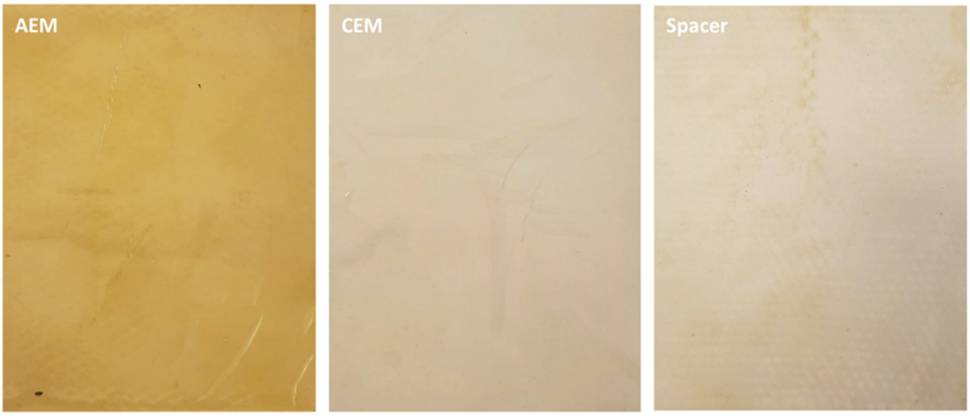


**Figure S5.6** Representative pictures of the membranes and spacer. Due to interactions with humic acids, AEMs turned brown after the experiment, while CEMs preserved visually the same characteristics of a clean membrane. On the spacers, some fouling accumulation can be seen on the connections of the net, mostly characterized by green light colour due to the presence of algae.

**References**


[1] K. Nijmeijer, S. Metz, Chapter 5 Salinity Gradient Energy, Elsevier, 2010. https://doi.org/10.1016/S1871-2711(09)00205-0.

[2] R.E. Lacey, Energy by reverse electrodialysis, Ocean Engineering. 7 (1980) 1–47. https://doi.org/10.1016/0029-8018(80)90030-x.

[3] J. Veerman, M. Saakes, S.J. Metz, G.J. Harmsen, Reverse electrodialysis: Evaluation of suitable electrode systems, J Appl Electrochem. (2010). https://doi.org/10.1007/s10800-010-0124-8.

[4] R.E. Pattle, Production of electric power by mixing fresh and salt water in the hydroelectric pile, Nature. (1954). https://doi.org/10.1038/174660a0.

[5] A. Nazif, H. Karkhanechi, E. Saljoughi, S.M. Mousavi, H. Matsuyama, Recent progress in membrane development, affecting parameters, and applications of reverse electrodialysis: A review, Journal of Water Process Engineering. 47 (2022) 102706. https://doi.org/10.1016/j.jwpe.2022.102706.

[6] Y. Mei, C.Y. Tang, Recent developments and future perspectives of reverse electrodialysis technology: A review, Desalination. (2017). https://doi.org/10.1016/j.desal.2017.10.021.

[7] R.A. Tufa, S. Pawlowski, J. Veerman, K. Bouzek, E. Fontananova, G. di Profio, S. Velizarov, J. Goulão Crespo, K. Nijmeijer, E. Curcio, Progress and prospects in reverse electrodialysis for salinity gradient energy conversion and storage, Appl Energy. 225 (2018) 290–331. https://doi.org/10.1016/j.apenergy.2018.04.111.

[8] J.W. Post, C.H. Goeting, J. Valk, S. Goinga, J. Veerman, H.V.M. Hamelers, P.J.F.M. Hack, Towards implementation of reverse electrodialysis for power generation from salinity gradients, Desalination Water Treat. 16 (2010) 182–193. https://doi.org/10.5004/dwt.2010.1093.

[9] J.W. Post, H.V.M. Hamelers, C.J.N. Buisman, Influence of multivalent ions on power production from mixing salt and fresh water with a reverse electrodialysis system, J Memb Sci. (2009). https://doi.org/10.1016/j.memsci.2008.12.042.

[10] D.A. Vermaas, J. Veerman, M. Saakes, K. Nijmeijer, Influence of multivalent ions on renewable energy generation in reverse electrodialysis, Energy Environ Sci. (2014). https://doi.org/10.1039/c3ee43501f.

[11] Z.Y. Guo, Z.Y. Ji, Y.G. Zhang, F.J. Yang, J. Liu, Y.Y. Zhao, J.S. Yuan, Effect of ions (K+, Mg2+, Ca2+ and SO42−) and temperature on energy generation performance of reverse electrodialysis stack, Electrochim Acta. 290 (2018) 282–290. https://doi.org/10.1016/j.electacta.2018.09.015.

[12] A.H. Avci, R.A. Tufa, E. Fontananova, G. di Profio, E. Curcio, Reverse Electrodialysis for energy production from natural river water and seawater, Energy. 165 (2018) 512–521. https://doi.org/10.1016/j.energy.2018.09.111.

[13] E. Güler, W. van Baak, M. Saakes, K. Nijmeijer, Monovalent-ion-selective membranes for reverse electrodialysis, J Memb Sci. (2014). https://doi.org/10.1016/j.memsci.2013.12.054.

[14] T. Rijnaarts, E. Huerta, W. Van Baak, K. Nijmeijer, Effect of Divalent Cations on RED Performance and Cation Exchange Membrane Selection to Enhance Power Densities, Environ Sci Technol. (2017) 13028–13035. https://doi.org/10.1021/acs.est.7b03858.

[15] S. Mehdizadeh, Y. Kakihana, T. Abo, Q. Yuan, M. Higa, Power generation performance of a pilot-scale reverse electrodialysis using monovalent selective ion-exchange membranes, Membranes (Basel). 11 (2021) 1–25. https://doi.org/10.3390/membranes11010027.

[16] E.H. Hossen, Z.E. Gobetz, R.S. Kingsbury, F. Liu, H.C. Palko, L.L. Dubbs, O. Coronell, D.F. Call, Temporal variation of power production via reverse electrodialysis using coastal North Carolina waters and its correlation to temperature and conductivity, Desalination. 491 (2020) 114562. https://doi.org/10.1016/j.desal.2020.114562.

[17] S. Mehdizadeh, M. Yasukawa, T. Abo, M. Kuno, Y. Noguchi, M. Higa, The effect of feed solution temperature on the power output performance of a pilot-scale reverse electrodialysis (RED) system with different intermediate distance, Membranes (Basel). 9 (2019). https://doi.org/10.3390/membranes9060073.

[18] D.A. Vermaas, D. Kunteng, M. Saakes, K. Nijmeijer, Fouling in reverse electrodialysis under natural conditions, Water Res. (2013). https://doi.org/10.1016/j.watres.2012.11.053.

[19] R.S. Kingsbury, F. Liu, S. Zhu, C. Boggs, M.D. Armstrong, D.F. Call, O. Coronell, Impact of natural organic matter and inorganic solutes on energy recovery from five real salinity gradients using reverse electrodialysis, J Memb Sci. 541 (2017) 621–632. https://doi.org/10.1016/j.memsci.2017.07.038.

[20] B. Vital, E. v. Torres, T. Sleutels, M.C. Gagliano, M. Saakes, H.V.M. Hamelers, Fouling fractionation in reverse electrodialysis with natural feed waters demonstrates dual media rapid filtration as an effective pre-treatment for fresh water, Desalination. 518 (2021). https://doi.org/10.1016/j.desal.2021.115277.

[21] D.A. Vermaas, D. Kunteng, J. Veerman, M. Saakes, K. Nijmeijer, Periodic feedwater reversal and air sparging as antifouling strategies in reverse electrodialysis, Environ Sci Technol. (2014). https://doi.org/10.1021/es4045456.

[22] J. Moreno, N. de Hart, M. Saakes, K. Nijmeijer, CO 2 saturated water as two-phase flow for fouling control in reverse electrodialysis, Water Res. (2017). https://doi.org/10.1016/j.watres.2017.08.015.

[23] E.J. Bodner, M. Saakes, T. Sleutels, C.J.N. Buisman, H.V.M. Hamelers, The RED Fouling Monitor: A novel tool for fouling analysis, J Memb Sci. (2019). https://doi.org/10.1016/j.memsci.2018.10.059.

[24] D. Pintossi, M. Saakes, Z. Borneman, K. Nijmeijer, Electrochemical impedance spectroscopy of a reverse electrodialysis stack: A new approach to monitoring fouling and cleaning, J Power Sources. 444 (2019) 227302. https://doi.org/10.1016/j.jpowsour.2019.227302.

[25] D.A. Vermaas, M. Saakes, K. Nijmeijer, Power generation using profiled membranes in reverse electrodialysis, J Memb Sci. (2011). https://doi.org/10.1016/j.memsci.2011.09.043.

[26] S. Pawlowski, T. Rijnaarts, M. Saakes, K. Nijmeijer, J.G. Crespo, S. Velizarov, Improved fluid mixing and power density in reverse electrodialysis stacks with chevron-profiled membranes, J Memb Sci. (2017). https://doi.org/10.1016/j.memsci.2017.03.003.

[27] J.Y. Nam, K.S. Hwang, H.C. Kim, H. Jeong, H. Kim, E. Jwa, S.C. Yang, J. Choi, C.S. Kim, J.H. Han, N. Jeong, Assessing the behavior of the feed-water constituents of a pilot-scale 1000-cell-pair reverse electrodialysis with seawater and municipal wastewater effluent, Water Res. 148 (2019) 261–271. https://doi.org/10.1016/j.watres.2018.10.054.

[28] C. Simões, D. Pintossi, M. Saakes, Z. Borneman, W. Brilman, K. Nijmeijer, Electrode segmentation in reverse electrodialysis: Improved power and energy efficiency, Desalination. 492 (2020). https://doi.org/10.1016/j.desal.2020.114604.

[29] J. Hu, S. Xu, X. Wu, D. Wu, D. Jin, P. Wang, Q. Leng, Multi-stage reverse electrodialysis: Strategies to harvest salinity gradient energy, Energy Convers Manag. (2019). https://doi.org/10.1016/j.enconman.2018.11.032.

[30] C. Simões, D. Pintossi, M. Saakes, W. Brilman, Optimizing multistage reverse electrodialysis for enhanced energy recovery from river water and seawater: Experimental and modeling investigation, Advances in Applied Energy. (2021). https://doi.org/10.1016/j.adapen.2021.100023.

[31] J. Veerman, M. Saakes, S.J. Metz, G.J. Harmsen, Reverse electrodialysis: Performance of a stack with 50 cells on the mixing of sea and river water, J Memb Sci. (2009). https://doi.org/10.1016/j.memsci.2008.11.015.

[32] J. Veerman, Reverse Electrodialysis : Co- and Counterflow Optimization of Multistage Configurations for Maximum Energy Efficiency, Membranes (Basel). (2020) 1–13. https://doi.org/10.3390/membranes10090206.

[33] M. Tedesco, P. Mazzola, A. Tamburini, G. Micale, I.D.L. Bogle, M. Papapetrou, A. Cipollina, Analysis and simulation of scale-up potentials in reverse electrodialysis, Desalination Water Treat. (2015). https://doi.org/10.1080/19443994.2014.947781.

[34] J. Hu, S. Xu, X. Wu, S. Wang, X. Zhang, S. Yang, R. Xi, D. Wu, L. Xu, Experimental investigation on the performance of series control multi-stage reverse electrodialysis, Energy Convers Manag. 204 (2020). https://doi.org/10.1016/j.enconman.2019.112284.

[35] Z. Wang, J. Li, C. Zhang, H. Wang, X. Kong, Power production from seawater and discharge brine of thermal desalination units by reverse electrodialysis, Appl Energy. 314 (2022). https://doi.org/10.1016/j.apenergy.2022.118977.

[36] S. Xu, Q. Leng, X. Wu, Z. Xu, J. Hu, D. Wu, D. Jing, P. Wang, F. Dong, Influence of output current on decolorization efficiency of azo dye wastewater by a series system with multi-stage reverse electrodialysis reactors, Energy Convers Manag. 228 (2021). https://doi.org/10.1016/j.enconman.2020.113639.

[37] J. Hu, S. Xu, X. Wu, D. Wu, D. Jin, P. Wang, Q. Leng, Theoretical simulation and evaluation for the performance of the hybrid multi-effect distillation—reverse electrodialysis power generation system, Desalination. 443 (2018) 172–183. https://doi.org/10.1016/j.desal.2018.06.001.

[38] Y. Zhang, X. Wu, S. Xu, Q. Leng, S. Wang, A serial system of multi-stage reverse electrodialysis stacks for hydrogen production, Energy Convers Manag. 251 (2022). https://doi.org/10.1016/j.enconman.2021.114932.

[39] D. Pintossi, C. Simões, M. Saakes, Z. Borneman, K. Nijmeijer, Predicting reverse electrodialysis performance in the presence of divalent ions for renewable energy generation, Energy Convers Manag. 243 (2021). https://doi.org/10.1016/j.enconman.2021.114369.

[40] J. Moreno, E. Slouwerhof, D.A. Vermaas, M. Saakes, K. Nijmeijer, The Breathing Cell: Cyclic Intermembrane Distance Variation in Reverse Electrodialysis, Environ Sci Technol. (2016). https://doi.org/10.1021/acs.est.6b02668.

[41] P. Długołecki, K. Nymeijer, S. Metz, M. Wessling, Current status of ion exchange membranes for power generation from salinity gradients, J Memb Sci. (2008). https://doi.org/10.1016/j.memsci.2008.03.037.

[42] J. Moreno, S. Grasman, R. van Engelen, K. Nijmeijer, Up-scaling reverse electrodialysis, Environ Sci Technol. (2018). https://doi.org/10.1021/acs.est.8b01886.

[43] T. Rijnaarts, J. Moreno, M. Saakes, W.M. de Vos, K. Nijmeijer, Role of anion exchange membrane fouling in reverse electrodialysis using natural feed waters, Colloids Surf A Physicochem Eng Asp. 560 (2019) 198–204. https://doi.org/10.1016/j.colsurfa.2018.10.020.

[44] X. Ge, X. Wang, M. Zhang, S. Seetharaman, Correlation and prediction of activity and osmotic coefficients of aqueous electrolytes at 298.15 K by the modified TCPC model, J Chem Eng Data. (2007). https://doi.org/10.1021/je060451k.

[45] D.A. Vermaas, J. Veerman, N.Y. Yip, M. Elimelech, M. Saakes, K. Nijmeijer, High efficiency in energy generation from salinity gradients with reverse electrodialysis, ACS Sustain Chem Eng. (2013). https://doi.org/10.1021/sc400150w.

[46] L. S. Clesceri, A. E. Greenberg, A. D. Eaton, Standard Methods for the Examination of Water and Wastewater 22th Edition, 1999.

[47] A.W. Qurashi, A.N. Sabri, Biofilm formation in moderately halophilic bacteria is influenced by varying salinity levels, J Basic Microbiol. 52 (2012) 566–572. https://doi.org/10.1002/jobm.201100253.

[48] J. Veerman, J.W. Post, M. Saakes, S.J. Metz, G.J. Harmsen, Reducing power losses caused by ionic shortcut currents in reverse electrodialysis stacks by a validated model, J Memb Sci. (2008). https://doi.org/10.1016/j.memsci.2007.11.032.

[49] A. Culcasi, L. Gurreri, A. Zaffora, A. Cosenza, A. Tamburini, A. Cipollina, G. Micale, Ionic shortcut currents via manifolds in reverse electrodialysis stacks, Desalination. (2020). https://doi.org/10.1016/j.desal.2020.114450.

[50] N.Y. Yip, D.A. Vermaas, K. Nijmeijer, M. Elimelech, Thermodynamic, energy efficiency, and power density analysis of reverse electrodialysis power generation with natural salinity gradients, Environ Sci Technol. 48 (2014) 4925–4936. https://doi.org/10.1021/es5005413.

[51] D. Pintossi, C.L. Chen, M. Saakes, K. Nijmeijer, Z. Borneman, Influence of sulfate on anion exchange membranes in reverse electrodialysis, NPJ Clean Water. 3 (2020) 1–10. https://doi.org/10.1038/s41545-020-0073-7.

[52] M. Higa, A. Tanioka, K. Miyasaka, Simulation of the transport of ions against their concentration gradient across charged membranes, J Memb Sci. 37 (1988) 251–266. https://doi.org/10.1016/S0376-7388(00)82432-1.

[53] M. Vanoppen, G. Stoffels, C. Demuytere, W. Bleyaert, A.R.D. Verliefde, Increasing RO efficiency by chemical-free ion-exchange and Donnan dialysis: Principles and practical implications, Water Res. 80 (2015) 59–70. https://doi.org/10.1016/j.watres.2015.04.030.

[54] T. Rijnaarts, N.T. Shenkute, J.A. Wood, W.M. De Vos, K. Nijmeijer, Divalent Cation Removal by Donnan Dialysis for Improved Reverse Electrodialysis, ACS Sustain Chem Eng. (2018). https://doi.org/10.1021/acssuschemeng.8b00879.

[55] K. Chon, N. Jeong, H. Rho, J.Y. Nam, E. Jwa, J. Cho, Fouling characteristics of dissolved organic matter in fresh water and seawater compartments of reverse electrodialysis under natural water conditions, Desalination. 496 (2020) 114478. https://doi.org/10.1016/j.desal.2020.114478.

[56] L.O. Villacorte, S.A.A. Tabatabai, N. Dhakal, G. Amy, J.C. Schippers, M.D. Kennedy, Algal blooms: an emerging threat to seawater reverse osmosis desalination, Desalination Water Treat. 55 (2015) 2601–2611. https://doi.org/10.1080/19443994.2014.940649.

[57] T.H. Tan, C.P. Leaw, S. Chee, Y. Leong, L.P. Lim, S.M. Chew, Marine micro-phytoplankton of Singapore , with a review of harmful microalgae in the region, Raffles Bulletin of Zoology. (2016).

[58] J. Choi, W.-S. Kim, H.K. Kim, S.C. Yang, J.-H. Han, Y.C. Jeung, N.J. Jeong, Fouling behavior of wavy-patterned pore-filling membranes in reverse electrodialysis under natural seawater and sewage effluents, NPJ Clean Water. 5 (2022) 1–12. https://doi.org/10.1038/s41545-022-00149-2.

[59] J. Landoulsi, K.E. Cooksey, V. Dupres, Review - Interactions between diatoms and stainless steel: Focus on biofouling and biocorrosion, Biofouling. 27 (2011) 1105–1124. https://doi.org/10.1080/08927014.2011.629043.

[60] https://www.wetterzentrale.de/de/weatherdata_de.php (seen on 9th December 2021)

# Chapter 6

# Evaluation of chemical free cleaning techniques for RED fed with natural waters and stacks with profiled membranes

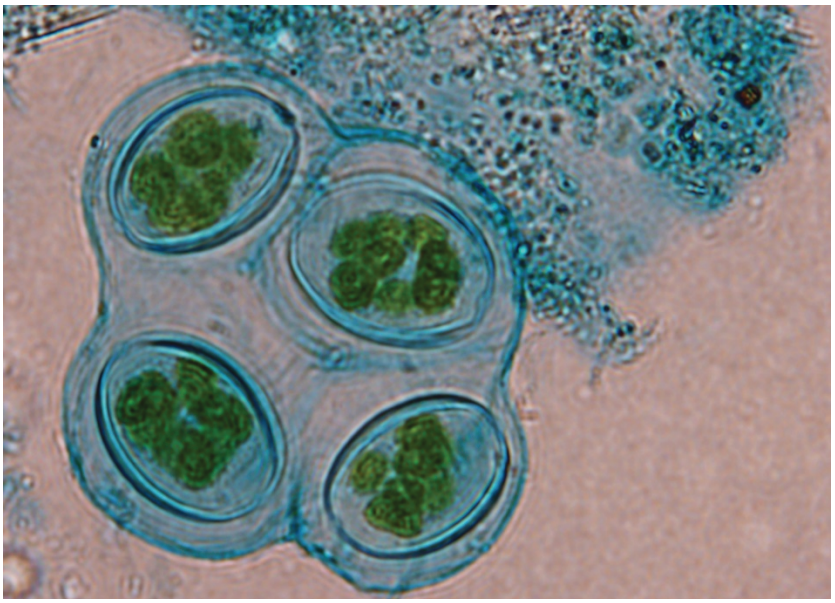

**Abstract:**

Reverse electrodialysis (RED) is a promising technology to harvest salinity gradient power (SGP) that is available where fresh and sea water mix, using anion (AEM) and cation exchange membranes (CEM) in a stack. Fouling of the membranes is one of the main challenges for RED, since it leads to a reduction in attainable net power output. In this study, we combined the use of profiled ion-exchange membranes (200 µm thick compartments) with a pre-treatment by a dual media filter for both natural water streams (Lake Ijssel and Wadden Sea), with four different cleaning procedures: (i) increased flow, (ii) reverse and increased flow, (iii) reverse flow and feed switch, and (iv) air sparging.

Cleaning with air sparging was the most effective technique, limiting the pumping losses and not influencing the power generation capacity. The cleaning with reverse flow and feed switch also showed to be suitable, keeping the pressure drop losses lower than 100 mbar for both water streams. Post experiment membrane autopsy showed that CEMs were more subjected to particulate fouling than AEMs, and that a lower accumulation of fouling by particulate resulted in a higher concentration of humic acids and biofouling on the membrane surface.

## 6.1 Introduction

Reverse electrodialysis (RED) is a promising technology that can be used to harvest the salinity gradient power (SGP), also known as Blue Energy, that is naturally available where fresh and sea water mix [1,2]. SGP is a renewable energy source that can be used in combination with other sustainable energy sources, such as solar and wind, as the SGP is a continuous source of energy and does not suffer from high fluctuations of yield due to weather conditions or day and night cycles [3]. The RED principle is based on exploiting the chemical potential difference from the controlled mixing of a low and high salinity streams separated by ion-exchange membranes converting it into an electrochemical potential difference [1,2,4]. Electrical energy can be harvested by alternating anion exchange membranes (AEM) and cation exchange membranes (CEM), which directs anions to the anode and cations to the cathode of the RED stack, and through redox reactions in the end compartments, using electrodes and an electrolyte solution [1].

Fouling of the ion exchange membranes is one of the main challenges hindering the viability of this technology, since it leads to a reduction of the exploitable net power [5,6]. Prevention and management of fouling is of utmost need for this technology to reach the market [5,7,8]. Fouling formation can be slower when using an effective pre-treatment of the inlet waters (sea and fresh), that removes a large amount of foulants even when the daily and seasonal variations in weather and climate result in varying inflow of foulants. Many pre-treatment methods have been tested on inlet water for RED in the past, such as a drum filter, cartridge filter, river bank filtration, coagulation with polyaluminum chloride (PAC) and sand filter [6,9,10]. The desired pre-treatment should be robust, durable, with simple operation and maintenance and, most important, with a low energy demand [11]. In previous studies we showed that a dual media filter, using anthracite and sand as media, could fulfil many of these requirements, being effective for both seawater and fresh water pre-treatment [12]. In our work, it was also shown that the formation of a fouling layer composed by particulate matter was the main contributor to pumping power losses in the process, but at the same time, its formation could also limit attachment and growth of microorganisms and thus biofouling [12,13]. Thus, the presence of small amounts of particulate matter can be beneficial, and fouling management through cleaning should consider this aspect.

Together with a robust pre-treatment, fouling management with cleaning techniques is necessary to avoid a loss in performance during long term RED operation [7,8,14]. This can be achieved by applying certain operational techniques, such as increased flow, or a proper cleaning procedure that includes the use of a cleaning agent such as compressed gas or chemical solution [7,14]. A combination of frequently applied operational technique and a less frequent cleaning with a cleaning agent could be considered to tackle different types of fouling at low energy expenditure. To make RED a viable and sustainable technology, the

desirable cleaning procedure should require low amounts of energy, be effective, not use harsh chemicals and not produce toxic by-products, since it is likely that cleaning residues will be disposed in the sea. In addition, it should not hamper RED stack performance and membrane properties or demand a long downtime in operation [8]. Previous research on this matter included the work of Post et al [15], who proposed switching of feed waters in the compartments' regularly to promote an osmotic shock of microorganisms and prevent biofouling development. Vermaas et al. [16] compared the periodic feed water switching with air sparging, with both techniques being applied every 30 min, and air sparging showed to be more effective on long-term operation. Moreno et al. [17] investigated the best configuration of operation for air and $CO_2$ sparging, implementing the use of short pulses of compressed gas. The main conclusion was that applying $CO_2$ was more effective since less stagnant bubbles were trapped on the spacers mesh, allowing for a more constant performance of stacks [17]. Finally, when using a basic solution as cleaning agent, Chon et al. showed that both organic and inorganic foulants were more effectively desorbed from the membrane surface in fresh and sea water in comparison to an acid solution, but no details on the potential by-products formed was presented [18].

In (reverse) electro-dialysis, it is common to use spacers to create the compartments for feed waters, but recent studies showed that the use of spacers could hinder stack performance, due to the spacer shadow effect and by enhancing the surface available for fouling attachment [8,19–21]. In addition, the spacers can have a negative effect when applying cleaning techniques, such as air sparging, by trapping bubbles and increasing the resistance of the cell [16,17]. Thus, an alternative for spacers was designed, by imprinting channels on the membranes surface to make the compartments, the so-called profiled membranes [21–23]. Profiled membranes have shown to yield better power output when using natural waters and allow for more customization of desired flow distribution inside the cell [16,19,23].

Despite the above-mentioned benefits, profiled membranes are not yet commercially available due to difficulties of profiling surfaces at large scale and a low demand for this type of membrane.

In this study, we combined the use of thermo-pressed profiled ion-exchange membranes, that created water compartments of 200 µm thickness, with dual media filter pre-treatment of both inlet waters and four different (new and more established) cleaning procedures, namely increased flow (IF), reverse and increased flow (RIF), reverse flow and feed switch (RFFS), and air sparging (AS). The selection of the techniques was based on results from previous research [16,17,19] and the above mentioned needs for RED to be a viable and sustainable technology.

The cleaning procedures were compared for their impact on stack performance and fouling removal potential. The applied cleaning techniques had different impacts on fouling build-

up and performance loss over long-term operation (67 days) under realistic operation conditions with natural waters. In addition, fouling removal and membrane autopsy analysis were carried out to investigate fouling layers' formation in time and the effects of each of the cleaning techniques on different kinds of fouling.

## 6.2 Materials and Methods

### 6.2.1 Experimental Set-up

Figure 6.1 presents a schematic representation of the set-up used in the experiment, built in the pilot plant installation at the REDstack BV facility (Breezanddijk, the Netherlands) located on de Afsluitdijk, a flood defence dike spanning between the provinces of North Holland and Friesland. Five RED stacks were operated in parallel, fed with equally pre-treated fresh and sea water. First, both waters were filtered with a drum filter with pore mesh of 40 µm, immediately followed by rapid dual media filtration, and stored in 30 m³ storage tanks. The rapid dual media filter consisted of two distinct layers: first an anthracite layer (1.2 mm – 2.0 mm) followed by a sand layer (0.5 mm – 1.0 mm). Operation of the filters was automated, and backwashing was done with treated water and compressed air.

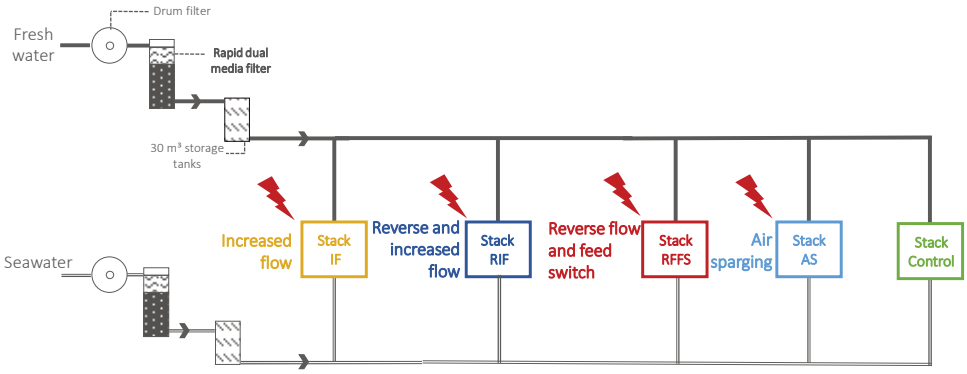


**Figure 6.1.** Schematic representation of the experimental set-up used for the experiments presented in this work. Five stacks were operated in parallel with equally pre-treated feed waters (via a drum sieve and a dual media filter) while a different cleaning technique was applied on each stack throughout the experiment. In stack control, no cleaning technique was applied.

All RED stacks were constructed identically and operated equally, with the only difference being the cleaning procedure applied. 10 x 10 cm crossflow stacks were supplied by REDstack BV (The Netherlands), and 5 cell pairs were used, totalizing a membrane area of 0.1 m². The stacks were run with a flow velocity of 1 cm/s and operated continuously for 67 days.

### 6.2.2 Profiled membranes and stack operation

The membranes used in the experiment were supplied by Ralex (Mega, Czech Republic), more specifically CMH-PES and AMH-PES, and the characteristics can be found in [21]. These membranes were chosen due to their suitability to make profiles with the thermo-pressing method, which employs heterogeneous membranes that can withstand temperatures up to 140°C [21,22,24].

CEM membranes were profiled on both sides, with perpendicular direction to maintain a cross flow pattern in the stack. Profiling was done as in [21], by applying 140°C for 10 minutes with 200 bar of pressure, after pre-heating the moulds for 2 minutes. Pressure was kept until cooling of the membranes was completed to approximately 45°C. A picture of a freshly prepared profiled CEM is shown in Figure 6.2, together with a cross section picture of a profile, showing the height of the channels of around 200 µm. AEMs were used flat, without any modifications. All membranes were stored and conditioned as recommended by the supplier.

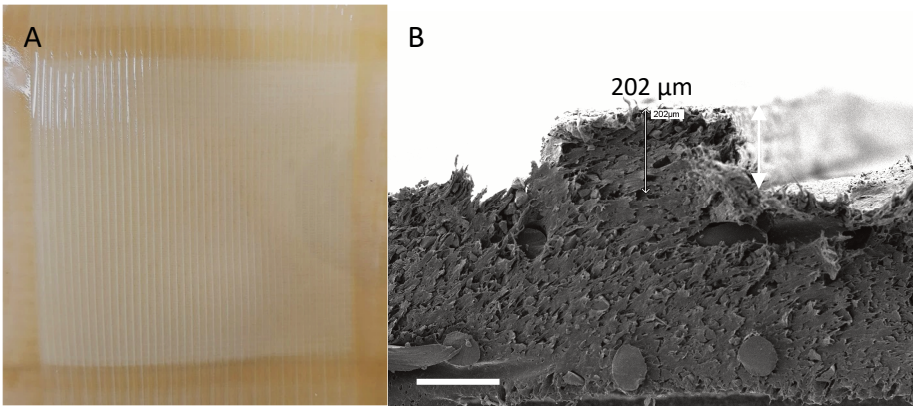


**Figure 6.2.** Image of a clean profiled CEM (A) and the SEM image (B) showing a detail of the profiles generated by thermos-pressing method. The profile/ridge height is around 200 µm. Scale bar is 200 µm.

The anode and the cathode of the stack consisted of titanium electrodes mesh with a galvanic platinum coating of 2.5 µm and with an active area of 10 x 10 cm (Magneto Special Anodes B.V., The Netherlands). The electrolyte solution was recirculated in the electrode compartments and kept at an over pressure of 0.3 bar and composed of 0.05 M $K_3Fe(CN)_6$, 0.05 M $K_4Fe(CN)_6$ and 0.25 M NaCl (VWR, USA). A pressure difference transmitter (Yokogawa, Japan) continuously measured pressure drop over the outlet and inlet of the stacks. A sensor connected to a data logger (Yokogawa, Japan) which recorded temperature and conductivity of the feed waters after treatment every 60 s.

Voltage of the stacks were measured using a potentiostat (Iviumstat, Ivium Technologies, The Netherlands) connected via a peripheral differential amplifier. Chrono potentiometric series were applied allowing for calculation of the open circuit voltage and gross power density based on obtained I-V curves. Net power density was calculated by subtracting the pumping power required to pump the feed waters to the stacks from the gross power density, as done in [25]. The chronopotentiometry series consisted of constant current density steps of 2 $A/m^2$, 3 $A/m^2$, 4 $A/m^2$, 5 $A/m^2$ and 6 $A/m^2$ applied for 80 s each, to allow the stack voltage to reach a constant value. The current steps were separated with 80 s without applied current, when the open cell voltage (OCV) could be measured. The results are shown as a day average of four measurements per day, which were done with 6 hours of interval. The rest of the time the stacks were operated at constant current density to simulate the RED process.

### 6.2.3 Cleaning techniques

The four cleaning procedures applied were selected for their suitability and potential of fouling removal, looking as well at how easily they can be implemented and performed.

- *Increase of flow to three times the original flow for 5 min (IF).* This technique aims to cause fouling detachment and release simply by increasing the shear forces along the membrane surface [26].
- *Reverse inlet and outlet of the stack coupled with flow increase to three times the original flow for 5 min (RIF)*. This procedure was chosen due to fouling starting to accumulate at the inlet of the stack, and by increasing the flow foulants are pushed out [13,19].
- *Reverse inlet and outlet of the stack coupled with switching the feed waters compartment's (RFFS)*. With this procedure, the compartment that was receiving fresh water in the inlet, now receives seawater from the outlet (new inlet). By switching water compartments, the difference of salinity of the feed water streams causes an osmotic shock which can lead to detachment of the fouling layer and to adverse conditions for organic and biofouling. This happens mostly when the previous freshwater compartment receives seawater, which acts as a draw solution to desorb the foulants that were absorbed or attached to the surface [15].
- *Air sparging (AS)*. In this procedure, compressed air is used as cleaning agent and flown inside the stack along with the feed water, causing a disturbance on the water compartment due to the high pressure of the air bubbles. This leads fouling to detach from the membrane and be washed out by the water flow [16,17,27].

***Combination of cleaning techniques***

A combination of techniques is expected to be required for fouling management in RED. Thus, an additional chemical cleaning was introduced and a concentrated salt solution was chosen instead of acid and base solutions that can damage membrane surface [8,28]. For this purpose, a brine of 90 g/L of sodium chloride was prepared and recirculated for 1 h 30 min in all stacks compartments on day 54, except in the stack control [28].

In addition, the frequency of treatment of all stacks was increased from day 60 until 64 to daily, to evaluate if more frequent cleaning could be beneficial. On day 64, after the normal cleaning of each stack, air sparging was performed in the four stacks receiving cleaning treatments, to test the possibility of combining the mechanical cleanings with a more intensive procedure with a cleaning agent (compressed air). The effluent water collected after the cleaning procedure was analysed for quantification of the removed fouling, with the same techniques as described in section 6.2.4.

### 6.2.4 Fouling removal water analysis and membrane autopsy

Samples of the outlet fresh and sea water from the stacks were taken during the cleaning procedures and analysed to quantify the fouling removal by means of organic carbon quantification via TOC analysis and LC-OCD, suspended solids concentration, particle size distribution (PSD), with the same procedures as described in [13].

At the end of the experiments, membrane autopsy was performed in all stacks to visually evaluate the effect of the cleaning procedures. Fouling appearance was visualized by naked eye and are presented with camera photos. Membrane pieces were cut in duplicate for microscopy investigation via optical and scanning electron microscopy (SEM). To visualize the carbohydrate fraction of the extracellular polymeric substance (EPS) characterizing biofilms and thus biofouling, membrane samples were stained with Alcian Blue 8 GX 0.1% solution (Sigma Aldrich, USA) for 30 min and washed with MilliQ water to remove excess dye [29,30]. For SEM analysis, membrane pieces were first fixed with 2.5% glutaraldehyde solution overnight and dehydrated with graded series (30, 50, 70, 90 and two times 100%) of ethanol for 20 minutes each step and finally dried for 30 minutes at 55ºC oven. The SEM analysis was performed with a JEOL JSM-6480LV (JEOL, Japan) at an acceleration voltage of 6 kV and magnifications up to 15,000x.

Finally, to study residual fouling on the membrane surface in more detail, membrane pieces of 2 x 5 cm were cut and placed in 30 ml of 90 g/L NaCl brine to extract as much foulants as possible from the membrane surface to a solution. The samples were placed for 30 min on a shaker, followed by 30 min on the ultrasonic bath and left overnight at 4°C. In the next

morning the samples were shaken for 30 min again, before the analysis were done. With the foulants in the brine solution, suspended solids and humic acids analysis were performed in the same way as for the outlet water collected during the cleaning procedures, described earlier in this section.

## 6.3 Results and discussion

The effect of the different cleaning strategies was evaluated by monitoring stack performance in time and by analysis of the effluent water after cleaning to get insights on the type and the amount of foulants removed. Moreover, at the end of the experiment, membrane autopsy was performed to identify different types of fouling on the membrane surface.

### 6.3.1 Stack performance

The experiment was carried out for 67 days and evaluated along time via monitoring the pressure drop (Fig. 6.3) and by measuring the electrochemical performance via OCV and gross power density measurements (Fig. 6.4). Finally, these parameters can be combined in the net power density (Fig. 6.4C), revealing the overall performance.

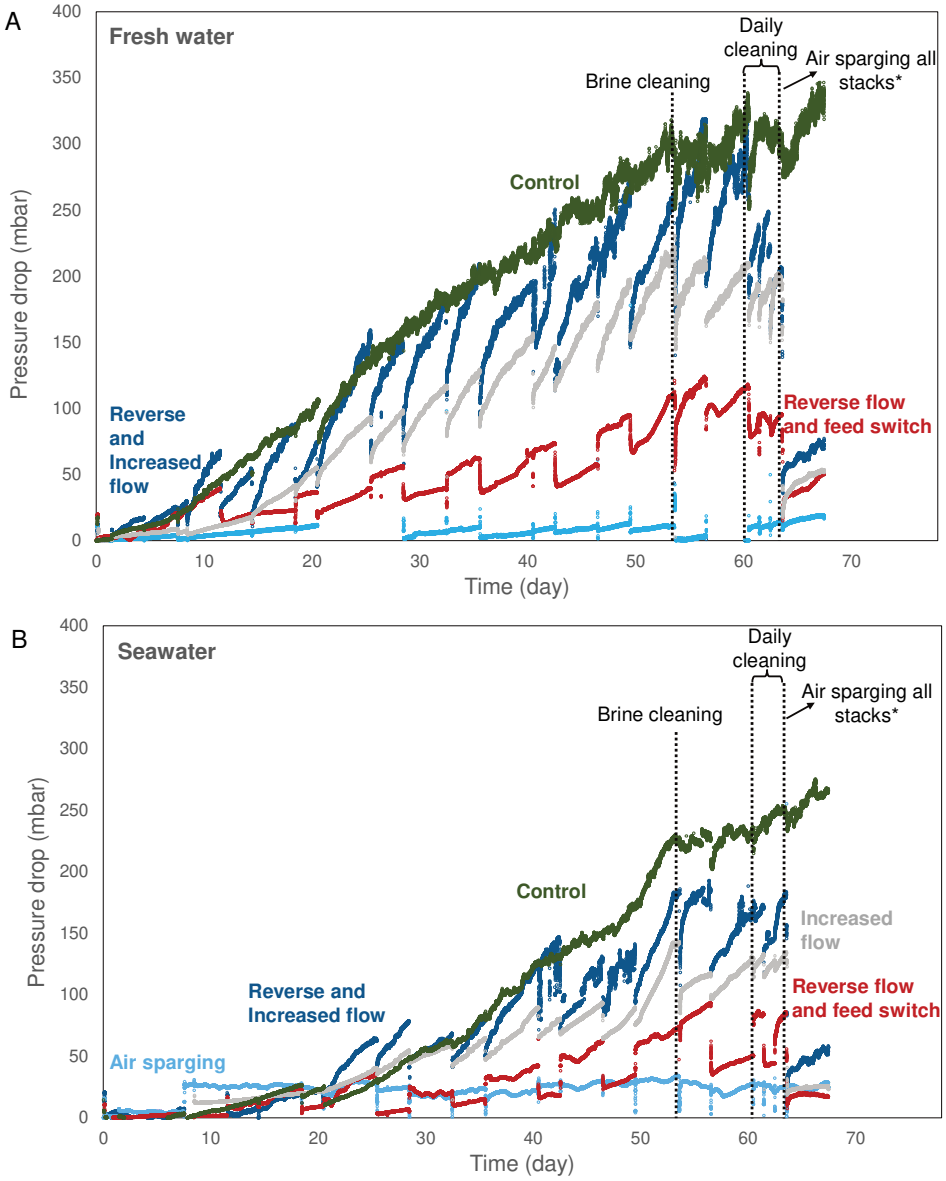


**Figure 6.3.** Pressure drop over the inlet and outlet of fresh water (A) and seawater (B) compartment of the five stacks in operation. The type of cleaning of each stack is positioned next to its curve in the graph. (*) Air sparging was performed on day 64 in all stacks receiving cleaning throughout the experiment.

The use of dual media filtration as pre-treatment showed to be effective in keeping the pressure drop at low values throughout the experiment, with a maximum pressure drop of 350 mbar for the stack Control (Fig. 6.3). This is about half of the values reported by Vermaas et al. [16] in an experiment using similar profiled membranes and natural waters, but a

different pre-treatment (a 10 µm cartridge filter). These results show that the pre-treatment with a dual media filter is reliable and performs better than a cartridge filter, which having a lower specific pore size needs to be replaced frequently. The results achieved by cleaning techniques, such as Air sparging and Reversed flow and feed switch are remarkable, keeping the pressure drop values below 100 mbar for more than 2 months of operation. In the study of Vermaas [16], the pressure drop values reached more than 400 mbar over the similar long period of operation when only a feed switch was performed. This underlines that the combination of a pre-treatment with a cleaning technique could achieve better results.

As shown in Fig. 6.3, the pressure drop constantly increased over time in both fresh water and seawater compartments due to fouling accumulation in the compartments. In all the stacks where a cleaning strategy was applied, the pressure drop was kept lower than the pressure drop in the control stack (Fig. 6.3). The lowest pressure drop in both seawater and freshwater compartments was observed in stack AS, highlighting a minimal fouling build-up (Fig. 6.3). This underlines the efficacy of the air sparging as a cleaning technique, which reduced the fouling to initial levels and that allows for longer intervals in between cleaning.

The reversed flow and feed switch (stack RFFS) cleaning technique was also shown to be effective, keeping pressures drop in the stack below 100 mbar for 67 days (Fig. 6.3). With this simple technique, we cannot assume that fouling was completely removed from the stack, but it was mitigated, due to changing of the nature of the waters in the compartments and by flushing foulants partially out.

The treatment with RIF and IF was not effective in keeping a low pressure drop, as the pressure drop quickly increased again after the cleaning procedure was applied (Fig. 6.3). These simple cleaning techniques were not able to decrease fouling to its initial levels, and thus new fouling layers can build-up fast, possibly leading to irreversible fouling [31,32]

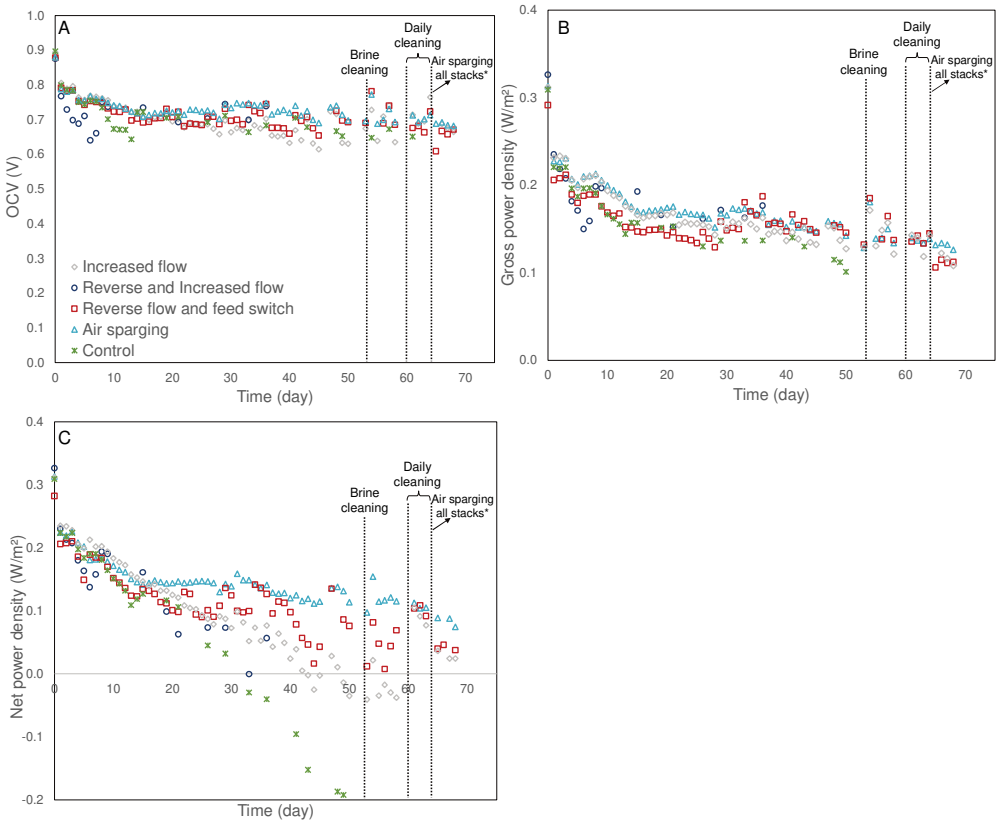


**Figure 6.4.** Electrical performance of the five stacks operated during the experiment, reported as OCV (A), gross power density (B), and net power density (C). (*) Air sparging was performed on day 64 in all stacks receiving cleaning throughout the experiment.

In terms of electrochemical performance the biggest impact is seen in the beginning of the experiments (from day 0 to day 1) (Fig. 6.4), when divalent ions poisoned the membrane and reduce OCV and consequently gross power density [33] (Fig. 6.4A and B). This decrease was observed in all stacks and can be attributed to the chemistry of the polymeric membranes. From day 2 until the end of the experiment, the gross power density of all stacks reduces similarly overtime; with stack Control having a bit sharper and faster decrease than other stacks (Fig. 6.4B). This overall decrease of performance is due to reduction in temperature of waters and variations of the salinity gradient, as shown on Figure S 6.1, but also due to the different types of fouling accumulation in the membrane surface. The temperature of both feed waters decreased around 6° C and reach about 10° C, which can impact the power density to a great extent [3]. The temperature decrease could also impact OCV, which dropped around 0.1 V per stack (Fig. 6.4) [3,16]. In addition, fouling by organics, such as humic acids present in natural waters, can get trapped inside the membrane and results in a loss of ion-exchange capacity of the membrane [18,32]. After

day 37 stack RIF, and at day 50 stack Control started to fail electrochemically (Fig. 6.4) and could not be evaluated at the end of the experiment. These two stacks were also the ones with highest pressure drops and most affected by fouling, which could have led to the power failure.

At the end of the experiment all the stacks produced a similar gross power density, except for the control and RIF stacks (Fig. 6.4B). That means that the fouling removal by the other three cleaning procedures had little effect on the electrical performance of the stacks, possibly due to the applied cleanings not affecting the kind of foulants that would influence the ion transfer through the membranes and consequently the electrical performance of the stack.

In conclusion, based on the pressure drop and the net power density air sparging showed the best cleaning performance.

It is important to highlight that three out of these four cleaning strategies did not use a cleaning agent and can be seen as an operational practice that can delay fouling formation and recover performance, at least partially, for some time. The cleaning with air sparging is seen as greater intervention on the stack operation, but still a simple technique since it uses only compressed air as a cleaning agent.

### 6.3.2 Analysis of foulants removed with cleaning

The cleaning techniques were evaluated in their potential to remove foulants from the stacks, by analysing the effluent water collected during the application of each technique. The removal of suspended solids (Fig. 6.5), confirmed that air sparging was most effective to remove foulants originating from both feed waters, which are known to cause an increase of pressure drop [26]. The removal was clearly larger in the freshwater compartments and that could be attributed to a higher content of suspended solids in this inlet water (~ 6 mg/L). The treatment with the dual media filter provides inlet seawater with a low content of suspended solids (~2 mg/L), but for fresh water the treatment is less effective and overtime this slightly higher concentration of solids entering the stacks accumulates in a fouling layer. The fouling build-up in the freshwater compartments is then tackled by the cleaning techniques, resulting in higher removals than from seawater compartments. It is worth to notice that the fouling from the freshwater feed is mostly of organic nature, as seen on the higher fraction of volatile suspended solids (Fig. 6.5), and that high amounts could be removed with the cleaning techniques.

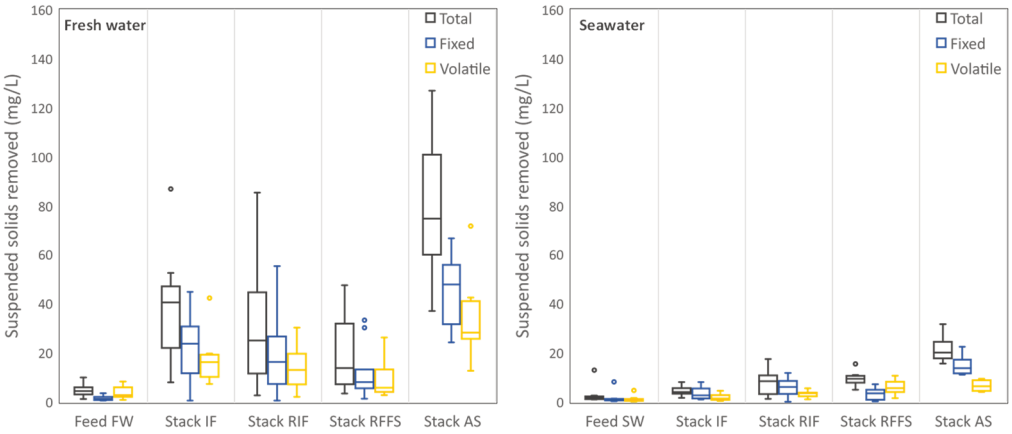


**Figure 6.5.** Box plot distribution of the suspended solids removed in the fresh water and seawater compartment of each stack when a cleaning technique was carried out. For reference, the content of suspended solids on both feed waters is shown. Stack IF received increased flow cleaning, stack RIF was cleaned with reverse and increased flow, stack RFFS received cleaning by reverse flow and feed switch and stack AS with air sparging.

Looking at other fractions of fouling, such as organic carbon and humic acids, little effect could be seen in their removal by the different cleaning techniques (Fig. 6.6, Fig. S 6.2 and Fig. S 6.3). The exception was the cleaning with reverse flow and feed switch that was the only technique that could remove humic acids from the freshwater compartment (Fig. 6.6).

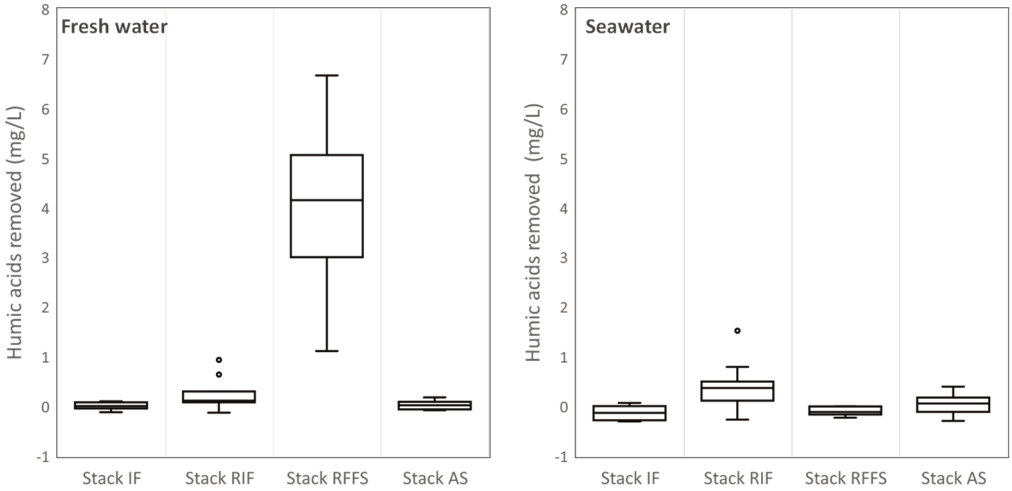


**Figure 6.6.** Box plot distribution of humic acids removal from fresh and sea water compartments for each cleaning procedure performed during the experiment. Stack IF received increased flow cleaning, stack RIF was cleaned with reverse and increased flow, stack RFFS received cleaning by reverse flow and feed switch and stack AS with air sparging.

When the feed waters were switched in stack RFFS, the fouling accumulated in the previous freshwater compartment was suddenly subjected to an osmotic stress when the compartment is switched to seawater. This caused an osmotic gradient that likely allowed the humic acids to desorb from the fouling layer to the feed water compartment (Fig. 6.6), with seawater acting as a draw solution for this foulant [15,16] .

The lack of removal of humic acids from the seawater compartments (Fig. 6.6) can be explained by freshwater feed not being able to desorb humic acids from the seawater compartments. Fresh water bodies are known to have high concentration of humic acids, while seawater is less affected by it [18]. Thus, the fouling layer in the seawater compartment has a lower content of humic acids and that possibly allows for a fast equalization of concentration of the humic content, together with a fast reduction of the osmotic gradient between the fouling layer and the feed water.

### 6.3.3 Combination of cleanings strategies

Besides the previously discussed cleaning procedures, also combinations of cleaning strategies were used to help maintain stack performance.

A cleaning with brine was performed on day 54 to assess the effect of a chemical technique on fouling and consequent stack performance and the effect was evaluated by the impact on pressure drop (Fig. 6.3), electrochemical performance (Fig. 6.4) and suspended solids and COD measurements on the water recovered from the cleaning procedure (Fig. S 6.4).

The pressure drop was not greatly impacted by this technique (Fig. 6.3), proving that a brine cleaning has little effect on particulate fouling, which is the type of fouling mostly responsible for increased pressure drop [26]. When the brine cleaning was applied on both seawater and freshwater compartments, removal of suspended solids was comparable or lower than what was achieved with the other cleaning methods already in use (Fig. 6.5 and Fig. S 6.4).

On the other hand, the gross power density was momentously positively affected by the brine cleaning (Fig. 6.4B). This can be expected, since the amount of salt present in the stack and membranes after the cleaning could reduce the feed's resistance and increase the power output [16,34]. However, the benefit of this technique was limited to the moment of the cleaning only.

Another attempt to restore the performance was to perform the cleaning procedures more frequently, in this case every day for 4 days in a row, and the impact on pressure drop (Fig. 6.3) showed that there was a benefit from more frequent cleaning on decreasing the loss of performance for all stacks. This could be attributed to the cleaning being performed in a shorter time span than needed for fouling build-up. However, this benefit was limited, as shown by the pressure drop reduction; it was only kept at a slightly lower pressure drop during these 4 days but did not return to initial values (Fig. 6.3). Thus, a more frequent cleaning can help to keep a lower pressure drop and limit the effects of fouling build-up. Even with the daily cleaning, the estimated downtime needed is less than 1% of the full-time operation, considering 24 hours of continuously operation.

Due to the effectiveness of air sparging in reducing pressure drop (Fig. 6.3), at day 64 this cleaning method was applied on the stacks that were receiving a different cleaning procedure, namely IF, RIF and RFFS. After application of air sparging, the amount of suspended solids removed from these stacks was up to 10x higher than what was observed with their initial cleaning procedure, before day 64 (Fig. 6.5 and Fig. 6.7), showing that most of the fouling still present in the stacks was reversible with a more intensive cleaning. This resulted in low values of pressure drop, which were close to the initial ones (Fig. 6.3). In the case of stack IF, the effect on pressure drop was three times higher than the average reduction observed with the increased flow cleaning alone during the 2 months of operation (Fig. S 6.5). Similar results were achieved with stack RIF, while for stack RFFS the effect was not so evident, but this is due to a previous lower accumulation of foulant (Fig. 6.3 and S 6.5). The results also showed that a larger fraction of the suspended solids removed is composed of inorganic compounds (non-volatile SS, Fig. 6.7), highlighting that minerals from sediments constitute a large part of the reversible fouling. Air sparging is a more robust cleaning strategy to remove a large fraction of reversible fouling that is still effective even when applied less frequently.

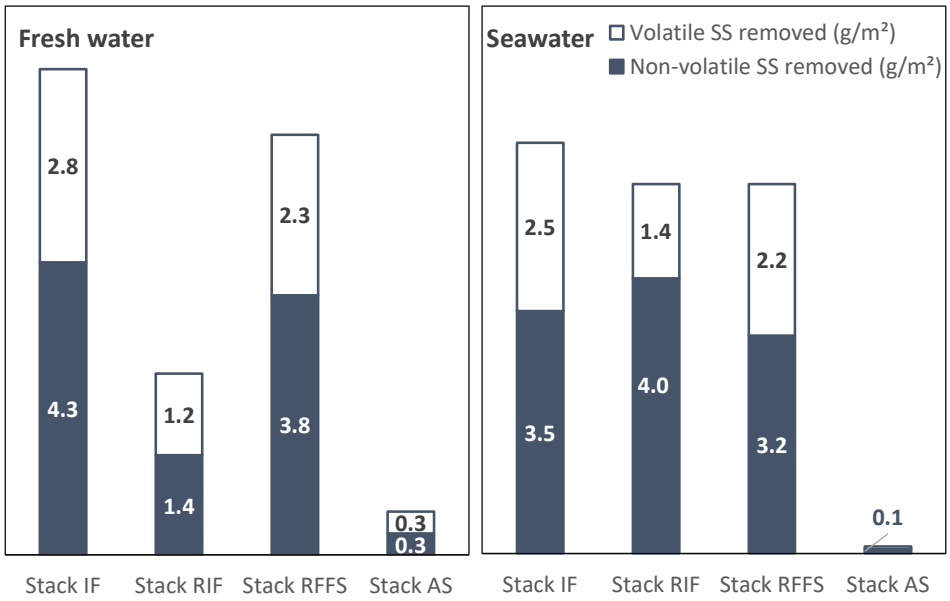


**Figure 6.7.** Suspended solids (SS) and the relative volatile and non-volatile fractions removed when air sparging was applied to the four stacks receiving cleaning procedure during the experiment for the fresh and sea water compartments. Stack IF received increased flow cleaning, stack RIF was cleaned with reverse and increased flow, stack RFFS received cleaning by reverse flow and feed switch and stack AS with air sparging.

### 6.3.4 Membrane autopsy

By the end of the experiment (day 67), all stacks were opened and subjected to membrane autopsy, and membrane samples were visually analysed. As air sparging was performed in all stacks receiving cleaning at the end of the experiment, almost no fouling could be detected on the membranes by naked eye, apart from stack Control (Fig. S 6.6), used as reference. SEM micrographs (Fig. 6.8), and optical microscopy images (Fig. S 6.7) confirmed that the control stack had a significant fouling layer in comparison to others. In the profiled CEMs, fouling was mostly found in between membrane ridges, as showed via visual (Fig. S 6.6) and SEM (Fig. 6.8) analysis. This happens due to the top of the ridges being in contact with the AEM and space for accumulation was limited.

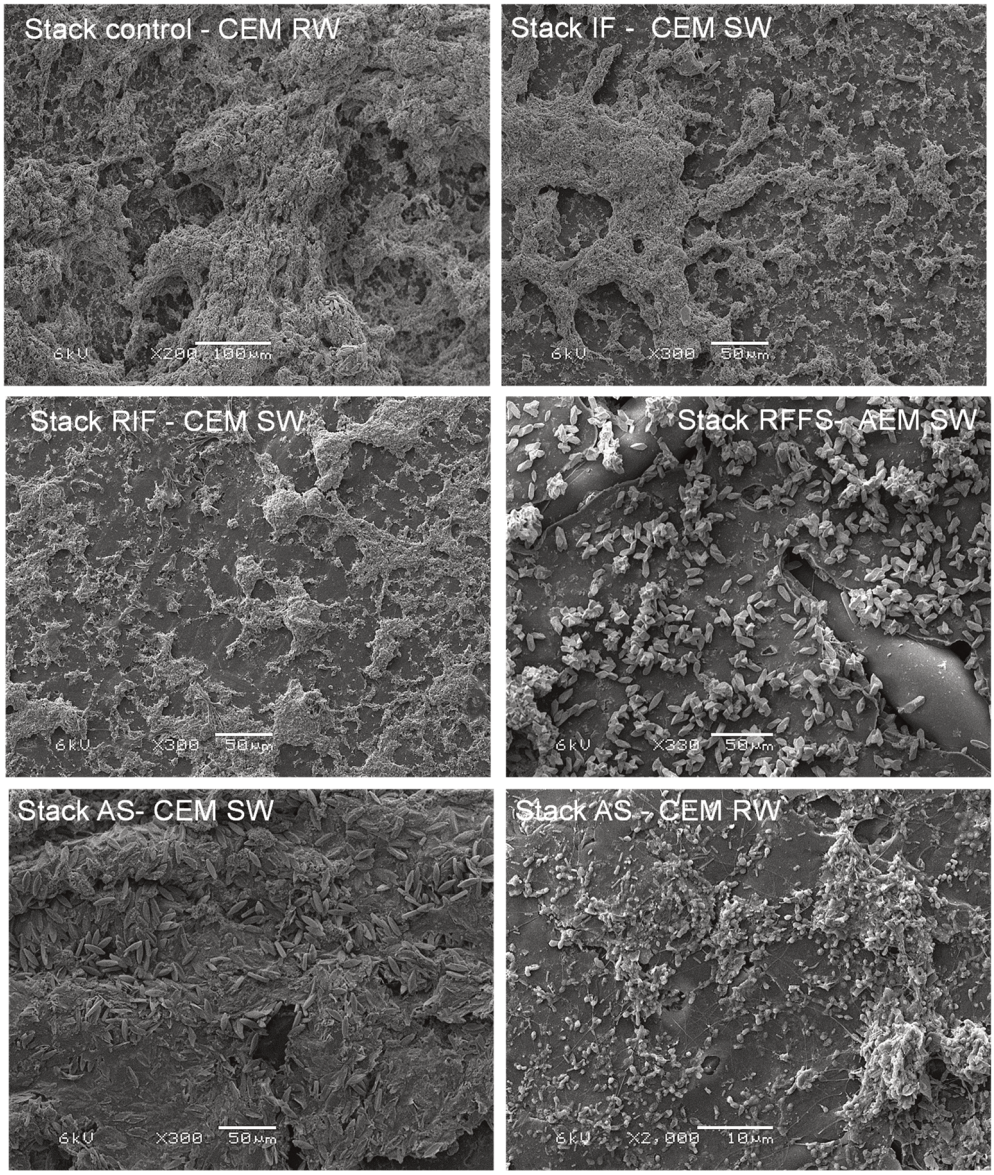


**Figure 6.8.** SEM images of fouling layer of all stacks operated in the experiment. Stack IF received increased flow cleaning, stack RIF was cleaned with reverse and increased flow, stack RFFS received cleaning by reverse flow and feed switch and stack AS with air sparging.

Despite the air sparging step was applied to the stacks by the end of the process, different types of fouling were identified in each stack, highlighting that the different cleaning techniques applied to them during the experiment were selecting for a certain type of foulant(s). In stack AS, fouling development involved biological components as bacterial cells and diatoms (Fig. 6.8) but low coverage of biofilm, as highlighted by the low amount

of EPS detected after applying alcian blue staining (Fig. S 6.7). The diatoms were more commonly found in the CEMs, probably due to favourable charge interactions between the outer 'shell' of the diatom, which is usually negative [35], and the positive ionic charge caused by concentration polarization around the negative charge of the cationic membrane. Vermaas [6] observed accumulation of diatoms and mineral silica at the AEMs, but in that study both AEM and CEM were profiled and that could interfere on the fouling attachment and formation. As previous studies showed [12,13], when there is less incidence of fouling by particulate matter, there is more available ideal surface area for attachment and growth of bacteria and EPS layer, as well as diatoms, resulting in pronounced biofouling. Biofouling is more difficult to remove during the cleaning procedure, even when using air sparging [15]. However, despite the presence of low biofouling, the performance of stack AS was not really affected during the experiment, biofouling.

In stack RFFS scaling in the form of calcium precipitates was observed using EDX analysis of the fouling layer (Table S1). The precipitation of salts could have happened due to the switching of feed waters compartments, with a sudden osmotic shock and local changes of pH. Additionally, diatoms were found on the CEMs (Fig. S 6.7), highlighting that the presence of biofouling could not be removed with the performed cleanings, similar to the observation of stack AS.

Fouling in stacks IF and RIF was found in similar amounts, and no special type of fouling could be identified with the techniques applied, such as typical traits of biofouling. The two cleaning techniques applied on the two stacks were very similar, with the only difference being the first one includes reversing the flow direction before increasing the flow. The stacks also performed very similar, as shown in pressure drop measurements for both fresh and seawater (Fig. 6.3).

Overall, particulate fouling was found in small amounts in the stacks subjected to the cleaning procedures. This was confirmed by the residual fouling found during autopsy, quantified as suspended solids and humic acids (Fig. 6.9). As reference, the amount of residual suspended solids in the control stack was about 7 g/m² of membrane area on the CEM membrane (Fig. 6.9).

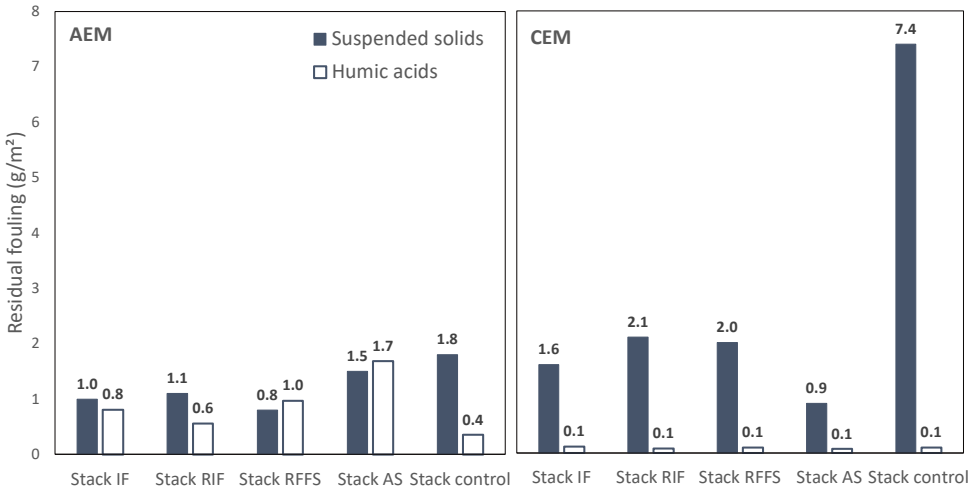


**Figure 6.9**. Estimation of the residual fouling on membrane surfaces on each membrane type (AEM and CEM) of each stack, estimated on the basis of suspended solids and humic acids from the membrane autopsy. Stack IF received increased flow cleaning, stack RIF was cleaned with reverse and increased flow, stack RFFS received cleaning by reverse flow and feed switch and stack AS with air sparging.

In stack AS, the residual suspended solids on the CEM were slightly lower than other stacks receiving cleaning, as expected by the pressure drop values (Fig. 6.3). It is interesting to notice that more residual suspended solids were found on CEM membranes of all stacks compared to their AEMs counterparts, except for stack AS (Fig. 6.9). EDX analysis showed that suspended solids were mostly composed of natural organic matter debris and silica and aluminium sediments found in the natural waters that could not be removed in the pre-treatment (Table S1). This type of foulants is usually negatively charged, and, surprisingly, were more attracted to the CEM then to the AEM. This could be due to concentration polarization of positively charged species on the membrane surface or because most of the solids are found on fresh water feed (Fig. 6.5) and due to the electric field are attracted to the anode and thus the CEMs [32].

For the residual humic acids, AEMs had higher accumulation than CEMs (Fig. 6.9), which is in accordance with the observed brown colour of the first membranes (Fig. S 6.7) and due to the negative charge interaction of the humic acids with the positive charge of the AEMs, as previously reported in the literature [16,24,36]. In the fresh water compartments, AEMs acquire a very intense brown colour, while the seawater compartment have a faded brown coloration, as shown on Figure S 6.6, and reported in [24].

Humic acids were found in lower concentrations on the stacks with higher accumulation of pressure drop, such as Stack RIF and Control (Fig. 6.3 and 6.9), and, as observed for

biofouling, this could be due to the protection of the membrane surface from being in contact with the larger organic molecules, such as humic acids.

In summary, the cleaning strategies that allowed maintaining a good performance throughout the experiment were air sparging and reverse flow and feed switch, which in combination with the use of profiled membranes resulted in an overall low-pressure drop. The use of spacers is known to hinder the use of air as a cleaning agent [17], thus the use of profiled membranes is important to achieve the mentioned results. Most cleaning procedures had no effect on chemical parameters associated with fouling, except for reverse flow and feed switch that could combine the effect of low pressure drop and removal of humic acids. In addition, membrane autopsy showed that the presence or absence of a fouling layer of particulate solids can affect the subsequent fouling formation, such as organic and biofouling. This is highly relevant for pre-treatment design and cleaning frequency and should be studied in more detail depending on the feed water sources.

**6.4 Conclusions**

The application of cleaning strategies in stacks operating for more than 2 months gives a good perspective on which cleaning method is preferred to use for different goals and composition of feed water. Air sparging removed particulate fouling well and it seems to be the best strategy to keep a low pressure drop when used in combination with a pre-treatment that allows some particulate matter in the effluent, as the dual media filtration. It was shown that the application of air sparging a few times a week could keep the pumping power losses to a minimum, like the initial operation values.

The application of reverse feed and flow switch shows to be effective in reducing fouling related to humic acids and is able to keep the pressure drop below 100 mbar. A combination of air sparging and flow switch could be the best method to keep lower amounts of fouling from humic acids and particulate matter and the frequency of cleaning can be adjusted to the desired level of pressure drop. Brine cleaning, that potentially could be suitable for removal of humic acids, did not show to be particularly effective in this matter and most benefits of this technique could be also achieved by performing flow switch.

Overall, simple, and chemical free methods for cleaning can be suitable to maintain the performance of RED stacks, allowing this technology to be considered environmentally friendly and without environmental damage.

The use of profiled membranes is needed for the further development of RED as they give higher power outputs compared to stacks with spacers and allowed for more efficient cleaning. Thus, the development of commercial profiled membranes for RED should be the next step to take this technology further.

**Supporting Information**

Feed waters temperature and conductivity were measured and recorded throughout the experiment and are presented in Figure S 6.1.

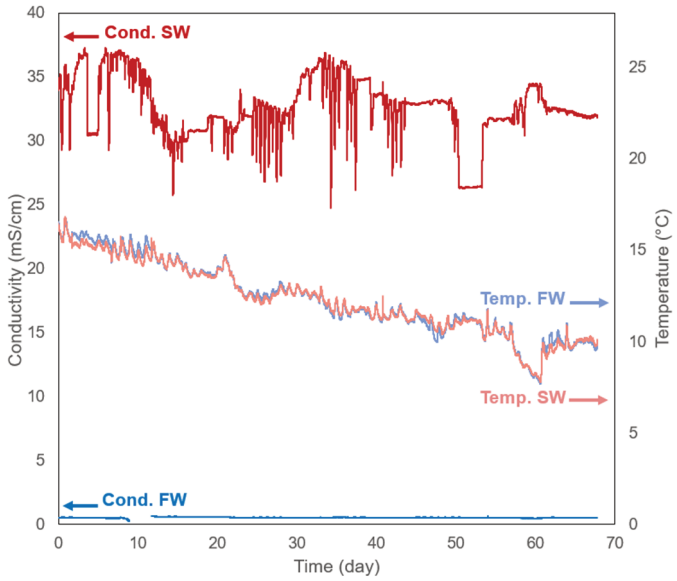


**Figure S 6.1.** Conductivity and temperature of both feed seawater (SW) and fresh water (FW) during the experiment.

Analysis of the water collected after each cleaning, showed that the TOC removed and particle size classification of the removed fouling variate little among the stacks receiving the different cleaning procedures, as shown on Figure S 6.2 and S 6.3.

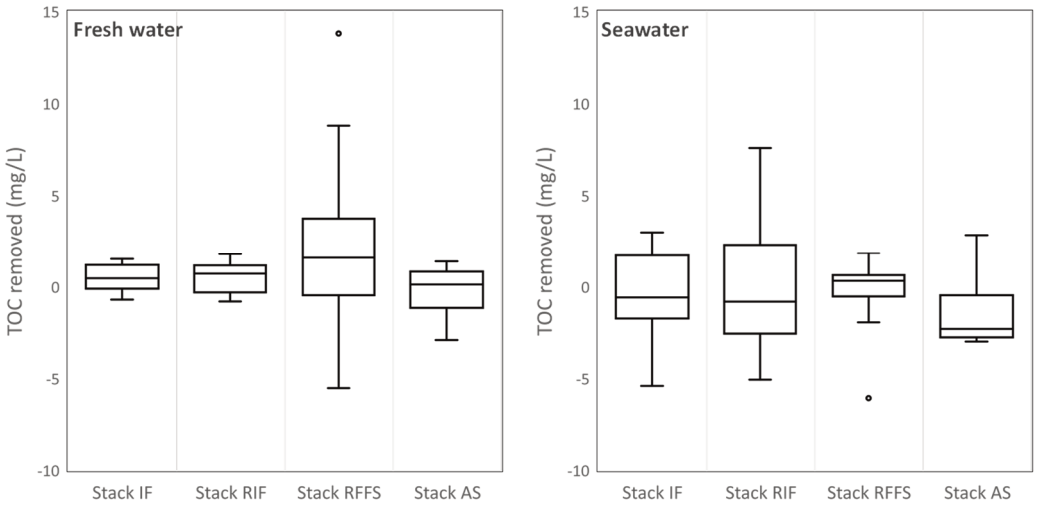


**Figure S 6.2.** TOC removed from each stack compartment just after cleaning.

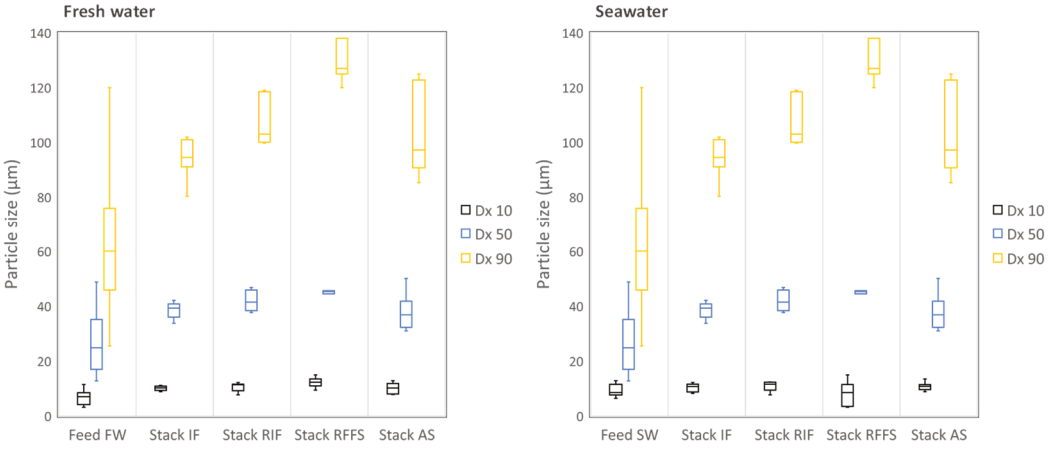


**Figure S 6.3.** Particle size fractions from water collected after each cleaning of each stack compartment.

In the cleaning with brine, each stack was evaluated by the removal of COD and suspended solids, as shown in Figure S 6.4. In terms of COD, the highest removal was in Stack AS in the freshwater compartment, followed by similar removals from stacks RIF and IF. The higher removal obtained in Stack AS with fresh water can be attributed to this compartment having a lower incidence of suspended solids fouling and more membrane area was available to be impacted by organic fouling, which was then removed at higher levels with the brine technique.

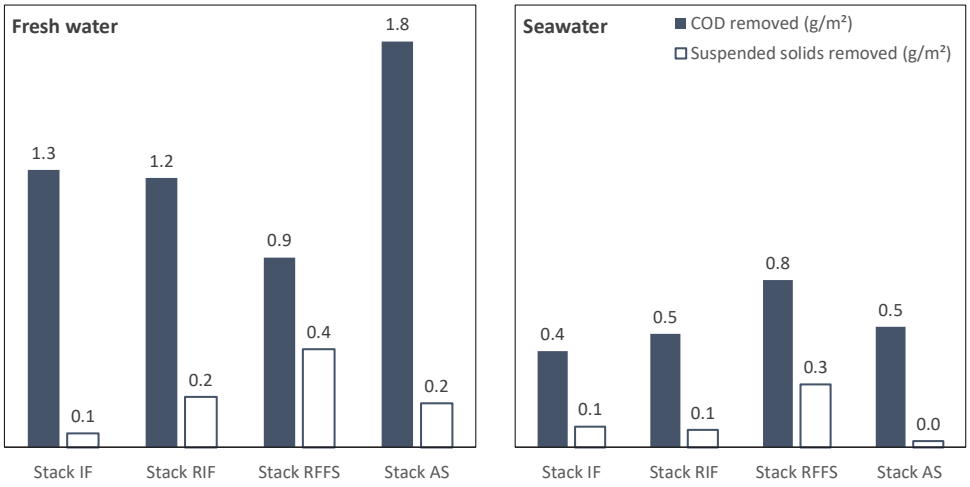


**Figure S 6.4.** Suspended solids fractions and COD removed from each stack compartment with additional brine cleaning performed on day 54.

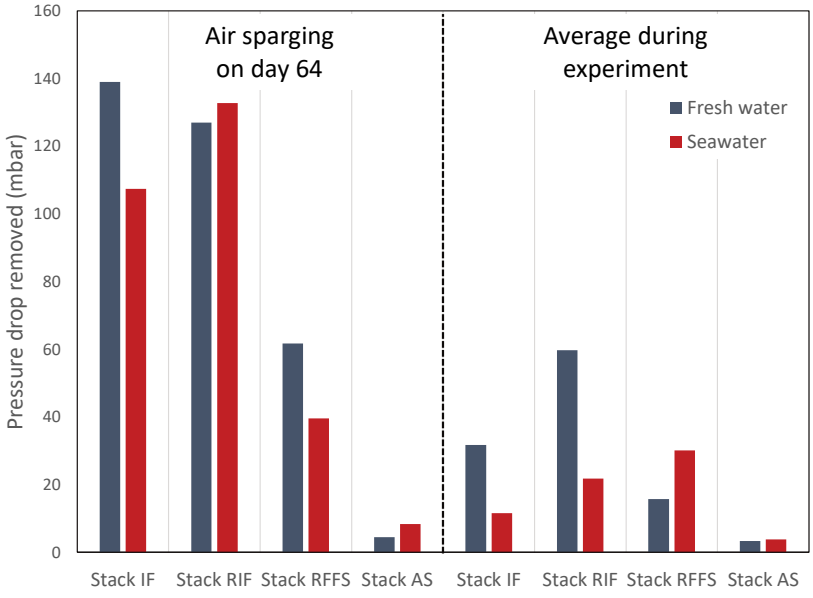


**Figure S 6.5.** Comparison of the pressure drop that was removed with application of air sparging on day 64 and the average pressure drop removed with the respective technique applied to each stack during the whole experiment. For stacks IF, RIF and RFFS the removal with air sparging was around 3 times more than the average achieved during the experiment.

**Membrane autopsy**

Figures S 6.6 and S 6.7 show images of the membrane autopsy. In stacks IF, RIF and Control large areas covered with a cloud of foulants can be seen in both CEM and AEM samples (Fig. S 6.7). These foulants are mostly particulate matter, composed of silica and aluminium compounds, as shown on Table S 6.1. In stacks RFFS and AS more fouling by diatoms (CEMs) and organic matter (AEM) marked by the blue tone of the alcian blue can be seen on the images.

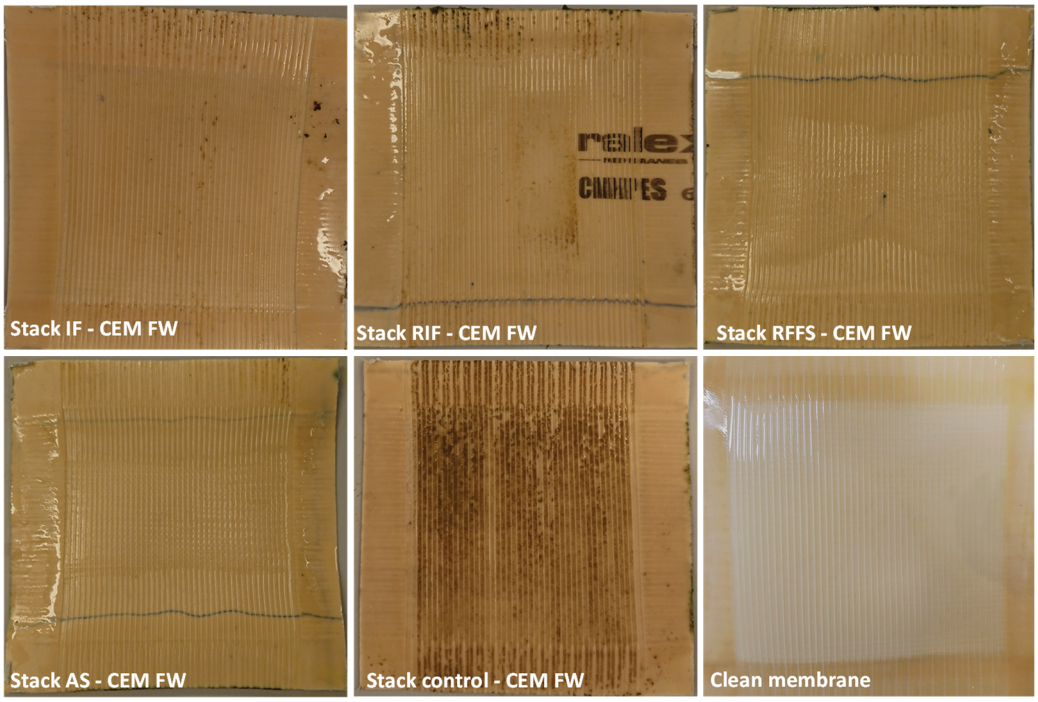


**Figure S 6.6.** Images of profiled CEM membranes in contact with fresh water. Visual inspection of CEMs showed that most membranes look clean after more than 2 months experiment due to the cleaning procedures applied to them, with exception of the stack Control, that did not experience any cleaning procedure.

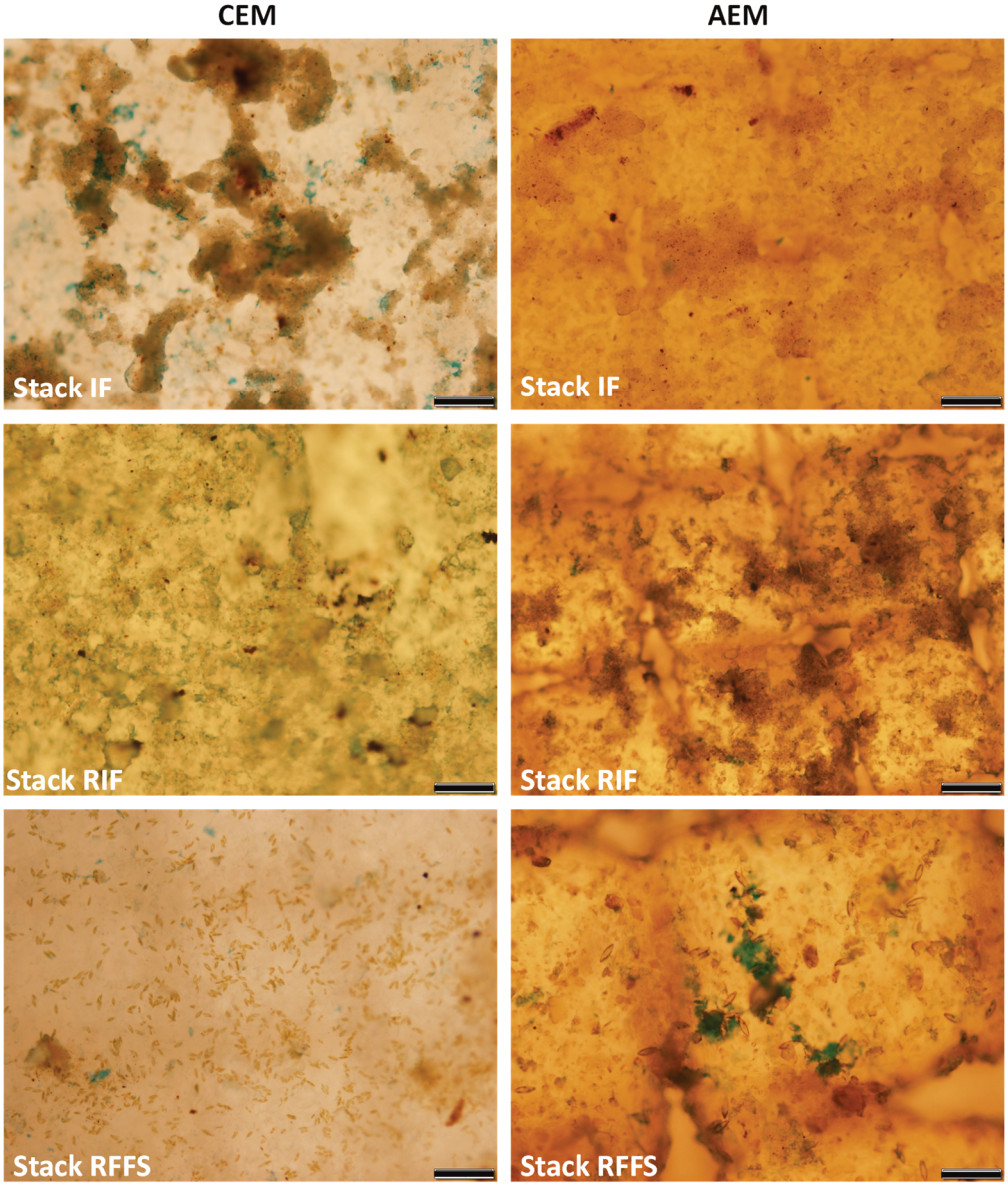
CEM
AEM
Stack IF
Stack IF
Stack RIF
Stack RIF
Stack RFFS
Stack RFFS

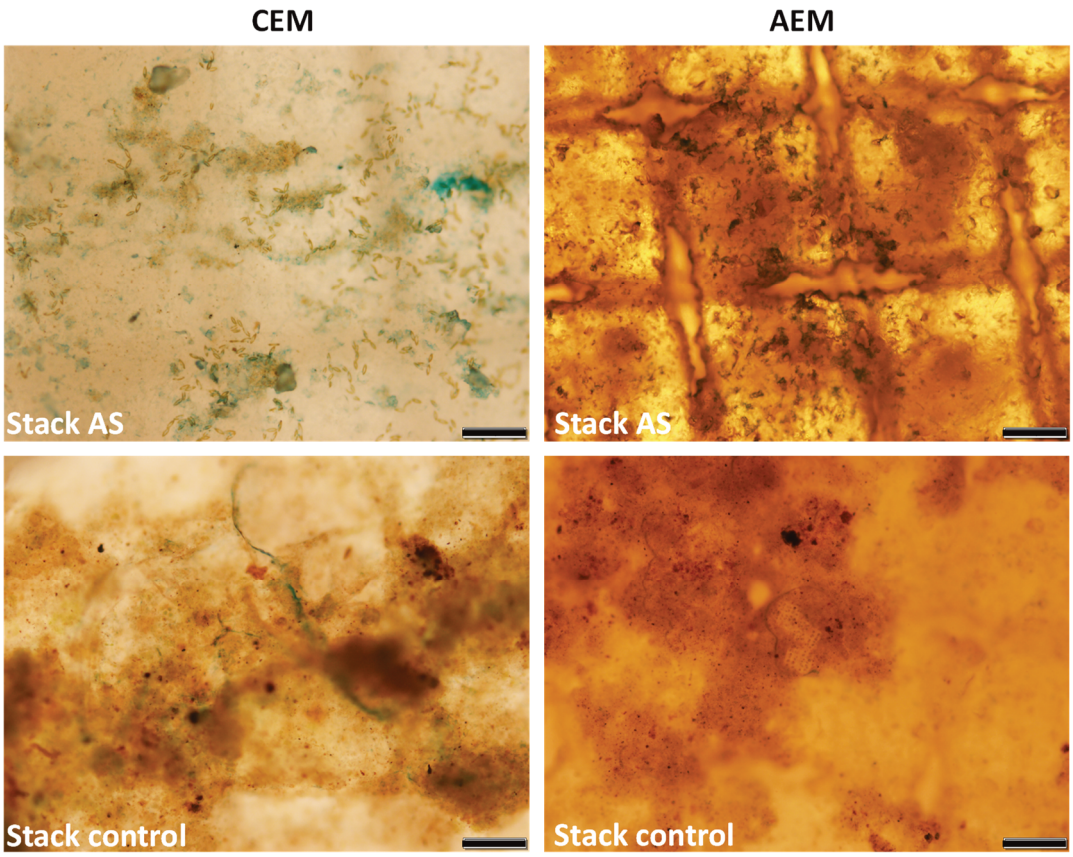


**Figure S 6.7.** Microscopy images from both CEM and AEMs membranes stained with alcian blue, targeting acidic polysaccharides. Scale bars are 100 µm, except on the image of Stack RIF CEM and Stack RFFS AEM, where is 50 µm.

Table S 6.1 shows the atomic compoistion of the remarkable samples scanned by EDX. The sample on Stack AS (CEM-SW) represents the composition of an area covered by diatoms. The sample of Stack RFFS (AEM-SW) represents the composition of an area covered by precipitates. While the sample of Stack IF (CEM-SW) shows the composition of a typical area found in many samples, that are a mix of sediments, diatoms, bacteria, and precipitates.

**Table S 6.1** – EDX atomic composition of samples.

| Element (%) | Stack AS CEM-SW | Stack RFFS AEM-SW | Stack IF CEM-SW |
|---|---|---|---|
| **C** | 51.7 | 46.4 | 61.5 |
| **O** | 40.5 | 43.3 | 32.0 |
| **Na** | 0.2 | - | 0.1 |
| **Mg** | 0.1 | 0.3 | 0.3 |
| **Al** | 0.5 | - | 1.3 |
| **Si** | 6.4 | 0.5 | 3.4 |
| **S** | 0.2 | 0.4 | 0.3 |
| **Cl** | - | 0.4 | - |
| **K** | 0.1 | - | 0.3 |
| **Ca** | 0.3 | 8.8 | 0.5 |
| **Fe** | - | - | 0.4 |

**References**

[1] J.W. Post, J. Veerman, H.V.M. Hamelers, G.J. Euverink, S.J. Metz, K. Nymeijer, C.J. Buisman, Salinity-gradient power: Evaluation of pressure-retarded osmosis and reverse electrodialysis, Journal of Membrane Science 288 (2007) 218–230.

[2] R. E. Pattle, Production of Electric Power by mixing Fresh and Salt Water in the Hydroelectric Pile, Nature 174 (1954) 660.

[3] E.H. Hossen, Z.E. Gobetz, R.S. Kingsbury, F. Liu, H.C. Palko, L.L. Dubbs, O. Coronell, D.F. Call, Temporal variation of power production via reverse electrodialysis using coastal North Carolina waters and its correlation to temperature and conductivity, Desalination 491 (2020) 114562.

[4] R.E. Lacey, Energy by reverse electrodialysis, Ocean Engineering 7 (1980) 1–47.

[5] S. Pawlowski, R.M. Huertas, C.F. Galinha, J.G. Crespo, S. Velizarov, On operation of reverse electrodialysis (RED) and membrane capacitive deionisation (MCDI) with natural saline streams: A critical review, Desalination 476 (2020) 114183.

[6] D.A. Vermaas, D. Kunteng, M. Saakes, K. Nijmeijer, Fouling in reverse electrodialysis under natural conditions, Water research 47 (2013) 1289–1298.

[7] I. Merino-Garcia, S. Velizarov, New insights into the definition of membrane cleaning strategies to diminish the fouling impact in ion exchange membrane separation processes, Separation and Purification Technology 277 (2021) 119445.

[8] A. Nazif, H. Karkhanechi, E. Saljoughi, S.M. Mousavi, H. Matsuyama, Recent progress in membrane development, affecting parameters, and applications of reverse electrodialysis: A review, Journal of Water Process Engineering 47 (2022) 102706.

[9] S. Mehdizadeh, M. Yasukawa, T. Suzuki, M. Higa, Reverse electrodialysis for power generation using seawater/municipal wastewater: Effect of coagulation pretreatment, Desalination 481 (2020) 114356.

[10] M. Vanoppen, T. van Vooren, L. Gutierrez, M. Roman, L.J.-P. Croué, K. Verbeken, J. Philips, A. Verliefde, Secondary treated domestic wastewater in reverse electrodialysis: What is the best pre-treatment?, Separation and Purification Technology 218 (2019) 25–42.

[11] J. Ju, Y. Choi, S. Lee, C.-G. Park, T. Hwang, N. Jung, Comparison of Pretreatment Methods for Salinity Gradient Power Generation Using Reverse Electrodialysis (RED) Systems, Membranes 12 (2022).

[12] B. Vital, E.V. Torres, T. Sleutels, M.C. Gagliano, M. Saakes, H.V.M. Hamelers, Fouling fractionation in reverse electrodialysis with natural feed waters demonstrates dual media rapid filtration as an effective pre-treatment for fresh water, Desalination 518 (2021) 115277.

[13] B. Vital, T. Sleutels, M.C. Gagliano, H.V.M. Hamelers, Reversible fouling by particulate matter from natural seawater reduces RED performance while limiting biofouling, Desalination 548 (2023) 116262.

[14] S. Mikhaylin, L. Bazinet, Fouling on ion-exchange membranes: Classification, characterization and strategies of prevention and control, Advances in colloid and interface science 229 (2016) 34–56.

[15] J.W. Post, Blue energy: Electricity production from salinity gradients by reverse electrodialysis. Wageningen, Univ., Diss., 2009, 2009.

[16] D.A. Vermaas, D. Kunteng, J. Veerman, M. Saakes, K. Nijmeijer, Periodic feedwater reversal and air sparging as antifouling strategies in reverse electrodialysis, Environmental science & technology 48 (2014) 3065–3073.

[17] J. Moreno, N. de Hart, M. Saakes, K. Nijmeijer, CO2 saturated water as two-phase flow for fouling control in reverse electrodialysis, Water research 125 (2017) 23–31.

[18] K. Chon, N. Jeong, H. Rho, J.-Y. Nam, E. Jwa, J. Cho, Fouling characteristics of dissolved organic matter in fresh water and seawater compartments of reverse electrodialysis under natural water conditions, Desalination 496 (2020) 114478.

[19] J. Choi, W.-S. Kim, H.K. Kim, S.C. Yang, J.-H. Han, Y.C. Jeung, N.J. Jeong, Fouling behavior of wavy-patterned pore-filling membranes in reverse electrodialysis under natural seawater and sewage effluents, npj Clean Water 5 (2022).

[20] E. Güler, R. Elizen, M. Saakes, K. Nijmeijer, Micro-structured membranes for electricity generation by reverse electrodialysis, Journal of Membrane Science 458 (2014) 136–148.

[21] D.A. Vermaas, M. Saakes, K. Nijmeijer, Power generation using profiled membranes in reverse electrodialysis, Journal of Membrane Science 385-386 (2011) 234–242.

[22] S. Pawlowski, J.G. Crespo, S. Velizarov, Profiled Ion Exchange Membranes: A Comprehensible Review, International journal of molecular sciences 20 (2019).

[23] S. Pawlowski, V. Geraldes, J.G. Crespo, S. Velizarov, Computational fluid dynamics (CFD) assisted analysis of profiled membranes performance in reverse electrodialysis, Journal of Membrane Science 502 (2016) 179–190.

[24] S. Pawlowski, C.F. Galinha, J.G. Crespo, S. Velizarov, 2D fluorescence spectroscopy for monitoring ion-exchange membrane based technologies - Reverse electrodialysis (RED), Water research 88 (2016) 184–198.

[25] J. Moreno, E. Slouwerhof, D.A. Vermaas, M. Saakes, K. Nijmeijer, The Breathing Cell: Cyclic Intermembrane Distance Variation in Reverse Electrodialysis, Environmental science & technology 50 (2016) 11386–11393.

[26] J. Di Luque Salvo, A. Cosenza, A. Tamburini, G. Micale, A. Cipollina, Long-run operation of a reverse electrodialysis system fed with wastewaters, Journal of environmental management 217 (2018) 871–887.

[27] Cornelissen E. R., Vrouwenvelder J. S., Heijman S. G. J., Van der Kooij D., Viallefont X. D., Wessles L. P, Periodic air/water cleaning for control of biofouling in spiral wound membrane elements, Journal of Membrane Science 287 (2007) 94–101.

[28] M.-E. Langevin, L. Bazinet, Ion-exchange membrane fouling by peptides: A phenomenon governed by electrostatic interactions, Journal of Membrane Science 369 (2011) 359–366.

[29] O'Toole, G. A., Pratt, L. A., Watnick, P. I., Newman, D. K., Weaver, V. B., and Kolter, R., Genetic approaches to study of biofilms., Methods Enzymol 310 (1999) 91–109.

[30] J. Ramus, Alcian blue: A quantitative aqueous assay for algal acid and sulfated polysaccharides, Journal of Phycology 13(4) (1977) 345–348.

[31] U. Metzger, P. Le-Clech, R.M. Stuetz, F.H. Frimmel, V. Chen, Characterisation of polymeric fouling in membrane bioreactors and the effect of different filtration modes, Journal of Membrane Science 301 (2007) 180–189.

[32] D. Pintossi, M. Saakes, Z. Borneman, K. Nijmeijer, Electrochemical impedance spectroscopy of a reverse electrodialysis stack: A new approach to monitoring fouling and cleaning, Journal of Power Sources 444 (2019) 227302.

[33] J. Moreno, V. Díez, M. Saakes, K. Nijmeijer, Mitigation of the effects of multivalent ion transport in reverse electrodialysis, Journal of Membrane Science 550 (2018) 155–162.

[34] M. Tedesco, A. Cipollina, A. Tamburini, G. Micale, Towards 1 kW power production in a reverse electrodialysis pilot plant with saline waters and concentrated brines, Journal of Membrane Science 522 (2017) 226–236.

[35] N. Poulsen, M. Sumper, N. Kröger, Biosilica formation in diatoms: Characterization of native silaffin-2 and its role in silica morphogenesis, Proceedings of the National Academy of Sciences 100 (2003) 12075–12080.

[36] M. Grzegorzek, K. Majewska-Nowak, The influence of humic acids on desalination process with the use of electrodialysis, E3S Web Conf. 17 (2017) 27.

# Chapter 7

## General discussion and outlook

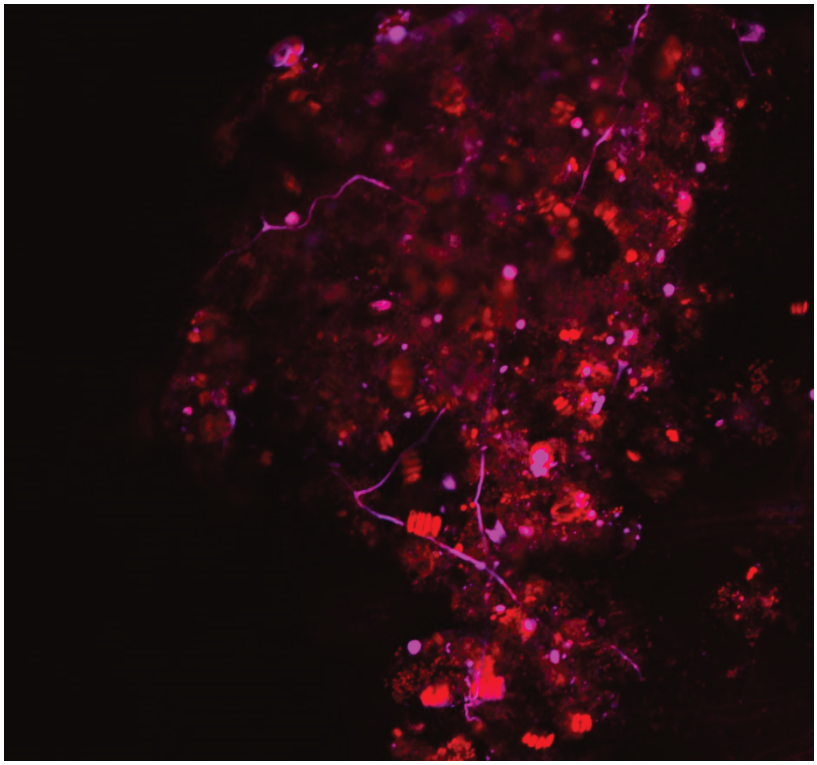

Fouling in reverse electrodialysis (RED) can lead to a decrease of the power output and is a major concern for application of the technology at full scale. This thesis focused on identifying and analysing fouling caused by components of natural feed waters in RED and proposing solutions. First, a deeper understanding of the kind of foulants that are of concern for RED performance was discussed (Chapters 2 and 3) and later pre-treatment and cleaning strategies were proposed as possible solutions regarding the process design to prevent fouling formation and mitigate the power losses (Chapters 4, 5 and 6). Based on what we learned in this study, we will discuss in this chapter how fouling by real feed waters and the proposed solutions can impact the design of a RED facility and its feasibility.

To represent fouling in real applications, the experiments of this thesis were carried out at a pilot plant located at the Afsluitdijk, The Netherlands, which is a potential location for the implementation of the process. Most previous research in RED has been carried out with the use of model feed waters, which hardly translate into the effects caused by real foulants. However, using natural feedwaters has the disadvantage that the experimental conditions are intrinsically related to the location of the pilot plant and composition of the feedwaters, making it a unique case study. Anyhow, the insights gathered with this case study can still be extrapolated to other locations and feedwater conditions, and that is more meaningful than making conclusions when using just model waters.

Thus, in this chapter, first some considerations are made regarding the effects of fouling in RED and its implications. Next, a discussion about how to reduce this effect, focusing on the design of the pre-treatment step is made. Lastly, some input for future projects on RED is given, focusing on location and sustainability of the process.

## 7.1 The effects of foulants

Chapters 2 and 3 showed that biofouling caused by microbial growth does not affect the electrochemical performance in terms of gross power production. The largest impact from fouling was observed as a result of the accumulation of particulate matter, which increases the pressure drop over the stack, reducing the available net power density. From this we can conclude that is more important to tackle the development of a large fouling layer of (in)organic particulate matter with a tailored pre-treatment method than to focus on the removal of other more specific foulants. The same is valid for the cleaning procedures, as shown in Chapter 6, which should primarily focus on the removal of particulate fouling and that is achievable with simple techniques with low energy requirements rather than the application of more sophisticated techniques or involving the use of chemicals.

In Chapters 2 and 3, a new methodology was developed for detection and analysis of biofouling on ion-exchange membranes used in RED stacks. This consisted in using microscopy techniques, such as SEM-EDX to visualize the shape and chemical nature of fouling layers, and CLSM and optical microscopy using dyes to identify biofouling elements (for example, cells and extracellular polymeric substances, forming biofilms). For the first time in this field, by using these techniques together, the occurrence of biofouling could be evaluated and related to feed water composition and performance of the stacks, leading to the conclusion that biofouling is limited and not causing appreciable process losses. Those results made possible to establish a relation between the pre-treatment and the fouling layer: it seems like that the particles that pass a dual media filter pre-treatment and adhere to the membrane surface have a protective effect against biofilm formation on the surface itself. We believe this phenomenon was avoiding the decline of obtainable gross power output in RED, even with the use of natural feeds and presence of foulants.

However, biofouling is seen as a big problem in pressure driven membrane processes, such as nanofiltration (NF) and reverse osmosis (RO) [1], and many approaches were made in an attempt of reducing these problems, but up to our knowledge, no relation between the presence of particulate matter and biofouling was established. Even though the processes (RED and pressure driven systems) are of different nature, further studies could focus on applying a compound that has similar characteristics to the particulate matter on the membranes and that does not cause clogging of the membranes pores but helps prevent biofouling in these membrane processes. The reasons for biofouling being of less concern when particulate matter is adhering on membranes can be due to a combination of factors:

- In pressure driven process, there is always the formation of a concentrate, which means that the microorganisms are being continuously concentrated at the membrane surface, which can lead to a condition that favours the attachment and growth of biofouling. In RED that does not happen, the feed waters are just passing through the stacks and the change in the concentration of most foulants are not changing drastically.
- In RO or NF usually, a stricter pre-treatment method removes the suspended solids of the feed and leaves only dissolved foulants on the feed of these processes. The presence of these particulate solids in RED can act as a protection of the membrane surface, and due to different charge interactions from the particles and the membrane surface, could be that the microorganisms find more difficulties in attaching and growing, due to repulsing charges near the membrane. In addition, less membrane surface is available for attachment with the presence of solids.

- In this thesis, most of the experiments were performed in waters with low temperature (below 15°C), which could have also favoured that the bioactivity was low and more specific to certain conditions, such as the absence of particulate matter.

## 7.2 Reducing the effects of fouling

It was shown that the stack design in RED should focus on maximizing the gross power output, while pre-treatment and cleaning will focus on the removal of foulants that if present would increase pumping losses and thus reduce the net power production. In this way, a sustainable energy output can be achieved and maintained. However, the energy requirements for the pre-treatment and cleaning, have not been sufficiently considered in literature. In the next section, an evaluation will relate the operational conditions of the pre-treatment with the energy requirements and area needed, applying these results to other possible locations.

### 7.2.1 Energy requirements for the pre-treatment

In this thesis and in several previous works, net power density was defined by considering the losses related only to the power needed to pump the water through the stack, and not the power needed to pump water from a source point to the stack, or other energy expenditures, such as the pre-treatment. This is a simplification that has been adopted in literature, in the expectation that energy requirements for pumping and pre-treatment would not account for a significant reduction when estimating the total produced energy. Most scientific work on this technology is done at lab scale and with small stacks and consequently small membrane area, making it difficult to estimate the real amount of energy that can be harvested with the technology in perspective. However, a shift towards a more realistic net energy calculation is needed for further development of RED technology.

The energy expense of pre-treatment for RED can be depicted with a simple model using the results from Chapters 4 and 5. The power needed for the pre-treatment has two components: the power spent to pump the water through the filtration media, and the additional power need due to the increase of pressure caused by fouling accumulation on the media granules. The first, depends on the type of media (in this case sand and anthracite), characteristics of the feed water and the flow velocity applied to the filter. The latter is mostly related to the fouling potential of the influent.

The power spent to pump the water through the filters is given by $P_{pump}$ (W):

$$P_{pump} = \phi_{fw}\Delta P_{fw} + \phi_{sw}\Delta P_{sw} \quad \text{(Eq. 7.1)}$$

with $\Delta p_{fw}$ and $\Delta p_{sw}$ (Pa) are the pressure drop over the inlet and outlet of the freshwater and seawater filters and $\phi_{fw}$ and $\phi_{sw}$ ($m^3/s$) are the flow rates of fresh and seawater.

Using Ergun's Equation (Eq. 7.2) for calculating the pressure drop of the media bed (Δp, Pa) over the column of the filters, it is possible to estimate the pumping power needed to run the filters at different flow velocities:

$$\Delta p = \frac{150\mu L}{D_p^2}\frac{(1-\epsilon)^2}{\epsilon^3}v_s + \frac{1.75L\rho}{D_p}\frac{(1-\epsilon)}{\epsilon^3}v_s^2 \qquad \text{(Eq. 7.2)}$$

where μ is dynamic viscosity of the fluid, L is the length of the bed, $D_p$ is the equivalent spherical diameter of the bed material, ϵ is the porosity of the bed, $v_s$ is the superficial velocity, and ρ is the density of the fluid. The values of μ and ρ were found in literature for fresh water and seawater at 10 °C [2], $D_p$ is estimated by the particle distribution given by the manufacturer for sand and anthracite used in the experiments, ϵ was calculated by estimation of the void space with water, and L and $v_s$ are given by the conditions applied to the filters. All the values used for this calculation can be found in the Appendix section.

For an estimation of the pressure drop increase in the filters due to fouling, experimental values of pressure drop from Chapter 4 were fitted with the load removed. For an analysis of the pumping energy needed for the pre-treatment of 1 $m^3/h$ of seawater and 1 $m^3/h$ of freshwater at different flow velocities, it was assumed an inlet turbidity of 50 NTU and an outlet turbidity of 15 NTU, and results are shown in Figure 7.1.

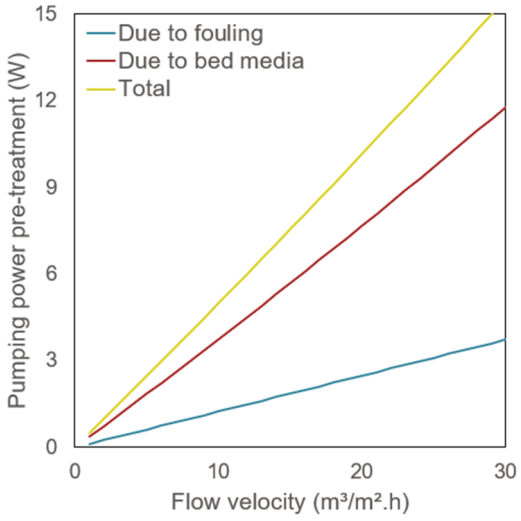


**Figure 7.1.** Pumping power needed to produce 1 $m^3/h$ of seawater and 1 $m^3/h$ of freshwater with the dual media filter pre-treatment at different flow velocities.

With the dual media filter running at 20 $m^3/m^2.h$, approximately 10 W of power is needed to treat 1 $m^3/h$ of each feed water. The power required at lower flow velocity, for example at 4 $m^3/m^2.h$ is substantially lower, around 2 W. That is mostly related to the pumping power needed to the water go through the bed media, which accounts for most of the energy requirement. However, despite the higher energy expenses, the flow velocity at 20 $m^3/m^2.h$ has two key advantages: (1) it allows for the reduction of the constructed area of the filters, leading to less capex costs as discussed in the next section. (2) There is also a reduction in the material needed for filtration, such as anthracite, sand, or activated filter media (AFM), which again reduces the capex costs. In addition, the use of high filtration velocity makes better use of the filtration media column in between each backwash, by accumulating foulants over the whole column, and limited effect on the pressure drop of the filter [3].

### 7.2.2 Comparison of energy produced versus energy spent

For a comparison of the power output that can be obtained with RED and the amount of water treated at high velocity with the dual media filter, some assumptions about stack operation are made. For the net power density, a low, yet realistic, value of 0.3 $W/m^2$ was obtained experimentally in this thesis, with two stacks of 22 cm x 22 cm in a multistage configuration (Chapter 5). With 100 cell pairs each and running at 1 cm/s flow velocity, the membrane area available (2 stacks) is 19.4 $m^2$, thus, it is possible to produce 5.8 W per couple of stacks. The flow rate and the flow velocity are intrinsically related, thus in such a stack, the flow rate of each feed compartment ($\phi$) can be calculated as:

$$\phi = \mathrm{v} * N_{cp} * A \qquad \text{(Eq. 7.3)}$$

where v is the flow velocity in the stack (cm/s), $N_{cp}$ is the number of cell pairs in the stack (dimensionless), and A is the cross-sectional area available for the flow ($cm^2$). These results show that the stacks should be run at 120 L/h to achieve the flow velocity of 1 cm/s. With the 1 $m^3/h$ of flow produced by the dual media filters thus is possible to run at least 8 couple of stacks, which would result in a total produced power of **46 W** produced. Thus, the pre-treatment at 20 $m^3/m^2.h$ would consume about **22 %** of the produced power (10 W), which for this scale of operation seems realistic. It is possible to reduce this percentage still, by increasing the power density of the stacks or by lowering the flow velocity of the pre-treatment, at the expense of increasing the area needed for filtration. The value for the power density used here is taken from this thesis where the salinity of the feed waters is not optimal for the process. Improvement of stacks operation or increasing the concentration gradient can yield a better power density and decrease the fraction of power consumed in the pre-treatment. Still, how this power requirement relates to the potential production of a full-scale RED plant depends on many other variables, such as membrane type, fouling phenomena, stack configuration, etc.

The energy required for the cleaning procedure is considered negligible in comparison to the power expense due to the pre-treatment. The cleaning procedures studied in Chapter 6 were low in energy demand, which could be performed with simple valves switch and compressed air. The cleaning procedures demanded only around 1 % downtime, so energy could be continuously produced, and the losses due to fouling quickly recovered. Because of that, the power requirement for the cleaning procedures was not included in this evaluation.

### 7.2.3 Area required for pre-treatment

In Chapter 4, the pre-treatment of feed water with dual media filters was studied, aiming for an improved operation for application in RED, which translates into a smaller surface area footprint of the filters. The goal was to produce an effluent with low concentration of solids with the minimum energy and area requirement. By applying high flow velocity (i.e. 20 $m^3/m^2.h$) to the filters, the volume of treated water produced per total surface area of the filter increases, allowing to have a smaller surface area, decreasing construction costs of the filters. Using values acquired experimentally in Chapter 4, the area of filter needed to guarantee the production of a certain flow, can be estimated with equation 7.4, and related to the flow velocity, as shown in Figure 7.2.

$$A_f = \frac{Q_f}{V_{produced}} * t_{cycle} \qquad \text{(Eq. 7.4)}$$

With $A_f$ ($m^2$) the area of the filter, $Q_f$ ($m^3/h$) the flow passing the filter, $V_{produced}$ ($m^3/m^2$) the net volume of produced water per area of filter, already accounting for the volume used for backwashing and $t_{cycle}$ (h) the total time of a filtration cycle, including the time to produce water and the downtime to perform backwash. The total time of the filtration cycle was assumed to be linear with the flow velocity, and the values were acquired by regression of the experimentally determined values (i.e., 4 $m^3/m^2.h$ and 20 $m^3/m^2.h$)

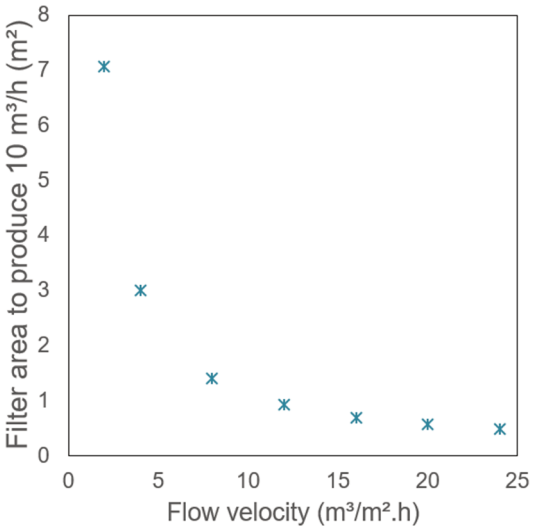


**Figure 7.2.** Filter area needed to produce 10 $m^3$/h related to the flow velocity applied to the filter

Thus, if we consider having a working flow of 10 $m^3$/h of treated water, the surface area needed for the filter at high velocity is 0.56 $m^2$, while at low velocity the area needed is 3 $m^2$.

This is important for RED technology because it can reduce the initial construction costs of such pre-treatment in a power plant and makes the use of the filter bed column more efficient, since with the higher filtration velocity the bed is used to a higher extent to remove load before backwash is performed. In Chapter 4, we showed that a more frequent backwashing is needed due to the higher velocity applied, but this is not necessarily a disadvantage, since even when considering the volume of water needed for backwashing the production of treated water at high velocity is more efficient and would not result in an increase of operation costs.

The use of AFM in the dual media filter showed to be beneficial, by partly compensating for the decrease of effluent quality of the filters running at high velocity and achieving better removal than sand. Ju et al. [4] also observed the benefit of using AFM, but in their study included the removal of organic compounds, which was not seen in this study. The observed removal is probably an artefact due to the short experimental time of the experiments not being meaningful. The use of an activated media increases the surface area and charge density of the media and that contributes to better filtration, however that did not change the types of foulants that could be removed with the media, and we believe that this is mostly related to extended times of operation. This difference in

results shows the importance of running experiments that are designed to be similar to real operation, including larger scale, extended operation time and use of natural waters.

The application of high flow velocity had the disadvantage of decreasing the effluent quality of the filters, leading to an increase of pressure drop in the stacks and a loss of performance. However, the resulting decrease of stack performance is not critical, as it was mostly below 100 mbar in the period of two weeks. As shown in Chapter 6, a frequent cleaning can solve this problem, as the increase of pressure drop is due to particulate fouling, and thus cleaning should be able to restore the performance to initial levels.

### 7.2.4 What if we use cleaner feed water?

This thesis focused on the Dutch water bodies, more specifically IJsselmeer and Wadden sea, as source of feed water for RED technology, both cointaning considerable amount of particulate matter [5]. According to the main results of Chapters 2 and 3, suspended solids are the main cause of performance loss due to fouling and required an adequate pre-treatment. Thus, when searching for an ideal location for a RED process plant and considering the impact of such particulate fouling in the process, water bodies with less particulate matter should be ideally chosen.

A simulation of the pumping power needed for the pre-treatment when the inlet water is cleaner can be made with the same model used in section 7.2.1. The estimation of the pumping power needed with a reduction of influent turbidity from 50 to 25 NTU is shown in Figure 7.3.

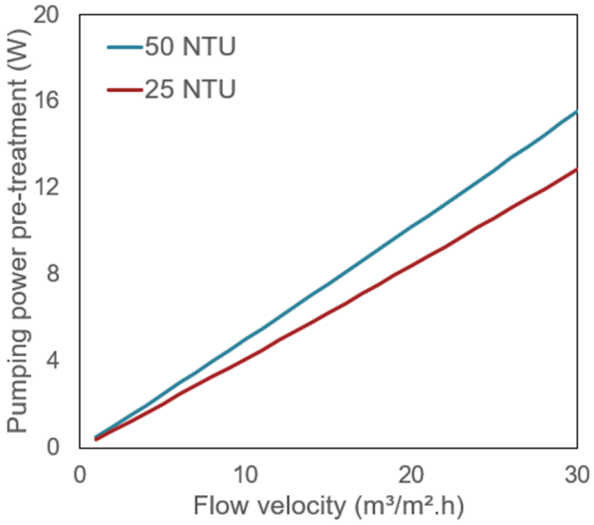

**Figure 7.3.** Estimation of the pumping power needed for the pre-treatment of 1 $m^3/h$ of each feed water with 50 NTU and 25 NTU inlet turbidity and 15 NTU outlet turbidity varying with the flow velocity applied to the filters.

So, in the case of a lower influent turbidity the pumping power needed for the pre-treatment is reduced from 10 W to 8.4 W when the filter is operated at 20 $m^3/m^2.h$, which corresponds to **18%** of the net power produced with RED stacks, as shown in section 7.2.2.

## 7.3 Input for future RED design

RED is a technology involving many variables in its operation. It needs two water sources that need to go through a pre-treatment, two types of membranes with different properties, use of spacers or profiled membranes and other stack configuration parameters, such as length, flow velocity and intermembrane distance. Here, some of these variables will be discussed in the light of the impact of fouling.

### 7.3.1 Location and feed water composition

Every water body that can be used for RED application will have different characteristics and composition that will result in different power output. The characteristics of the feed water are closely related to the location, thus chosing an ideal location for the process is key for its success. To achieve a high gross power output from the mixing of the two streams, a few things can be considered, such as maximizing the salinity gradient, large flow of water available and high temperature of the waters, for example. However, every location is conditioned to seasonal variations that will ultimately affect the power output of the process. The variations impact mostly the freshwater sources, since freshwater bodies are more prone to seasonal conditions, such as flow discharge regime and sediment transport, and variability of temperature [6].

In this thesis, we focused on studying how the feed water composition related to foulants can affect the performance of RED. The need to reduce the energy losses from fouling is an important feature for the future development of RED technology, and we have showed that they can be managed and controlled with the application of adequate pre-treatment and cleaning procedures. We have performed experiments in different seasons and feed water conditions, resulting in the observation of different types of fouling. In the warmer months, the gross power production was higher due to the water temperature, but more fouling was observed due to algae activity, as well as more variation in the available salinity gradient, due to human activities around the sourcing point and rainfall events. In contrast, in autumn and winter, while the gross power was reduced by the colder water temperature, fouling was mostly caused by particulate matter and that could be managed with the pre-treatment and cleaning procedures discussed earlier.

When choosing a location for RED, the water quality of the location is crucial as it determines the gross power density and the losses due to fouling. Water quality of river water depends on its (natural) course and sediment suspension regime, besides the human uses upstream and human activities like wastewater discharge. Seasonal variation of the flow is also a key point as it determines the power production profile throughout the year. For seawater, the human activities nearby can affect the salinity gradient and the (re)suspension of solids, besides tidal range being a key factor of the suitability of the location [7].

For instance, the Ebro river and the Rhone river were considered suitable for RED exploitation based on the flow and salinity gradient with the Mediterranean sea, already considering the energy spent for pumping the feeds to a potential location of a plant [7]. As regarding fouling potential from the Ebro river, due to dams constructed upstream, the amount of sediment discharge in the delta was reduced up to 99% its original values [8], potentially favouring the reduction of fouling impact. In the Rhone river delta, sediment discharge is highly dependent on the season and meteorological events, such as floods in winter and high precipitation events in summer contributing to more sediment discharge and creating conditions for ocean life and marine ecosystem development [9].

As for the fouling coming from the seawater source, in the case of the Mediterranean Sea, less issues with suspended solids are expected due to its clear waters but, as the water is warmer, potentially more bioactivity can occur, which can lead to more issues with biofouling than what has been seen in the case described in this thesis.

A clear separation of salinity gradient favors successful exploitation of RED. Thus, RED technology is favoured when located in a dike, where seawater and fresh water sources are located close to each other but still clearly separated by land, where the plant can be located. With the rising sea levels, it is expected that more dikes or levees are going to be built, especially near big cities by the seashore [10]. In these cases, the low salinity feed water could be a river delta or the effluent of wastewater treatment plants. Known examples are New York and Venice, where the rise of sea level and flood management are known issues for a long time already. These regions are also located where energy demands are high and the use of renewable and non-polluting sources are especially needed, due to high population density and environment impact from other activities already polluting the surrounding areas.

### 7.3.2 Stack variables

The use of spacers versus the use of profiled membranes in RED has been discussed in previous works, with the use of spacers being known to decrease the overall electrochemical performance and constitute an additional surface for fouling

attachment. In chapters 4 and 6, the use of profiled membranes was preferred and fouling was better controlled in agreement with previous studies [11]. The problem for future implementation of the technique for real scale application is, that to our knowledge, no technique has been developed to produce such membranes on industrial scale. The use of thermo-press method, which increases the temperature of the membrane and press it into a mold for reshaping, is basically manual and further development of the membranes properties is also needed to make this method suitable. The use of the casting method, by shaping the membranes with a mold since the production phase with a casting solution, has more potential for industrialization. More recently [12], 3D printing was also used for making profiled membranes and has somewhat potential for a scaled-up manufacturing technique. That is of utmost need to enable the adoption of profiled membranes in RED.

The intermembrane distance also heavily influences RED performance and fouling impact. As seen in Chapter 5, when using spacers and a small intermembrane distance (~ 150 μm), the impact of fouling in the pressure drop over the inlet and outlet of the stacks was substantially higher than in the other experiments, with larger intermembrane distance or profiled membranes. The smaller the intermembrane distance, the higher is the gross power output, but it also requires an increase of pumping power and can lead to a faster blocking of the channels by foulants, reducing the obtained net power. Thus, a balance is needed between these variables, the channels should be smaller as possible, considering the fouling potential of the channel and the feedwater [13].

### 7.3.3 Sustainability and ecological impact

Although salinity gradient energy is considered sustainable, the whole process must be analysed for its impact on the environment. A life cycle assessment of a RED plant was discussed by [14] and most of the environmental impact of a RED power plant using natural waters as source comes from the production of the membranes, more specifically from the AEM monomer molecules. This impact is highly dependent on the membrane area needed for the process, which correlates mostly to the power density achieved with the feed waters and still many uncertainties are present. However, when using the good case scenarios, the impacts associated with RED are still less than the other comparable renewable energy technologies, such as solar and wind [14].

One of the biggest concerns for the RED process is that during the operation of a plant, ecological damage can occur [15]. That would be mostly related to the pre-treatment, since during the filtration of the feed waters, organic and inorganic sediments is concentrated in a stream and usually later discharged in one point, normaly in the sea. This concentraded stream of foulants could impact micro and macro fauna in the coastal ecosystems, which is already under pressure due to other human activities. It is difficult to estimate the extent of the ecological impact that could be caused by the operation of

a full-scale plant with natural waters, since that will depend on the specific characteristics of each site. The research carried out for the impact of the operation of the RED pilot plant in the Afsluitdijk, the Netherlands, [16] concluded that there was an impact on the microfauna mostly due to difference of salinity at the discharge point and the impact on the macrofauna was the low survival rate at the intake systems. However, most of these impacts could be limited if properly mitigated. Some solutions could be: (i) the use of wedge-wire screens that prevent small organism to enter the pumping system, (ii) keep the low and high salinity streams separated in the source and (iii) mix the low and high salinity streams at the discharging point in a way that does not extremely change the salinity of the area. The main environmental impact would be due to space requirement for a full-scale plant, including the pre-treatment system and the disposal of the concentrate from the pre-treatment. The discharge of large quantities of concentrate in the Wadden Sea is expected to be complicated, as this is a protected area from UNESCO World Heritage [17], being the largest tidal flats in the world, with specific fauna and habitats that can be sensitive to changes in the surrounding conditions. However, other ecosystems around the world could be more resilient to variations of sediments and salinity or other solutions could be designed. The impact of a larger installation is expected to be greater than what was observed for the pilot plant and proper adaptations and mitigation of the impacts will demand further research and implementation to reduce the impact.

### 7.4 Conclusion

Substantial knowledge was gathered with this thesis on the type of foulants in natural feedwaters and their effect on RED technology performance, along with alternatives for the design of a RED plant, focusing on the pre-treatment system. For future reference, water sample analysis can give first insights on type of fouling expected and its possible impact on the RED process based on the knowledge acquired with this thesis and important design parameters of the pre-treatent were discussed with a view in the energy requirements for application in Blue Energy. We showed that RED is a suitable technology for production of renewable energy to be further developed at larger scale and that fouling related issues can be prevented and mitigated during operation with adequate procedures. The available sites around the world with potential to explore the salinity gradient energy is relevant and certain characteristics of RED are advantgeous compared to other renewable energy sources, making it a good potential addition to the electricity matrix of many countries.

**References**


[1] J.S. Vrouwenvelder, S.M. Bakker, L.P. Wessels, J. van Paassen, The Membrane Fouling Simulator as a new tool for biofouling control of spiral-wound membranes, Desalination 204 (2007) 170–174.

[2] Joel T. Park, Ph. D. and Angelo Olivieri, Fresh Water and Seawater Properties.

[3] P. Ncube, M. Pidou, T. Stephenson, B. Jefferson, P. Jarvis, The effect of high hydraulic loading rate on the removal efficiency of a quadruple media filter for tertiary wastewater treatment, Water research 107 (2016) 102–112.

[4] J. Ju, Y. Choi, S. Lee, C.-G. Park, T. Hwang, N. Jung, Comparison of Pretreatment Methods for Salinity Gradient Power Generation Using Reverse Electrodialysis (RED) Systems, Membranes 12 (2022).

[5] G. C. CADÉE, Reappraisal of the production and import of organic carbon in the Western Wadden Sea6, Netherlands Journal of Sea Research 14 (1980) 305–322.

[6] O.A. Alvarez-Silva, A.F. Osorio, C. Winter, Practical global salinity gradient energy potential, Renewable and Sustainable Energy Reviews 60 (2016) 1387–1395.

[7] O. Alvarez-Silva, C. Winter, A.F. Osorio, Salinity Gradient Energy at River Mouths, Environ. Sci. Technol. Lett. 1 (2014) 410–415.

[8] J.W. Day, C. Ibáñez, D. Pont, F. Scarton, Status and Sustainability of Mediterranean Deltas: The Case of the Ebro, Rhône, and Po Deltas and Venice Lagoon, in: Eric Wolanski, John W. Day, Michael Elliott, Ramesh Ramachandran (Ed.), Coasts and Estuaries, Elsevier, 2019, pp. 237–249.

[9] A.M. Pruski, J. Rzeznik-Orignac, P. Kerhervé, G. Vétion, S. Bourgeois, E. Péru, P. Brosset, F. Toussaint, C. Rabouille, Dynamic of organic matter and meiofaunal community on a river-dominated shelf (Rhône prodelta, NW Mediterranean Sea): Responses to river regime, Estuarine, Coastal and Shelf Science 253 (2021) 107274.

[10] J.H. Nienhuis, J.R. Cox, J. O'Dell, D.A. Edmonds, P. Scussolini, A global open-source database of flood-protection levees on river deltas (openDELvE), Nat. Hazards Earth Syst. Sci. 22 (2022) 4087–4101.

[11] D.A. Vermaas, D. Kunteng, J. Veerman, M. Saakes, K. Nijmeijer, Periodic feedwater reversal and air sparging as antifouling strategies in reverse electrodialysis, Environmental science & technology 48 (2014) 3065–3073.

[12] J. Choi, W.-S. Kim, H.K. Kim, S. Yang, N.J. Jeong, Ultra-thin pore-filling membranes with mirror-image wave patterns for improved power density and reduced pressure drops in stacks of reverse electrodialysis, Journal of Membrane Science 620 (2021) 118885.

[13] D.A. Vermaas, D. Kunteng, M. Saakes, K. Nijmeijer, Fouling in reverse electrodialysis under natural conditions, Water research 47 (2013) 1289–1298.

[14] K.E. Mueller, J.T. Thomas, J.X. Johnson, J.F. DeCarolis, D.F. Call, Life cycle assessment of salinity gradient energy recovery using reverse electrodialysis, Journal of Industrial Ecology 25 (2021) 1194–1206.

[15] C. Seyfried, H. Palko, L. Dubbs, Potential local environmental impacts of salinity gradient energy: A review, Renewable and Sustainable Energy Reviews 102 (2019) 111–120.

[16] Luca van Duren, Peter Herman, Zwanette Jager, Lodewijk van Walraven, Simon Grasman, Jeroen Wijsman, Rik Siebers, Onderzoek Omgevingseffecten Blue Energy: Synthese van vier jaar onderzoek, Deltares, 2020.

[17] UNESCO World Heritage Centre, Wadden Sea - description, https://whc.unesco.org/en/list/1314/, accessed 26 May 2023.

**Appendix**

μ freshwater at 10°C: 0.001306 Pa.s

μ seawater at 10° C: 0.001397 Pa.s

ρ freshwater at 10° C: 999.7025 kg/m³

ρ seawater 10°C: 1027 kg/m³

$D_p$ sand: 0.0006 m

$D_p$ anthracite: 0.0013 m

$v_s$ : 0.00556 m/s

ϵ sand: 0.36

ϵ anthracite: 0.47

L bed: 0.45 m

Area filter 0.052 m²

## Acknowledgements

For everyone that reads only this section of the thesis: no hurt feelings, I understand it is the most interesting part of it! :)

Thanks for the committee for taking the time to read and evaluate this work, it is well appreciated.

Bert, thank you for sharing a small piece of your knowledge and experience with me in the last 4.5 years. I learned a lot from our meetings, not only about fouling and reverse electrodialysis but also about life and the importance of communication. Your sharp thinking together with your questioning nature triggered me to always go a step further, even if at first I would not agree. In the end, you were always right and you convinced me to push my limits.

Tom, you were always there to help me, thank you. I appreciate all the times that you calmed me down and that nothing can change your good mood. Your determination to make me start writing was of the utmost need for the creation of this book, together with all the repeated corrections you have made to my drafts when I would make the same mistakes again and again. With you I learned how to build a story and make it concise enough for writing a paper.

Cristina, you were my first contact at Wetsus, and I am glad you are part of my story until the end. You picked my CV from the "trash" and 5 years later we have a thesis to tell the rest of the story. Thanks for pushing me to do more and striving for better. Also, thank you for all the knowledge you have shared about the tiny living organisms that can grow in membranes systems. Your feedback as an "outsider" of the electrochemistry field was also very valuable.

Michel, you were the first to take me to the lab, since day one. I was completely lost on how to start this project and you showed me, with your practical way, that we just start in the lab and see what we can do. That was very helpful and fitted me perfectly, thank you. You were always open to discuss anything related to electrochemistry and also gave me many ideas on things I could try in the lab, unfortunately some were too elaborate for me, but anyhow it was an immense help.

Philipp, you joined in later, but I appreciate all the thinking along and input you brought. You always had a new idea on how to solve the many problems I had with my setup in the Afsluitdijk, and you were always available for help, thanks. Antoine, your help with the students was super valuable but also great fun. I enjoyed the meetings we had but specially all the knowledge on membranes that you shared with me.

John, your help with building and adapting the setup many and many times was beyond important for the continuation of my project. Thanks for your critical look on what needed to be done but mostly for your availability to go to the setup and think along on solutions. I hope you enjoy your deserved retirement.

To REDStack, more specifically Simon, Pieter, Jordi and Joost, thank you for all the valuable input on my research and the use of the facility in the Afsluitdijk. At some point, I felt like home when I was there, and I really hope that the pilot is only the first step of a successful story for Blue Energy. I extend my thank you to the Blue Energy theme and all the nice discussions we had during the meetings, it made this book more relevant for the world.

For the ones on the Fouling meetings, especially Caroline for organizing it, thank you for the good discussions and the possibility to share different insights about fouling.

To the students that chose my project to make their own, thank you so much! Marta, Eduardo, Duwayne, Alvaro, André and Fouad, I am grateful you were not afraid to make your hands dirty and that together we overcame many challenges, from faulty pumps to some “showers” in the pilot plant. Each of you brought in new ideas to the research, but most important your enthusiasm made me keep going many times. I especially enjoyed that we had nice and deep talks about everything and nothing on the long drives to the Afsluitdijk.

To the very diverse staff at Wetsus, thank you so much, you are the ones responsible to keep Wetsus running. Jannie, thank you so much for your help with my crazy schedule with the caddy and to always have a smile and a nice talk even when I had difficult requests. The same goes for Trienke, Anita, Tineke, Jeanette, Laura , Roely and all the others that were always available to help at the reception/secretary. Hester, thanks for all the support in ESEE and for pushing me to run further and faster, I hope I can follow your steps one day.

For the canteenies, thank you for supplying us food when we need the most! Gerben, Catherina, Karin and Riet, you were responsible for making the day lighter and brighter when I could not find it in many other places.

Lab team, you are amazing! It gives me confidence that there is good research being done at Wetsus when we have such a great team to help us with all the measurements and analysis. Lisette, Mieke, Jan Willem, Marianne and Jelmer, keep up the good work. The same goes for the microlab people, you helped me a lot in the beginning of my thesis, Bianca, Agnieszka and Alicia.

Technical team, thank you for being there to solve all the issues that a two left-handed person like me can have! Jan, Ernst, Harm, John, JJ, Johan, Wim and Wiebe, you were

always ready to help, thank you! Rienk, thanks for solving all the IT problems I had on the last years.

To my office mates of the most boring office at Wetsus, thank you for the great time we had. Rose, you were the first to say welcome, I wish your endeavours are successful. Kaustub, thanks for the help with all the WUR stuff. Diego, Emad and Gosia, it was very nice to share the theme and the office with you, theme meeting weeks were crazy but after we could have a laugh together. Rebeca, thanks for introducing me to PhD life. Emanuel, thanks for all the pausas, talks, parties, lab sessions and advice we shared. I will never forget the horoscope reading on Friday afternoons. Jolanda, thanks for bearing my mood in the mornings and for the nice talks. Ragne, Sam, Kestral, Arunitha and Ruix, I am glad we could share the office for at least some time and I wish all the luck with your projects.

To the Portuguese crowd that adopted me almost as an equal (cough cough) Catarina, Mariana, Emanuel, João, Rita, Sara and Raquel, thank you for good moments we shared. You helped me to bring a bit of home into the Netherlands by our talks in Portuguese. Mariana, your time managing skills were always crazy to me, but I had fun with all the dinners and moments we shared. Thanks for showing us your home, it is amazing! Catarina, we shared many things in this journey, and I could not be more happy to have found a friend on you! Thank you for being there in the good and the bad, and specially in all the ways to partner up as a paranymph. Gijs, your jokes were never appropriate and never made me laugh, but thanks for the time shared in the Afsluitdijk and in the Portuguese dinners. João, I am glad we share one more milestone together that is the defense date. Thanks for bringing in your organizational skills for this event.

To my Brazilians fellows, thank you for keeping alive some of our most distinctive traditions. Evelyn our long but very rare breaks are known at Wetsus, and it was the time to share all the frustrations but also the achievements we had. These were completely needed. Thanks for being my paranymph. Luewton, thanks for the warm welcome since the first day and sharing all your knowledge about life adaption in Leeuwarden. Filipe, thanks for the all the talks, coffees and dinners inside and outside Wetsus.

To all the others that I had a nice talk and an update in life every now and then, Shuyana, Paulina, Qingdian, Ruizhe, Amanda, Carlo, Wokke, Sebastian, Danielle, Olga S. and Olga B. thanks for that, it made my day.

Aos meus queridos amigos que mesmo a distância me incentivaram de alguma forma a continuar, muito obrigada. Mayra, Bia, Ade, Lígia, Paty, Sara, Tsuka, Laís, Cauê é sempre bom me sentir acolhida quando nos vemos ou falamos!

Marianne, lieverd, it is hard to know if this thesis would have been here if I had not met you in the process. Thank you for all the times you heard my complains and gave me (un)wanted advice, you make me a better person. I look forward to share with you all the next adventures to come! Pieter, Heleen, Imke, Sierd, Pieter Jr., Gonnie and Jurre, thanks for welcoming me in your family.

À minha família, um obrigada especial por todo o apoio e incentivo que recebi desde pequena. Regina, foi você quem despertou meu interesse em estudar e aprender mais sobre o mundo, obrigada. Tias Socorro, Sueli, Sule e Selni e tios Ademir e Tonho, obrigada por sempre me apoiarem. Mãe, você que possibilitou que eu chegasse até aqui, que me guiou em todos os meus passos e me fez almejar sonhos mais altos, meu muito obrigada! A distância não é facil, mas sei que seu orgulho de ver sua filhota como doutora ajuda a amenizar. A minha vó Luiza, obrigada por todos os ensinamentos e o carinho que compartilhamos, voce está sempre comigo.

**About the author**

Bárbara Vital was born on 15th January 1990 in Curitiba, Brazil. In 2008 she started her studies in Environmental Engineering at University of São Paulo in Brazil. With her degree she started working at Aqualogy Brasil as Environmental Engineer, but then decided to join an Erasmus Mundus master's degree in Environmental Engineering and Technology (IMETE) from Ghent University, UNESCO-IHE in Delft and VSCHT in Prague. Bárbara developed a master thesis project about fouling of forward osmosis membranes in the treatment of acid mine drainage in Chile. In 2017, back in Brazil, she worked at Engecorps as Environmental Engineer, in a multidisciplinary team for a project about evaluation of planned infrastructure for mitigation of impact caused by floods and droughts at national level. Looking for a new challenge abroad, in the end of 2018, she joined the "Blue Energy" theme at Wetsus as a PhD candidate from Wageningen University. In this project, she focused on studying fouling in reverse electrodialysis and developing an adequate pre-treatment and cleaning strategy for mitigation of the effects from fouling.

**List of Publications**

**Related to this thesis:**

B. Vital, T. Sleutels, M.C. Gagliano, H.V. Hamelers – Reversible fouling by particulate matter from natural seawater reduces RED performance while limiting biofouling. Desalination 548 (2023) 116262 (doi.org/10.1016/j.desal.2022.116262).

C. Simões, B. Vital, T. Sleutels, M. Saakes, W. Brilman – Scaled-up multistage reverse electrodialysis pilot study with natural waters. Chemical Engineering Journal 450 (2022) 138412. (doi.org/10.1016/j.cej.2022.138412)

B. Vital, E.V. Torres, T. Sleutels, M.C. Gagliano, M. Saakes, H.V. Hamelers – Fouling fractionation in reverse electrodialysis with natural feed waters demonstrates dual media rapid filtration as an effective pre-treatment for fresh water. Desalination 518 (2021) 115277. (doi.org/10.1016/j.desal.2021.115277)

**Other:**

B. Vital, J. Bartacek, J.C. Ortego-Bravo, D. Jeison. Treatment of acid mine drainage by forward osmosis: Heavy metal rejection and reverse flux of draw solution constituents. Chemical Engineering Journal (2018), volume 332, p. 85-91. (https://doi.org/10.1016/j.cej.2017.09.034)

This work was performed in the cooperation framework of Wetsus, European Centre of Excellence for Sustainable Water Technology. Wetsus is co-funded by the Dutch Ministry of Economic Affairs and Climate Policy, the European Union Regional Development Fund, the City of Leeuwarden, the Province of Fryslân, the Northern Netherlands Provinces, and the Netherlands Organization for Scientific Research. The author would like to thank the participants of the Wetsus research theme “Blue Energy” for their financial support and fruitful discussions.

Financial support from Wetsus and Environmental Technology Group (Wageningen University) for printing this thesis is gratefully acknowledged.

Cover photo by Paul de Ruiter Architects and design by RidderPrint

Printed by RidderPrint on recycled paper.

*Netherlands Research School for the*
*Socio-Economic and Natural Sciences of the Environment*

# D I P L O M A

## *for specialised PhD training*

The Netherlands research school for the
Socio-Economic and Natural Sciences of the Environment
(SENSE) declares that

## *Bárbara Vital*

born on the 15th of January 1990 in Curitiba, Brazil

has successfully fulfilled all requirements of the
educational PhD programme of SENSE.

Wageningen, 11th of September 2023

Chair of the SENSE board

Prof. dr. Martin Wassen

The SENSE Director

Prof. Philipp Pattberg

*The SENSE Research School has been accredited by the Royal Netherlands Academy of Arts and Sciences (KNAW)*

K O N I N K L I J K E N E D E R L A N D S E

The SENSE Research School declares that **Bárbara Vital** has successfully fulfilled all requirements of the educational PhD programme of SENSE with a work load of 38.7 EC, including the following activities:

## SENSE PhD Courses

- Environmental research in context (2018)
- Research in context activity: 'Co-organising the European Symposium on Electrochemical Engineering (2021)'

## Selection of Other PhD and Advanced MSc Courses

- Bath Electrochemistry Winter School, Bath University, United Kingdom (2019)
- Data Analysis and Modelling using Python, Wageningen University (2019)
- Novel Batteries for Electrical Energy Storage, Wetsus (2019)
- How to supervise BSc/MSc students, Wetsus/Van Zelf (2019)
- Brain Training, Wageningen Graduate Schools (2019)
- Communication Styles, Wetsus/ How company (2019)
- Presentation skills, Wetsus/ Van Zelf (2019)
- Illustrations for scientific publications, Wetsus/ Somersault (2019)
- Project and Time Management, Wageningen Graduate Schools (2020)
- Scientific writing, Wageningen Graduate Schools (2020)
- Career perspectives, Wetsus (2021)

## Management and Didactic Skills Training

- Supervising two MSc students with thesis entitled 'Study of fouling incidence on Reverse Electrodialysis for power generation using real waters' (2020) and 'Anti-fouling strategies for anion and cation exchange membranes in Blue Energy' (2021)
- Supervising BSc student with thesis entitled 'Natural water data analysis for understanding fouling behavior in Reverse Electrodialysis' (2020)
- Supervising High School students in 'Blue Energy – Het zandfilter' (2019)
- Supervising Literature review assignments (2019-2021)

## Oral and Poster Presentations

- **Best poster award**: *Reversible fouling by particulate matter from natural seawater reduces RED performance but prevents biofouling*. Wetsus congress, 4-5 October 2021, Leeuwarden, The Netherlands
- *Cleaning techniques for RED fed with natural waters using profiled membranes*. Euromembrane 20-24 November 2022, Sorento, Italy
- *Particulate fouling in natural seawater reduces reverse electrodialysis performance but is reversible and prevents biofouling*. Young Water Professional Benelux, 04-06 April 2022, Delft, The Netherlands

SENSE coordinator PhD education

Dr. ir. Peter Vermeulen